



HELLENIC REPUBLIC

UNIVERSITY OF IOANNINA

SCHOOL OF ENGINEERING

DEPARTMENT OF MATERIALS SCIENCE AND ENGINEERING

**A 3d-enabled Visual Representation Tool as a Progressive Web
Application (PWA) based on the WebAssembly specification**

Mohammed A. Abo Arab

PhD Thesis

IOANNINA 2025



ΕΛΛΗΝΙΚΗ ΔΗΜΟΚΡΑΤΙΑ
ΠΑΝΕΠΙΣΤΗΜΙΟ ΙΩΑΝΝΙΝΩΝ
ΠΟΛΥΤΕΧΝΙΚΗ ΣΧΟΛΗ
ΤΜΗΜΑ ΜΗΧΑΝΙΚΩΝ ΕΠΙΣΤΗΜΗΣ ΥΛΙΚΩΝ

**Ένα εργαλείο οπτικής αναπαράστασης με δυνατότητα 3D ως
προοδευτική εφαρμογή ιστού (PWA) με βάση την προδιαγραφή
WebAssembly**

Mohammed A. Abo Arab

ΔΙΔΑΚΤΟΡΙΚΗ ΔΙΑΤΡΙΒΗ

ΙΩΑΝΝΙΝΑ 2025

«Η έγκριση της διδακτορικής διατριβής από το Τμήμα Μηχανικών Επιστήμης Υλικών της Πολυτεχνικής Σχολής του Πανεπιστημίου Ιωαννίνων δεν υποδηλώνει αποδοχή των γνωμών του συγγραφέα Ν. 5343/32, άρθρο 202, παράγραφος 2».

Date of application of Mr. Abo Arab: 14.10.2021

Date of appointment of PhD Advisory Committee: 27.10.2021

Members of the 3 member Advisory Committee:

Thesis Advisor

Dimitrios I. Fotiadis, Professor of Department of Materials Science and Engineering, School of Engineering, University of Ioannina.

Members

Leonidas Gergidis, Professor of Department of Materials Science and Engineering, School of Engineering, University of Ioannina.

Nenad Filipovic, Professor, University of Kragujevac, Serbia.

Date of Thesis subject definition: 27.10.2021

Topic: «A 3d-enabled Visual Representation Tool as a Progressive Web Application (PWA) based on the WebAssembly specification».

Date of appointment of the seven-member Examination Committee: 21.05.2025

Members of the seven-member Advisory Examination Committee:

1. Dimitrios Fotiadis, Professor, Department of Materials Science and Engineering, University of Ioannina
2. Leonidas Gergidis, Professor, Department of Materials Science and Engineering, University of Ioannina
3. Nenad Filipovic, Full Professor at the Faculty of Engineering Sciences at the University of Kragujevac, Serbia
4. Yorgos Goletsis, Associate Professor, Department of Economics of the University of Ioannina
5. Costas Papaloukas, Professor, Department of Biological Applications and Technology, University of Ioannina
6. Themis Exarchos, Associate Professor, Department of Informatics, Ionian University, Corfu
7. Andrzej Skalski, Associate Professor, Department of Measurement and Electronics, AGH University of Krakow, Poland

The PhD thesis is approved, with «Excellent» on 13.06.2025

The Head of the Department



Prof. Simeon Agathopoulos



The Secretary of the Department



Maria Kontou

Ημερομηνία αίτησης του κ. Abo Arab: 14.10.2021

Ημερομηνία ορισμού Τριμελούς Συμβουλευτικής Επιτροπής: 27.10.2021

Μέλη Τριμελούς Συμβουλευτικής Επιτροπής:

Επιβλέπων

Δημήτριος Ι. Φωτιάδης, Καθηγητής, Τμήμα Μηχανικών Επιστήμης Υλικών, Πολυτεχνική Σχολή, Πανεπιστήμιο Ιωαννίνων.

Μέλη

Λεωνίδας Γεργίδης, Καθηγητής, Τμήμα Μηχανικών Επιστήμης Υλικών, Πολυτεχνική Σχολή, Πανεπιστήμιο Ιωαννίνων.

Nenad Filipovic, Καθηγητής, Πανεπιστήμιο του Kragujevac, Σερβία.

Ημερομηνία ορισμού θέματος: 27.10.2021

Θέμα: «Ένα εργαλείο οπτικής αναπαράστασης με υποστήριξη 3D ως Προοδευτική Ιστοεφαρμογή (PWA) βασισμένο στην προδιαγραφή WebAssembly».

Ημερομηνία διορισμού της επταμελούς Εξεταστικής Επιτροπής: 21.05.2025

ΔΙΟΡΙΣΜΟΣ ΕΠΙ ΑΜΕΛΟΥΣ ΕΞΕΤΑΣΤΙΚΗΣ ΕΠΙΤΡΟΠΗΣ:

1. Δημήτριος Φωτιάδης, Καθηγητής του Τμήματος Μηχανικών Επιστήμης Υλικών του Πανεπιστημίου Ιωαννίνων,
2. Λεωνίδας Γεργίδης, Καθηγητής του Τμήματος Μηχανικών Επιστήμης Υλικών του Πανεπιστημίου Ιωαννίνων,
3. Nenad Filipovic, Professor at the Faculty of Engineering Sciences at the University of Kragujevac, Serbia,
4. Γεώργιος Γκολέτσης, Αναπληρωτής Καθηγητής του Τμήματος Οικονομικών Επιστημών του Πανεπιστημίου Ιωαννίνων,
5. Κωνσταντίνος Παπαλουκάς, Καθηγητή του Τμήματος Βιολογικών Εφαρμογών και Τεχνολογιών του Πανεπιστημίου Ιωαννίνων,
6. Θεμιστοκλής Έξαρχος, Αναπληρωτής Καθηγητής του Τμήματος Πληροφορικής του Ιονίου Πανεπιστημίου,
7. Andrzej Skalski, Associate Professor AGH University of Science and Technology, Poland

Έγκριση Διδακτορικής Διατριβής με βαθμό «Άριστα» στις 13.06.2025

Ο Πρόεδρος του Τμήματος


Συμεών Αγαθόπουλος
Καθηγητής



Η Γραμματέας του Τμήματος


Μαρία Κόντου

Dedication

*To the soul of my beloved sister, Sara, may she rest in peace,
and to the soul of my dear grandfather, Elsaied, may he rest in peace.*

Acknowledgements

I consider myself fortunate to have undertaken my PhD journey under the guidance of my supervisor, *Prof. Dimitrios I. Fotiadis*, who hosted me in his laboratory, MedLAB, at the University of Ioannina, in the beautiful city of Ioannina. His exceptional mentorship, and continuous support have profoundly shaped my academic path and made this journey truly rewarding. I am also grateful to my co-supervisors, *Prof. Leonidas Gergidis* (University of Ioannina) and *Prof. Nenad Filipovic* (University of Kragujevac), for their guidance and feedback. I extend my appreciation to *Dr. Vassiliki Potsika* for her support and guidance throughout the DECODE project. Her cheerful demeanor and unwavering encouragement from our very first meeting made every challenge more manageable.

I also appreciate the collaborative environment within DECODE, especially the early-stage researchers at the National and Kapodistrian University of Athens for providing the dataset. My sincere gratitude to *Prof. Andrzej Skalski* (AGH University of Krakow) for his contributions during my secondment, and to *Georgios Gkois* (MedLAB) for his insights into software implementation. Special thanks to *Prof. Amira Ashour* (Tanta University) for her guidance in resolving critical challenges.

On a deeply personal note, I extend my warmest gratitude to my beloved parents, *Abdelrahman* (father) and *Nadia* (mother), whose unwavering support and sacrifices have been my greatest source of inspiration. I owe immense gratitude to my wonderful wife, *Heba*, who has patiently endured the challenges of my PhD journey with love. During this journey, we were blessed with our son, *Hamza*, whose presence brought immense joy. I also cherish the love and encouragement of my siblings—my late sister, *Sara* (may her soul rest in peace), and my brothers, *Elsaied*, *Hamdy*, and *Belal*—who have always supported me.

My sincere appreciation extends to my friends and colleagues at MedLAB, particularly those with whom I shared an office—*Orestis Gkaintes*, *Dr. Panagiotis Siogkas*, *Dimitrios Pleouras*, *Ioannis Pappas*, and *Sokratis Dimos*—whose camaraderie and support enriched my work environment. Special thanks to *Alexandra Zouvgia* for her administrative assistance.

Finally, I am deeply grateful to the European Union's *Marie Skłodowska-Curie* Fellowship, funded under the Horizon 2020 Framework Programme (DECODE Project - grant agreement No 956470), for Funding my doctoral research.

Table of Contents

Chapter 1: Introduction	1
1.1 Background on peripheral artery disease (PAD)	1
1.1.1 Pathophysiology of PAD	1
1.1.2 Epidemiology and prevalence.....	3
1.1.3 Diagnostic Methodologies for PAD.....	4
1.1.4 Clinical and Economic Impact.....	5
1.2 Limitations of Conventional PAD Treatment.....	6
1.2.1 Limitations in Treatment Options.....	6
1.2.1.1 Pharmacotherapy and lifestyle modifications.....	6
1.2.1.2 Surgical and endovascular interventions	7
1.2.2 Challenges in PAD visualization	7
1.2.2.1 Limitations of conventional imaging modalities	8
1.2.3 Advanced Imaging Solutions.....	8
1.2.3.1 3D WebGL volume rendering and DICOM visualization.....	9
1.3 Role of Clouds in Medical Imaging.....	9
1.3.1 Cloud technologies in healthcare	9
1.3.2 Cloud-Driven Innovations in Medical Imaging.....	10
1.3.3 Peripheral artery disease (PAD) diagnosis and management	11
1.4 Objectives and Scope of the Thesis	13
1.4.1 Thesis Objectives	13
1.4.2 Structure of the Thesis	15
Chapter 2: Literature Review.....	19
2.1 Evolution of Web-Based Medical Visualization Platforms.....	19
2.2 Technical advantages: Accessibility, real-time data, and multi-user collaboration.....	22
2.3 Advancements in 3D medical imaging	25
2.4 Advancements in Web-Based DICOM Viewers	26
2.5 WebGL-based medical imaging	29
2.6 Advancements in 3D WebGL volume rendering.....	30
2.7 Cloud-Based Solutions for PAD Management.....	33
2.8 Cloud Computing and AI in Medical Imaging	35
2.9 Cloud-based multidisciplinary platforms.....	35
2.10 Contribution of this Thesis.....	36

Chapter 3: Computational Modeling of Drug-Eluting Balloons	41
3.1 Introduction.....	41
3.2 Intervention methods for PAD.....	43
3.2.1 Balloon Angioplasty	44
3.2.2 Comparative Insights into Balloon Angioplasty Technologies	49
3.3 Computational methods and applications	52
3.3.1 Computational fluid dynamics (CFD)	53
3.3.2 Structural Analysis.....	54
3.3.3 Fluid–structure interaction (FSI) analysis.....	56
3.3.4 Molecular dynamics (MD).....	57
3.3.5 Monte Carlo (MC)	57
3.3.6 Density functional theory (DFT)	58
3.3.7 Machine Learning and Artificial Intelligence.....	59
3.4 Discussion.....	61
3.4.1 Contextualizing Computational Modeling in DEBs.....	61
3.4.2 Implications for Clinical Translation and Practice	63
3.4.3 Challenges and Limitations in Current Computational Techniques.....	64
3.4.4 Future Directions for DEB Research	65
3.5 Conclusion	66
Chapter 4: Advancing Progressive Web Applications for Medical Imaging Visualization	69
4.1 Introduction.....	69
4.2 Objectives	71
4.3 Technical Framework and Methodology	71
4.3.1 Architectural Framework.....	71
4.3.2 Multiplanar reconstruction algorithm	73
4.3.2.1 Weighted Bilinear Interpolation for Nonedge Pixels	74
4.3.2.2 Bicubic Interpolation	74
4.3.3 Application Implementation	76
4.4 Experimental Findings and Performance Analysis.....	77
4.4.1 Experimental Design.....	78
4.4.2 Performance across Multiple Platforms.....	81
4.4.2.1 Private Mode Impact on Loading (T1) and Volume Rendering (T2).....	81

4.4.2.2 Performance evaluation on Windows, Linux, and macOS on the LAN and WAN	81
4.5 Qualitative and Quantitative Evaluation	82
4.6 Discussion	85
4.6.1 Principal Findings	85
4.6.2 Limitations	87
4.6.3 Comparison With Prior Work	87
4.7 Contributions and Future Directions	92
Chapter 5: DECODE-3DViz: High-Fidelity Web-Based Visualization and Automated Risk Classification for Peripheral Artery Disease	93
5.1 Introduction	93
5.2 Objectives	95
5.3 System Design and Implementation	96
5.3.1 System Design	96
5.3.2 Preprocessing Pipeline	96
5.3.3 Large-Scale Volume Rendering	100
5.4 Automated Risk Classification of PAD	104
5.4.1 Real-Time Dynamic Illumination	104
5.4.2 Plaque density analysis	106
5.4.3 Vascular Curvature Analysis	107
5.4.4 PAD Risk Classification	108
5.5 Validation and Performance Evaluation	109
5.5.1 Analytical evaluation	109
5.5.2 Clinical evaluation	109
5.5.3 User feedback via questionnaire	109
5.6 Results	110
5.6.1 Effects of Visualization Parameters on Peripheral Artery CT Images	110
5.6.2 Level of detail optimization in large-scale data management	112
5.6.3 Effect of Light Controls on CT DICOM Peripheral Artery Imaging	114
5.6.4 Validation of the Proposed Framework for PAD Risk Classification	116
5.6.5 Analytical Performance and Evaluation	117
5.6.6 Clinical evaluation	118
5.6.7 Questionnaire and Assessment Protocol	119

5.6.7.1 Visual characteristics	119
5.6.7.2 Additional Questions	120
5.6.7.1 Open-End Questions	122
5.7 Discussion	122
5.7.1 Comparative evaluation of DECODE-3DViz and other modalities on a large-scale dataset 123	
5.7.1 Innovations and Robustness in DECODE-3DViz	126
5.7.2 Clinical impact of DECODE-3DViz in a real-world clinical setting	126
5.7.3 Limitations and Future Work.....	127
5.8 Conclusions.....	127
Chapter 6: DECODE: An Open-Source Cloud-Based Platform for the Noninvasive Management of Peripheral Artery Disease	129
6.1 Introduction.....	129
6.2 Materials and methods	131
6.2.1 Conceptual Design	131
6.2.2 Implementation	132
6.2.3 DECODE Cloud Platform Layers.....	133
6.2.4 Distribution of the DECODE Cloud Computing Services to Stakeholders.....	135
6.3 Modules Design and Architecture	137
6.3.1 User Authentication and Access Control	137
6.3.2 Data Providers.....	138
6.3.3 Data Management and Data Quality Control.....	140
6.3.4 Workflow Manager Module	141
6.3.5 Visualization	141
6.3.5.1 WebXR (eXtended Reality).....	141
6.3.5.2 DECODE-3DViz: WebGL	141
6.3.6 Routing Architecture of the DECODE Cloud Platform	142
6.3.7 Flowchart of the DECODE Cloud Platform	144
6.4 Evaluation	145
6.5 Results.....	146
6.5.1 SUS evaluation.....	147
6.5.2 TAM evaluation	147
6.5.3 Correlation analysis between the SUS and TAM metrics	147

6.6 Discussion	148
6.7 Conclusion	152
Chapter 7: Conclusions and Future Work	153
7.1 Advancements in Cloud-Based Medical Imaging and Computational Vascular Modeling	153
7.2 Future Work	155
Bibliography	159
Appendix.....	191
Author's Publications	203
Short CV	205

List of Figures

Figure 1.1 Diagrammatic representation of atherosclerosis in the lower limbs leading to peripheral arterial disease [2].	2
Figure 1.2 PAD prevalence comparison across regions [11, 16].	4
Figure 3.1 Trends and Comparative Analysis of Balloon Angioplasty Publications (2015–2024): (A) PubMed, (B) Scopus, (C) ScienceDirect, and (D) Stacked Comparison of Article Counts Across Databases.	44
Figure 3.3 Decision-Making Process for Selecting Balloon Angioplasty Techniques Based on Stenosis Type [173-175].	52
Figure 3.2 Comparative Distribution of Clinical Metrics for Conventional Balloons, Drug-Coated Balloons (DCBs), and Drug-Eluting Balloons (DEBs) [173-175].	52
Figure 3.4 Computational Modeling Techniques for Optimizing Drug-Eluting Balloons in Peripheral Artery Disease [188, 211, 212].	61
Figure 4.1 Pipeline Architecture of DICOM and Multiplanar Reconstruction Visualization as a Progressive Web Application.	72
Figure 4.2 Multiplanar Reconstruction Protocol for Volumetric Data from DICOM Slices.	75
Figure 4.3 Clinical evaluation of multiplanar reconstruction accuracy, (A) measurement accuracy of the distal edge of the L1 vertebra in the dataset series of patient 1, (B) consistency in measuring the distal head of the femur bone in the dataset series of patient 2, and (C) consistency of reference lines across multiple planes for the dataset series of patient 3.	84
Figure 4.4 Comparison of the proposed application performances over the LAN with others, (Large-size data).	91
Figure 5.1 Workflow of 3D WebGL Volume Rendering for Peripheral Artery CT Imaging.	96
Figure 5.2 Schematic Diagram of the Preprocessing Pipeline for 3D WebGL Volume Rendering.	97
Figure 5.3 WebGL Volume Rendering Pipeline with Adaptive Resolution and LOD Algorithm.	100
Figure 5.4 Visualization and Parameter Effects on Peripheral Artery CT Images of Patient #17: (a) Top Series Axial View, (b) Bottom Series Axial View, (c) Coronal View, (d) Cropped Coronal View, (e) Cropped Front Coronal View of Region of Interest, (f) Cropped Back Coronal View of Region of Interest, (g) Enhanced Detailed View of Pelvic Arteries with Transfer Function Adjustments.	112

Figure 5.5 Visualization Results of Progressive Streaming and Level of Detail (LOD) Volume Rendering for Three Case Studies (a-c: Case Study 1; d-f: Case Study 2; g-i: Case Study 3).	113
Figure 5.6 Interactive Visualization of Peripheral Artery CT Imaging for Patient 9 with Dynamic Light Controls; (a) User interface for light control parameters; (b) Full CT volume visualization; (c-e) Region of interest under dynamic light variation; (f) Increased light rotation speed and maximum intensity amplitude; (g) Maximum light rotation speed and intensity amplitude; (h) Static lighting with medium intensity.	115
Figure 5.7 Minimum and Maximum Refresh Rate Performance of Visualization Tools on: (a) Laptop and (b) Desktop.	118
Figure 5.8 Performance Comparison of DECODE-3DViz and State-of-the-Art Visualization Tools which are IMAGE-IN, BlueLight, VolView, and Glance. (a) Render Time on Laptop, (b) Render Time on Desktop, (c) Frames Per Second (FPS) on Laptop, (d) FPS on Desktop, (e) GPU Memory Usage on Laptop, and (f) GPU Memory Usage on Desktop.....	122
Figure 6.1 Conceptual development phases of the DECODE cloud platform.	132
Figure 6.2 Package diagram of the DECODE Cloud Platform.	133
Figure 6.3 The DECODE Cloud Platform's multilayered hierarchical framework.	134
Figure 6.4 Architecture and Service Distribution of the DECODE Cloud Platform.....	136
Figure 6.5 Detailed architecture of the DECODE Cloud Platform.	137
Figure 6.6 User authentication workflow in the DECODE Cloud Platform.	138
Figure 6.7 Data provider architecture within the DECODE Cloud Platform.....	139
Figure 6.8 Data Ownership and Collaborative Healthcare Ecosystem.....	140
Figure 6.9 Flowchart of the DECODE Cloud Platform.....	145
Figure 6.10 Home Interface of the DECODE Cloud Platform.....	146
Figure 6.11 Correlation matrix between the system usability scale (SUS) and technology acceptance model (TAM) metrics.....	148
Figure 6.12 DECODE Cloud Platform ecosystem.	149

List of Tables

Table 2.1 Comparison of Advancements in Web-Based DICOM Viewers.	28
Table 2.2 Comparison of advancements in 3D WebGL volume rendering for medical imaging.	33
Table 2.3 Comparison of Cloud-Based Solutions for PAD Management	37
Table 3.1 Clinical outcomes of balloon angioplasty.....	50
Table 3.2 Comparative Overview of Balloon Angioplasty Technologies – Clinical Applications, Efficacy Metrics, Advantages, Limitations, and Technological Innovations. ...	51
Table 3.3 Comprehensive Analysis of Computational Modeling Approaches for Drug-Coated Balloons in the Treatment of Peripheral Artery Disease.	63
Table 4.1 DICOM image annotation and measurement tools and their functions.....	77
Table 4.2 Characteristics of the computed tomography dataset for peripheral artery patients used in the evaluation.....	79
Table 4.3 Computer specifications used in the experiments.....	79
Table 4.4 Performance Metric Details.	80
Table 4.5 Performance metrics for the proposed application across platforms, browsers, and modes (private and ordinary).	81
Table 4.6 Comparison of the proposed application performances over the LAN with others, (Low-size data).	90
Table 4.7 Comparison of the proposed application performances over the LAN with others, (Large-size data).	90
Table 5.1 Parameters and results of progressive streaming and level of detail volume rendering for three case studies.	114
Table 5.2 Quantitative Results of Plaque Density and Vascular Curvature Metrics Across Patients.....	116
Table 5.3 Analytical performance evaluation metrics of DECODE-3DViz and state-of-the-art visualization tools for 3D WebGL volume rendering (mean \pm std).	117
Table 5.4 Likert’s scale evaluation of volume rendering across Peripheral arteries structures and characteristics from the DECODE-3DViz and State-of-the-Art Tools.....	121
Table 5.5 Large-Size Dataset Specification for DECODE-3DViz validation and comparison with others.....	123
Table 5.6 Evaluation Metrics of DECODE-3DViz and State-of-the-Art Visualization Tools on Large-Size Dataset (mean \pm std).	125

Table 6.1 DECODE Cloud Platform Routes and Functional Modules. 143

List of Supplementary Figures

Supplementary Figure 1. Control measurements of the distal edge of the L1 vertebra for patient #1 using 3D Slicer (Version 5.6.2). (a) Measurements performed in the axial view, automatically reflected in the coronal and sagittal planes. (b) Manual measurements repeated in the coronal and sagittal planes. Minor differences (<0.5mm) observed between the views are attributed to the manual measurement process using the mouse cursor.191

List of Abbreviations

<i>Acronym</i>	<i>Meaning</i>
ABI	Ankle-Brachial Index
AGEs	Advanced Glycation End Products
AI	Artificial Intelligence
AJAX	Asynchronous JavaScript and XML
ApoB	Apolipoprotein B
AR	Augmented Reality
BIM	Building Information Modeling
BI	Biomimetic Intelligence
BEM	Boundary Element Method
CAD	Coronary Artery Disease
cMDT	Cloud-Based Multidisciplinary Team
CLTI	Critical Limb-Threatening Ischemia
CNN	Convolutional Neural Network
CRPs	Cardiac Rehabilitation Programs
CSS	Cascading Style Sheets
CT	Computed Tomography
CTA	Computed Tomography Angiography
CVR	Cinematic Volume Rendering
CUDA	Compute Unified Device Architecture

C++	C++ Programming Language
DCB	Drug-Coated Balloon
DEB	Drug-Eluting Balloon
DFUs	Diabetic Foot Ulcers
DFT	Density Functional Theory
DICOM	Digital Imaging and Communications in Medicine
DICOMweb	Web-Based DICOM API
DWV	DICOM Web Viewer
DL	Deep Learning
DSL	Domain-Specific Language
EHR	Electronic Health Record
ESS	Endothelial Shear Stress
FAIR	Findable, Accessible, Interoperable, Reusable
FEA	Finite Element Analysis
FEM	Finite Element Method
FSI	Fluid-Structure Interaction
GDPR	General Data Protection Regulation
GIS	Geographic Information Systems
GPU	Graphics Processing Unit
HIPAA	Health Insurance Portability and Accountability Act
HTML	HyperText Markup Language

HTML5	HTML Version 5
IC	Intermittent Claudication
LDL	Low-Density Lipoprotein
LOD	Level of Detail
MC	Monte Carlo
MD	Molecular Dynamics
MITK	Medical Imaging Interaction Toolkit
ML	Machine Learning
MPR	Multiplanar Reconstruction
MRI	Magnetic Resonance Imaging
NLP	Natural Language Processing
PACS	Picture Archiving and Communication System
PAD	Peripheral Artery Disease
PWA	Progressive Web Application
PET	Positron Emission Tomography
QoE	Quality of Experience
QoS	Quality of Service
REST	Representational State Transfer
ROI	Region of Interest
SAMP-Viz	Scalable Advanced Medical Processing Visualization
SGLT2i	Sodium-Glucose Cotransporter 2 Inhibitors

SOA	Service-Oriented Architecture
SUS	System Usability Scale
TAM	Technology Acceptance Model
TBI	Toe-Brachial Index
TcPO2	Transcutaneous Oxygen Pressure
VLDL	Very Low-Density Lipoprotein
VTK	Visualization Toolkit
WebGL	Web Graphics Library
WebXR	Web Extended Reality

List of symbols

<i>Symbol</i>	<i>Meaning</i>
ρ	Fluid density
∇	Divergence operator
u	Velocity vector
p	Pressure
μ	Dynamic viscosity
g	External forces
C	Drug concentration
D	Diffusion coefficient
$R(C)$	Biochemical reactions within the arterial wall
σ_{ij}	Stress tensors
ϵ_{kl}	Strain tensors
C_{ijkl}	Fourth-order elasticity tensor
C_1	Material constants
C_2	Material constants
I_1	The first invariants of the Cauchy–Green strain tensor
I_2	The second invariants of the Cauchy–Green strain tensor
σ_c	Contact stress
F	Applied force
a	Contact radius

K	Stiffness matrix
m	Mass
h	Planck constant
∇^2	Laplacian operator
$v_{eff}(r)$	Effective potential
$\varphi_i(r)$	The wave function
y_i	The true value
\hat{y}_i	Predicted value
$V_i[k]$	The value of pixel
M_i	The $i - th$ measured value (in the coronal or sagittal view),
G_i	The corresponding ground truth value
$I(D)$	Intensity of the light
I_0	Initial intensity of the light
$\tau(t)$	The optical depth or attenuation coefficient at position t
$C(s)$	Color or emission at positions
$\alpha(v)$	Opacity transfer function
$c(v)$	Color transfer function
G	Gaussian function
$\alpha(t)$	The opacity at point t
$\tau(s)$	Optical depth or attenuation coefficient at positions
$L(t)$	The light direction vector

$\eta(t)$	Noise factor
ω	Light frequency
A	Amplitude of oscillation
β	Damping factor
α	Angular frequency
(ρ_p)	Plaque density
N_c	The number of calcified plaque voxels
N_s	The number of soft plaque voxels
N_v	The total number of vascular tissue voxels
k_i	The curvature
\bar{k}	The average curvature
ρ_p	The computed plaque density
F	The F-statistic

Abstract

This thesis focuses on the development of advanced cloud-based medical imaging frameworks, high-fidelity visualization techniques, and computational modeling solutions for the noninvasive management of peripheral artery disease (PAD). The primary objective is to bridge critical gaps in diagnostic precision, clinical workflow efficiency, and personalized treatment strategies by leveraging web technologies, deep learning models, and computational simulations. This thesis introduces the DECODE Cloud Platform, an open-source cloud-based ecosystem that integrates AI-powered vascular segmentation, real-time 3D visualization, and predictive modeling for PAD risk assessment and treatment planning.

The first chapter provides a detailed introduction to PAD, its pathophysiology, and the limitations of current diagnostic and treatment approaches, highlighting the need for innovative computational solutions. It outlines the role of web-based imaging, cloud computing, and AI in advancing PAD diagnostics and the foundation for research objectives.

The second chapter presents a comprehensive review of state-of-the-art technologies in digital health, web-based medical imaging, and cloud-based platforms for PAD management. It explores advancements in web visualization, AI-powered vascular segmentation, and computational hemodynamics, establishing the theoretical background for the research. In addition, it discusses emerging trends and limitations in noninvasive vascular imaging and introduces the novel contributions of this work.

The third chapter examines the computational modeling of drug-eluting balloons (DEBs) for PAD treatment. A systematic analysis of fluid–structure interaction (FSI), molecular dynamics (MD), finite element modeling (FEM), and machine learning (ML) techniques is conducted to optimize drug diffusion, vascular response, and patient-specific intervention planning. This chapter explores how computational simulations enhance DEB design and performance, addressing therapeutic efficacy and *in-silico* validation.

The fourth chapter focuses on advancing progressive web applications (PWAs) for medical imaging visualization, particularly DICOM and multiplanar reconstruction (MPR) visualization. It presents the technical architecture, algorithmic enhancements, and performance evaluations of the system. Key innovations include the implementation of bicubic and weighted bilinear interpolation techniques, ensuring high-precision 3D reconstructions, cross-platform compatibility, and offline-accessible imaging workflows.

The fifth chapter introduces DECODE-3DViz, a WebGL-based high-fidelity visualization platform optimized for large-scale peripheral artery CT imaging. The research addresses WebGL texture constraints and real-time performance bottlenecks by integrating a level-of-detail (LOD) algorithm, dynamic downsampling, and data chunk streaming. In addition, this chapter presents the automated PAD risk classification framework, which employs optimized volume rendering, dynamic illumination, and quantitative vascular analysis to improve diagnostic accuracy and clinical decision support. A detailed performance validation study demonstrated the efficacy of DECODE-3DViz in enabling interactive 3D visualization for vascular diagnostics.

The sixth chapter details the DECODE Cloud Platform, an open-source, cloud-native infrastructure designed for AI-driven PAD diagnostics and *in-silico* clinical trials. It integrates deep learning-based vascular segmentation, computational hemodynamic modeling, and real-time 3D visualization, providing a scalable, regulatory-compliant framework for multi-institutional collaboration. The usability evaluation via the System Usability Scale (SUS) and Technology Acceptance Model (TAM) confirms high adoption potential, underscoring its clinical viability and integration into real-world medical workflows.

The seventh chapter presents the conclusions and future directions of this research. This thesis highlights the impact of AI-driven vascular imaging, web-based visualization, and computational modeling in redefining PAD diagnostics and noninvasive therapeutic planning. Future research will focus on WebGPU-enhanced visualization, AI-driven multimodal fusion (CT, MRI, and ultrasound), federated learning for privacy-preserving AI training, and real-time *in-silico* simulations for optimizing drug-coated balloon (DCB) therapy. The integration of blockchain-based regulatory compliance mechanisms and automated AI-generated radiology reports will further expand the clinical adoption of DECODE, ensuring its role as a pioneering platform in AI-assisted precision vascular medicine.

The main contributions of this thesis can be summarized as follows: (i) The development of a web-based DICOM and MPR visualization system within a PWA framework ensures cross-platform compatibility, offline accessibility, and optimized real-time rendering for high-resolution vascular imaging. (ii) The introduction of DECODE-3DViz, a high-fidelity WebGL-based visualization pipeline that incorporates LOD algorithms and chunk streaming, significantly enhances real-time interactive visualization of large-scale CT images while optimizing GPU memory and performance efficiency. (iii) The design and validation of an

automated PAD risk classification framework integrating dynamic illumination models, optimized volume rendering, and quantitative vascular analysis improve diagnostic accuracy, reduce interobserver variability, and enable real-time clinical decision support. (iv) The application of computational modeling techniques for DEBs, utilizing FSI, MD, and finite element simulations, to enhance drug delivery, optimize device performance, and advance patient-specific treatment strategies. (v) DECODE, an open-source cloud-based platform that integrates AI-driven vascular segmentation, computational hemodynamic modeling, and real-time 3D visualization, ensures scalability, interoperability, and seamless clinical integration into digital healthcare ecosystems, was developed. This thesis establishes a new benchmark in cloud-based vascular imaging, risk classification, and computational modeling, providing a scalable and clinically viable solution for noninvasive PAD management and precision vascular medicine.

Περίληψη

Αυτή η διατριβή επικεντρώνεται στην ανάπτυξη προηγμένων πλαισίων ιατρικής απεικόνισης βασισμένων στο νέφος, τεχνικών υψηλής πιστότητας οπτικοποίησης και λύσεων υπολογιστικής μοντελοποίησης για τη μη επεμβατική διαχείριση της Περιφερικής Αρτηριακής Νόσου (ΠΑΝ). Ο κύριος στόχος είναι η γεφύρωση κρίσιμων κενών στην ακρίβεια της διάγνωσης, την αποδοτικότητα των κλινικών ροών εργασίας και τις εξατομικευμένες στρατηγικές θεραπείας, αξιοποιώντας διαδικτυακές τεχνολογίες, μοντέλα βαθιάς μάθησης και υπολογιστικές προσομοιώσεις. Αυτή η διατριβή παρουσιάζει την Πλατφόρμα DECODE Cloud, ένα υπολογιστικό οικοσύστημα ανοιχτού κώδικα βασισμένο στο νέφος, το οποίο ενσωματώνει αγγειακή τμηματοποίηση με τεχνητή νοημοσύνη, τρισδιάστατη οπτικοποίηση σε πραγματικό χρόνο και προγνωστική μοντελοποίηση για την εκτίμηση κινδύνου ΠΑΝ και τον σχεδιασμό θεραπείας.

Το πρώτο κεφάλαιο παρέχει μια λεπτομερή εισαγωγή στην ΠΑΝ, τη φυσιοπαθολογία της και τους περιορισμούς των τρεχουσών διαγνωστικών και θεραπευτικών προσεγγίσεων, αναδεικνύοντας την ανάγκη για καινοτόμες υπολογιστικές λύσεις. Περιγράφει τον ρόλο της διαδικτυακής απεικόνισης, του υπολογιστικού νέφους και της τεχνητής νοημοσύνης στην εξέλιξη της διάγνωσης της ΠΑΝ και θέτει τα θεμέλια για τους ερευνητικούς στόχους.

Το δεύτερο κεφάλαιο παρουσιάζει μια ολοκληρωμένη ανασκόπηση των πλέον σύγχρονων τεχνολογιών στην ψηφιακή υγεία, την ιατρική απεικόνιση μέσω διαδικτύου και τις πλατφόρμες βασισμένες στο νέφος για τη διαχείριση της ΠΑΝ. Εξετάζει τις προόδους στην οπτικοποίηση ιστού, την αγγειακή τμηματοποίηση με τεχνητή νοημοσύνη και την υπολογιστική αιμοδυναμική, εδραιώνοντας το θεωρητικό υπόβαθρο της έρευνας. Επιπλέον, συζητά τις αναδυόμενες τάσεις και τους περιορισμούς στη μη επεμβατική αγγειακή απεικόνιση και εισάγει τις καινοτόμες συνεισφορές αυτής της μελέτης.

Το τρίτο κεφάλαιο εξετάζει την υπολογιστική μοντελοποίηση των επικαλυμμένων με φάρμακο μπαλονιών (Drug-Eluting Balloons - DEBs) για τη θεραπεία της Περιφερικής Αρτηριακής Νόσου (ΠΑΝ). Διεξάγεται μια συστηματική ανάλυση της αλληλεπίδρασης ρευστού-δομής (Fluid-Structure Interaction - FSI), της μοριακής δυναμικής (Molecular Dynamics - MD), της μοντελοποίησης πεπερασμένων στοιχείων (Finite Element Modeling - FEM) και των τεχνικών μηχανικής μάθησης (Machine Learning - ML), με στόχο τη βελτιστοποίηση της διάχυσης του φαρμάκου, της αγγειακής απόκρισης και του σχεδιασμού εξατομικευμένων θεραπευτικών παρεμβάσεων. Το κεφάλαιο διερευνά τον τρόπο με τον οποίο οι υπολογιστικές προσομοιώσεις

ενισχύουν τον σχεδιασμό και την απόδοση των DEB, βελτιώνοντας τη θεραπευτική τους αποτελεσματικότητα και την *in-silico* επικύρωση.

Το τέταρτο κεφάλαιο επικεντρώνεται στην προώθηση των Progressive Web Applications (PWAs) για την οπτικοποίηση ιατρικής απεικόνισης, ιδιαίτερα της απεικόνισης DICOM και της Πολυεπίπεδης Ανακατασκευής (Multiplanar Reconstruction - MPR). Παρουσιάζει την τεχνική αρχιτεκτονική, τις αλγοριθμικές βελτιώσεις και τις αξιολογήσεις απόδοσης του συστήματος. Βασικές καινοτομίες περιλαμβάνουν την υλοποίηση τεχνικών κυβικής παρεμβολής και στάθμισης διγραμμικής παρεμβολής, διασφαλίζοντας υψηλής ακρίβειας τρισδιάστατες ανακατασκευές, διαλειτουργικότητα μεταξύ πλατφορμών και ροές εργασίας απεικόνισης προσβάσιμες εκτός σύνδεσης.

Το πέμπτο κεφάλαιο παρουσιάζει το DECODE-3DViz, μια πλατφόρμα οπτικοποίησης υψηλής πιστότητας βασισμένη στο WebGL, βελτιστοποιημένη για απεικόνιση περιφερικών αρτηριών με αξονική τομογραφία μεγάλης κλίμακας. Η έρευνα αντιμετωπίζει τους περιορισμούς των υφών WebGL και τα σημεία συμφόρησης της απόδοσης σε πραγματικό χρόνο, ενσωματώνοντας έναν αλγόριθμο Επίπεδου Λεπτομέρειας (Level of Detail - LOD), δυναμική υποδειγματοληψία και ροή δεδομένων ανά τμήματα. Επιπλέον, το κεφάλαιο παρουσιάζει το αυτοματοποιημένο πλαίσιο ταξινόμησης κινδύνου ΠΑΝ, το οποίο χρησιμοποιεί βελτιστοποιημένη ογκομετρική απεικόνιση, δυναμικό φωτισμό και ποσοτική αγγειακή ανάλυση για τη βελτίωση της διαγνωστικής ακρίβειας και της υποστήριξης κλινικών αποφάσεων. Μια λεπτομερής μελέτη επικύρωσης της απόδοσης αποδεικνύει την αποτελεσματικότητα του DECODE-3DViz στην παροχή διαδραστικής τρισδιάστατης οπτικοποίησης για αγγειακές διαγνώσεις.

Το έκτο κεφάλαιο περιγράφει λεπτομερώς την Πλατφόρμα DECODE Cloud, μια ανοιχτού κώδικα, εγγενώς βασισμένη στο νέφος υπολογιστική υποδομή, σχεδιασμένη για διαγνωστικές διαδικασίες ΠΑΝ με τεχνητή νοημοσύνη και *in-silico* κλινικές δοκιμές. Ενσωματώνει αγγειακή τμηματοποίηση με βαθιά μάθηση, υπολογιστική αιμοδυναμική μοντελοποίηση και τρισδιάστατη οπτικοποίηση σε πραγματικό χρόνο, παρέχοντας ένα επεκτάσιμο, συμβατό με κανονισμούς πλαίσιο για συνεργασία μεταξύ πολλαπλών ερευνητικών ιδρυμάτων. Η αξιολόγηση της χρηστικότητας μέσω της Κλίμακας Χρηστικότητας Συστήματος (System Usability Scale - SUS) και του Μοντέλου Αποδοχής Τεχνολογίας (Technology Acceptance Model - TAM) επιβεβαιώνει το υψηλό δυναμικό υιοθέτησης, υπογραμμίζοντας τη

βιωσιμότητά του στην κλινική πράξη και την ενσωμάτωσή του σε πραγματικά ιατρικά περιβάλλοντα.

Το έβδομο κεφάλαιο παρουσιάζει τα συμπεράσματα και τις μελλοντικές κατευθύνσεις αυτής της έρευνας. Τονίζει τον αντίκτυπο της αγγειακής απεικόνισης με τεχνητή νοημοσύνη, της διαδικτυακής οπτικοποίησης και της υπολογιστικής μοντελοποίησης στον επαναπροσδιορισμό της διάγνωσης της ΠΑΝ και του μη επεμβατικού θεραπευτικού σχεδιασμού. Οι μελλοντικές έρευνες θα επικεντρωθούν στη βελτιστοποίηση της οπτικοποίησης με WebGPU, στη συγχώνευση πολλαπλών απεικονιστικών δεδομένων (CT, MRI, υπερηχογράφημα) με τεχνητή νοημοσύνη, στην ομοσπονδιακή μάθηση για εκπαίδευση τεχνητής νοημοσύνης με διατήρηση της ιδιωτικότητας και στις προσομοιώσεις σε πραγματικό χρόνο για τη βελτιστοποίηση της θεραπείας με επικαλυμμένα με φάρμακο μπαλόνια (Drug-Coated Balloon - DCB). Η ενσωμάτωση μηχανισμών συμμόρφωσης με τους κανονισμούς μέσω blockchain και η αυτόματη παραγωγή ακτινολογικών αναφορών από τεχνητή νοημοσύνη θα επεκτείνουν περαιτέρω την κλινική υιοθέτηση του DECODE, διασφαλίζοντας τον ρόλο του ως πρωτοποριακή πλατφόρμα στην ιατρική ακριβείας με υποστήριξη τεχνητής νοημοσύνης.

Οι κύριες συνεισφορές αυτής της διατριβής μπορούν να συνοψιστούν ως εξής: (i) Η ανάπτυξη ενός διαδικτυακού συστήματος οπτικοποίησης DICOM και Πολυεπίπεδης Ανακατασκευής (Multiplanar Reconstruction - MPR) στο πλαίσιο μιας Progressive Web Application (PWA), διασφαλίζοντας διαλειτουργικότητα μεταξύ πλατφορμών, πρόσβαση εκτός σύνδεσης και βελτιστοποιημένη απόδοση σε πραγματικό χρόνο για αγγειακή απεικόνιση υψηλής ανάλυσης. (ii) Η εισαγωγή του DECODE-3DViz, μιας υποδομής οπτικοποίησης υψηλής πιστότητας βασισμένης στο WebGL, που ενσωματώνει αλγόριθμους Επίπεδου Λεπτομέρειας (LOD) και ροή δεδομένων ανά τμήματα, ενισχύοντας σημαντικά τη διαδραστική οπτικοποίηση μεγάλης κλίμακας αξονικής τομογραφίας σε πραγματικό χρόνο, ενώ παράλληλα βελτιστοποιεί τη μνήμη GPU και την αποδοτικότητα της απόδοσης. (iii) Ο σχεδιασμός και η επικύρωση ενός αυτοματοποιημένου πλαισίου ταξινόμησης κινδύνου για την Περιφερική Αρτηριακή Νόσο (ΠΑΝ), το οποίο ενσωματώνει δυναμικά μοντέλα φωτισμού, βελτιστοποιημένη ογκομετρική απεικόνιση και ποσοτική αγγειακή ανάλυση, βελτιώνοντας την ακρίβεια διάγνωσης, μειώνοντας τη διακύμανση μεταξύ παρατηρητών και επιτρέποντας την υποστήριξη κλινικών αποφάσεων σε πραγματικό χρόνο. (iv) Η εφαρμογή τεχνικών υπολογιστικής μοντελοποίησης για τα επικαλυμμένα με φάρμακο μπαλόνια (Drug-Eluting Balloons - DEBs), αξιοποιώντας την αλληλεπίδραση ρευστού-δομής (Fluid-Structure Interaction - FSI), τη μοριακή δυναμική (Molecular Dynamics - MD) και τις προσομοιώσεις πεπερασμένων στοιχείων (Finite Element

Simulations) για τη βελτίωση της απελευθέρωσης φαρμάκου, τη βελτιστοποίηση της απόδοσης της συσκευής και την προώθηση εξατομικευμένων θεραπευτικών στρατηγικών. (v) Η ανάπτυξη του DECODE, μιας ανοιχτού κώδικα πλατφόρμας βασισμένης στο νέφος, η οποία ενσωματώνει αγγειακή τμηματοποίηση με τεχνητή νοημοσύνη, υπολογιστική αιμοδυναμική μοντελοποίηση και τρισδιάστατη οπτικοποίηση σε πραγματικό χρόνο, διασφαλίζοντας επεκτασιμότητα, διαλειτουργικότητα και απρόσκοπτη κλινική ενσωμάτωση στα ψηφιακά οικοσυστήματα υγειονομικής περίθαλψης. Αυτή η διατριβή θέτει ένα νέο σημείο αναφοράς στην αγγειακή απεικόνιση βασισμένη στο νέφος, την ταξινόμηση κινδύνου και την υπολογιστική μοντελοποίηση, προσφέροντας μια επεκτάσιμη και κλινικά βιώσιμη λύση για τη μη επεμβατική διαχείριση της ΠΑΝ και την ιατρική ακριβείας στον αγγειακό τομέα.

Chapter 1: Introduction

- 1.1 Background on peripheral artery disease (PAD)
 - 1.2 Limitations of Conventional PAD Treatment
 - 1.3 Role of Clouds in Medical Imaging
 - 1.4 Objectives and Scope of the Thesis
-

1.1 Background on peripheral artery disease (PAD)

1.1.1 Pathophysiology of PAD

PAD is a chronic atherosclerotic condition that predominantly affects the arteries of the lower extremities [1, 2]. The disease arises from systemic atherosclerosis, which is characterized by endothelial dysfunction, chronic inflammation, and the progressive accumulation of lipid plaques within arterial walls. These plaques trigger immune responses, oxidative stress, and vascular remodeling, leading to arterial narrowing, reduced blood flow, and ischemia [3, 4]. Figure 1.1 illustrates the pathophysiological process of atherosclerosis leading to PAD, including plaque formation, arterial narrowing, and subsequent impaired blood flow.

The progression of PAD follows a continuum from asymptomatic stages to intermittent claudication (IC) and, in advanced cases, critical limb-threatening ischemia (CLTI) [5]. CLTI is characterized by severe ischemic damage, including rest pain, nonhealing ulcers, gangrene, and a heightened risk of limb loss. In patients with diabetes mellitus (DM), the pathophysiology of PAD is further exacerbated by hyperglycemia, which promotes the formation of advanced glycation end products (AGEs), vascular calcification, and smooth muscle cell proliferation [6]. These changes reduce vascular compliance, impair repair mechanisms, and amplify oxidative

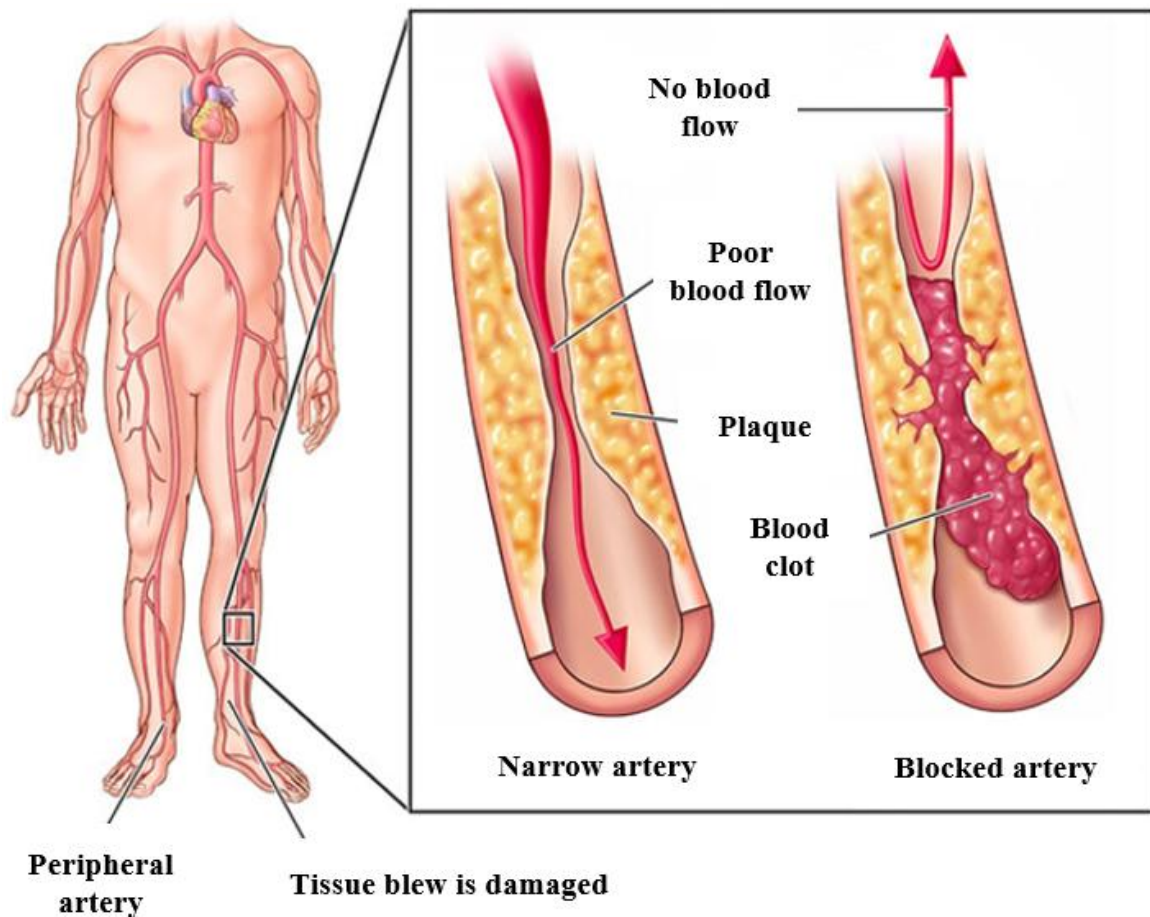


Figure 1.1 Diagrammatic representation of atherosclerosis in the lower limbs leading to peripheral arterial disease [2].

stress, resulting in ischemic injury.

The systemic nature of PAD is evident in its frequent coexistence with coronary and cerebrovascular disease, reflecting shared atherogenic pathways. Emerging evidence highlights the role of atherogenic lipoproteins, particularly apolipoprotein B (ApoB)-containing particles and extra-small very-low-density lipoproteins (XS.VLDL.P), which drive PAD progression [7, 8]. These lipoproteins infiltrate the arterial intima, forming foam cells that accelerate plaque buildup and vascular obstruction. In addition, thromboembolic events and in-situ thrombosis, which are distinct from coronary artery disease (CAD) mechanisms, contribute to the unique pathology of PAD.

Sex-specific differences further influence PAD pathophysiology. In women, the protective effects of estrogen delay endothelial dysfunction [9], but postmenopausal hormonal changes increase oxidative stress and inflammation, leading to more severe disease progression and reduced collateral circulation. Furthermore, microvascular dysfunction and inadequate

angiogenesis have been implicated in advanced PAD, particularly in patients transitioning to CLTI.

In addition to arterial obstruction, PAD impacts skeletal muscle atrophy, mitochondrial dysfunction, and impaired oxygen metabolism, which limit functional capacity and mobility. These localized effects, coupled with systemic cardiovascular risk factors such as smoking, hypertension, and dyslipidemia, underscore the complexity of PAD. Understanding these intricate mechanisms is critical for developing targeted therapeutic strategies that address both the localized and systemic dimensions of the disease.

1.1.2 Epidemiology and prevalence

PAD represents a growing global health burden, affecting over 237 million individuals worldwide [10]. The prevalence of PAD has nearly doubled in the last three decades, driven by aging populations, urbanization, and increasing rates of atherosclerotic risk factors, such as diabetes, smoking, hypertension, and obesity [11]. In the United States, PAD affects an estimated 8.5 to 12 million individuals, with prevalence rates ranging from 4% to 10% among adults aged 40 years and older and increasing to over 20% among those aged 80 years and above [12]. Figure 1.2 illustrates the regional differences in PAD incidence, highlighting the impact of socioeconomic and healthcare disparities on disease burden. Globally, PAD is more common in low- and middle-income countries, which now account for more than 70% of cases [11]. These regions face significant healthcare disparities that exacerbate the impact of PAD, limiting access to preventive care, timely diagnosis, and effective management.

The disease disproportionately affects certain populations. Compared with men, women present equal or higher prevalence rates across all age groups, with a marked increase in older women due to hormonal changes after menopause. The prevalence of black individuals is nearly twice as high as that of other racial groups, compounded by socioeconomic inequities and systemic barriers to care. Furthermore, individuals with diabetes are two to seven times more likely to develop PAD, particularly in distal arteries such as the dorsalis pedis [13, 14]. Diabetic foot ulcers (DFUs), which are common complications in these patients, significantly increase the risks of lower limb amputation and mortality.

Geographic and demographic disparities are pronounced. In high-income countries, PAD is the third leading cause of atherosclerotic morbidity after CAD and stroke [15]. However, the burden is rising most rapidly in low- and middle-income regions, where limited access to healthcare intensifies the toll of PAD. Studies in the Asia–Pacific region, e.g., reported prevalence rates of

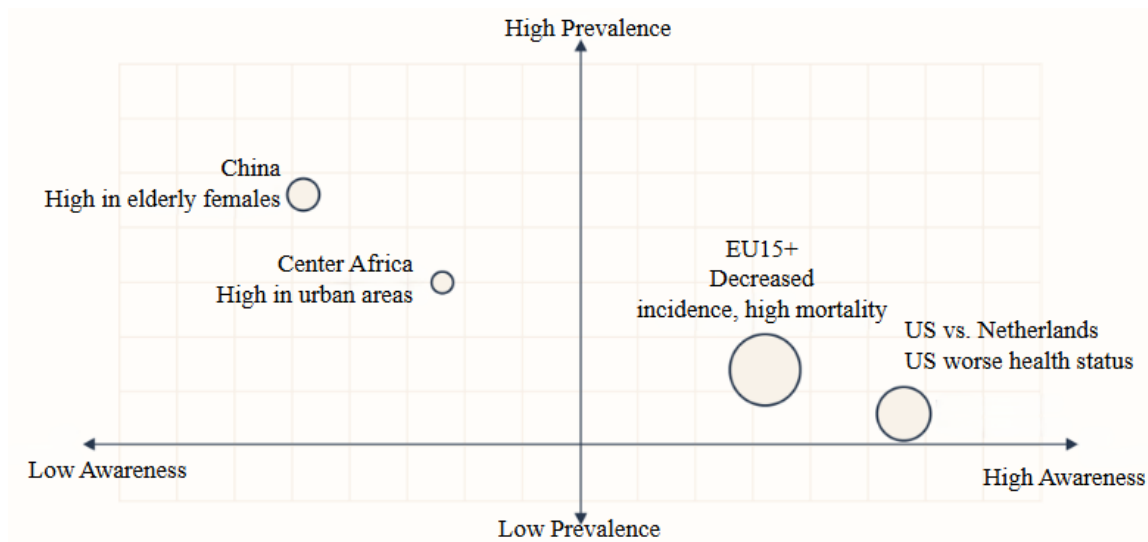


Figure 1.2 PAD prevalence comparison across regions [11, 16].

5% in the Philippines, 8.2% in Singapore, and 12.1% in Japan [16]. Data from large registries, such as the Veterans Affairs Million Veteran Program, underscore the widespread impact of PAD, with African Americans, nonwhite women, and individuals from lower socioeconomic backgrounds disproportionately affected [17].

Age is a critical determinant of PAD incidence. The incidence doubles each decade after the age of 50, reaching over 20% in individuals aged 70 and older [18]. Despite its high prevalence, PAD often remains underdiagnosed, particularly in asymptomatic or atypically presenting individuals. Alarming, 90% of PAD cases in women are undetected, highlighting the pressing need for improved diagnostic outreach and public health strategies. This growing epidemiological burden underscores the urgent need for targeted screening, early intervention, and equitable healthcare policies. Addressing geographic, racial, and socioeconomic disparities is essential to reducing the morbidity and mortality associated with PAD, particularly as global populations continue to age and chronic disease prevalence increases.

1.1.3 Diagnostic Methodologies for PAD

Accurate and early diagnosis of PAD is essential for effective management and improved patient outcomes. The cornerstone diagnostic tool is the ankle-brachial index (ABI), a simple and noninvasive method that compares systolic blood pressure in the ankle to that in the arm. An $ABI \leq 0.90$ confirms PAD, with a sensitivity of 90% and specificity of 98% [19]. In cases of arterial calcification, which may result in falsely elevated ABI readings, common among patients with diabetes or chronic kidney disease, alternative tests such as the toe-brachial index

(TBI) and transcutaneous oxygen pressure (TcPO₂) [20] are employed for enhanced diagnostic accuracy.

Advanced imaging modalities are critical for detailed vascular assessment and treatment planning. Duplex ultrasound provides real-time visualization of arterial stenosis and blood flow dynamics, serving as a first-line imaging technique. Computed tomography angiography (CTA) and magnetic resonance angiography (MRA) offer high-resolution vascular mapping, enabling precise characterization of arterial occlusions and stenotic regions [21]. In severe cases, particularly when surgical or endovascular intervention is planned, catheter-based angiography remains the gold standard for preoperative planning, offering unparalleled details of vascular anatomy.

1.1.4 Clinical and Economic Impact

PAD exerts profound clinical and economic burdens on patients and healthcare systems worldwide. Clinically, PAD significantly reduces mobility, impairs quality of life, and increases the risk of severe cardiovascular events, including myocardial infarction, stroke, and cardiovascular death [10]. Advanced stages of the disease, such as CLTI, lead to chronic ischemic pain, nonhealing ulcers, gangrene, and increased risks of amputation and mortality. Complications such as DFUs in patients with comorbid diabetes further increase morbidity, necessitating prolonged hospital stays and extensive rehabilitative care.

Economically, the management of PAD is resource intensive. Annual healthcare costs associated with PAD in the United States alone are estimated to range from \$84 billion to \$380 billion, driven by advanced diagnostics, surgical interventions, and long-term care for severe cases [22]. Patients with diabetes or CLTI often face disproportionately higher costs, with some Medicare beneficiaries incurring over \$120,000 annually in treatment-related expenses. Hospitalizations, revascularization procedures, and the management of chronic complications such as limb amputation further escalate the financial burden [23]. Globally, the economic losses is particularly severe in low- and middle-income countries, where limited healthcare access exacerbates outcomes and increases costs related to preventable complications [24].

Disparities in healthcare access significantly worsen clinical and economic outcomes. Rural, low-income, and minority populations, including Black Americans and nonwhite women, face disproportionately higher risks of amputation, delayed treatment, and reduced access to limb-salvage therapies. Compared with men, women with PAD often experience worse functional outcomes, such as reduced walking capacity and lower extremity strength [25], highlighting gaps in equitable care delivery and underutilization of guideline-based therapies. These

systemic inequities underscore the urgent need for targeted public health strategies and resource allocation to mitigate the societal and financial impacts of PAD.

Emerging solutions, including artificial intelligence (AI) and machine learning (ML), offer promising avenues to streamline diagnostics and personalize treatment strategies [26], potentially reducing healthcare costs and improving patient outcomes. Innovative therapeutic approaches, such as lipid-lowering therapies targeting ApoB-containing particles and antithrombotic treatments [27], also hold promise in alleviating the clinical and economic burden of PAD. Comprehensive care models that emphasize early diagnosis, aggressive risk factor management, and equitable access to advanced therapies are essential to address PAD's multifaceted challenges effectively.

1.2 Limitations of Conventional PAD Treatment

PAD presents significant clinical challenges because of its multifaceted nature, which affects both the macrovascular and microvascular systems [28]. Despite advances in medical and surgical interventions, conventional PAD treatments often fail to adequately address the complexity of the disease [29], resulting in suboptimal patient outcomes. These limitations are further compounded by disparities in healthcare access, particularly among underserved populations. This section explores the inherent limitations of current PAD treatment options, underscoring the need for innovative, personalized, and noninvasive therapeutic approaches.

1.2.1 Limitations in Treatment Options

Conventional PAD treatments primarily involve pharmacotherapy, lifestyle modifications, and surgical interventions [30]. While these approaches provide symptomatic relief and risk reduction, they are often limited by limited efficacy, safety concerns, and accessibility issues, particularly in advanced stages of PAD.

1.2.1.1 Pharmacotherapy and lifestyle modifications

Pharmacological management of PAD relies heavily on antiplatelet agents, lipid-lowering therapies, and antihypertensives aimed at reducing cardiovascular risk [31]. However, these systemic treatments fall short in addressing localized ischemia or reversing arterial narrowing, particularly in advanced cases such as chronic limb-threatening ischemia (CLTI). Medications such as cilostazol provide modest symptomatic relief but are contraindicated in certain populations, such as those with heart failure, owing to adverse effects [32]. In addition, emerging therapies such as sodium–glucose cotransporter 2 inhibitors (SGLT2i) and glucagon-like peptide-1 receptor agonists (GLP-1 RAs) show promise in improving cardiovascular [33]

outcomes but remain inaccessible or underutilized owing to their cost and limited clinical adoption.

Lifestyle modifications, including smoking cessation and supervised exercise programs, are recommended for risk reduction and symptom management [34]. However, patient noncompliance, socioeconomic barriers, and systemic healthcare disparities limit their effectiveness. Furthermore, these interventions demonstrate variable efficacy across different demographic groups, particularly among women and underserved populations.

1.2.1.2 Surgical and endovascular interventions

Revascularization techniques, including endovascular procedures (angioplasty and stenting) and surgical bypass, are the mainstays of PAD management aimed at restoring blood flow and alleviating ischemic symptoms [35]. However, these interventions are associated with high rates of restenosis, graft failure, and procedural complications, particularly in patients with extensive calcification, multilevel occlusions, or comorbid conditions such as diabetes and chronic kidney disease. Drug-coated technologies and drug-eluting stents (DESs), although promising, exhibit variability in clinical outcomes across patient subgroups and inconsistencies between controlled trials and real-world applications [36].

Surgical bypass, while effective for limb salvage in advanced PAD patients, is invasive and poses substantial perioperative risks, especially in elderly patients or those with complex comorbidities. In addition, anatomical variations, such as infrapopliteal disease and heavily calcified vessels, complicate procedural success, leading to inconsistent therapeutic outcomes [35]. The invasiveness and high cost of these interventions limit their accessibility, particularly in low-resource settings, exacerbating health inequities.

1.2.2 Challenges in PAD visualization

Accurate visualization of the PAD is fundamental for effective diagnosis, risk stratification, and treatment planning [35]. However, conventional imaging modalities face significant challenges due to the complex nature of PAD, its heterogeneous presentation, and anatomical variations among patients. These challenges are further compounded by the limitations of existing technologies in capturing both macrovascular and microvascular changes, leading to suboptimal diagnostic accuracy and therapeutic outcomes. This section examines the key challenges in PAD visualization, highlighting the need for advanced, noninvasive imaging solutions that offer comprehensive, high-resolution, and dynamic assessments.

1.2.2.1 Limitations of conventional imaging modalities

1. Duplex ultrasound (DUS)

Duplex ultrasound is a commonly employed, noninvasive modality that offers real-time imaging and hemodynamic assessments. However, its effectiveness is limited by operator dependency, leading to variability in diagnostic accuracy. In addition, DUS has reduced sensitivity in visualizing distal arterial branches and heavily calcified vessels, which are common in diabetic PAD patients [37]. This limitation is further exacerbated by motion artifacts and suboptimal contrast resolution, impacting the detection of complex lesions or dynamic blood flow changes.

2. Computed Tomography Angiography (CTA) and Magnetic Resonance Angiography (MRA)

CTA and MRA are advanced imaging techniques that provide high-resolution, three-dimensional vascular mapping, enabling detailed assessments of stenosis, plaque morphology, and arterial occlusions [38]. However, CTA is associated with radiation exposure and the risk of contrast-induced nephropathy, limiting its use in patients with chronic kidney disease. MRA, while avoiding ionizing radiation, is cost intensive and contraindicated in patients with implanted devices or severe comorbidities. Both modalities demonstrate limited efficacy in detecting microvascular disease, nonobstructive PAD, or functional perfusion deficits, which are critical for comprehensive PAD assessment.

3. Invasive Angiography

Catheter-based angiography remains the gold standard for detailed vascular imaging and intervention planning. However, it is an invasive procedure associated with risks such as arterial dissection, vascular injury, and contrast-induced nephropathy [39]. Its invasive nature, high cost, and requirement for specialized expertise restrict its widespread application, particularly in low-resource settings. In addition, invasive angiography focuses on macrovascular anatomy and lacks the ability to assess microvascular dysfunction or dynamic blood flow changes [40, 41].

1.2.3 Advanced Imaging Solutions

Recent advancements in imaging technologies have transformed PAD diagnostics by overcoming the limitations of conventional methods [42]. Innovations such as 3D WebGL volume rendering, DICOM visualization, and MPR enable more detailed and accurate

assessments of vascular structures [43]. These advanced imaging methods not only enhance diagnostic precision but also facilitate personalized therapeutic planning and improve patient outcomes. This section explores the latest advancements in imaging technologies, emphasizing the integration of web-based visualization tools, AI, and hybrid imaging modalities.

1.2.3.1 3D WebGL volume rendering and DICOM visualization

1) Real-Time 3D Volume Rendering Using WebGL

3D WebGL volume rendering has revolutionized PAD visualization by enabling real-time, high-fidelity representations of complex vascular structures. This technique uses GPU acceleration for interactive rendering, allowing clinicians to explore volumetric data from multiple angles and depths [44]. By leveraging web-based platforms, 3D WebGL volume rendering facilitates remote diagnostics and collaborative decision-making, bridging geographical disparities in healthcare access. In addition, the integration of level-of-detail (LOD) algorithms optimizes rendering performance, ensuring smooth visualization even on low-bandwidth devices. These advancements enhance diagnostic accuracy, particularly in complex cases involving calcified plaques or multilevel stenoses.

2) DICOM and Multiplanar Reconstruction (MPR) Visualization

DICOM visualization, combined with MPR, provides comprehensive anatomical assessments by reconstructing 2D slices into 3D volumetric representations. MPR allows for interactive exploration of axial, sagittal, and coronal planes, enabling detailed evaluations of lesion morphology and vessel patency [45]. This approach enhances the detection of complex arterial abnormalities, including bifurcations, calcifications, and plaque composition. By integrating the MPR with 3D WebGL rendering, clinicians can achieve precise localization of vascular lesions, improving procedural planning and therapeutic outcomes. These web-based visualization tools also enable seamless integration with cloud platforms, supporting remote consultations and collaborative diagnostics.

1.3 Role of Clouds in Medical Imaging

1.3.1 Cloud technologies in healthcare

Cloud technologies fundamentally transform healthcare by enabling scalable, secure, and efficient solutions for data storage, processing, and collaboration [46]. In the realm of medical imaging, cloud platforms are revolutionizing data management and accessibility, particularly for 3D WebGL volume rendering, DICOM visualization, and MPR. These advanced cloud-

based solutions provide the high-performance computing resources necessary for real-time rendering and remote diagnostics, enabling collaborative decision-making and enhancing diagnostic accuracy in PAD management.

Cloud platforms provide the computational power required for high-fidelity 3D WebGL volume rendering, supporting interactive and real-time visualization of complex vascular structures [47]. By leveraging GPU acceleration through cloud computing, clinicians can explore volumetric data with dynamic lighting and shading effects, enhancing the visualization of calcified plaques and stenoses. This cloud-based architecture eliminates the limitations of local hardware, allowing users to access advanced rendering capabilities on any device with an internet connection.

Cloud technologies enable centralized storage and seamless access to large-scale DICOM datasets, streamlining the workflow for MPR. By utilizing cloud-based DICOM viewers, healthcare providers can navigate axial, sagittal, and coronal planes interactively, facilitating detailed assessments of lesion morphology and vessel patency. This cloud integration enhances collaborative diagnostics by allowing multidisciplinary teams to access and analyze DICOM images simultaneously, regardless of geographic location [48].

The implementation of level-of-detail (LOD) algorithms in cloud-based 3D volume rendering optimizes performance by dynamically adjusting the resolution of volumetric data on the basis of the user's viewpoint and device capabilities. This approach reduces latency and enhances rendering efficiency, ensuring smooth visualization even in low-bandwidth scenarios. The integration of LODs with cloud computing provides a scalable and responsive solution for complex vascular imaging, supporting accurate risk stratification and personalized treatment planning in PAD management.

1.3.2 Cloud-Driven Innovations in Medical Imaging

Cloud-driven innovations have fundamentally transformed medical imaging by addressing critical challenges in data storage, processing, and analysis. By leveraging cloud infrastructure, healthcare institutions can now handle vast volumes of imaging data generated by advanced modalities such as CT, MRI, and PET scans [49]. This capability ensures secure, scalable, and cost-effective storage solutions, eliminating the limitations of on-premises systems.

One of the most significant advancements in cloud-based medical imaging is real-time image processing powered by GPU-accelerated computation. This allows complex tasks such as 3D volume rendering, image segmentation, and reconstruction to be performed rapidly and

accurately, enhancing diagnostic precision and reducing turnaround times. These capabilities are particularly valuable in time-sensitive scenarios, such as emergency care and PAD management, where timely and accurate imaging is critical for clinical decision-making.

Hybrid cloud models have emerged as powerful solutions, combining the security of private clouds with the scalability and computational power of public clouds [50]. This architecture allows sensitive patient data to be stored locally while leveraging cloud-based resources for intensive image processing and analytics. Moreover, hybrid models ensure compliance with healthcare regulations such as the HIPAA and GDPR, [51] maintaining data privacy and security without compromising performance.

Cloud-based medical imaging also supports remote collaboration and telemedicine by enabling radiologists and specialists to access and annotate images from anywhere, breaking geographical barriers and facilitating global consultations. This capability enhances multidisciplinary teamwork, ensuring comprehensive evaluations and personalized treatment planning. Real-time data sharing and annotation tools foster collaborative decision-making, improving diagnostic confidence and accelerating patient care workflows.

Furthermore, cloud-driven platforms integrate seamlessly with electronic health records (EHRs) and picture archiving and communication systems (PACSs) [52], creating unified ecosystems that increase operational efficiency. This interoperability ensures that imaging data are readily available within the broader clinical context, streamlining workflows and reducing diagnostic delays.

In conclusion, cloud-driven innovations in medical imaging are revolutionizing the field by providing scalable, efficient, and secure solutions that enhance diagnostic accuracy, operational efficiency, and patient outcomes. By democratizing access to advanced computational resources and enabling collaborative, data-driven care, cloud technologies are setting new standards in medical imaging, paving the way for next-generation diagnostic and therapeutic paradigms.

1.3.3 Peripheral artery disease (PAD) diagnosis and management

The integration of cloud and web technologies has revolutionized the diagnosis and management of PAD, addressing limitations in traditional diagnostic methods and enhancing patient care [53]. By leveraging advanced imaging platforms powered by cloud infrastructure, healthcare providers can access comprehensive, high-resolution visualizations of vascular structures, enabling early detection and precise risk stratification for PAD patients.

Cloud-based imaging methods, such as CTA, MRA, and Doppler ultrasound, provide centralized storage and real-time processing of complex vascular datasets. These platforms support advanced functionalities such as 3D reconstructions and dynamic perfusion analysis, offering clinicians a holistic view of arterial health. By enabling seamless integration with AI algorithms, these systems automate tasks such as plaque segmentation, stenosis quantification, and calcification analysis, significantly increasing diagnostic accuracy while reducing interobserver variability.

One of the most transformative aspects of cloud-driven PAD diagnostics is real-time collaboration and remote accessibility [54]. Specialists, including vascular surgeons, interventional radiologists, and primary care physicians, can securely access and annotate imaging studies from any location, breaking down geographical barriers and ensuring a coordinated, multidisciplinary approach to PAD management. Telemedicine platforms, integrated with cloud-based imaging tools, further increase accessibility, particularly in underserved or remote regions, enabling timely consultations and second opinions without the need for patient transfers.

Web-based imaging tools are pivotal in democratizing access to advanced diagnostic capabilities. These platforms leverage modern web technologies, including progressive web applications (PWAs), to deliver high-performance imaging experiences directly through standard browsers [55]. This eliminates the need for dedicated hardware or software installations, reducing deployment costs and making sophisticated imaging tools accessible even in resource-constrained settings. Features such as offline functionality, cross-platform compatibility, and cloud synchronization ensure uninterrupted access to imaging data, supporting continuous workflows and enhancing clinical productivity.

The integration of AI-driven analytics in web-based platforms provides automated diagnostic support, including anomaly detection, disease classification, and treatment planning. For example, AI models trained on PAD-specific datasets can identify microvascular abnormalities [56], predict plaque rupture risk, and suggest personalized therapeutic strategies, significantly improving clinical decision-making. In addition, predictive analytics powered by cloud-based AI can predict disease progression, enabling proactive intervention and reducing the incidence of critical limb ischemia or amputation.

Wearable devices integrated with cloud platforms further revolutionize PAD management by enabling continuous monitoring of hemodynamic parameters, including the ankle-brachial

index (ABI), oxygen saturation, and blood flow dynamics [57]. These real-time data streams are analyzed on cloud-based platforms, providing actionable insights into patient status and facilitating early detection of critical events, such as ischemia or thrombosis. This proactive approach ensures timely interventions, reduces hospitalization rates and improves overall patient outcomes.

The scalability and cost-effectiveness of cloud solutions democratize access to cutting-edge PAD diagnostics and management tools, bridging healthcare disparities between urban and rural populations. By eliminating the need for expensive on-premises infrastructure and supporting pay-as-you-go models, cloud technologies enable smaller clinics and resource-limited healthcare settings to access state-of-the-art diagnostic resources [58]. Moreover, hybrid cloud models combine the security of private clouds with the computational power of public clouds, ensuring compliance with healthcare regulations such as the HIPAA and GDPR while maintaining operational efficiency.

Cloud and web technologies are also driving large-scale PAD research and innovation. By aggregating deidentified imaging datasets across multiple institutions, cloud platforms support multi-institutional studies, advancing our understanding of PAD pathophysiology [59], risk factors, and therapeutic outcomes. These platforms facilitate the development of federated learning models, where AI algorithms are trained on diverse, decentralized datasets, enhancing the robustness and generalizability of diagnostic solutions while preserving patient privacy.

In conclusion, cloud and web technologies redefine PAD diagnosis and management by delivering scalable, secure, and efficient solutions that enhance diagnostic accuracy, operational efficiency, and patient outcomes. By enabling advanced imaging analytics, facilitating real-time collaboration, and supporting personalized care pathways, these innovations are setting new standards in vascular health management. The ongoing integration of AI, cloud computing, and web technologies continues to transform PAD care, bridging gaps in accessibility, improving equity in healthcare delivery, and ultimately enhancing the quality of life for PAD patients worldwide.

1.4 Objectives and Scope of the Thesis

1.4.1 Thesis Objectives

The objectives of this PhD thesis are centered on advancing medical imaging analysis, high-fidelity visualization, and noninvasive management solutions for PAD through innovative computational frameworks and cloud-based platforms. By integrating web-based technologies,

optimized volume rendering, and state-of-the-art computational modeling, this research aims to bridge critical gaps in diagnostic precision, clinical workflow efficiency, and personalized treatment strategies for PAD. The specific objectives are as follows:

1) Web-based medical image visualization via PWAs

To evaluate the integration of Digital Imaging and Communications in Medicine (DICOM) and MPR visualization into web platforms via PWAs. This involves: (i) Addressing challenges related to cross-platform compatibility and integration capabilities. (ii) Enabling high-resolution image reconstruction for medical image visualization. (iii) The offline capabilities and enhanced performance features of PWAs can be leveraged to provide seamless medical image access across various devices, thereby enhancing accessibility and usability in clinical environments.

2) High-Fidelity Visualization of Large-Scale CT Datasets

To optimize the visualization pipeline for large-scale peripheral artery CT datasets via the DECODE-3DViz platform, we focus on the following: (i) Efficient WebGL Texture Management: Techniques using a level of detail (LOD) algorithm are developed to render large datasets without performance degradation or errors, overcoming WebGL texture size limitations. (ii) Memory Optimization and Dynamic Downsampling: Implementing memory management techniques to prevent browser memory allocation errors and establishing dynamic downsampling guided by the LOD algorithm to maintain high visual fidelity. (iii) Chunk Streaming and ROI Rendering: Enabling chunk streaming to efficiently manage large datasets while maintaining application responsiveness and facilitating region of interest (ROI) rendering for high-resolution visualization of critical anatomical structures. (iv) Performance and Usability Improvement: Increasing the performance, accuracy, and usability of web-based medical imaging applications to support improved diagnostic outcomes.

3) Automated Risk Classification Framework for PAD

To introduce an automated risk classification framework for PAD by leveraging optimized volume rendering, dynamic illumination, and quantitative vascular analysis. This objective includes the following: (i) Enhancing Diagnostic Precision: Automating plaque density and vascular curvature analysis to improve diagnostic accuracy. (ii) Reducing interobserver variability: Standardizing risk classification to minimize variability in clinical assessments. (iii) Supporting early intervention: Enabling personalized patient management through accurate risk stratification. (iv) Clinical Validation: Demonstrating the clinical effectiveness of the

framework using real patient data to validate its potential for transforming PAD diagnostics and advancing clinical decision-making.

4) Computational Modeling for Drug-Eluting Balloons (DEBs) in PADs

To systematically examine the application of computational modeling techniques to DEBs for PAD treatment. This involves: (i) Evaluating Computational Approaches: Assessing the effectiveness of various modeling techniques, such as fluid–structure interaction (FSI), molecular dynamics (MD), and ML, for optimizing DEB design. (ii) Impact Analysis of Device Performance: Investigating how these computational approaches improve DEB performance and therapeutic efficacy. (iii) Exploring Emerging Trends and Challenges: Identifying emerging trends, challenges, and future directions in DEB research. (iv) Advancing Patient-Specific Modeling: Enhancing patient-specific modeling and *in-silico* simulations to optimize treatment strategies and outcomes for PAD patients.

5) Development of DECODE: An Open-Source Cloud-Based Platform

To present DECODE, an innovative open-source cloud-based platform for the noninvasive management of PAD, with the following objectives: (i) Integrating AI-driven vascular segmentation and computational modeling: Enhancing PAD diagnostics and intervention planning through advanced segmentation modules and real-time 3D visualization. (ii) Enabling Personalized Treatment Strategies: Utilizing finite element modeling (FEM) for personalized simulations of balloon angioplasty and DCB therapy. (iii) Real-Time Visualization and AR Integration: Providing real-time volumetric rendering and augmented reality (AR)-assisted procedural planning through DECODE-3DViz, powered by WebGL/WebXR technologies. (iv) Ensuring scalability and interoperability: Supporting seamless clinical integration with RESTful API compatibility for PACS and EHRs. (v) Advancing Precision Vascular Medicine: Establishing DECODE as a transformative tool in precision vascular medicine by bridging the gap between AI-powered imaging, interactive visualization, and *in-silico* simulations.

1.4.2 Structure of the Thesis

This thesis is organized into seven chapters, systematically addressing the challenges and advancements in medical imaging visualization, risk classification, and noninvasive management strategies for PAD. This research integrates state-of-the-art web technologies, high-fidelity visualization techniques, and advanced computational modeling to bridge

significant gaps in diagnostic precision, clinical workflow efficiency, and personalized treatment strategies for PAD.

Chapter 1: Introduction

The first chapter establishes the foundational context of the thesis by presenting an exploration of PAD, focusing on its epidemiology, pathophysiology, and clinical implications. This chapter provides a comprehensive overview of conventional diagnostic tools and the limitations associated with existing PAD treatment and visualization approaches. This chapter emphasizes the necessity for advanced imaging solutions and introduces the role of cloud-based and web technologies in enhancing medical imaging functionalities. It concludes by defining the research objectives and the scope of the thesis.

Chapter 2: State of the Art

This chapter offers a critical review of the literature and state-of-the-art technologies relevant to PAD management and medical imaging. It explores technical advancements, including digital health technologies, web-based visualization tools, and cloud-based platforms. The chapter also investigates clinical innovations in PAD care, emphasizing evolving diagnostic practices and patient-centric visualization approaches. It examines emerging trends and future directions in comprehensive visualization platforms, establishing a strong theoretical foundation for the methodologies and innovations proposed in this thesis. It concludes by defining the key contributions.

Chapter 3: Computational Modeling of Drug-Eluting Balloons

Chapter 3 provides an examination of computational modeling techniques applied to DEBs for PAD treatment. It systematically analyzes a wide range of computational methods, including MD, finite element analysis (FEA), computational fluid dynamics (CFD), and ML. This chapter evaluates their contributions to optimizing DEB design, enhancing drug release accuracy, and improving patient-specific therapeutic outcomes. It contextualizes computational modeling within clinical translation and identifies challenges, limitations, and future research directions, thus highlighting the importance of advanced modeling techniques in precision vascular medicine.

Chapter 4: Advancing Progressive Web Applications for Medical Imaging Visualization

This chapter explores the integration of DICOM and MPR visualization into web environments via PWAs. It presents the technical framework and architectural design, introducing novel MPR

algorithms employing bicubic and weighted bilinear interpolation to enhance image reconstruction quality. The chapter details the implementation process, experimental findings, and performance analysis across multiple platforms. This demonstrates the effectiveness of the proposed solutions in achieving cross-platform compatibility, offline access, and high-resolution medical imaging visualization, thus contributing to enhanced diagnostic capabilities.

Chapter 5: DECODE-3DViz: High-Fidelity Web-Based Visualization and Automated Risk Classification for Peripheral Artery Disease

Chapter 5 presents DECODE-3DViz, an innovative WebGL-based high-fidelity visualization pipeline designed for large-scale peripheral artery CT datasets, and integrates an automated risk classification framework for PAD. The combined approach leverages optimized volume rendering, dynamic illumination, and quantitative vascular analysis to increase diagnostic accuracy and clinical decision support.

The chapter details the system design and implementation of DECODE-3DViz, focusing on the integration of level-of-detail (LOD) algorithms and data chunk streaming to optimize rendering performance. It presents a comprehensive validation and performance evaluation through analytical and clinical assessments, demonstrating significant improvements in rendering time, GPU memory efficiency, and diagnostic precision. Building on the visualization capabilities of DECODE-3DViz, this chapter introduces the automated risk classification framework, which utilizes advanced algorithms for real-time plaque density and vascular curvature assessments. By validating the system via real clinical data, this chapter confirms its potential to transform PAD diagnostics and highlights its contributions to personalized patient management and noninvasive risk assessment.

This integrated presentation of DECODE-3DViz and the automated risk classification framework not only establishes a high-fidelity visualization pipeline but also introduces a transformative approach to risk classification, setting a new standard for web-based medical imaging and precision vascular medicine.

Chapter 6: DECODE: An Open-Source Cloud-Based Platform for Noninvasive Peripheral Artery Disease Management

This chapter presents the development and validation of DECODE, an open-source, cloud-based platform designed for the noninvasive management of PAD by integrating AI-driven vascular segmentation, computational hemodynamic modeling, and real-time 3D visualization. The platform leverages deep learning (DL) algorithms for high-precision peripheral artery

segmentation, intima–media thickness (IMT) analysis, and automated plaque characterization, enhancing diagnostic accuracy and risk stratification. Additionally, finite element modeling (FEM) enables personalized vascular simulations for optimized treatment planning, particularly in balloon angioplasty and drug-coated balloon (DCB) therapy. Built on a cloud-native microservice architecture, DECODE ensures scalability, real-time accessibility, and multi-institutional collaboration. System usability evaluations, including system usability scale (SUS) and technology acceptance model (TAM) metrics, confirm high adoption potential, with an SUS score of 87.5 and TAM acceptance rating of 4.21, demonstrating its clinical viability. By bridging AI-driven vascular imaging, real-time 3D visualization, and predictive computational modeling, including *in-silico* simulations for treatment optimization, DECODE establishes a scalable framework for precision vascular medicine and digital PAD diagnostics.

Chapter 7: Conclusions and Future Work

The final chapter presents the conclusions and future directions in cloud-based medical imaging and computational vascular modeling, emphasizing their role in advancing noninvasive PAD diagnostics and treatment planning. This research introduces a web-based DICOM and MPR system that integrates AI-driven vascular segmentation, real-time 3D visualization, and predictive modeling within a scalable cloud-native framework. Future research will focus on enhancing WebGPU-based rendering for high-performance visualization; integrating AI-powered multimodal fusion for CT, MRI, and ultrasound data; and developing federated AI models for privacy-preserving learning. In addition, advancements in cloud-edge AI optimization, *in-silico* simulations for DCB therapy, automated NLP-driven report generation, and blockchain-based regulatory compliance mechanisms will further establish DECODE as a pioneering AI-driven platform for precision vascular medicine.

Chapter 2: Literature Review

- 2.1. Evolution of Web-Based Medical Visualization Platforms
 - 2.2. Technical advantages: Accessibility, real-time data, and multiuser collaboration
 - 2.3. Advancements in 3D medical imaging
 - 2.4. Advancements in Web-Based DICOM Viewers
 - 2.5. WebGL-based medical imaging
 - 2.6. Advancements in 3D WebGL volume rendering
 - 2.7. Cloud-Based Solutions for PAD Management
 - 2.8. Cloud Computing and AI in Medical Imaging
 - 2.9. Cloud-based multidisciplinary platforms
 - 2.10. Contribution of this Thesis
-

2.1 Evolution of Web-Based Medical Visualization Platforms

The evolution of web-based medical visualization platforms has been one of the most transformative developments in the management of complex health conditions such as PAD [60]. Driven by the increasing volume and complexity of clinical data, particularly from diagnostic imaging, interventional studies, and procedural datasets, these platforms have drastically changed how clinicians, researchers, and patients interact with medical information. Historically, medical visualization tools have been constrained by local software installations that limit accessibility and real-time collaboration, creating significant barriers to efficient care and communication.

The shift from desktop-based systems to cloud-based, web-enabled platforms marks a pivotal evolution in medical visualization [61]. Early tools such as 3D Slicer [62] and Medical Imaging Interaction Toolkit (MITK) [63], which are powerful for image analysis, required significant hardware and were isolated within specific research facilities. They were restricted to environments that lacked flexibility, collaboration potential, and scalability. However, the integration of cloud computing and web technologies has overcome these challenges, enabling remote access and centralized data storage, thus allowing a more seamless integration of imaging, clinical, and patient information.

In the realm of PAD, the transition to web-based visualization has mirrored this broader trend. Initially, PAD imaging relied primarily on 2D static images. As technology has advanced, so has the sophistication of visualization tools, evolving into 3D interactive models capable of rendering complex vascular geometries derived from coronary and peripheral angiograms [64]. These web-based platforms not only visualize anatomical structures but also support dynamic simulations, providing clinicians with an integrated view of patient-specific vascular health. The progression from basic image viewing to full 3D modeling represents a profound leap forward in diagnostic capabilities and treatment planning.

One key development in these platforms is the integration of geographic information systems (GISs) and building information modeling (BIM), which parallels advancements in medical visualization [65]. This shift has been mirrored in medical visualization, where detailed structural information, such as vascular life cycles, device performance, and procedural outcomes, can now be integrated into dynamic 3D models. This transformation has enabled a deeper understanding of vascular geometries and how procedural changes impact disease progression in conditions such as PAD [66].

With the integration of real-time data visualization, these platforms have revolutionized how clinicians interact with both historical data and real-time updates. For example, in cardiac rehabilitation programs (CRPs) for PAD patients, web-based platforms track exercise performance, angiographic imaging, and vascular data in an integrated manner [67]. They allow dynamic overlays of real-time data with historical trends, offering a comprehensive, patient-specific view of progress, which is essential for both diagnostics and treatment planning. These platforms allow for the visualization of vascular improvements following therapeutic interventions or exercise regimens, underscoring their crucial role in PAD management.

Another significant innovation in this space is the integration of wearable devices, EHRs, and clinical imaging. Web-based platforms now incorporate data interoperability, enabling seamless integration of patient information from diverse sources [68]. This evolution reflects a shift toward more proactive care for PAD, moving away from reactive methods and emphasizing prevention and long-term management. This is exemplified in PAD risk assessment tools that combine clinical, diagnostic, and patient-reported data into unified, actionable visualizations.

In terms of computational power, the leap from desktop-based systems to cloud-enabled platforms has been fundamental. Tools such as WebGL and WebRTC have made it possible to visualize and render complex 3D medical images in real time without relying on local installations [69]. These technologies have allowed for cross-platform functionality, eliminating the barriers imposed by hardware limitations. For example, volume rendering, MPR, and segmentation are now seamlessly integrated into web-based systems that provide diagnostic capabilities previously restricted to powerful desktop systems. This has been particularly beneficial for preoperative planning and intervention simulation, where real-time data and detailed anatomical modeling are critical for successful outcomes.

The inclusion of EHRs and automated prognostic tools within medical visualization platforms is another critical advancement. Traditional visualization tools operate in isolated environments and require manual data entry and retrospective analysis. Today, platforms that integrate with EHR systems not only visualize patient-specific anatomical data but also incorporate real-time prognostic information [70]. This allows clinicians to receive automated risk calculations, helping them make better-informed decisions at the point of care. Platforms now support continuous, automated updates, refining patient management strategies over time on the basis of integrated, up-to-date data streams.

In PAD management, this evolution has enhanced clinical decision-making by incorporating advanced computational techniques, such as phenotyping algorithms and community-level datasets. These allow for real-time visualization of prognostic information that is directly integrated into patient records. For example, automated survival prediction tools for PAD are now embedded within these platforms, providing a more sophisticated understanding of disease progression and guiding therapeutic decisions [71].

A particularly notable development is the rise of low-code/no-code platforms such as CdB (Cinco de Bio) [72], which democratize access to powerful computational tools. Historically, medical imaging and visualization required deep technical expertise, which limited accessibility

to only a small pool of professionals. Platforms such as CdB, which offer modular, service-oriented architectures (SOAs) and domain-specific languages (DSLs) for biomedical research, empower a broader group of users, including researchers, clinicians, and even nontechnical professionals, to design and execute imaging workflows without needing specialized coding knowledge. This shift toward user-centered design is pivotal in fostering collaboration across disciplines, particularly in complex areas such as PAD research.

The integration of AI and ML into medical visualization platforms has further propelled their evolution. AI-driven tools such as natural language processing (NLP) and ML algorithms now assist in interpreting complex datasets, including vascular imaging and patient histories. For example, platforms equipped with CNNs (convolutional neural networks) can classify stenosis and localize vascular abnormalities with precision comparable to that of radiologists [73]. The incorporation of real-time Doppler waveform analysis into visualization tools offers further insight into vascular health, enabling early detection and predictive modeling of disease progression.

The integration of biomimetic intelligence (BI) has also significantly enhanced the dynamic nature of medical visualization platforms [60]. Platforms that combine real-time data analytics with predictive modeling can now simulate the impact of various interventions on PAD patients. By incorporating 3D simulations and interactive data visualizations, these tools allow for more personalized treatment planning, considering factors such as vascular geometry, patient-specific health metrics, and genetic predispositions.

Finally, the evolution of educational technologies in medical visualization has been equally transformative. Traditionally, medical education relies on static resources such as textbooks and printed materials. However, the integration of interactive learning modules, virtual reality (VR) simulations, and AR tools has revolutionized how students and clinicians engage with complex medical data [74]. Web-based platforms that allow the simulation of vascular conditions and treatment outcomes exemplify how digital tools have shifted toward more interactive, immersive, and user-centric learning experiences.

2.2 Technical advantages: Accessibility, real-time data, and multi-user collaboration

Web-based visualization platforms have revolutionized the management of complex conditions such as PAD by offering unique technical advantages, particularly in terms of accessibility, real-time data integration, and multiuser collaboration [75]. These platforms not only streamline the management of PAD but also foster a more collaborative and efficient healthcare

environment. By democratizing access to diagnostic and therapeutic tools, they enable clinicians, researchers, and patients to engage with critical data and contribute to decision-making processes, regardless of their location or technical expertise.

a) Accessibility

One of the most significant advantages of web-based platforms is their unparalleled accessibility, particularly in managing conditions such as PAD [76]. Traditional medical imaging and visualization tools often require specialized hardware and installations, which limits their reach. In contrast, web-based platforms eliminate these barriers, enabling access through simple browser interfaces and making advanced tools available to healthcare providers and researchers worldwide. This democratization of access is particularly crucial for underserved regions where access to specialized care is limited. For example, web-based systems that visualize ABI measurements or walking performance metrics empower both patients and clinicians to track PAD progress remotely, adjusting treatment plans as needed [77]. This approach is transformative for PAD patients, who often need continuous monitoring and support between clinical visits.

The cloud-based architecture of these platforms ensures that medical imaging, procedural data, and patient information are centralized, providing consistent access across multiple institutions [78]. This universal accessibility means that researchers and clinicians—regardless of geographical constraints—can collaborate and make informed decisions on the basis of real-time patient data. Platforms such as trackPAD [79] offer accessible mobile apps that help PAD patients engage with supervised exercise therapy (SET) remotely, ensuring that they continue to adhere to recommended treatment regimens without needing to be physically present in clinics. This type of remote access enhances patient participation and promotes better health outcomes, particularly in resource-limited settings.

b) Real-Time Data

Another cornerstone of web-based platforms is their real-time data integration capability. In the management of PAD, timely access to accurate data can significantly influence clinical decisions and improve patient outcomes [35]. These platforms integrate data from diverse sources, such as clinical imaging, wearable devices, and patient-reported outcomes, providing clinicians with a comprehensive, up-to-date view of a patient's health status. The ability to visualize real-time metrics such as vascular responses, pain thresholds, and heart rate during supervised exercise therapy enhances treatment personalization and allows clinicians to adjust

protocols as needed to optimize results. In PAD rehabilitation programs, for example, clinicians can adjust therapy on the basis of real-time feedback on walking performance or vascular health, ensuring that patients receive the most appropriate interventions [35].

Moreover, real-time data also allow for dynamic procedural planning. Platforms that incorporate real-time hemodynamic data, such as blood flow or device performance metrics, provide immediate insights into the effectiveness of interventions such as drug-eluting stents [80-82]. For example, in the case of PAD, real-time updates from procedural systems allow for immediate adjustments to the intervention plan, facilitating more accurate decision-making and improving outcomes. By incorporating predictive analytics and automated risk stratification tools, these platforms enable clinicians to predict disease progression, predict complications such as critical limb ischemia, and adapt treatment strategies accordingly. This real-time capability fosters proactive management of PAD, allowing clinicians to intervene earlier, potentially preventing more severe complications.

c) Multiuser Collaboration

Web-based visualization platforms inherently support multiuser collaboration, which is essential in managing complex diseases such as PAD. Given the multidisciplinary nature of PAD care—requiring input from vascular surgeons, cardiologists, rehabilitation specialists, and data scientists—collaborative features are crucial for optimizing patient outcomes [83, 84]. Web-based platforms facilitate the simultaneous interaction of multiple users across different specialties, allowing them to access, analyze, and annotate patient data in real time. This shared access fosters collaborative decision-making, ensuring that all stakeholders are on the same page when developing and adjusting treatment plans.

In clinical settings, such as during interventions involving drug-eluting stents, the ability to share angiographic findings and perform quantitative analyses across multidisciplinary teams allows for dynamic treatment planning. In PAD, this could mean that interventional radiologists can work closely with surgeons and rehabilitation specialists, all accessing the same visualization of a patient's vascular structure and procedural data [85]. Through web-based systems, shared dashboards allow real-time discussion and modification of treatment strategies, making it easier to align treatment goals and decisions across specialties. This collaborative environment is vital for holistic care—ensuring that PAD treatment is comprehensive and tailored to the individual patient.

2.3 Advancements in 3D medical imaging

In medical imaging diagnosis, the importance of three-dimensional (3D) visualization is paramount, as it enhances the ability to display volumetric organs on screens, allowing observation from various perspectives [86]. This capability facilitates diagnostic assistance, comprehensive analysis, decision support, and educational purposes. One of the most widely used 3D medical image visualization techniques in clinical practice is MPR, which reconstructs 3D representations from multiple two-dimensional (2D) images obtained from modalities such as computed tomography (CT) or magnetic resonance imaging (MRI) [87]. MPR methods enhance both visual and diagnostic capacities, contributing significantly to the accuracy and efficiency of clinical workflows.

Currently, clinical environments benefit from a variety of advanced medical imaging processing tools, including high-performance desktop applications and workstations designed to handle complex computations. In parallel, there is a growing trend toward cloud-based medical imaging applications and repositories, which offer cost-effective, scalable, and flexible alternatives for biomedical research [88, 89]. These cloud solutions enable the storage and retrieval of medical images as cloud resources, paving the way for enhanced collaboration among healthcare professionals.

To address evolving clinical needs, researchers have developed open-source web-based DICOM viewers equipped with both basic and advanced features [90]. These viewers are applicable not only in general diagnostic settings but also in telemedicine and clinical research platforms. Integrating web-based DICOM viewers within a PACS offers a strategic advantage by simplifying image access and interaction with remote data sources without requiring application downloads. This integration enhances practicality and accessibility, fostering seamless collaboration among radiologists and researchers.

The advancement of internet technologies has significantly contributed to the development of web-based applications that rival traditional desktop and workstation solutions [91]. These versatile web applications have permeated diverse sectors, including healthcare and driving radiologists, to engage in the design of specialized web applications for radiological use.

A critical gap remains in the domain of DICOM visualization on the web, particularly concerning the adoption of PWAs. This thesis addresses this gap by exploring the integration of DICOM visualization into web environments via PWAs, which offer unique attributes such as offline accessibility, enhanced performance, and an improved user experience [92]. By

leveraging these features, this study aims to overcome current technological challenges, contributing to the advancement of web-based medical imaging applications and ultimately benefiting radiologists and the broader healthcare community.

In addition to these challenges, the development of medical imaging applications must address critical aspects of web applications, including cross-platform compatibility, integration capabilities, speed, scalability, and overall performance. An effective approach to these factors is essential for enhancing the functionality and efficiency of medical imaging applications in today's digital landscape.

A particular challenge relevant to MPR for medical image visualization lies in producing high-resolution images on the web, especially when visualizing volumetric structures such as sagittal and coronal views derived from DICOM slices [93]. This complexity necessitates a detailed examination, and this study seeks to elucidate and overcome these challenges, ultimately driving forward the capabilities of web-based medical imaging systems.

2.4 Advancements in Web-Based DICOM Viewers

Web-based DICOM viewers have emerged as pivotal tools in modern medical imaging, offering advanced functionalities that enhance diagnostic workflows and clinical collaboration. Researchers have explored various technologies and approaches to overcome traditional limitations, leading to significant advancements in this domain. Min *et al.* [94] investigated the potential of HTML5 and WebGL to address challenges in web-based medical imaging. Their study focused on developing a comprehensive application that enables remote access for radiologists, demonstrated through a CT colonography prototype. The evaluation across different browsers and operating systems confirms that HTML5 and WebGL are well suited for real-time 2D and 3D imaging, ensuring platform independence and improved accessibility. However, minor browser compatibility issues were noted, highlighting areas for further improvement. Despite these limitations, the study concludes that HTML5 and WebGL provide promising foundations for remote medical imaging applications.

Similarly, Hazarika *et al.* [95, 96] introduced an innovative approach by developing DICOM-based medical image repositories via DSpace. This solution is designed to increase visibility and reduce storage costs for medical professionals. By integrating DICOM standards with DSpace through JavaScript, the system achieves efficient image accommodation and retrieval, which is supported by a robust indexing mechanism. Although they are effective for smaller datasets, scalability challenges are observed when datasets exceed 5000 images. This work

demonstrates the feasibility of a cost-effective web platform for DICOM users, paving the way for scalable solutions in future developments. Wadali *et al.* [97] focused on evaluating free, open-source, web-based DICOM viewers for integration with eSanjeevani, the Indian National Telemedicine Service. Conducted by the Health Informatics & Electronics Division in Mohali, India, this study assesses six viewers, ultimately recommending the DICOM Web Viewer (DWV) for its comprehensive features and compatibility. Although the research identifies the strengths and weaknesses of each viewer, no single solution fully satisfies all the requirements, highlighting the need for customized solutions tailored to specific clinical workflows.

In the realm of specialized imaging applications, Gorman *et al.* [98] introduced Slim, an open-source, web-based, DICOM-compliant slide microscopy viewer developed for the NCI Imaging Data Commons. Slim facilitates interactive visualization of diverse microscopy images while adhering to FAIR principles, supporting advanced imaging data science. This approach shows practical utility in standardized image annotations for ML applications. However, challenges in standardization, interoperability, and data format consistency underscore the need for further advancements in cross-platform integration.

Another influential contribution was made by Ziegler *et al.* [99], who presented the OHIF Viewer, a flexible, web-based medical image viewer widely adopted in cancer research. The OHIF Viewer supports both basic and advanced imaging functionalities, seamlessly integrating into clinical research platforms. Its highly customizable framework reduces software development redundancy, streamlining research workflows. Nevertheless, deployment challenges for nontechnical users and the need for improved community documentation remain areas for enhancement. Chen *et al.* [100] contributed to the field with the development of BlueLight, an open-source DICOM viewer built on low-cost computation algorithms via JavaScript. Designed for stability and speed, particularly on mobile devices, BlueLight supports both 2D and 3D imaging, leveraging CSS transformations and DICOMweb connectivity. Although it demonstrates efficient rendering for 3D medical images, the study suggests potential improvements in rendering performance, particularly for mobile applications.

Exploring novel approaches in medical image reconstruction, Ghoshal *et al.* [101] proposed a 3D spine MRI reconstruction algorithm using bicubic and bilinear interpolation from a single sequence of 2D slices. This method achieves high accuracy in reconstructing 3D images while reducing MRI scan times and associated costs. However, the study has several limitations, such as the absence of direct comparisons and performance variability across different datasets,

indicating the need for further clinical validation. Finally, Fajar *et al.* [102] presented an innovative algorithm for reconstructing and resizing 3D images from DICOM files, effectively addressing metadata variations. The method uses histogram equalization and trilinear interpolation to manage large 3D image data sizes, supporting ML applications in 3D image generation. This approach enhances the efficiency of 3D image processing, contributing significantly to the field of medical image analysis.

Collectively, these advancements illustrate the transformative potential of HTML5, WebGL, and PWAs in overcoming traditional limitations associated with web-based DICOM viewers. Table 2.1 provides a comparative overview of these innovations, highlighting their key contributions and limitations. By addressing existing challenges and leveraging emerging technologies, these studies have contributed to the continuous evolution of web-based medical imaging applications. This progression not only advances diagnostic precision but also enhances clinical workflows, paving the way for more accessible and efficient medical imaging solutions.

Table 2.1 Comparison of Advancements in Web-Based DICOM Viewers.

Refs.	Technology/Approach	Key Features	Limitations
[94]	HTML5 and WebGL for Remote Imaging	Supports real-time 2D/3D imaging, platform-independent	Minor browser compatibility issues
[95]	DICOM Repositories via DSpace	Increases visibility, reduces storage costs, robust indexing	Scalability challenges with datasets >5000 images
[97]	Evaluation of Free Web-Based Viewers	Recommends DICOM Web Viewer (DWV) for telemedicine	No single viewer fully meets clinical needs
[98]	DICOM-Compliant Microscopy Viewer	Supports microscopy images, adheres to FAIR principles	Challenges in standardization and interoperability
[99]	Customizable Web-Based Medical Image Viewer	Highly customizable, widely used in cancer research	Deployment challenges for nontechnical users
[100]	JavaScript-Based Low-Cost DICOM Viewer	Optimized for mobile devices, CSS-based transformations	Performance limitations in mobile 3D rendering
[101]	3D Spine MRI Reconstruction	Bicubic and bilinear interpolation for 3D MRI reconstruction	Performance variability, lacks direct comparisons
[102]	3D Image Reconstruction and Resizing	Histogram equalization and trilinear interpolation for large datasets	Metadata variations, requires further validation

2.5 WebGL-based medical imaging

The rapid evolution of medical imaging technologies has led to the development of powerful tools for visualizing complex volumetric data, particularly from CT and MRI. Among these tools, 3D WebGL volume rendering has emerged as a prominent technique, leveraging WebGL—a JavaScript API for interactive 3D graphics within web browsers [103]—to enable real-time visualization of detailed medical images. The accessibility and cross-platform compatibility of WebGL eliminate the need for additional plugins, increasing usability for medical professionals [43]. Despite its potential, several challenges hinder its effectiveness when it is applied to large-scale medical datasets.

a) WebGL Texture Size Constraints

One of the primary challenges is the limitation on texture size in WebGL, which can restrict the direct uploading and rendering of extensive medical datasets [104]. These constraints often lead to performance degradation and visualization errors. Efficient dataset segmentation and handling techniques are essential for maintaining high visualization quality while ensuring smooth rendering.

b) Browser Memory Allocation Issues

High-resolution medical imaging data demand substantial memory resources. When memory allocation exceeds the browser's limits, it results in incomplete rendering and potential loss of diagnostic information [105]. The development of optimized memory management strategies is crucial for handling large datasets efficiently within the browser environment.

c) Impact of Large Datasets on Browser Performance

Rendering large CT imaging datasets can overwhelm browser memory and WebGL capabilities, leading to crashes or unresponsiveness [106]. This significantly impacts usability and performance. The implementation of techniques such as progressive rendering and LOD can help maintain application performance while providing high-quality visualizations.

d) Data downsampling and its drawbacks

To conform to WebGL texture size limits, datasets are often downsampled, which reduces the resolution and compromises essential diagnostic details. This poses a challenge in maintaining visualization quality. Implementing adaptive downsampling methods that preserve critical details while enhancing performance is crucial for effective diagnostic imaging [107].

e) High-resolution rendering in specific regions

Detailed analysis in medical imaging often requires a focus on specific regions of interest (ROIs). Downsampled datasets may not provide sufficient resolution in these areas. Adaptive rendering techniques that allow for high-resolution visualization in selected regions can enhance diagnostic accuracy and clinical decision-making [108].

These challenges underscore the necessity for innovative solutions to optimize the visualization pipeline in WebGL-based medical imaging. This thesis aims to address these limitations by developing advanced rendering techniques that maintain performance, accuracy, and usability, ultimately enhancing diagnostic workflows and improving patient outcomes.

2.6 Advancements in 3D WebGL volume rendering

Advancements in 3D WebGL volume rendering have been motivated primarily by the need to address the complex challenges associated with visualizing large-scale medical datasets. This section systematically examines the key contributions of contemporary research, emphasizing innovative methodologies, their advantages, and the limitations they aim to overcome. Understanding these developments provides a contextual framework for the evolution of WebGL-based medical imaging solutions while identifying potential pathways for further advancements.

The advancement toward effective WebGL volume rendering commenced with foundational studies that sought to resolve the inherent challenges of multidimensional data visualization. Zhang *et al.* [109] made significant strides with SAMP-Viz, a tool that synergizes subspace clustering with RadViz to increase the interpretability of complex datasets. This tool facilitates the dynamic exploration of multidimensional data, which is particularly valuable in medical imaging, where temporal changes in volumetric data are crucial for accurate diagnosis. By employing a technology stack comprising C++, OpenGL, QT, and CUDA, SAMP-Viz shows potential for high-performance medical data visualization. Nevertheless, the study revealed limitations in managing time-varying data, thus highlighting the necessity for more adaptable visualization frameworks.

Building on this foundational work, Zhang [110, 111] further advanced the field through two pivotal projects. The first project utilized server-side scripting with PHP and MySQL to enable real-time visualization, interactive analysis, and secure data management. While comprehensive in scope, this approach was constrained by WebGL2's data storage limitations, affecting its scalability for extensive medical datasets. The second project innovatively leverages JavaScript

(Node.js) for web-based rendering, incorporating enhanced interpolation techniques to address missing voxels. In addition, the integration of WebCL facilitated high-performance parallel computing, thereby overcoming earlier performance bottlenecks. These contributions not only demonstrated the evolving capabilities of WebGL for medical imaging but also underscored the pressing need for robust data storage solutions to accommodate the growing complexity of medical datasets.

With the increasing demand for efficient web-based medical image rendering, researchers have explored diverse strategies to increase performance and usability. Lajara *et al.* [112] significantly contributed to this domain by focusing on the web-based visualization of whole slide images conforming to DICOM standards. Their novel approach involved preconstructing the pyramidal structure within the middleware layer rather than on the web platform. This architectural enhancement led to more efficient frame transmission, thus optimizing the rendering speed and ensuring consistent medical image visualization. This strategic innovation emphasized the critical role of middleware architecture in achieving scalable and high-performance medical imaging solutions.

In continuation of this trend, Visutsak *et al.* [113] employed marching cubes with histogram pyramids for 3D medical volumetric rendering, aiming to increase feature extraction precision. Despite methodological advancements, challenges related to surface roughness due to unused voxels persist. This limitation underscores the necessity for advanced algorithms capable of refining voxel utilization, ultimately enhancing visualization quality. The study highlighted the critical importance of accurate voxel processing in optimizing medical image rendering.

Rendering high-quality medical images within the constraints of browser memory remains a significant challenge in WebGL volume rendering. In response, Xu *et al.* [114] introduced cinematic volume rendering (CVR) via JavaScript, which aims to achieve high-fidelity in-browser rendering of medical images. Although CVR presented a groundbreaking approach, it encountered memory limitations that hindered its practical deployment, especially in rendering complex volumetric datasets. This highlighted an ongoing challenge within the field, necessitating the development of more sophisticated memory management strategies to fully exploit the potential of cinematic rendering in web applications.

To address these challenges, Li *et al.* [104] introduced a real-time online medical image rendering and 3D visualization framework using WebGL and HTML5. Their focus was on designing advanced interpolation techniques to manage missing voxels effectively, which

significantly improved image quality and rendering accuracy. By addressing voxel interpolation challenges, this study contributes to smoother real-time rendering, paving the way for more interactive and responsive medical imaging applications.

To enhance the user experience and optimize rendering performance, researchers have explored advanced resolution techniques and dynamic interaction mechanisms. Boutsis *et al.* [115] developed a multiresolution rendering technique utilizing JavaScript, HTML, CSS, PHP, and AJAX, integrated with Nexus.js for real-time parameter adjustments and Draco compression for efficient mesh data optimization. This technique enables real-time manipulation of 3D models, optimizing rendering times for even the most complex medical datasets. The study illustrated the substantial potential of multiresolution rendering to deliver interactive, high-fidelity medical imaging experiences on the web.

To further enhance interactive visualization, Zhu *et al.* [116] introduced an adaptive resolution enhancement method that leverages spatial interpolation and eye tracking. This technique dynamically adjusts the resolution on the basis of the user focus, thereby optimizing the rendering efficiency and improving the accuracy of medical image analysis. This study demonstrated the ability of adaptive resolution techniques to maximize diagnostic precision by strategically concentrating rendering power on regions of interest. Kumar *et al.* [117] extended this trajectory by introducing RadVolViz, a multivariate volume visualization tool utilizing the RadViz and HSL colormaps, implemented through WebGL, JavaScript, and ThreeJs. This tool enhances visual differentiation for correlated channels and optimizes the manual brushing interface, providing an intuitive and detailed visualization experience. By employing RadViz, the tool facilitated enhanced discrimination of complex anatomical structures, thereby supporting more informed diagnostic decision-making processes.

The cumulative innovations presented in these studies underscore the transformative potential of 3D WebGL volume rendering in addressing longstanding challenges in web-based medical imaging. Through the strategic utilization of HTML5, WebGL, and PWAs, these advancements have significantly enhanced the accessibility, accuracy, and interactivity of medical imaging solutions. Table 2.2 provides a comparative overview of these approaches, highlighting their key contributions and limitations in optimizing memory management, real-time rendering, and resolution adaptability.

Building on these foundational advancements, this thesis aims to address ongoing challenges, including WebGL texture size constraints, browser memory allocation issues, and resolution

degradation due to downsampling. By integrating adaptive rendering techniques, progressive loading strategies, and region-specific high-resolution rendering, this chapter aims to improve the performance, accuracy, and usability of web-based applications for visualizing large-scale medical datasets, particularly in peripheral artery CT imaging.

Table 2.2 Comparison of advancements in 3D WebGL volume rendering for medical imaging.

Refs.	Rendering Approach	Key Features	Limitations
[109]	PHP and MySQL for Real-Time Visualization	Enables interactive analysis and secure data management	Limited scalability due to WebGL2 storage constraints
[112]	Pyramidal Structure Middleware	Optimizes rendering speed using middleware	Requires middleware-based optimizations
[113]	Marching Cubes with Histogram Pyramids	Improves feature extraction for 3D volumetric data	Surface roughness due to unused voxels
[114]	Cinematic Volume Rendering (CVR)	Achieves high-fidelity in-browser rendering	Memory limitations restrict deployment
[104]	WebGL and HTML5 for Real-Time Rendering	Advanced interpolation for missing voxels	Voxel interpolation challenges remain
[115]	Multiresolution Rendering with Nexus.js	Real-time model manipulation with mesh compression	Processing-intensive, dependent on Nexus.js
[116]	Adaptive Resolution with Eye Tracking	Dynamic resolution adjustment for focused regions	High computational cost for eye tracking
[117]	RadViz and HSL Colormap-based Visualization	Improves visualization of correlated anatomical structures	Manual brushing interface requires refinement

2.7 Cloud-Based Solutions for PAD Management

The integration of cloud-based platforms in PAD management has demonstrated significant potential in enhancing patient outcomes and accessibility to therapeutic interventions. TrackPAD, introduced by Paldán *et al.* [118], supports supervised exercise therapy (SET) for PAD patients, resulting in improvements in walking distance and quality of life. Despite its effectiveness, the platform relies on manual input and lacks AI-driven automation, limiting its scalability and adaptability. In a similar vein, Paredes *et al.* [119] developed a mobile application for home-based exercise therapy that incorporates GPS tracking and pain assessment. However, patient adherence has remained low, and the absence of AI-driven adjustments has hindered its potential for personalized care.

To further advance digital health interventions, Kim *et al.* [120] introduced the HOBBIT-PAD, an mHealth platform integrated with wearable devices to support exercise interventions for

PAD patients. Positive usability feedback was received, but limitations included restricted compatibility (available only on Android), a small sample size for validation, and a lack of AI-based personalization for real-time adaptation. In a broader review, Wu *et al.* [121] analyzed the effectiveness of SET for PAD patients with IC, confirming its benefits but highlighting low enrollment rates. They emphasized the need for enhanced digital-assisted therapies and AI-driven supervision to improve long-term adherence.

Reinforcing these findings, Khoury *et al.* [79] investigated SET as a primary intervention for PAD, noting that only 2% of eligible patients participated because of limited awareness and accessibility. They suggested that hybrid digital health solutions could improve SET adoption; however, existing platforms lack real-time AI monitoring, automated adjustments, and predictive analytics. Collectively, these studies underscore the necessity for AI-integrated cloud-based platforms to enhance patient engagement, personalized interventions, and long-term adherence in PAD management.

In the context of PAD, digital health applications have shown varying degrees of success. Shalan *et al.* [122] introduced YORwalk, an application designed to promote exercise and track walking ability in PAD patients. Although the concept is promising, its effectiveness requires further validation through patient feedback and clinical trials. Harzand *et al.* [123] conducted a Smart Step trial for a smartphone-enabled exercise program but encountered challenges in terms of participant engagement and adherence, particularly in low-resource settings. Addressing these challenges, Lortz *et al.* [124] emphasized the need for improved disease literacy and SET support in mobile interventions, although their study was limited by a small sample size and limited generalizability.

In addition to advancing the field of AI applications in PAD, Flores *et al.* [125] explored ML and AI tools to enhance PAD outcomes but highlighted challenges related to data interoperability, algorithm bias, and the need for extensive validation. Similarly, Forghani *et al.* [126] developed an intelligent oscillometric system for PAD detection with high accuracy, although further validation across different age groups is needed to account for age-related variations. In a comparative study, Collins *et al.* [127] evaluated a smartphone app combined with motivational interviewing (MI) for improving walking distance and weight loss in PAD patients and concluded that MI was more effective. However, limitations included a small sample size, inconsistent app usage, and the absence of an iOS version.

2.8 Cloud Computing and AI in Medical Imaging

Cloud computing integrated with AI is revolutionizing medical imaging by enabling scalable, efficient, and real-time diagnostics. Sakellarios *et al.* [128] developed a cloud-based platform for CAD management that integrates ML, computational modeling, and clinical decision support systems (CDSSs). Although the platform demonstrated scalability and adaptability, it was specific to CAD and lacked modules tailored to PAD, particularly in terms of real-time AI-driven automation. By extending the application of AI-cloud integration, Wu *et al.* [129] demonstrated enhanced diagnostic efficiency for lung cancer and COVID-19 via cloud-based AI systems. However, challenges related to AI standardization and dataset quality persist, highlighting the need for more robust and PAD-specific solutions.

Similarly, Chen *et al.* [54] examined the impact of AI-enhanced cloud computing on medical imaging and reported significant improvements in segmentation, feature extraction, and predictive diagnostics. Despite these advancements, the absence of clinical validation and real-world implementation has limited its applicability to PAD diagnostics. On the other hand, Putzier *et al.* [130] investigated cloud adoption in German hospitals, emphasizing data privacy, interoperability, and regulatory compliance. While successfully implemented at Charité University Hospital, the system lacked AI-driven clinical decision support and was confined to a single facility, indicating limited scalability.

To further expand on cloud-based medical imaging, Schweitzer *et al.* [131] developed a teleophthalmology platform with cloud-based DICOM storage integrated with the OHIF Viewer for remote image annotation and diagnostics. Although the platform demonstrated interoperable cloud workflows, it struggled with image retrieval latency and did not incorporate AI-driven automation or real-time computational modeling. These studies collectively highlight the need for enhanced AI integration, real-time computational modeling, and broader clinical validation to fully realize the potential of cloud computing in medical imaging for PAD.

2.9 Cloud-based multidisciplinary platforms

In addition to single-domain applications, cloud-based multidisciplinary platforms are emerging as pivotal tools for comprehensive patient care and collaborative clinical workflows. Zhang *et al.* [132] developed a cloud-based multidisciplinary team (cMDT) platform aimed at improving oncology treatment coordination, resulting in increased response times and better adherence to clinical guidelines. However, the system relies heavily on manual expert input and lacks AI-driven clinical decision-making and predictive analytics for personalized treatment pathways.

Building on cloud-based AI-driven platforms, Peng *et al.* [133] introduced AIScholar, an OpenFaaS-based cloud platform designed for intelligent medical data analytics. This platform demonstrated scalability and real-time clinical data processing, enhancing diagnostic precision and workflow efficiency. Nevertheless, its focus on structured medical data without comprehensive imaging diagnostics and real-time computational modeling limits its applicability to more complex scenarios such as PAD management.

Collectively, these studies highlight the evolving landscape of cloud-based multidisciplinary platforms. They underscore the necessity for enhanced AI integration, real-time decision support, and comprehensive interoperability to optimize clinical workflows and improve patient outcomes across various healthcare domains.

Cloud-based solutions have demonstrated significant potential in enhancing PAD management by improving accessibility and patient engagement. However, challenges such as low adherence, limited AI-driven automation, and scalability constraints persist. Table 2.3 presents a comparative overview of these solutions, emphasizing the necessity for AI integration, real-time decision support, and enhanced interoperability to optimize digital health interventions for PAD.

2.10 Contribution of this Thesis

This PhD thesis explores innovative solutions to advance medical imaging visualization, risk classification, and noninvasive management strategies for PAD. Through the integration of web-based technologies, high-fidelity visualization, and state-of-the-art computational modeling, this research addresses critical challenges in diagnostic precision, clinical workflow efficiency, and personalized treatment strategies. The scope and contributions of the thesis are presented in the context of five main research areas, each contributing to the advancement of PAD diagnostics and treatment planning.

Integration of DICOM and MPR visualization via progressive web applications (PWAs)

This thesis explores the integration of DICOM and MPR visualization into web environments via PWAs. This research aims to overcome significant technological challenges, including cross-platform compatibility, integration capabilities, speed, and scalability, particularly within medical imaging workflows. By leveraging PWAs' offline access and enhanced performance features, this study seeks to enable seamless medical image visualization across various devices, thus enhancing accessibility and usability for healthcare professionals. This research

specifically focuses on PAD imaging, aiming to provide radiologists with high-resolution medical images that maintain diagnostic accuracy even in offline scenarios. This study introduces a novel approach to web-based DICOM and MPR visualization, emphasizing offline access, enhanced performance, and an improved user experience. It proposes an MPR algorithm that uses bicubic and weighted bilinear interpolation to enhance edge detail, effectively addressing the limitations found in conventional implementations.

Table 2.3 Comparison of Cloud-Based Solutions for PAD Management.

Refs.	Platform Type	Key Features	Limitations
[118]	Supervised Exercise Therapy (SET)	Supports SET; Improves walking distance and quality of life	Manual input, lacks AI-driven automation
[119]	Home-based Exercise Therapy	Incorporates GPS tracking and pain assessment	Low patient adherence, lacks AI-driven adjustments
[120]	mHealth with Wearables	Wearable-integrated exercise interventions	Limited compatibility (Android only), small validation sample, no AI personalization
[121]	SET for PAD Patients	Analyzed effectiveness of SET for PAD	Low enrollment rates, lacks AI-driven supervision
[79]	Hybrid Digital Health Solutions	Suggested hybrid digital health for SET adoption	Low participation (2%), no real-time AI monitoring
[122]	Exercise Tracking App	Tracks walking ability	Requires more clinical validation
[123]	Smartphone Exercise Program	Smartphone-enabled exercise program	Low engagement and adherence in low-resource settings
[124]	Mobile Intervention for Disease Literacy	Supports SET in mobile interventions	Small sample size, limited generalizability
[125]	AI and ML for PAD	ML and AI for PAD outcomes	Challenges in data interoperability and algorithm bias
[126]	Intelligent Oscillometric System	PAD detection with high accuracy	Needs validation across different age groups
[127]	Motivational Interviewing App	Walking distance & weight loss tracking	Small sample size, inconsistent app usage, no iOS version
[128]	Cloud-Based CAD Platform	ML, computational modeling, CDSSs	Specific to CAD, lacks PAD modules and AI automation
[129]	Cloud-Based AI for Diagnostics	Enhanced diagnostic efficiency	Challenges in AI standardization and dataset quality
[54]	AI-Enhanced Cloud Computing	Improvements in segmentation and feature extraction	Lacks clinical validation & real-world implementation
[130]	Cloud Adoption in Hospitals	Implemented in German hospitals	Lacks AI-driven clinical decision support, limited scalability
[131]	Teleophthalmology Cloud Platform	Cloud-based DICOM storage with OHIF Viewer	Image retrieval latency, no AI-driven automation
[132]	Cloud-Based Multidisciplinary Team (cMDT)	Improved oncology treatment coordination	Heavy reliance on manual expert input, lacks AI decision-making
[133]	Cloud-Based AI Medical Analytics	Scalable real-time medical data processing	Focuses on structured data, lacks imaging diagnostics

In addition, the study examines cross-platform performance variations, recommending optimal configurations to ensure consistent functionality. By demonstrating superior loading times and reconstruction efficiency compared with existing platforms, this research establishes a new benchmark for web-based medical imaging systems. This validates the proposed solution using CT scans from PAD patients, thus confirming its potential to enhance diagnostic capabilities and clinical workflows.

High-Fidelity Visualization of Large-Scale Peripheral Artery CT Datasets via DECODE-3DViz

This thesis addresses the challenges of rendering high-resolution volumetric medical imaging datasets, specifically for peripheral artery CT images, via WebGL technology. It introduces the DECODE-3DViz pipeline, which uses level-of-detail (LOD) algorithms and data chunk streaming to optimize the visualization pipeline, ensuring real-time interactivity and high-fidelity visualization. This approach effectively manages WebGL texture size constraints and memory limitations, enabling the visualization of large-scale medical images within browser environments without performance degradation. The scope of this research includes enhancing real-time interaction, maintaining high visual fidelity, and overcoming browser memory limitations to support accurate medical diagnostics and clinical decision-making.

Compared with state-of-the-art visualization tools, the DECODE-3DViz pipeline significantly improves rendering performance, achieving up to a 98% reduction in rendering time while maintaining a high frame rate. By efficiently managing GPU memory usage, this platform enables real-time, high-fidelity interactions with large-scale datasets. This research enhances diagnostic accuracy by providing detailed visualizations of the peripheral vasculature, supporting advanced diagnostic and treatment planning for complex vascular pathologies. It also improves user accessibility through a web-based platform, facilitating widespread clinical adoption and enhancing user engagement with interactive real-time rendering adjustments. The open-source nature of DECODE-3DViz promotes further research and development in medical imaging visualization.

Automated risk classification framework for PAD

This thesis proposes a novel computational framework for the automated risk classification of PAD, leveraging optimized volume rendering, dynamic illumination, and quantitative vascular analysis. It integrates real-time plaque density and vascular curvature assessments to enhance

PAD diagnostics by automating risk stratification. The framework aims to improve diagnostic precision, reduce interobserver variability, and streamline clinical workflows, thereby enabling personalized patient management and early intervention. This research validates the effectiveness of this approach via real clinical data, demonstrating its potential for accurately classifying PAD risk levels and supporting clinical decision-making.

The framework introduces a real-time dynamic illumination model to enhance depth perception and the realism of vascular geometry. It also implements an automated plaque density and vascular curvature analysis algorithm, enabling precise risk classification. The system outperforms existing tools by offering advanced automated functionalities, including risk classification and quantitative vascular analysis. The research highlights the clinical decision support capabilities of the framework, demonstrating its effectiveness in reducing interobserver variability and enhancing diagnostic accuracy. By utilizing real clinical data for validation, this study confirms the framework's practical applicability in clinical settings and its potential to transform PAD diagnostics.

Computational Modeling of Drug-Eluting Balloons for PAD Treatment

This thesis systematically examines the application of computational modeling techniques to optimize DEBs for PAD treatment. It evaluates a comprehensive range of computational approaches, including MD, FEA, computational fluid dynamics (CFD), and ML. Research has focused on simulating drug transport, release kinetics, and hemodynamic responses within complex vascular geometries, thereby optimizing DEB design and therapeutic efficacy. The study also explores emerging trends, challenges, and future directions in DEB research, emphasizing patient-specific modeling to enhance predictive accuracy and improve clinical outcomes.

This work provides an in-depth examination of advanced computational techniques for optimizing DEB design, highlighting their role in enhancing drug release accuracy, mechanical stability, and patient-specific therapeutic outcomes. This study demonstrated how computational models can improve drug retention, hemodynamic flow patterns, and plaque morphology. This study emphasizes the importance of patient-specific simulations for personalized medicine, highlighting their potential to refine DEB strategies tailored to individual patient profiles. By identifying limitations in existing models and proposing future

directions such as multiscale modeling and AI-driven predictive analytics, this research paves the way for next-generation DEBs with enhanced efficacy and safety profiles.

Development of DECODE: An Open-Source Cloud-Based Platform for Noninvasive Peripheral Artery Disease Management

This thesis presents DECODE, an innovative open-source cloud-based platform designed to revolutionize PAD diagnosis and treatment planning. This platform integrates AI-driven vascular segmentation, computational modeling, and real-time 3D visualization to provide an end-to-end solution for PAD management. It combines DL segmentation with finite element modeling (FEM) for personalized simulations of balloon angioplasty and DCB therapy. This research addresses challenges in interoperability, scalability, and real-time diagnostics through a cloud-integrated ecosystem, ensuring seamless clinical integration and accessibility for healthcare professionals.

DECODE introduces advanced visualization capabilities through DECODE-3DViz, which supports real-time volumetric rendering and AR-assisted procedural planning. It achieves high-fidelity visualization and GPU memory efficiency, enhancing real-time interactions with large-scale datasets. The platform also integrates predictive modeling for PAD interventions, enabling personalized vascular drug delivery strategies. By ensuring cross-platform accessibility and seamless integration with EHRs, DECODE has established itself as a transformative tool in precision vascular medicine. As an open-source solution, it enables further research and sets a new benchmark for noninvasive PAD management and personalized patient care.

Chapter 3: Computational Modeling of Drug-Eluting Balloons

- 3.1. Introduction
 - 3.2. Intervention Methods for PAD
 - 3.3. Computational Methods and Applications
 - 3.4. Discussion
 - 3.5. Conclusion
-

3.1 Introduction

Cardiovascular disease (CVD) continues to pose a significant global health challenge, affecting over 500 million individuals and contributing to 20.5 million deaths in 2021 [134]. A recent systematic review revealed that the prevalence of peripheral arterial disease (PAD) has risen by more than 17%, equating to an additional 30 million people over five years [135]. PAD is a vascular condition characterized by narrowing or obstruction of arteries that supply the extremities, leading to reduced blood flow and impaired tissue perfusion [136]. Traditional interventions such as balloon angioplasty have shown limitations in maintaining long-term vessel patency and preventing restenosis. Drug-eluting stents (DESs), while offering benefits, are associated with restenosis in approximately 10% of patients within two years—a figure that doubles in those with comorbid conditions such as diabetes [137]. DESs also present risks of late or very late stent thrombosis, often caused by inflammatory reactions to polymeric excipients, which delay vessel healing.

In response to these challenges, DEBs and DCBs have emerged as promising alternatives. These devices combine mechanical dilation with localized drug delivery, typically using paclitaxel to

inhibit neointimal hyperplasia and improve clinical outcomes. Unlike DESs, DCBs avoid long-term exposure to polymeric excipients, potentially reducing the risk of delayed vessel recovery and late thrombosis [138]. DCBs have demonstrated superiority over balloon angioplasty for the treatment of both de novo and in-stent restenotic lesions in femoropopliteal and below-the-knee occlusive diseases. They have also been found to be equivalent to DESs and superior to balloon angioplasty in treating coronary in-stent restenosis [139]. Owing to their smaller therapeutic footprint, DCBs are particularly advantageous in cases where DESs may be less effective, such as in-stent restenosis, bifurcation lesions, and diffuse atherosclerotic segments.

Optimizing the therapeutic impact of DCBs requires a sophisticated understanding of their mechanical dynamics, drug release kinetics, and distribution profiles within the arterial wall. While experimental studies provide crucial insights, the complexity, ethical considerations, and high costs associated with *in-vivo* testing highlight the role of computational modeling as an essential, complementary tool. Computational modeling enables researchers to explore DCB drug transport and tissue retention dynamics under controlled conditions, providing a systematic approach to assess therapeutic efficacy and improve device design [140].

In recent years, computational modeling and simulation have become pivotal in developing and refining DEBs and DCBs, allowing detailed analysis of device–tissue interactions, drug uptake, and retention. Through advanced 3D models, studies have investigated drug transport behaviors during balloon deployment, accounting for variables such as inflation time, arterial composition, and drug washout. Computational methods have also been instrumental in predicting how coating microstructures influence drug transfer and retention, highlighting critical parameters that drive therapeutic outcomes. The convergence of computational modeling with experimental and clinical data holds significant potential for advancing PAD treatments. These models deepen our understanding of drug delivery mechanisms and offer insights that can inform the next generation of DEBs and DCBs with enhanced efficacy and safety profiles. In addition, computational simulations pave the way for personalized treatment strategies, supporting device customization and deployment techniques on the basis of individual patient anatomy and pathology [141]. Despite substantial progress, the application of computational modeling to DEBs remains limited compared with that to DESs. Much of the current research still relies on simplified geometries and uniform drug coating assumptions, which restricts model accuracy. However, recent advancements in 3D modeling and the integration of hybrid *in-silico* and *in-vitro* methods have enhanced the predictive power of

simulations for long-term therapeutic outcomes. Coupling computational methods with *in-vitro* studies, ML, and nanotechnology offers a promising pathway toward the comprehensive optimization of drug-eluting devices, underscoring the need for further research to overcome existing limitations [142].

This chapter systematically examines the application of computational modeling techniques to DEBs for PAD treatment, evaluating the range of computational approaches, their contributions to DCB design, and their impact on optimizing device performance. Through an analysis of the current literature and modeling advancements, this review identifies emerging trends, challenges, and future directions in the computational modeling of DEBs, with a focus on improving outcomes for PAD patients.

3.2 Intervention methods for PAD

PAD treatment strategies span a wide range of modalities aimed at alleviating symptoms and improving vascular health. Initial interventions typically include lifestyle modifications and pharmacotherapy, the use of antiplatelet agents, lipid-lowering drugs, and vasodilators to increase circulation and prevent disease progression. For more advanced cases, revascularization procedures, such as surgical bypass grafting and minimally invasive endovascular approaches, become essential. Techniques such as atherectomy—mechanical removal of plaque—are often combined with other interventions to optimize outcomes in challenging lesions. Among implantable devices, DESs have demonstrated efficacy in maintaining vessel patency; however, their long-term use is associated with risks, including late thrombosis and restenosis, primarily due to inflammatory responses to polymeric coatings.

As shown in Figure 3.1, when publication trends across PubMed, Scopus, and ScienceDirect are analyzed, DEBs dominate research activity, reflecting their clinical importance and increasing adoption. The consistent increase in the number of DEB-related publications across all three databases highlights their effectiveness in addressing the limitations of other interventions, including DCBs, conventional balloon angioplasty (CBA), high-pressure balloon angioplasty (HPBA), and cutting balloon angioplasty. DEBs integrate two key mechanisms, mechanical dilation and localized drug delivery, providing an effective solution to restenosis, particularly in complex cases such as in-stent restenosis and heavily calcified lesions.

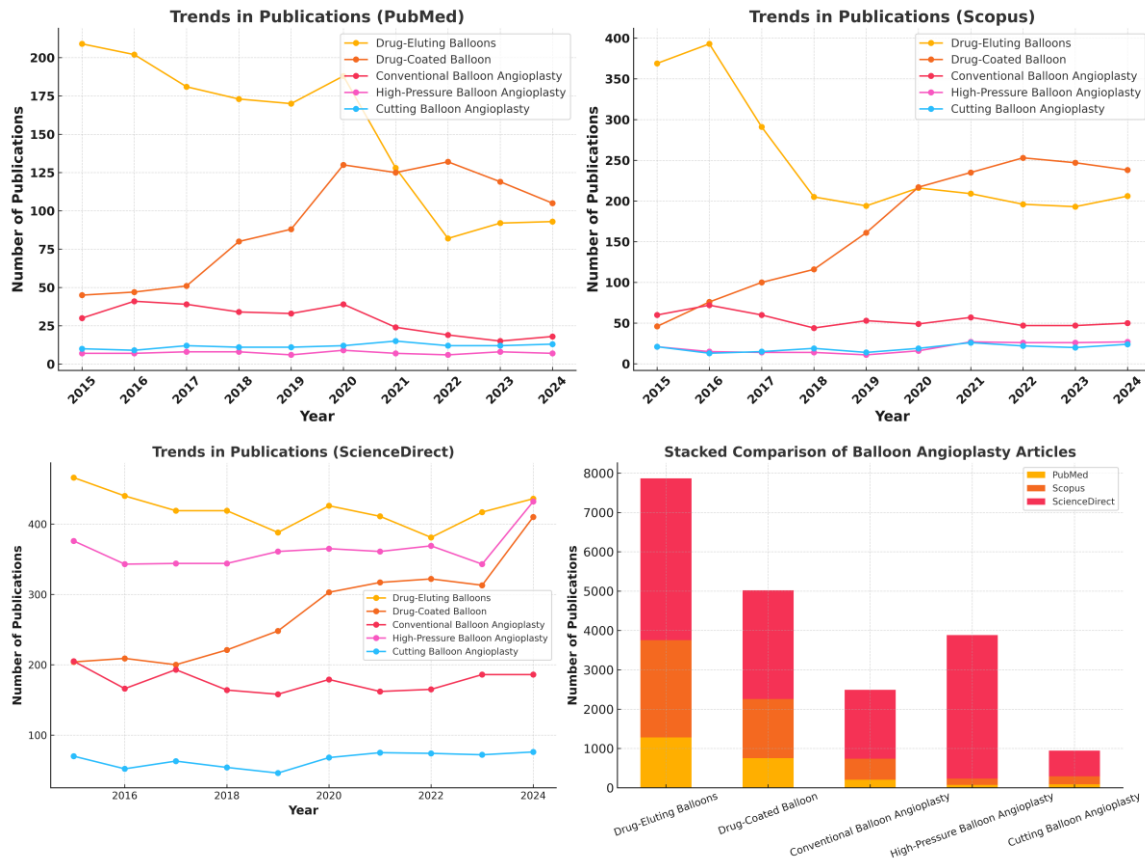


Figure 3.1 Trends and Comparative Analysis of Balloon Angioplasty Publications (2015–2024): (A) PubMed, (B) Scopus, (C) ScienceDirect, and (D) Stacked Comparison of Article Counts Across Databases.

In addition, they avoid complications associated with permanent implants, such as inflammation and late-stage thrombosis, making them a transformative option in PAD management.

This dominance of DEBs in the research landscape underscores their ability to address mechanical and pharmacological challenges simultaneously, reduce procedural risks, and improve long-term outcomes. Figure 3 also emphasizes the growing interest in DEBs compared with other techniques, validating their role as a central focus in advancing PAD treatment.

3.2.1 Balloon Angioplasty

Balloon angioplasty, also known as percutaneous transluminal angioplasty (PTA) [143, 144], is a minimally invasive procedure used to open narrowed or blocked blood vessels, typically arteries. This technique involves the insertion of a small balloon-tipped catheter into the affected artery. Once in place, the balloon is inflated to widen the artery, improving blood flow [145]. This procedure is commonly used to treat conditions such as PAD, CAD, and stenosis in arteriovenous (AV) fistulas and grafts used for hemodialysis. Types of balloon angioplasty:

a) Conventional balloon angioplasty (CBA)

CBA, also known as plain old balloon angioplasty (POBA) [146], involves the use of an uncoated balloon to dilate the artery. While effective in the short term, this method often faces challenges such as vessel recoil and restenosis, where the artery narrows again after the procedure. Studies have shown that while POBA can improve blood flow, it does not significantly reduce the long-term need for revascularization or improve clinical outcomes such as limb salvage and mortality [147].

b) Drug-Coated Balloon (DCB)

DCBs are an advanced form of balloon angioplasty that involves coating the balloon with antiproliferative drugs, such as paclitaxel [148]. These drugs are released into the arterial wall during inflation of the balloon, inhibiting the growth of neointimal tissue, which can lead to restenosis.

Efficacy and safety: Multiple studies have demonstrated the superior efficacy of DCBs over standard balloon angioplasty [148]. For instance, the IN.PACT SFA trial revealed that DCBs had a significantly higher primary patency rate at 12 months than did POBA (82.2% vs. 52.4%, $P < 0.001$) and a lower rate of clinically driven target lesion revascularization (2.4% vs. 20.6%, $P < 0.001$) [149]. Another study, the EffPac Trial, confirmed these findings, showing that DCBs maintained superior efficacy over conventional balloons at 2 years, with primary patency rates of 90.2% for DCBs compared with 62.7% for POBA [150].

Long-term outcomes: The durability of the treatment effect with DCBs has been a focus of recent research. The IN.PACT SFA trial reported that at 24 months, DCBs continued to result in significantly greater primary patency (78.9% vs. 50.1%, $P < 0.001$) and lower rates of clinically driven target lesion revascularization (9.1% vs. 28.3%, $P < 0.001$) than did POBA [151]. However, there were concerns about higher overall mortality rates in the DCB group, which necessitates further investigation.

Clinical and functional outcomes: While DCBs have shown clear advantages in terms of anatomical endpoints such as primary patency and restenosis rates, their impact on clinical outcomes such as limb salvage, mortality, and quality of life remains less clear. A comprehensive meta-analysis of 45 randomized trials indicated that DCBs significantly reduced the rate of target lesion revascularization but did not significantly affect mortality or recurrent acute ischemic events compared with conventional revascularization strategies [152].

Technological innovations: Recent advancements in DCB technology include the development of novel coatings and delivery mechanisms. For example, a study on a novel paclitaxel-nanocoated balloon demonstrated improved outcomes in terms of late lumen loss and primary patency compared with POBA, with no significant safety concerns. In addition, the combination of DCBs with other treatment modalities, such as atherectomy or laser ablation, has shown promising results in overcoming the limitations of calcified lesions [153].

c) Drug-Eluting Balloon (DEB)

DEB angioplasty, similar to DCB angioplasty, involves the use of balloons coated with drugs that elute over time to prevent restenosis [154]. This method has demonstrated significant improvements in patency rates and cost-effectiveness, particularly in the treatment of failing dialysis access and PAD.

Efficacy and Outcomes: Compared with plain balloon angioplasty (PBA) and PTA, DEB angioplasty has shown superior outcomes in various studies. A meta-analysis of randomized controlled trials (RCTs) revealed that DEB angioplasty significantly reduces late lumen loss, restenosis, and the need for target lesion revascularization (TLR) in patients with femoral-popliteal and infrapopliteal diseases without increasing the risk of major amputation or mortality [155]. Another study confirmed that DEBs are more effective than uncoated balloons in maintaining primary vessel patency and reducing binary restenosis rates for up to five years [156].

Clinical Trials and Evidence: Several clinical trials have supported the efficacy of DEB angioplasty. For example, the PACUBA trial demonstrated that paclitaxel-eluting balloon angioplasty provides significantly higher patency rates and lower TLR rates than does standard PTA in patients with in-stent restenosis of the femoropopliteal artery [157]. In addition, the IN.PACT SFA trial reported that DEB angioplasty resulted in greater primary patency and lower CD-TLR rates at 24 months than did PTA, with similar functional improvements and fewer reinterventions [158].

Cost-effectiveness: Despite the higher initial cost of DEBs than of uncoated balloons, their long-term benefits in reducing the need for repeat interventions and improving vessel patency make them a cost-effective option for treating PAD [159]. The durability of the treatment effect of DEBs, as evidenced by long-term follow-up studies, further supports their cost-effectiveness.

Limitations and Future Directions: While DEB angioplasty has shown promising results, some studies have reported no significant differences in clinical endpoints, such as amputation, death,

or changes in the ankle–brachial index (ABI), compared with uncoated balloon angioplasty [160]. Moreover, the heterogeneity in trial designs, patient populations, and follow-up durations necessitates further well-designed RCTs with long-term follow-up to fully establish the clinical and economic benefits of DEBs [161].

d) High-Pressure Balloon Angioplasty (HPBA)

HPBA is a technique that utilizes balloons capable of withstand higher pressures, making them particularly suitable for treating more resistant lesions [162]. This method is often employed in conjunction with other techniques to improve clinical outcomes.

Technical Aspects and Efficacy: HPBA involves the use of noncompliant balloons that can be inflated to high pressures, typically ranging from 22 to 24 atmospheres, to effectively dilate resistant and calcified arterial lesions. This high-pressure capability is crucial for achieving technical success in complex cases, such as long and calcified infrapopliteal and inframalleolar lesions. A previous study reported a technical success rate of 95.7% with no procedure-related complications, highlighting the feasibility and safety of this approach [163].

Comparative effectiveness: Compared with conventional balloon angioplasty, HPBA has shown superior outcomes in specific scenarios. For example, in the treatment of long infrapopliteal calcified lesions, HPBA achieved high rates of limb salvage and wound healing over a follow-up period of up to three years [164]. In addition, the use of ultrahigh-pressure balloons in pediatric patients with pulmonary artery stenosis associated with congenital heart defects has a success rate of 78.4%, with predictors of success including a larger balloon-to-waist ratio and the presence of therapeutic tears [165].

In combination with other modalities, HPBA is often used in combination with other revascularization strategies to optimize outcomes. For example, the combination of atherectomy and balloon angioplasty has improved patency rates and reduced the need for bailout stenting in femoropopliteal lesions [166]. Similarly, DCBs have been used following HPBA to maintain vessel patency and reduce the incidence of TLR. A meta-analysis indicated that DCBs significantly reduced TLR rates compared with conventional balloon angioplasty, particularly in patients with PAD [152].

Safety Considerations: While HPBA is generally safe, it is not without risks. Potential complications include vessel dissection, recoil, and restenosis. However, studies have shown that with careful patient selection and procedural planning, these risks can be minimized. For

example, the use of long balloons with prolonged inflation times has been recommended to mitigate the risk of dissection and recoil in infrapopliteal arteries [167].

e) Cutting balloon angioplasty

Cutting balloon angioplasty is a specialized technique used to treat more fibrotic or calcified lesions in PAD patients [167]. This method involves a balloon equipped with small blades that make precise incisions in the plaque as the balloon is inflated. The primary advantage of this technique is its ability to facilitate the fracturing of calcified plaques, which are often resistant to conventional balloon angioplasty.

Mechanism and efficacy: Cutting balloon blades creates controlled microincisions in calcified plaques, which helps reduce resistance to balloon expansion and allows for more effective lesion dilation. This is particularly beneficial in cases where calcification is severe and circumferential, as conventional balloons may fail to achieve adequate expansion, leading to suboptimal outcomes such as stent underexpansion and an increased risk of restenosis and thrombosis [168]. FEA has shown that the effectiveness of cutting balloons is significantly influenced by the balloon-to-diameter ratio and the number of blades facing the calcified lesion. For example, models with two blades facing the calcification generate greater principal stresses in the calcified plaque, facilitating better expansion even with undersized balloons. This approach also reduces the stress on the adjacent arterial wall, thereby minimizing the risk of vessel dissection and perforation [169].

Clinical Outcomes: Clinical studies have demonstrated that cutting balloon angioplasty can be a safe and effective method for treating heavily calcified lesions. For example, the use of scoring balloons, which operate on a similar principle, has shown promising results in terms of procedural success and long-term patency. However, the benefits of cutting balloons over conventional angioplasty techniques, such as POBA or DCB angioplasty, are still being evaluated [170]. In a study comparing the Wolverine™ cutting balloon with a noncompliant balloon catheter, the cutting balloon achieved higher dilation success rates at lower pressures. This was attributed to the increased stresses generated by the cut blades, which effectively fractured the calcified plaque. Another study highlighted that vessel preparation with cutting balloons before stent implantation could reduce the need for additional stenting and lower the incidence of flow-limiting dissections [171].

Limitations and Future Directions: Despite these advantages, cutting balloon angioplasty has the same limitations. The technique requires precise positioning of the blades to maximize

efficacy and minimize complications. In addition, the long-term benefits of cutting balloons in reducing restenosis rates and improving overall limb outcomes in PAD patients need further investigation through large-scale, randomized controlled trials [172].

3.2.2 Comparative Insights into Balloon Angioplasty Technologies

A comprehensive overview of the clinical outcomes and applications of various balloon angioplasty techniques is presented in Table 3.1, offering a systematic comparison of their effectiveness, patency rates, and safety across diverse clinical scenarios. For example, while CBA serves as a standard treatment for PAD, its high restenosis rates highlight the critical need for advanced alternatives. Both DCBs and DEBs demonstrate superior patency rates and safety profiles [173-175], establishing themselves as transformative solutions for complex vascular lesions. Moreover, specialized techniques such as HPBA and cutting balloon angioplasty are tailored for resistant or calcified lesions, providing targeted solutions for challenging cases. The comparative metrics of these technologies, visualized in Figure 3.2, reveal the superior performance of DCBs and DEBs in terms of patency, target lesion revascularization rates, and safety. Notably, DEBs further excel in cost-effectiveness, positioning them as pivotal innovations in PAD treatment.

The decision-making framework in Figure 3.3 outlines critical considerations for intervention selection, emphasizing tailored approaches on the basis of stenosis type, lesion complexity, and patient-specific factors. This structured perspective underscores the importance of individualized care in optimizing clinical outcomes. Table 3.2 deepens this analysis by highlighting the nuanced clinical applications, efficacy metrics, and technological innovations across balloon angioplasty technologies. For example, DCBs are particularly effective for managing ISR and small vessel diseases, offering outcomes comparable to those of DESs while preserving vasomotor function. In contrast, DEBs excel in addressing severe PAD and heavily calcified lesions, reducing restenosis rates and procedural risks without the complications associated with permanent implants. In addition, advanced solutions such as Ultra-High-Pressure (UHP) Balloons deliver precise therapeutic benefits in resistant lesions, and Cutting Balloons enable effective plaque modification for calcified vessels. The systematic comparison in Table 3.2 complements the graphical insights from Figure 3.2 and Figure 3.3, collectively reinforcing the indispensable role of innovations such as DCBs and DEBs in addressing the limitations of traditional techniques. These technologies not only advance angioplasty efficacy and safety but also exemplify the alignment of innovation with patient-centric care. As the data

reveal, careful selection of balloon technology, on the basis of lesion complexity and patient needs, is paramount in driving optimal clinical outcomes and cost efficiency.

Table 3.1 Clinical outcomes of balloon angioplasty.

Technique	Effectiveness	Patency Rates	Safety
Conventional Balloon Angioplasty (CBA / POBA)	Effective in short-term; limited by vessel recoil and restenosis; does not significantly reduce revascularization or improve clinical outcomes	12-month: 52.4% [149] 2-year: 62.7% [151]	Generally safe; minimal procedural complications, but high restenosis and TLR rates
Drug-Coated Balloon (DCB)	Superior to POBA in reducing restenosis and TLR; improves vessel patency; supported by multiple RCTs (e.g., IN.PACT SFA, EffPac)	12-month: 82.2% [149] 2-year: 90.2% [151]; 24-month: 78.9% vs. 50.1% (DCB vs. POBA) [152]	Generally safe; concerns raised about higher long-term mortality, but not consistently supported
Drug-Eluting Balloon (DEB)	Similar to DCB; effective in femoropopliteal and infrapopliteal arteries; superior to POBA in long-term outcomes (e.g., PACUBA, IN.PACT SFA)	Up to 5-year patency significantly better than POBA [156, 157]	Safe; no significant increase in amputation or mortality; considered cost-effective
High-Pressure Balloon Angioplasty (HPBA)	Highly effective in calcified/resistant lesions; high technical success rate (~95.7%) in complex infrapopliteal lesions	Long-term limb salvage and wound healing outcomes favorable [165, 166]	Generally safe; dissection and recoil risks mitigated with technique (e.g., long balloons, prolonged inflation)
Cutting Balloon Angioplasty	Effective in fibrotic and calcified plaques; micro-incisions improve dilation; facilitates optimal stent expansion	Higher dilation success at lower pressures; improved outcomes in specific lesion types [172]	Requires precision; reduced vessel stress and dissection risk when used correctly; long-term benefit still under study

Table 3.2 Comparative Overview of Balloon Angioplasty Technologies – Clinical Applications, Efficacy Metrics, Advantages, Limitations, and Technological Innovations.

Refs.	Balloon Technology	Clinical Applications	Limitations	Technological Innovations
[157]	DEB	In-Stent Restenosis (ISR) in femoropopliteal arteries	Higher upfront costs; paclitaxel-associated risks	Paclitaxel-coated balloons with innovative coatings
[174]	DEB	Complex ISR, severe PAD	Limited evidence for long-term durability in ISR and calcified lesions	Biodegradable and crystalline drug delivery matrices
[169]	Cutting Balloons	Calcified coronary lesions, moderate stenosis	Requires precise blade positioning; high technical expertise needed	Finite element analysis for optimization; undersized balloons for reduced risks
[175]	DCB	Unprotected left main (LMS) coronary disease, bifurcation lesions	Limited efficacy for complex bifurcation lesions (Medina 1,1,1: proximal main vessel, distal main vessel, and side branch all involved); may require provisional DES in some cases	OCT-guided intervention (Optical Coherence Tomography); advanced delivery systems
[138]	DCB	ISR, small vessel disease, de novo lesions, bifurcation, calcified lesions	Limited data for calcified and diffuse long lesions; technical challenges in drug transfer	Paclitaxel and sirolimus coatings; nanotechnology-based delivery systems
[165]	UHP	Pulmonary artery stenosis in children with congenital heart defects (CHD)	Higher restenosis rates compared to stents; limited long-term data	Cross-matrix woven ultrahigh molecular weight polyethylene for durability
[173]	DEB	Coronary artery lesions, ISR, PAD	Cytotoxicity of paclitaxel; limited data for long-term safety	Nano-needle designs; micropatterned coatings for efficiency

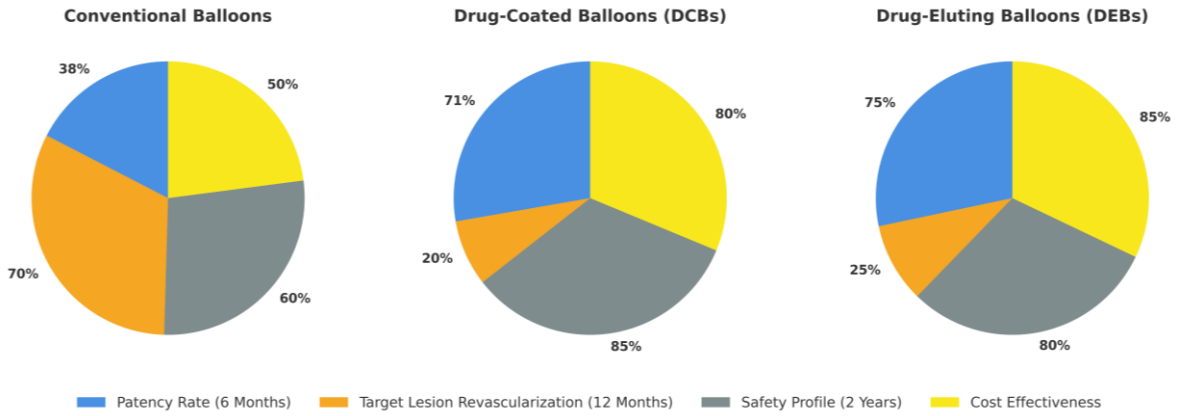


Figure 3.3 Comparative Distribution of Clinical Metrics for Conventional Balloons, Drug-Coated Balloons (DCBs), and Drug-Eluting Balloons (DEBs) [173-175].

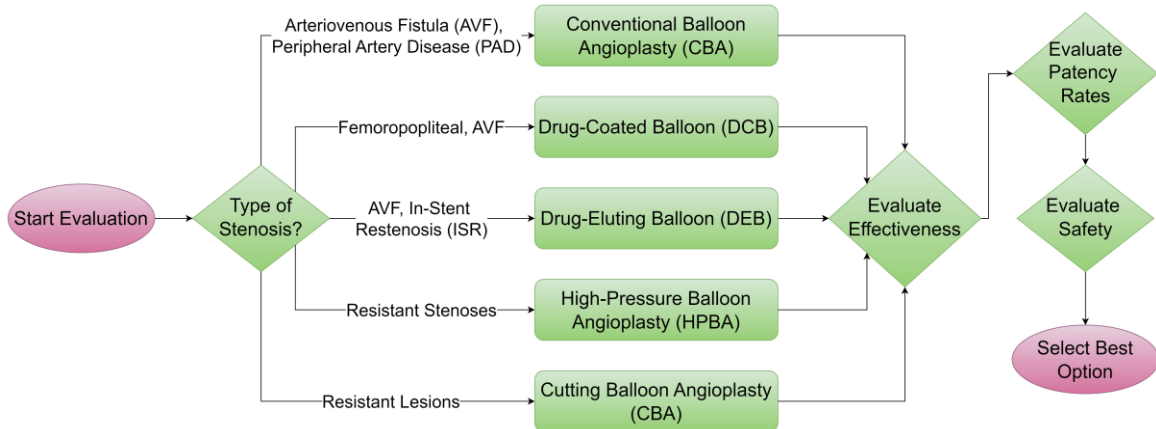


Figure 3.2 Decision-Making Process for Selecting Balloon Angioplasty Techniques Based on Stenosis Type [173-175].

3.3 Computational methods and applications

Computational methods have fundamentally enhanced DEB technology for PADs by offering precise insights into drug release, device–tissue interactions, and patient-specific responses [176]. Core techniques, such as computational fluid dynamics (CFD) and FEA, model drug transport and structural dynamics to ensure optimal flow dynamics and mechanical stability, which are critical for drug efficacy under physiological conditions [177]. ML and AI contribute predictive power, enabling personalized treatment approaches by optimizing parameters such as dosage and coating properties [178]. At the molecular scale, MD simulations reveal essential drug interactions, whereas Monte Carlo (MC) and density functional theory (DFT) methods predict release kinetics and stability with probabilistic and molecular-level precision. Advanced fluid–structure interaction (FSI) models integrate CFD and FEA to simulate blood flow impacts

on device stability, whereas patient-specific modeling and statistical optimization refine these models to reflect anatomical variability [179]. Together, these computational advancements are pivotal in developing DEBs with superior, patient-tailored efficacy, marking significant progress toward personalized PAD treatment.

3.3.1 Computational fluid dynamics (CFD)

Currently, CFD is a pivotal tool for simulating blood flow and drug delivery dynamics under conditions such as PAD [180]. Using finite volume analysis, CFD solves fluid dynamics equations, including the Navier–Stokes equations, and models drug transport through convection–diffusion–reaction (CDR) equations. The CFD process involves segmenting medical imaging data to create patient-specific *in-silico* arterial models, meshing the geometry, applying boundary conditions, and iteratively solving these equations to generate precise pressure and velocity profiles. This patient-specific approach allows CFD to simulate interventions such as balloon angioplasty or stent deployment, providing insights into drug interactions with vascular walls and facilitating dosage optimization.

In CFD analyses for incompressible flows, the Navier–Stokes and continuity equations govern mass and momentum conservation [181]:

$$\partial\rho/\partial t + \nabla \cdot (\rho * u) = 0, \quad (3.1)$$

$$\rho(\partial u/\partial t + u \cdot \nabla u) = -\nabla p + \mu \nabla^2 u + \rho g, \quad (3.2)$$

where ρ is the fluid density, ∇ is the divergence operator, u is the velocity vector, p denotes the pressure, μ is the dynamic viscosity, and g represents the external forces [182]. Drug transport dynamics are modeled using the following CDR equation:

$$\frac{\partial C}{\partial t} + \nabla \cdot (u * C) = D \nabla^2 C + R(C), \quad (3.3)$$

where C is the drug concentration, u represents convection, D is the diffusion coefficient, and $R(C)$ accounts for biochemical reactions within the arterial wall.

Boundary conditions in CFD are crucial for accurate modeling of fluid behavior, particularly in simulating drug diffusion in biological environments. These conditions, derived from experimental or patient-specific data, ensure physiological realism. The CFD modeling process

includes acquiring anatomical data, performing digital segmentation, meshing, applying boundary conditions, running simulations, extracting data, and validating results against clinical benchmarks [183]. CFD provides high-resolution insights into hemodynamic factors such as wall shear stress (WSS) and time-averaged WSS (TAWSS), aiding in optimizing drug-eluting devices and supporting noninvasive testing for therapy planning and device enhancement. This technique is invaluable for evaluating localized drug delivery, improving drug efficiency, and minimizing side effects.

Recent advancements in CFD have refined the design of stent- and balloon-based DDSs, although clinical adoption remains limited by model simplifications and computational demands. Notably, Rikhtegar *et al.* [184] explored the effects of flow on drug retention in coronary arteries but were constrained by biological variability, and Tzafriri *et al.* [185] analyzed coating micromorphology but lacked long-term tissue healing data. More recent works, such as those of Totorean *et al.* and Jain *et al.* [186, 187], introduced patient-specific data and models focused on balloon drug delivery, although computational demands and simplified wall models have limited their applicability. Black *et al.* and Xu *et al.* [188, 189] enhanced hemodynamic simulations with 4D flow-MRI data and angiography-based models, respectively, although their generalizability was affected by sample size and boundary conditions. These studies confirm the critical role of CFD in drug delivery optimization while highlighting the need for advanced models and validation to increase clinical utility.

3.3.2 Structural Analysis

Structural analysis, grounded in the FEA method, plays a critical role in understanding the mechanical behavior of DDSs, particularly DCBs and stents. FEA discretizes both the device and the surrounding tissue into smaller elements, enabling an elementwise analysis that predicts the overall structural response under applied mechanical forces, including stresses and strains. This method is essential for optimizing device design, ensuring mechanical durability, and assessing how interactions with the arterial wall influence drug release dynamics. The FEA process comprises meshing, application of boundary conditions, and assignment of material properties to each element, allowing researchers to iteratively solve governing equations for stress, strain, and deformation, ensuring both structural integrity and efficient drug delivery [190]. For anisotropic materials, such as vascular tissues, the stress–strain relationship is often represented in tensor form to capture directional variations in material properties [191]:

$$\sigma_{ij} = C_{ijkl}\epsilon_{kl}, \quad (3.4)$$

where σ_{ij} and ϵ_{kl} are the stress and strain tensors, respectively, and C_{ijkl} is the fourth-order elasticity tensor. This approach is necessary to model the complex, anisotropic behavior of arterial walls. In addition, for hyperelastic materials that undergo large deformations, as observed in vascular tissues, strain energy density functions, such as the Mooney–Rivlin model, are used to represent material behavior [192]:

$$W = C_1(I_1 - 3) + C_2(I_2 - 3), \quad (3.5)$$

where C_1 and C_2 are material constants and I_1 and I_2 are the first and second invariants of the Cauchy–Green strain tensor, respectively. FEA also incorporates contact mechanics to simulate the interface behavior between the device and arterial wall, with stress determined by Hertzian contact mechanics [193]:

$$\sigma_c = \frac{3F}{2\pi a^2}, \quad (3.6)$$

where σ_c is the contact stress, F is the applied force, and a is the contact radius. This interaction is crucial for understanding localized stresses at the arterial interface, which can impact drug release efficacy and the tissue response. The force–displacement relationship is formulated through a matrix equation [194]:

$$K \cdot u = F, \quad (3.7)$$

where K represents the stiffness matrix, u is the displacement vector, and F is the force vector. This equation is central to determining the structural response of drug delivery devices under physiological conditions.

Boundary conditions are essential in accurately modeling device response under physiological loads, such as blood pressure on stents, where fixed supports and applied forces simulate realistic pressures. Initial conditions in drug delivery devices capture preexisting stress or strain from manufacturing processes, such as stent crimping, to increase model accuracy [195]. FEA model construction includes definitions of the geometry, meshing, material property

assignment, and application of boundary and initial conditions, followed by simulations and post-processing for data extraction and validation against clinical benchmarks [190].

In PAD treatment, FEA provides high-resolution simulations of stent–artery interactions, optimizing drug release while minimizing restenosis risk. These findings support accurate localized drug delivery analysis, ultimately improving therapeutic outcomes and informing next-generation DDS design with applications in personalized cardiovascular care [196]. Despite its extensive use in optimizing DDSs, FEA's clinical applicability faces limitations. Studies by Mandal *et al.* [197, 198] demonstrated insights into tissue heterogeneity and drug retention, but empirical dependencies reduced generalizability, emphasizing the need for further validation. Escuer *et al.* and McQueen *et al.* [199, 200] advanced the understanding of mechanical deformation and drug effects but used idealized models, limiting their physiological accuracy. Liang *et al.* and Psarras *et al.* [201, 202] examined device resilience and failure risk, revealing progress in the scope of FEA; however, reliance on simplified geometries has restricted real-world application. Recent work by Shazly *et al.* and Kim *et al.* [203, 204] explored coating microstructures and novel stent geometries, revealing improvements in drug delivery and mechanical performance, although controlled conditions necessitate further *in-vivo* validation for clinical relevance. These studies affirm FEA's potential in DDS refinement while highlighting the need for validated, physiologically relevant models to advance clinical impact.

3.3.3 Fluid–structure interaction (FSI) analysis

FSI analysis combines CFD and FEA to simulate the interactions between blood flow and the structural elements of drug delivery devices, such as stents or balloons, providing a holistic view of drug delivery dynamics and device stability under physiological conditions [205]. The process begins with CFD to calculate fluid parameters (velocity, pressure, and shear stress), which are then integrated with FEA to assess the structural response, enabling precise modeling of drug kinetics. FSI simulations require boundary and interface conditions to maintain the continuity of stress and velocity at the device–blood interface, with initial conditions capturing the physiological state of both fluid and structural elements [206].

The development of FSI models involves various stages, including clinical imaging (CT, MRI) for anatomy capture, segmentation, digital reconstruction, and discretization focused on fluid–structure interfaces [207]. FSI applications have yielded valuable insights into vascular medicine; Lee *et al.* [208] reported nonuniform drug distribution due to stent-induced deformation, highlighting the need for design optimization, whereas McKittrick *et al.* [209]

noted limitations in simplified transport parameters for sirolimus-eluting stents. Anbalakan *et al.* [210] proposed biphasic release for DCBs, although assumptions limited generalization. More recent studies have extended the application of FSI, such as that of Fadhil *et al.* [211], who examined the impact of smoking on blood viscosity, although idealized models have restricted their clinical relevance. Shahrulakmar *et al.* [212] advocated for complex, patient-specific geometries to improve PAD hemodynamic modeling, whereas Khairulin *et al.* [213] explored multilayered artery models affecting stress–strain responses. Collectively, these studies demonstrate the versatility of FSI in vascular simulations, with a continued emphasis on patient-specific validations to improve clinical applicability.

3.3.4 Molecular dynamics (MD)

MD simulations operate at the atomic scale, enabling precise modeling of interactions between atoms and molecules within DDSs. These simulations are pivotal for understanding drug binding, stability, and diffusion, offering insights essential for optimizing drug coatings, analyzing release mechanisms, and predicting formulation efficacy. MD is widely applied in DDS research and involves liposomes, micelles, and nanoparticles to examine complex interactions such as hydrophobic effects, van der Waals forces, electrostatics, and hydrogen bonding [214].

MD simulations utilize boundary conditions to define the simulation box, often employing periodic boundaries to simulate bulk environments. The initial particle conditions are based on experimental data or randomized within realistic ranges for accurate system representation [215]. The key equations in MD include Newton’s second law for particle motion:

$$F = m \cdot a, \tag{3.8}$$

where F is the force, m is the mass, and a is the acceleration.

3.3.5 Monte Carlo (MC)

MC simulations are a probabilistic technique used to model complex drug release behaviors, particularly where random interactions, such as diffusion through heterogeneous tissue, are significant. MC simulations predict how drug molecules disperse through tissues by defining the drug and environment as probabilistic events and running numerous iterations to observe possible outcomes [216]. This approach is invaluable for understanding drug diffusion and absorption patterns, providing insights into release kinetics, bioavailability, and reaction rates.

In addition, MC simulations can be used to evaluate drug distribution patterns, uptake efficiency, and potential interactions with biological environments, making them highly versatile for analyzing various aspects of DDSs [217].

The MC simulation process involves (a) defining the problem and identifying system inputs and outputs, (b) generating random input values on the basis of probability distributions, (c) running simulations with these values to calculate outputs, (d) repeating simulations to create a statistical distribution of results, and (e) analyzing results to estimate system behavior probability distributions. This iterative process enables MC simulations to represent drug delivery stages from source release to tissue dispersion [216]. MC simulations account for molecular interactions with the environment and are dynamically adjusted on the basis of concentration gradients and tissue characteristics.

3.3.6 Density functional theory (DFT)

DFT is a quantum mechanical modeling approach used to study the electronic structure of atoms and molecules in drug delivery systems (DDSs). Examination of the electron density distribution provides detailed insights into drug–receptor interactions, which are crucial for optimizing drug design, chemical stability, and binding affinity. DFT helps predict the binding affinity between drugs and receptors, optimize drug structure and stability, and enhance bioavailability and solubility—key factors in drug delivery. It also assists in designing drug delivery vehicles such as liposomes, dendrimers, and micelles, thereby reducing the need for empirical methods [218]. The Kohn–Sham equation [219], which is foundational to DFT calculations, is represented as:

$$\left(-\frac{\hbar^2}{2m} \nabla^2 + v_{eff}(r) \right) \varphi_i(r) = \varepsilon_i \varphi_i(r), \quad (3.9)$$

where \hbar is the reduced Planck constant, m is the mass of the electron, ∇^2 represents the Laplacian operator, $v_{eff}(r)$ is the effective potential, $\varphi_i(r)$ denotes the wave function of the i -th electron, and ε_i is the corresponding energy eigenvalue. The equation accounts for the kinetic energy of the electrons, as well as their interactions with the effective potential arising from electron–electron interactions and external fields.

3.3.7 Machine Learning and Artificial Intelligence

ML and AI have become integral in drug delivery research, enhancing drug release optimization and prediction accuracy for complex therapeutic outcomes [220]. By processing large datasets, ML and AI identify key parameters for precise drug targeting, enabling real-time adjustments and personalized treatment plans [221]. These methods simulate intricate drug release scenarios, optimizing variables such as coating thickness, release rates, and patient-specific factors, thus complementing traditional computational methods such as CFD and FEA. This fusion of data-driven models with conventional computational techniques yields a more flexible and accurate approach in drug delivery research.

In ML model development for DDSs, training, validation, and test conditions are critical. The data are split into training, validation, and test sets: the training set adjusts the model parameters, the validation set fine-tunes hyperparameters and mitigates overfitting, and the test set evaluates model efficacy. These datasets often include patient-specific data, drug release patterns, and experimental outcomes. Initial conditions for ML models involve initial weights, typically initialized randomly or with techniques such as Xavier initialization to ensure effective training [222]. Loss functions, which are essential for AI model optimization, commonly use the mean squared error (MSE) for regression and cross entropy for classification:

$$(MSE) = \left(\frac{1}{n}\right) \cdot \sum_{i=1}^n y_i - \hat{y}_i, \quad (3.10)$$

$$(Cross\ Entropy) = - \sum_{i=1}^{y_i} y_i, \quad (3.11)$$

where y_i represents the true value for the $i - th$ data point, \hat{y}_i is the predicted value for the $i - th$ data point, and n denotes the total number of data points. In the case of classification, cross-entropy loss measures the difference between the predicted probabilities \hat{y}_i and the actual class labels y_i , providing a measure of prediction accuracy.

AI and ML are transforming DDSs by enabling sophisticated analysis of biological and chemical interactions, optimizing drug release, and supporting personalized treatment. AI-driven DDSs utilize sensor data for intelligent dosing adjustments, refining parameters such as dosage and timing to mitigate adverse effects. AI has also accelerated the 4D printing of responsive materials that adapt to environmental changes, offering innovative applications in

DDSs. In addition, ML enhances drug discovery through virtual screening, expedites the identification of drug candidates and refines molecular targets using DL tools such as the automated hit identification and optimization tool (A-HIOT). Furthermore, ML predicts critical physicochemical properties, including solubility and permeability, reducing the number of experimental trials and guiding drug stability. These predictive capabilities extend to pharmacokinetics, enabling tailored DDSs that optimize efficacy while minimizing side effects, particularly in personalized medicine.

MLs and AI have had substantial impacts on drug discovery and DDS development. Gupta *et al.* [223] used ML and DL in virtual screening, peptide synthesis, and toxicity prediction, although they highlighted computational limits and the need for experimental integration. Wang *et al.* [224] demonstrated AI's potential in computational pharmaceuticals, applying neural networks for formulation enhancement but encountering data scarcity challenges. Castro *et al.* [225] employed ML to predict 3D printing parameters for DDSs, achieving accuracy yet requiring standardized datasets. Staszak *et al.* [226] reviewed AI in drug design, demonstrating the ability of neural networks to predict structure–activity relationships, but noted the importance of comprehensive datasets. Patel and Shah [227] reported AI-driven gains in drug discovery efficiency, although data diversity remains a constraint. Vora *et al.* [178] explored AI in drug interaction prediction, with further experimental validation suggested. Sarkar *et al.* [228] applied DL to protein structure analysis, calling for more validation to manage biological complexity. Greenberg *et al.* [229] highlighted AI's role in extracellular vesicle (EV)-based drug targeting, pointing to the need for EV standardization to manage heterogeneity. Visan *et al.* [230] emphasized AI in drug repurposing and target identification, focusing on data integration for cost efficiency but noting clinical validation requirements. Hamilton and Kingston [231] discussed AI in nanoparticle design for targeted delivery, stressing *in-vivo* validation for computational insights. Xin *et al.* [232] highlighted the potential of AI in cosmetic formulations and reported that ingredient optimization is beneficial, although further validation for multicomponent systems is needed.

Advancing DEB technologies demands a multidisciplinary approach that integrates macroscopic modeling of vascular mechanics with microscopic analyses of drug dynamics. Computational methods such as CFD and FEA enable detailed insights into blood flow patterns, drug diffusion, and arterial wall interactions, whereas MD, DFT, and MC simulations focus on molecular-scale drug behavior, structural optimization, and probabilistic variations in drug release. These methodologies, coupled with multiscale analysis, provide a comprehensive

framework for capturing the complexities of DEB performance in both physiological and clinical settings.

The incorporation of ML and AI further enhances this framework by enabling real-time predictions, optimizing drug delivery strategies, and tailoring treatments to individual patient profiles. As illustrated in Figure 3.4, these diverse modeling techniques synergistically advance the design, optimization, and clinical implementation of DEBs. Key limitations in current approaches include challenges in replicating complex *in-vivo* environments, capturing patient-specific variability, and addressing the dynamic nature of arterial wall responses. Overcoming these hurdles is essential for enhancing accuracy and clinical applicability. The next generation of DEBs aims to integrate AI-driven predictive modeling, real-time patient data, and dynamic boundary conditions, ensuring tailored and efficient interventions. This integrated approach underscores the transformative potential of computational tools in enhancing treatment efficacy and advancing precision medicine in PAD.

3.4 Discussion

3.4.1 Contextualizing Computational Modeling in DEBs

Recent advancements in computational modeling have significantly enhanced our understanding of DCBs for targeted vascular treatments, particularly in addressing peripheral and CADs. By moving from traditional 2D models to more sophisticated 3D and multilayered frameworks [233], these simulations now provide greater precision in analyzing drug diffusion, binding kinetics, and mechanical interactions within complex vascular geometries. For

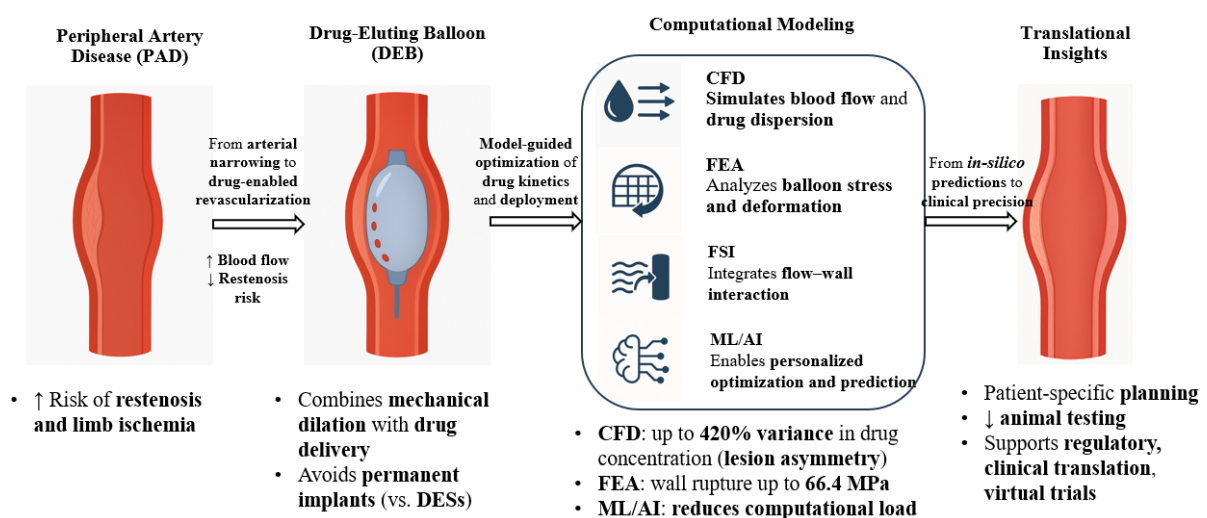


Figure 3.4 Computational Modeling Techniques for Optimizing Drug-Eluting Balloons in Peripheral Artery Disease [188, 211, 212].

example, 3D mass transport models and CDR equations capture the nuances of drug delivery across calcified and healthy tissue layers within superficial femoral arteries [186], simulating physiological conditions more accurately and predicting therapeutic outcomes more reliably.

In addition, patient-specific CFD models, calibrated with 4D flow-MRI data, offer a refined approach to capturing intricate hemodynamics in the aorta and coronary arteries [188, 212]. These models adapt boundary conditions on the basis of individual vascular profiles, thus reflecting patient-specific flow patterns and providing a basis for personalized treatment planning. Furthermore, innovations in FEA and FSI models help assess mechanical stresses and strain distributions within arterial walls, as seen in applications exploring stent performance and angioplasty treatments [211, 213]. Such analyses extend to understanding endothelial dynamic strain (EDS) metrics, which gauge the immediate impact of DCB inflation on arterial integrity, further advancing the safety and efficacy of DCB therapies. As summarized in Table 3.3, various studies have adopted computational modeling approaches to address different aspects of DCB performance, from stent simulations to drug release models and validation techniques. The diversity of methodologies underscores the versatility of computational tools in enhancing our understanding of DCB dynamics.

MD simulations and AI-driven predictive modeling also play critical roles in optimizing the drug delivery performance of DCBs. These methods enable the selection of materials, such as hydrogels and polymers, that offer controlled release properties suitable for complex environments [234]. Simulations evaluating nanoparticle and metal–organic framework (MOF) behaviors highlight their ability to target and adhere to plaque-laden regions within arteries [235]. Functionalized carbon nanotubes and MOF-based carriers, which are modeled for their interaction with vascular tissues, have the potential to improve drug retention and localization, increasing the efficiency of DCBs in achieving site-specific drug delivery [236]. The integration of AI and ML algorithms into computational modeling offers further optimization potential by rapidly identifying ideal release profiles, material combinations, and configurations tailored to the targeted disease area [231, 232]. These innovations in computational and AI-based approaches underscore the evolving role of *in-silico* methodologies in advancing DCB technologies, providing a comprehensive and robust framework for improving patient outcomes in vascular treatments.

Table 3.3 Comprehensive Analysis of Computational Modeling Approaches for Drug-Coated Balloons in the Treatment of Peripheral Artery Disease.

Refs.	Stent/Balloon Simulation	Drug Release Model	Validation
[233]	DCB for superficial femoral artery with calcified plaque	Diffusion-reaction equation for paclitaxel	Validated through comparison with clinical drug retention studies and coating retention analysis
[196]	FEA of atherosclerotic vessels	Not applicable	Validated with <i>ex-vivo</i> pressure-inflation testing on human arteries
[211]	FSI in a 3D artery under varied blood viscosities	Not applicable	Results compared for different viscosity effects on velocity, pressure, and stress on artery walls
[212]	Hemodynamic simulation in PAD	Not applicable	Reviewed existing studies with validation based on WSS and flow patterns
[188]	Focus on aorta boundary condition calibration, not specific to stents or balloons	Not applicable	Validated by comparing CFD results with clinical measurements and literature
[189]	DCB for de novo coronary lesions	Angiography-based EDS	Validated against clinical angiography data
[197]	DCB angioplasty for in-stent restenosis and PAD	Convection-diffusion-reaction equation for sirolimus release	Compared with existing models for drug concentration and retention in varied plaque compositions
[204]	DCB with hydrophilic excipients for PAD	Computational and <i>ex-vivo</i> model for paclitaxel transfer	<i>Ex-vivo</i> validation using porcine femoral arteries with SEM and LC-MS quantification
[203]	Novel PLLA bioresorbable stents with varied geometries	Not applicable	Validated by <i>in-vitro</i> mechanical testing (radial strength, and flexibility)
[213]	Stenting performance in multilayered artery with CoCr stents	Not applicable	Validated by comparing WSS values in different stent designs with clinical data
[202]	FEA of angioplasty with stent and plaque models	Not applicable	Comparison with literature-based mechanical limits and interlaminar failure criteria

3.4.2 Implications for Clinical Translation and Practice

The clinical translation of computational modeling for DCBs emphasizes critical optimization of treatment parameters, including inflation duration and vessel wall composition, to increase drug retention and efficacy [233]. Studies indicate that variations in arterial wall properties, particularly calcification levels, markedly affect drug uptake, with reduced penetration observed in calcified regions [186]. These findings support tailored DCB applications in PADs to achieve optimal drug delivery. Models also reveal that parameters such as diffusion coefficients, binding

rates, and boundary conditions can refine drug dosage and application, thereby enhancing the safety and personalization of DCB therapy.

Patient-specific CFD models provide precise hemodynamic insights, helping to identify high-risk regions, such as aneurysm-prone sites in the aorta. By enabling the visualization of flow patterns and the WSS, these models can aid clinicians in crafting individualized treatment plans on the basis of specific anatomical and flow characteristics [213]. Similarly, EDS evaluations indicate that vessel size influences DCB efficacy, with smaller vessels showing greater reductions in posttreatment strain, a crucial factor in planning DCB interventions for optimized outcomes [212].

In CAD, advances in DCB and DES technologies, including polymer-free coatings and bioresorbable scaffolds, offer the potential to mitigate restenosis and thrombosis, thus addressing long-term safety. Computational models underscore the importance of imaging data in DCB planning, as plaque characteristics, including dense calcium and necrotic cores, may hinder drug delivery. This insight promotes a more personalized approach, allowing clinicians to adapt interventions to each patient's vascular profile [211].

In addition to vascular therapy, computational insights have driven advancements in material selection and scaffold design across fields such as bone tissue engineering, dentistry, and oncology. Specific stent geometries and surface modifications have shown efficacy in optimizing drug retention and release, ensuring controlled delivery in high-stress environments and enhancing implant durability. Models also highlight the impact of the DCB coating microstructure on drug retention, with findings indicating that optimized coating aggregation improves PTX transfer [204], thereby promoting targeted and efficient drug delivery in PADs. The integration of AI further refines DCB precision, enabling rapid optimization of drug formulations, hydrogels, and surfactants for adaptive, patient-specific release profiles. AI models effectively predict and tailor release kinetics and material interactions, reducing experimental costs and facilitating more targeted drug delivery [231, 232]. As AI-driven methodologies evolve, they hold significant potential to enhance DCB design and advance personalized medicine, creating DCBs that are responsive to individual patient conditions and therapeutic requirements.

3.4.3 Challenges and Limitations in Current Computational Techniques

While computational modeling for DCBs has advanced significantly, current techniques still face notable limitations, primarily due to the need for idealized conditions that do not fully

replicate the complexity of *in-vivo* environments. Many models rely on simplified geometries and static or uniform boundary conditions, omitting critical biological factors such as dynamic blood flow, tissue interactions, and patient-specific anatomical variations [189]. For example, models using idealized two-material wall compositions or constant diffusivity assumptions may not account for the layered structure and specific morphologies of arterial walls, thus impacting their predictive accuracy [202].

High computational demands further constrain model realism, especially when incorporating detailed anatomical or patient-specific data. To manage these demands, models frequently assume rigid arterial walls or laminar blood flow, sacrificing accurate representation of complex physiological responses and interactions in dynamic vascular settings [176, 203]. Such simplifications, though necessary, limit the ability of the models to capture the full mechanical and physiological complexity of DCBs *in-vivo*.

Moreover, MD, FEA, and DFT simulations, while powerful at the molecular level, are often constrained by idealized conditions. Factors such as multilayer plaque heterogeneity, non-Newtonian blood properties [235, 237], and long-term material degradation remain underexplored, limiting the ability of these models to predict drug performance over extended periods. In addition, MD and FEA simulations often focus on short-term effects, overlooking the long-term stability critical for sustained clinical outcomes.

AI and ML offer potential for refining DCB design; however, their effectiveness relies heavily on high-quality, comprehensive datasets. Limited data availability and the challenges of generalizing across diverse biological environments restrict these models. The complexity of biological interactions demands extensive experimental validation for reliable AI predictions, as factors such as tissue variability and environmental influences introduce complexities that are difficult to model accurately *in-silico* [231, 232]. These challenges, ranging from oversimplified geometries and computational limitations to the constraints of current molecular and AI models, highlight the need for integrating multiscale models and combining computational approaches with experimental validation. Progress in capturing patient-specific variations and adapting to the dynamic *in-vivo* environment is essential to improve DCB modeling reliability and clinical applicability.

3.4.4 Future Directions for DEB Research

The future of DEB research will focus on advancing computational models to capture patient-specific characteristics and replicate complex physiological environments with greater

precision. By incorporating real-time clinical imaging data and patient-specific geometries alongside multilayered arterial models [202, 204], these simulations can account for individual anatomy, plaque heterogeneity, and structural dynamics. Multiscale modeling techniques, covering cellular to systemic responses, could deepen the understanding of DCB interactions across arterial layers, thus enhancing personalized treatment options for PAD and other conditions. Future research will also benefit from dynamic boundary conditions that reflect blood pulsatility, arterial compliance, and varied plaque compositions, allowing for more accurate predictions of drug retention, release, and uptake. Larger, diverse patient cohorts and advanced calibration algorithms are needed to better capture transient hemodynamic changes, extending the applicability of DCB simulations to a wide range of clinical scenarios [189].

Further research into biodegradable and bioresorbable materials, polymer-free coatings, and ultrathin struts could reduce adverse effects such as restenosis and inflammation [208]. Computational models can play a crucial role in simulating drug diffusion and material degradation, enabling long-term predictions of vascular responses tailored to individual needs. Continued examination of coating microstructures, balloon designs, and drug formulations will refine DCB technology, promoting more targeted drug delivery, especially in challenging cases with calcified or stenotic vessels. The incorporation of realistic flow conditions, such as non-Newtonian blood properties and pulsatile flow [211, 213], along with dynamic drug release profiles and tissue interactions, increases model accuracy. Integrating data on arterial elasticity, plaque morphology, and biochemical markers will validate and strengthen these models. The combination of computational predictions with experimental *in-vitro* and *in-vivo* validation will support the design of next-generation DCBs for tailored therapies [235].

AI and ML offer promising pathways for accelerating DCB development [231, 232]. Building extensive datasets of patient-specific variables and drug-material interactions can improve model accuracy and adaptability. Integrating AI-driven predictive models with real-time clinical data will allow DCBs to become adaptive systems that respond to specific patient variables, such as blood flow and tissue composition. This AI-driven approach can optimize DCB efficacy, minimize side effects, and significantly advance the role of DCBs in personalized medicine.

3.5 Conclusion

Advanced computational modeling and data-driven techniques are revolutionizing DEB applications in vascular interventions, enabling precision in patient-specific treatment

approaches. With the integration of multilayer arterial models and adaptive boundary conditions, simulations now capture unique plaque characteristics, drug transport dynamics, and mechanical responses in real time, thus supporting a more personalized strategy for PAD therapy. Emerging methods such as fluid–structure interaction (FSI), MD, and ML have improved our understanding of drug release mechanisms and optimized DEB performance tailored to individual patient profiles. However, current models still struggle to fully replicate *in-vivo* complexities, such as dynamic blood flow, tissue compliance, and long-term drug stability. Advancements in multiscale modeling and the incorporation of real-world clinical data will be pivotal to enhancing the clinical relevance of DEB technology. AI further facilitates this progress, enabling adaptive DEB systems that modify drug release on the basis of specific patient factors, marking a step toward truly personalized vascular treatment. As DEB technology evolves, rigorous *in-vitro* and *in-vivo* validation will be essential to ensure clinical precision and efficacy. This combination of computational innovation, AI, and clinical application represents a new paradigm in DEB research, promising for increasing therapeutic precision and improving outcomes for PAD patients and related vascular conditions.

Chapter 4: Advancing Progressive Web Applications for Medical Imaging Visualization

- 4.1. Introduction
 - 4.2. Objectives
 - 4.3. Technical Framework and Methodology
 - 4.4. Experimental Findings and Performance Analysis
 - 4.5. Qualitative and Quantitative Evaluation
 - 4.6. Discussion
 - 4.7. Contributions and Future Directions
-

4.1 Introduction

PWAs, particularly DICOM and MPR visualization, have emerged as transformative technologies in medical imaging. Traditional medical imaging solutions are typically restricted to high-performance desktop workstations, which limits accessibility and scalability. In contrast, PWAs provide a flexible, cross-platform solution that enhances the user experience through offline functionality, seamless updates, and improved performance [55]. Leveraging modern web technologies, PWAs enable efficient and accurate visualization of complex medical images, thus addressing the growing demand for remote diagnostic tools in healthcare.

The modular design architecture of PWAs plays a crucial role in enhancing medical image visualization. By utilizing React.js [238] and Cornerstone.js [239], seamless DICOM image

processing is achieved with advanced user interface components and interactive functionalities. This integration facilitates intuitive manipulation of medical images, including zooming, panning, and measurement tools, which are critical for accurate clinical analysis. The use of advanced interpolation techniques such as bicubic and weighted bilinear interpolation significantly enhances volume reconstruction accuracy and visual fidelity, ensuring that precise multiplanar views are essential for diagnostic accuracy.

Efficient data management is a cornerstone of PWA implementation in medical imaging. The use of Dexie.js for *IndexedDB* storage enables the efficient handling of large DICOM datasets directly within the browser [240], ensuring rapid image retrieval and offline access. This approach minimizes latency and enhances the user experience, particularly in clinical environments where quick access to medical images is critical. Cross-browser compatibility and responsive design are also integral to the architecture, enabling consistent performance across various platforms, including desktops, tablets, and mobile devices. Performance optimization is a key focus, with comprehensive evaluations conducted across multiple platforms and browsers, including Google Chrome, Firefox, Safari, and Microsoft Edge. The PWA demonstrates superior performance in loading times, volume rendering, and slice navigation, outperforming state-of-the-art platforms such as DicomViewer.net [241], Image-IN [242], and BlueLight [100]. Notably, Google Chrome exhibited the fastest performance across all the tested platforms, particularly for volume rendering tasks, whereas Firefox performed excellently in slice navigation. These findings highlight the importance of choosing the right browser for specific clinical tasks to optimize workflow efficiency.

Advanced MPR algorithms are implemented to achieve high-resolution image reconstructions, particularly for sagittal and coronal views. By employing a combination of bicubic and weighted bilinear interpolation, the PWA enhances edge detail and visual fidelity. This approach effectively addresses the limitations of conventional linear interpolation methods used in existing platforms, thereby improving diagnostic capabilities for complex anatomical structures. The incorporation of PWAs in medical imaging also addresses critical challenges such as cross-platform compatibility, integration capabilities, speed, and scalability. By leveraging service workers for offline functionality and advanced caching strategies, uninterrupted access to medical images can be ensured, even in low-connectivity environments. This is particularly beneficial for remote healthcare settings and telemedicine applications. Moreover, the PWA architecture is designed to integrate seamlessly with existing PACSs [243],

enhancing interoperability and facilitating streamlined workflows for radiologists and healthcare professionals.

The potential impact of PWAs on clinical practice extends beyond enhanced visualization. The ability to access high-resolution medical images on any device empowers healthcare providers with flexible diagnostic tools, reducing the dependency on specialized workstations. This contributes to improved patient care by enabling faster decision-making and facilitating collaborative consultations among medical teams across different locations. In addition, the scalability of PWAs allows for future integration with emerging technologies such as AI and ML, paving the way for advanced diagnostic analytics and predictive modeling in medical imaging. PWAs represent a significant advancement in medical imaging, particularly for DICOM and MPR visualization. Their modular architecture, efficient data management, advanced interpolation techniques, and cross-platform compatibility offer a comprehensive solution to the challenges faced by traditional desktop-based imaging systems. By delivering high-performance, accurate, and accessible medical image visualization, PWAs are poised to transform diagnostic workflows and enhance patient care in the digital era of healthcare.

4.2 Objectives

This chapter investigates the integration of DICOM and MPR visualization into web environments through PWAs, with the goal of overcoming current technology disparities and improving web-based medical imaging functionalities. By using the distinctive attributes of PWAs, including seamless offline access and improved performance, this chapter presents a holistic solution to address challenges such as cross-platform compatibility, integration capabilities, speed, and scalability. The ultimate aim was to benefit radiologists and the health care community, particularly in addressing issues related to PAD. The code of this work is available on GitHub [34].

4.3 Technical Framework and Methodology

The architectural framework and design features of our DICOM and MPR web visualizations are presented in the following sections.

4.3.1 Architectural Framework

The architectural framework of the DICOM and MPR PWA was designed with modular components to provide a seamless user experience, enabling a smooth transition from data upload to visualization. Metadata and image information play pivotal roles in retrieving crucial

details such as transfer syntax, service-object pair classes and instances [244], pixel representations, planar configurations, viewer elements, and image loading. As shown in Figure 4.1, the design encompasses several key modules that work together to facilitate efficient DICOM image handling and MPR. The DICOM image loading (step 1) module is responsible for parsing DICOM files via the Cornerstone library, which includes the *dicomParser* tool. This process extracts metadata and image data from DICOM files, storing them locally in Dexie.js to ensure that the images are prepared and ready for visualization and manipulation within the application. In contrast, the web integration (step 7) module focuses on integrating DICOM data with the broader web environment. This includes functionalities for uploading and downloading DICOM datasets, allowing users to interact with remote DICOM stores. Dexie.js manages the storage and retrieval of data during these interactions. The key distinction between steps 1 and 7 lies in their scope—step 1 handles the initial parsing and local loading of DICOM images, whereas step 7 manages the integration of these images into a web-based workflow, encompassing data transfer operations between the client and server. The DICOM viewer (step 2), tool integration (step 3), and MPR (step 4) modules further enhance the application by providing React.js components for the user interface, integrating Cornerstone tools for image manipulation, and implementing algorithms for orthogonal plane reconstructions, respectively.

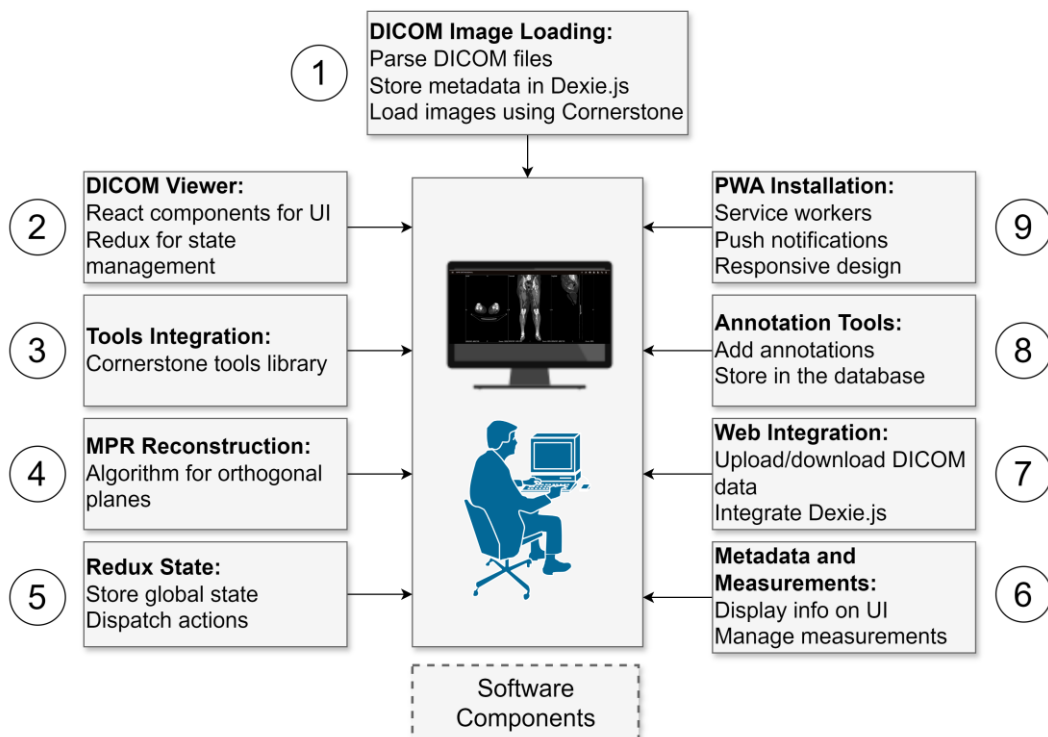


Figure 4.1 Pipeline Architecture of DICOM and Multiplanar Reconstruction Visualization as a Progressive Web Application.

Both frameworks, Cornerstone.js and React.js, improve performance but face limitations, particularly with complex state management and ensuring cross-platform compatibility. The Redux state (step 5) module is used for global state management, ensuring consistent state handling across the application. Additional features include metadata and measurements (step 6), which manage the display of crucial image information and measurements, and PWA installation (step 9), which enables offline access and enhances performance.

The DICOM web application integration functions play an instrumental role in establishing connectivity to the DICOM store, facilitating the search and loading of specific studies, and retrieving DICOM instances for detailed analysis. Leveraging the PWA approach, seamless DICOM stores connectivity; focused study examination; and web-based viewer controls for zooming, moving or panning, and resetting are ensured by the application. The functionality of reference lines and planes is tailored to create reference lines for aligning and comparing DICOM images within the MPR views [245]. This involves the construction of 3D lines and planes to represent spatial relationships, as well as the coordination of transformations for converting 3D perspectives into 2D images. DICOM viewer rendering within the PWA is achieved through the setting of DICOM image references, handling image clicks, identifying localizer images, and synchronizing DICOM slices [246, 247].

4.3.2 Multiplanar reconstruction algorithm

In the MPR from CT DICOM images, the integration of bicubic interpolation and weighted bilinear interpolation plays a significant role in improving the accuracy and visual fidelity of the reconstructed volumes. Bicubic interpolation, which uses a smooth and differentiable interpolation function across a 4×4 grid, proves valuable in addressing edge cases and delivering high-quality reconstructions [248]. The overall interpolation process benefits from the straightforward cubic interpolation method, which contributes to computational efficiency while maintaining a satisfactory level of smoothness in the interpolated values [249]. In addition, a balance between simplicity and effectiveness is achieved through the application of weighted bilinear interpolation for nonedge pixels. This technique combines the weighted contributions of neighboring pixels, facilitating the generation of interpolated values, which are crucial in constructing detailed and coherent representations of volume from DICOM images. The integration of these interpolation methods enhances the robustness and accuracy of the MPR, ultimately improving the diagnostic capabilities of the reconstructed volumetric data in the field of peripheral arterial diagnosis.

4.3.2.1 Weighted Bilinear Interpolation for Nonedge Pixels

Weighted bilinear interpolation is applied to non-edge pixels for the generation of interpolated planes between original planes in a volumetric dataset. Given an interpolation weight w derived from the relative position of the target pixel within the interpolation interval, the value of an interpolated pixel $P(k)$ at position k is calculated via a weighted average of its neighboring pixels in the original planes [250]. The interpolation considers the direct neighbor pixels along the same axis in both the current and the next interval planes. The weighting factors for the neighbors are adjusted to account for the distance from the interpolated position, emphasizing closer neighbors more significantly. For a non-edge pixel k located at a position where $k - 1 > 0$ and $k + 1 < \text{length}$, the interpolated pixel value $P(k)$ is given as follows [251, 252]:

$$P(k) = P_i(k) + P_{i+1}(k), \quad (4.1)$$

$$\begin{aligned} P_i(k) = & (V_i[k] \times (1 - w) \times 0.5 + \\ & V_i[k - 1] \times (1 - w) \times 0.25 + \\ & V_i[k + 1] \times (1 - w) \times 0.25), \end{aligned} \quad (4.2)$$

$$\begin{aligned} P_{i+1}(k) = & (V_{i+1}[k] \times w \times 0.5 + \\ & V_{i+1}[k - 1] \times w \times 0.25 + \\ & V_{i+1}[k + 1] \times w \times 0.25), \end{aligned} \quad (4.3)$$

where $V_i[k]$ denotes the value of pixel k in the original plane at interval i and where $V_{i+1}[k]$ is the value of pixel k in the next original plane at interval $i + 1$. For edge cases, where $k - 1 < 0$ or $k + 1 \geq \text{in length}$, the interpolation simplifies the prioritization of available neighboring pixels, reducing the weighting factors to 0.75 for the pixel itself and 0.25 for the available neighbor, accordingly adjusted by the interpolation weight.

4.3.2.2 Bicubic Interpolation

Bicubic interpolation extends cubic interpolation to two dimensions, providing a smooth and continuous interpolation function. Given an 4×4 grid of data points P_{ij} and two interpolation parameters u and v , the bicubic interpolation equation is as follows [248, 253]:

$$P(k, v) = \sum_{i=0}^3 \sum_{j=0}^3 a_{ij} u^i v^j, \quad (4.4)$$

The coefficients a_{ij} are determined on the basis of the values of P_{ij} and their partial derivatives. Bicubic interpolation is commonly used for reconstructing detailed and high-resolution images from CT DICOM slices. These interpolation methods are fundamental in the reconstruction process, contributing to the accurate representation of CT DICOM images in MPRs. The MPR protocol is structured as shown in Figure 4.2 to ensure comprehensive reconstruction of volumetric data from DICOM slices [100].

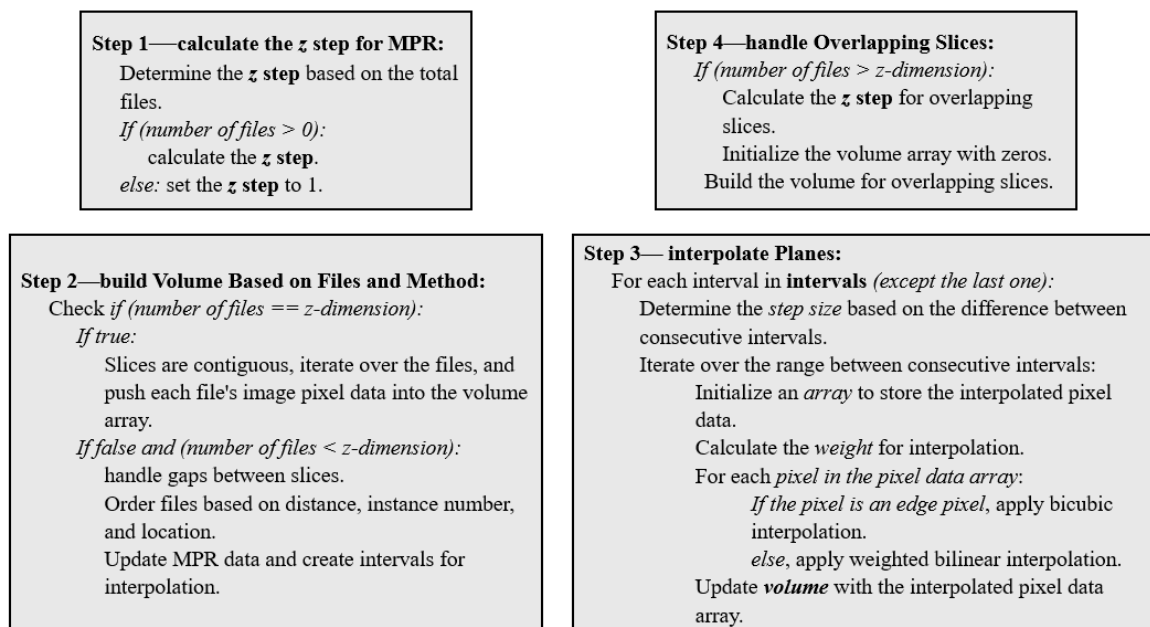


Figure 4.2 Multiplanar Reconstruction Protocol for Volumetric Data from DICOM Slices.

The design involves calculating the z step for the MPR, building a volume on the basis of files and method specifications, interpolating planes, and handling overlapping slices. In the calculation of the z step for the MPR, the protocol determines the z step on the basis of the total files and specified MPR dimensions, handling cases where the number of files is zero. The volume is contingent on whether the number of files matches the specified z -dimension. The protocol processes contiguous slices and handles gaps between slices, ordering files on the basis of distance, instance number, and location. Interpolating planes involves determining step sizes, iterating over intervals, and applying bicubic or weighted bilinear interpolation on the basis of pixel characteristics. The protocol addresses overlapping slices by calculating the z step for overlapping slices and selectively building the volume. This comprehensive protocol ensures

effective MPR, facilitating nuanced analysis of volumetric data from DICOM slices in medical imaging.

4.3.3 Application Implementation

a) Technology Stack

The DICOM and MPR web application is implemented as a PWA, leveraging the capabilities of React.js and Cornerstone.js [254].

b) PWA Implementation

PWAs offer a seamless and responsive user experience across various devices and platforms. DICOM and MPR web applications use the power of PWA, ensuring accessibility to different browsers and providing users with the ability to install the application on their devices [255].

c) Front-End Framework

React serves as the foundational front-end library for DICOM and MPR web implementation. Its component-based architecture facilitates the modular design of the application, enabling efficient updates and rendering of DICOM images. The React declarative approach enhances the predictability of the user interface, contributing to a smooth user experience [256].

d) DICOM image processing

Cornerstone.js, a robust JavaScript library designed for medical imaging, plays a pivotal role in DICOM image rendering and analysis within the proposed application. Cornerstone.js seamlessly integrates with React, providing a suite of tools tailored for DICOM image analysis, as shown in Table 4.1.

e) Data Storage

Dexie is a JavaScript library that simplifies interaction with IndexedDB. IndexedDB is used as a low-level data storage application programming interface, enabling the storage and retrieval of large amounts of data in the browser. Dexie provides a concise application programming interface that streamlines data management processes, contributing to a more intuitive developer experience [257].

f) Cross-Browser Compatibility and Platform Accessibility

DICOM and MPR visualization, built via PWA principles, ensure cross-browser compatibility, making the application accessible on various browsers, including Google Chrome, Firefox, Safari, and Microsoft Edge. The application’s responsive design guarantees optimal performance across different platforms, including desktops, tablets, and mobile devices [258].

The integration of React, Cornerstone.js, and Dexie empowers the development of DICOM- and MPR-based PWA with a robust foundation, advanced DICOM image analysis tools, and efficient data management capabilities. The adherence to PWA principles further extends the application’s accessibility and user engagement across diverse environments.

Table 4.1 DICOM image annotation and measurement tools and their functions.

DICOM Tool	Function
Length Tool	Allows measurement of distances on DICOM images
Pan Tool	Enables users to pan across DICOM images for detailed examination
Magnify Tool	Provides magnification capabilities for closer inspection of image details
Angle Tool	Facilitates angle measurements for anatomical analysis
Rectangle ROI Tool	Allows the creation of rectangular Regions of Interest (ROIs) on DICOM images
WWWC (Window Width and Window Center) Tool	Enables adjustment of the window width and window center for optimal image visualization
Zoom Touch Pinch Tool	Supports touch-based zooming gestures for enhanced user interaction
Probe Tool	Provides pixel value information at specific points on DICOM images
Elliptical ROI Tool	Allows the creation of elliptical Regions of Interest (ROIs) for focused analysis
Freehand ROI Tool	Enables the creation of freehand Regions of Interest (ROIs) on DICOM images
Stack Scroll Mouse Wheel Tool	Facilitates smooth scrolling through DICOM image stacks, enhancing the user's ability to navigate volumetric data

4.4 Experimental Findings and Performance Analysis

Detailed findings from 2 experiments on the DICOM-based PWA for medical image visualization and reconstruction are provided in this section. The key aspects include performance evaluation across platforms, dataset characteristics, computer specifications, and testing metrics. The experimental findings highlight various browser performances on different platforms for loading, volume rendering, and tool execution in local area network (LAN) and wide area network (WAN) environments, emphasizing Chrome’s (Google LLC) superiority in loading and rendering, whereas Firefox (Mozilla Foundation) excelled in viewing slices.

4.4.1 Experimental Design

In the experimental design phase, our application assisted radiologists in connecting to upload medical images seamlessly from local devices. The upload options included single files, folders, or links containing DICOM images. Once uploaded, our application provided a variety of essential tools for data access, annotation and measurements, image processing, and MPR, ensuring a comprehensive environment for image manipulation within a web browser. To assess the effectiveness of the DICOM- and MPR-based PWA for medical image visualization and reconstruction, 2 distinct experiments were performed. The first experiment aimed to gauge the application's performance across multiple platforms, ensuring compatibility and optimal functionality.

The second experiment was designed to evaluate the application's performance under controlled network conditions. Specifically, tests were conducted within an LAN to minimize the effect of internet variability, ensuring consistent bandwidth and reduced latency. This approach provided a stable environment for accurately assessing the software's inherent performance, whereas comparisons were also made under WAN settings to understand the impact of broader network conditions.

The dataset provided by the University of Athens was used to evaluate the performance of this work on different platforms and browsers. Each dataset series is characterized by its unique dimensions, which vary between $512 \times 512 \times 258$ pixels and $512 \times 512 \times 577$ pixels and represent the width, height, and depth of the CT scans. The dataset series sizes range from 128 to 290 MB. In addition, the dataset exhibits variability in slice thickness, spacing between slices, and pixel spacing, with values of 5.0, 0.976562, and 0.775391 mm, respectively. These details elucidate the characteristics of the dataset, providing a comprehensive understanding of its diversity, which is crucial for the thorough evaluation of the work across different platforms and browsers. A comprehensive overview of the dataset series is presented in Table 4.2, whereas details about the computers used in the experiments are shown in Table 4.3. Notably, the computers used were standard laptops accessible to regular users. React and PWAs are supported by all major browsers, including Firefox (version 125.0.3), Google Chrome (version 125.0.6422.78), Safari (Apple Inc), internet Explorer (Microsoft Corp), and Microsoft Edge (version 125.0.2535.67; Microsoft Corp).

Table 4.2 Characteristics of the computed tomography dataset for peripheral artery patients used in the evaluation.

Patient	Dimensions (pixels)	Size (MB)	Slice thickness (mm)	Spacing between slices (mm)	Pixel spacing (mm)
1	512 × 512 × 377	189	3.75	3.75	0.935547
2	512 × 512 × 274	138	3.75	3.75	0.960938
3	512 × 512 × 386	194	3.75	3.75	0.976562
4	512 × 512 × 531	267	2.5	2.5	0.841797
5	512 × 512 × 384	193	3.75	3.75	0.955078
6	512 × 512 × 258	130	5.0	0	0.8984375
7	512 × 512 × 577	290	2.5	2.5	0.912109
8	512 × 512 × 334	168	3.75	3.75	0.976562
9	512 × 512 × 350	176	3.75	3.75	0.976562
10	512 × 512 × 340	171	3.75	3.75	0.949219
11	512 × 512 × 352	177	3.75	3.75	0.888672
12	512 × 512 × 377	189	3.75	3.75	0.976562
13	512 × 512 × 277	139	5.0	5.0	0.976562
14	512 × 512 × 310	156	3.75	3.75	0.925781
15	512 × 512 × 255	128	5.0	5.0	0.976562
16	512 × 512 × 346	174	3.75	3.75	0.925781
17	512 × 512 × 374	188	3.75	3.75	0.902344
18	512 × 512 × 269	135	0.625	5.0	0.976562
19	512 × 512 × 298	150	3.75	3.75	0.939453
20	512 × 512 × 316	159	3.75	3.75	0.976562
21	512 × 512 × 341	171	3.75	3.75	0.896484
22	512 × 512 × 310	156	3.75	3.75	0.775391

Table 4.3 Computer specifications used in the experiments.

Computer	Type	Operation system	CPU	Memory	GPU
1	Laptop	Windows 11 Pro 64-bit	11th Gen Intel(R) Core (TM) i7-11800H @ 2.30 GHz, 16 cores	16 GB	NVIDIA GeForce RTX 3070
2	Laptop	Ubuntu 22.04.3 LTS	11th Gen Intel(R) Core (TM) i7-11800H @ 2.30 GHz, 16 cores	16 GB	NVIDIA GeForce RTX 3070
3	Laptop	Mac OS Sonoma 14	11th Gen Intel(R) Core (TM) i7-11800H @ 2.30 GHz, 4 cores	8 GB	NVIDIA GeForce RTX 3070
4	Tablet	Android 5.0.2 (Lollipop)	Quad-core 1.2 GHz Cortex-A7	1.5 GB	Adreno 305

The performance evaluation of the proposed system included several key metrics, as detailed in Table 4.4, which are essential for ensuring its clinical viability. T1 represents the performance time for loading a medical image dataset, assessing the time required to load an entire DICOM dataset into the application.

Table 4.4 Performance Metric Details.

Function	Label	Description	Measurement
Data access	T1	Performance time for loading a medical image dataset	Measured by JavaScript code
	T2	Performance time to build a medical image volume using Multiplanar Reconstruction (MPR) techniques	Measured by JavaScript code
	T3	Performance time for viewing a slice in a medical image dataset while scrolling	Measured by JavaScript code
Annotation and measurements tools	T4	Performance time for the following tools: 'Wwwc', 'Pan', 'Zoom', 'Length', 'Probe', 'EllipticalRoi', 'RectangleRoi', 'Angle', 'Magnify', and 'FreehandRoi' per slice	Measured by JavaScript code
Image processing	T5	Performance time for invert tool per slice	Measured by JavaScript code

This metric was selected because of the critical need for rapid image access in clinical settings, where delays could hinder diagnostic workflow efficiency. T2 evaluates the performance time to build a medical image volume via the MPR technique, reflecting the time necessary to reconstruct 3D volumes from 2D slices. This is crucial for providing clinicians with timely and accurate 3D representations, which are often essential for diagnostic and surgical planning. T3 monitors the performance time for viewing a slice while scrolling through a medical image dataset, a vital metric for ensuring that radiologists can efficiently navigate through large datasets to identify relevant anatomical structures. T4 focuses on the performance time for annotation and measurement tools per slice, which include tools such as “Wwwc,” “Pan,” “Zoom” and region-of-interest tools. The efficiency of these tools is directly linked to the accuracy and speed of clinical assessments. Finally, T5 measures the performance time for image processing tools, specifically the inverted tool per slice, which is essential for enhancing contrast and improving the visibility of subtle pathologies, thus assisting in more accurate diagnoses. By minimizing waiting times and enabling faster decision-making, these metrics directly correlate with the clinical efficiency and reliability of the application, ensuring that it meets the demands of medical professionals in real-world settings.

4.4.2 Performance across Multiple Platforms

In the initial experiment, we used a dataset of 22 patients via LAN to assess the application’s performance on various platforms. Our application was tested on computers running Windows, Linux, and macOS, each function was executed 5 times with different browsers, and the averages were calculated. Table 4.5 presents the average performance for each function across the entire dataset of 22 patients.

Table 4.5 Performance metrics for the proposed application across platforms, browsers, and modes (private and ordinary).

Platform	Windows				Linux		macOS		
	Google Chrome (s)	Microsoft Edge (s)	Firefox (s)	Internet Explorer (s)	Google Chrome (s)	Firefox (s)	Google Chrome (s)	Firefox (s)	Safari (s)
Private									
AT-T1 (LAN)	0.778	0.826	0.874	0.958	—	—	—	—	—
AT-T2 (LAN)	5.157	5.03	6.306	5.276	—	—	—	—	—
Ordinary									
AT-T1 (LAN)	1.036	1.22	0.89	1.305	1.101	6.45	4.434	5.736	6.443
AT-T2 (LAN)	5.215	5.344	6.33	5.277	5.06	6.664	7.69	9.26	19.559
AT-T1 (WAN)	1.212	1.119	0.842	1.263	1.412	5.914	4.823	5.388	5.943
AT-T2 (WAN)	5.068	5.202	6.478	5.39	5.175	6.277	7.276	9.057	19.6
AT-T3 (WAN)	0.00175	0.00188	0.0014	0.0019	0.00177	0.00168	0.00217	0.0015	0.00357
AT-T4 (WAN)	0.000155	0.00013	0.0005	0.00015	0.000135	0.0005	0.000155	0.0012	0.0006

4.4.2.1 Private Mode Impact on Loading (T1) and Volume Rendering (T2)

The private mode generally contributed to faster loading times (T1) across browsers. The impact on volume rendering times (T2) varied, with some browsers showing minor improvements in private mode. These findings provide insights for users seeking optimal performance during medical image visualization and reconstruction.

4.4.2.2 Performance evaluation on Windows, Linux, and macOS on the LAN and WAN

With respect to T1 loading, Google Chrome demonstrated superior performance on Windows (1.036 seconds), Linux (1.101 seconds), and macOS (4.434 seconds), whereas Firefox showed competitive performance on Windows at 0.89 seconds. With respect to T2 volume rendering, Google Chrome consistently outperformed other browsers on all platforms, with the shortest

times on Windows (5.215 s), Linux (5.06 s), and MacOS (7.69 s). Firefox demonstrated a competitive time of 6.33-second viewing slices on Windows in a medical image dataset while scrolling (T3). Firefox outperformed other browsers across all platforms in terms of scrolling performance within the medical image dataset (T3), achieving the fastest times on Windows (0.0014 s), Linux (0.00168 s), and Mac (0.0015 s).

With respect to T4 tool performance per slice, Google Chrome and Microsoft Edge on Windows exhibited the fastest times at 0.000155 and 0.00013 seconds, respectively. Google Chrome on Linux and macOS demonstrated efficiencies of 0.000135 and 0.000155 s, respectively. Google Chrome exhibited superior performance for T1 loading and T2 volume rendering, whereas Firefox outperformed T3, and Google Chrome or Microsoft Edge led in the execution of T4 tools per slice across different platforms in an LAN environment. In a WAN environment, for T1 loading, Google Chrome exhibited efficient performance across all platforms, with the shortest times on Windows (1.212 s), Linux (1.412 s), and MacOS (4.823 s). Firefox showed competitive performance on Windows, with 0.842 seconds. With respect to T2 volume rendering, Google Chrome consistently outperformed other browsers on all platforms, with the shortest times on Windows (5.068 seconds), Linux (5.175 seconds), and MacOS (7.276 seconds). Google Chrome demonstrated superior performance for both T1 loading and T2 volume rendering across Windows, Linux, and MacOS platforms in a WAN environment.

The experiments demonstrated that the performance time for 2D image processing, specifically for the inverted tool per slice (T5), consistently remained significantly at <1 second across all the computers. This finding leads to the conclusion that the application exhibits real-time performance capabilities for all the provided 2D tools, indicating its efficiency and responsiveness in handling the DICOM peripheral artery dataset.

4.5 Qualitative and Quantitative Evaluation

The proposed application, which focuses on the accuracy of MPR for both coronal and sagittal views, was evaluated by a board-certified medical doctor and surgeon with experience in the evaluation of CT images. This assessment used both qualitative and quantitative methods to ensure a comprehensive analysis of the application's performance in medicine through the random selection of some dataset series, as shown in Table 4.2. The measurements were conducted manually via the tools of our application. Bone structures were selected for measurements because of the high edge contrast of bones, which provides clearly visible edges for placing measurement points. Care was taken to ensure that the measurements corresponded

to the same structure, position, and plane across all 3 views: axial, coronal, and sagittal. In the axial view, which represents the data source, the structure is measured along 2 axes that represent the coronal and sagittal planes of that structure and are compared with the measurements of the same structure in the reconstructed coronal and sagittal planes. The measurement points were placed on the edges of the structures via the mouse cursor in a magnified view of the structure, ensuring that the pixels representing the exact edge were selected.

For the dataset series of Patient 1, the distal edge of the L1 vertebra was chosen as a measurement point. For the dataset series of Patient 2, the measurement focused on the distal head of the femur bone. Measurements for the dataset series of patients 3, 4, 10, and 20 were performed on the body of the femur bone. The results demonstrated consistent accuracy in the measurements of the reconstructions compared with the ground truth images across all the examined dataset, as shown in Figure 4.3. The error margin was computed by comparing the coronal and sagittal measurements (measured values, M) to the axial view (ground truth, G). The error for each measurement was calculated as follows:

$$error\ margin = \frac{1}{n} \sum_n^1 |M_i - G_i|, \quad (4.5)$$

where n represents the total number of measurements. M_i refers to the i – th measured value (in the coronal or sagittal view), and G_i refers to the corresponding ground truth value (from the axial view) at the same measurement point. The subscript i indexes each measurement point, running from 1 to n . This formula provides the average error per measurement. Across the dataset, the measurements consistently fell within an accepted error margin of less than 0.05 mm, which was attributed primarily to the inherent limitations of manual measurement methods, such as the placement of measurement points via the mouse cursor.

To further assess the accuracy of the MPR reconstructions, a comparative analysis was conducted via 3D Slicer (version 5.6.2; the Slicer Community) [259] on the same dataset series of Patient 1, as shown in (Supplementary Figure 1). The distal edge of the L1 vertebra was identified across all planes (axial, coronal, and sagittal) via a similar methodology. Measurements were performed via the native tool in 3D Slicer, where the markers were manually placed via the mouse pointer.

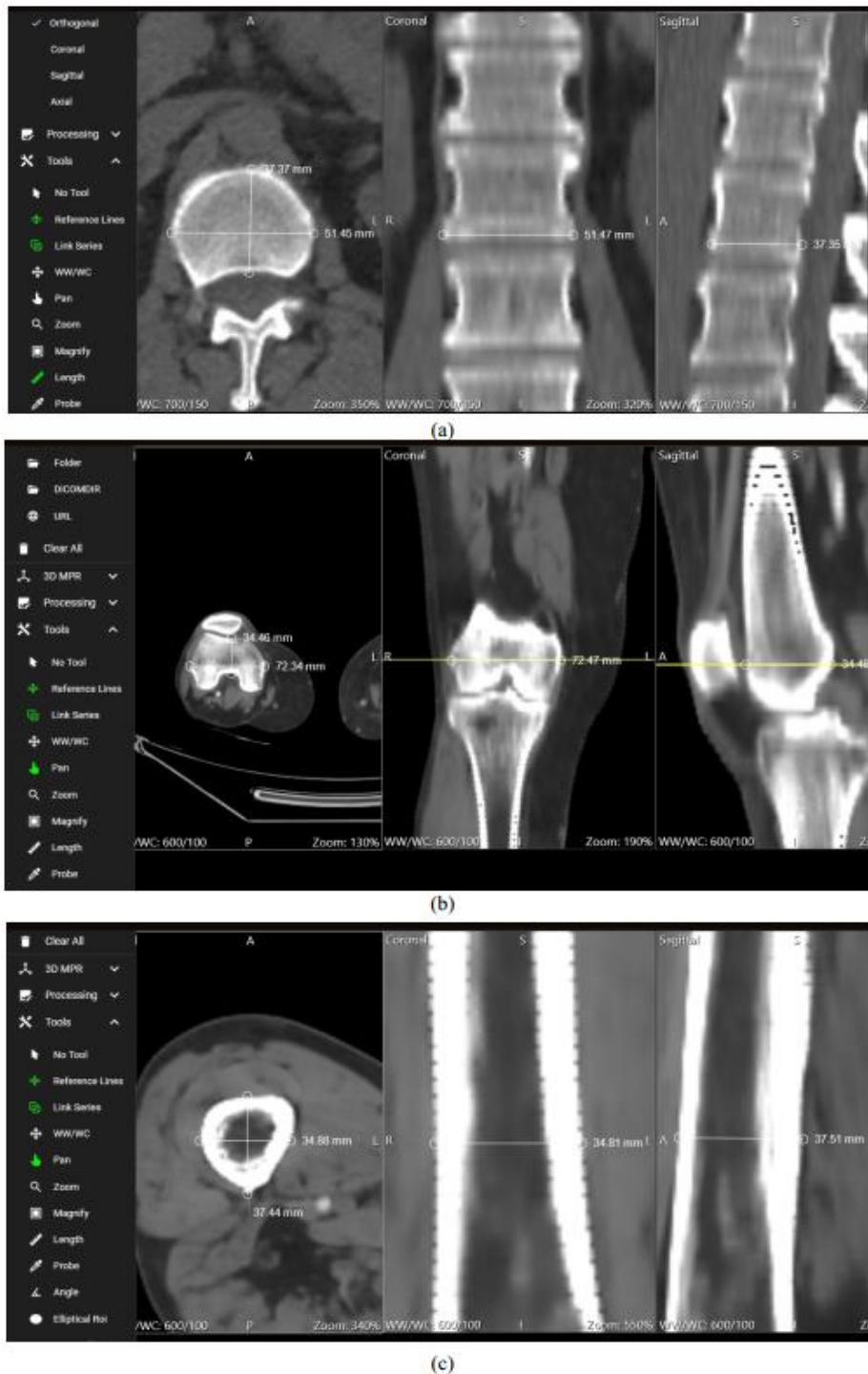


Figure 4.3 Clinical evaluation of multiplanar reconstruction accuracy, (A) measurement accuracy of the distal edge of the L1 vertebra in the dataset series of patient 1, (B) consistency in measuring the distal head of the femur bone in the dataset series of patient 2, and (C) consistency of reference lines across multiple planes for the dataset series of patient 3.

Measurements were first taken in the axial plane and then repeated in the coronal and sagittal planes. The measurements in the axial plane via 3D Slicer were nearly identical to those

obtained via the proposed PWA. Similarly, the measurements in the coronal and sagittal planes were consistent with both the axial plane results and the measurements obtained from the proposed PWA. As in the proposed PWA, the manual process of placing the cursor at the perceived edge of the structure introduced small variations (<0.5 mm) between measurements. These differences were attributed to the sensitivity of the mouse cursor positioning and the inherent limitations of manual measurement. The consistent appearance of this error margin in both the proposed PWA and 3D Slicer indicates that it is due to the manual measurement process. The findings of the evaluation indicate the ability of our application to deliver both qualitative and quantitative benefits in medicine. By offering precise measurements and consistent reference lines across various planes, the application represents a valuable tool for medical professionals.

4.6 Discussion

4.6.1 Principal Findings

The key contribution of this chapter lies in addressing the gap in the adoption of PWAs for DICOM and MPR visualization on the web. This chapter highlights the unique challenges in web-based medical imaging, such as cross-platform compatibility, integration capabilities, speed, and scalability. Specifically, focusing on the incorporation of DICOM visualization into web settings via PWAs, this chapter aims to provide a comprehensive and effective solution to enhance the functionality and efficacy of medical imaging applications in the digital era.

A significant finding of this chapter is the varying performance of the PWA across different browsers and platforms, which has direct implications for its deployment in clinical settings. Google Chrome outperforms other browsers in terms of loading times (T1) and volume reconstruction efficiency (T2), particularly on Windows and Linux, owing to its efficient V8 JavaScript engine. Firefox demonstrated strong performance in slice scrolling (T3) but exhibited slower (T2) performance on macOS, likely due to differences in memory management. Safari and Microsoft Edge lagged behind in T1 and T2, especially on macOS, with Safari showing the slowest performance.

These observations underscore the challenges of ensuring cross-platform consistency, with macOS generally showing a slower performance, particularly for T2. Given these findings, Google Chrome or Firefox on Windows is recommended for optimal performance, particularly in environments requiring rapid data access and processing. This chapter also highlights the importance of selecting the appropriate browser on the basis of the specific clinical setting, as

performance can vary significantly depending on the browser and platform used. This insight is critical for health care providers aiming to implement PWAs in their medical imaging workflows.

Furthermore, this chapter emphasizes the significance of uninterrupted offline access, enhanced performance, and improved user experience as distinctive characteristics of PWAs relevant to web-based DICOM applications. By doing so, this chapter aimed to overcome the identified technological hurdles and contribute to the advancement of web-based medical imaging applications. The choice of DICOM as the focus further solidifies the relevance of this chapter in the medical imaging domain, where standardization and interoperability are crucial.

In addition, this chapter contributes to the literature by addressing another challenge in the field of medical imaging applications, namely, the lack of an effective method for addressing variables inherent to web applications. The emphasis on cross-platform compatibility, integration capabilities, speed, and scalability underscores the commitment to providing a holistic solution that goes beyond DICOM and MPR visualization.

The discussion on MPR for medical image visualization adds depth to the contribution. The challenges related to generating high-resolution images on the internet and visualizing volumetric structures, especially sagittal and coronal views obtained from DICOM slices, are acknowledged. This chapter clarifies and addresses these issues, aiming to enhance web-based medical imaging capabilities, particularly in the field of peripheral artery imaging.

The MPR algorithm proposed in this chapter uses bicubic and weighted bilinear interpolation, which enhances edge detail, particularly in scenarios in which certain resolutions may result in missing intermediate points. This approach differs from conventional implementations such as XTK.js and VTK.js [30], which primarily use linear interpolation to prioritize computational efficiency. XTK.js adopts linear interpolation to balance smoothness and performance, whereas VTK.js supports multiple interpolation methods, including nearest neighbor and cubic methods.

The detailed description of the application's architectural framework, the implementation via React and Cornerstone.js, and the experimental results on multiple platforms provide practical insights into the feasibility and effectiveness of the proposed solution. The study's systematic approach, from design to implementation and evaluation, strengthens its contribution and applicability in real-world medical imaging scenarios.

4.6.2 Limitations

This chapter focused on peripheral artery CT imaging for 22 patients and used a single dataset type. This dataset limitation may affect how broadly our findings can be applied to different medical imaging scenarios. Moreover, the application's dependency on specific interpolation techniques for 3D reconstruction could limit its flexibility and efficiency in processing various types of medical imaging data. In addition, the application is designed to handle only DICOM formats, which may restrict its utility with other imaging formats prevalent in medicine. Furthermore, using vascular structures as reference points for comparing axial and reconstructed sagittal and coronal planes in the MPR can be challenging because of the uniformity of vascular structures, which often lack distinctive landmarks. This leads to inconsistencies in automatically produced reference lines and requires anatomical expertise for accurate validation.

4.6.3 Comparison With Prior Work

A comprehensive test of our application was conducted using 2 distinct series from the same dataset, representing extremes in size. These series correspond to patients 2 and 17, as listed in Table 4.2. The dataset for Patient 2 serves as a compact representation with dimensions of $512 \times 512 \times 5$ pixels and a size of 2.51 MB, exemplifying the lower end of the size spectrum. Conversely, the dataset for Patient 17 represents a substantial CT series with dimensions of $512 \times 512 \times 2339$ pixels, occupying 1.10 GB, highlighting the challenges associated with handling voluminous medical image data. These series vary significantly in slice thickness, spacing between slices, and pixel spacing, ensuring a thorough evaluation of the application's performance across diverse dataset sizes.

Highlighting the limitations encountered in the compared platforms, our work stands out as an innovative solution, as evidenced by the comprehensive performance analyses presented in Tables 4.5 and 4.6. To address compatibility concerns, our application surpassed competitors such as DicomViewer.net (version 3.2) [241], Image-IN (accessed February 2024) [242], BlueLight (accessed February 2024) [100], and VolView (accessed September 2024) [260]. DicomViewer.net, developed as an open-source project under the Open Health Imaging Foundation, is compatible with Google Chrome, Firefox, Safari, and Microsoft Edge and faces cross-browser compatibility issues on Firefox for macOS when dealing with both low- and large-size dataset series. Simultaneously, Image-IN, a web-based 3D visualizer for multidimensional DICOM microscopy images, encounters performance challenges on mobile

devices, particularly iPads, leading to suboptimal performance and browser crashes with large dataset series. BlueLight is an open-source DICOM viewer with a low-cost computation algorithm but lacks security and maintenance considerations.

In addition, the performance evaluation focused primarily on desktop browsers, and the compatibility and performance of mobile browsers or devices remain unclear. Addressing these limitations and conducting comprehensive evaluations across various platforms and scenarios would enhance the applicability and robustness of our proposed solution in real-world medical imaging contexts.

Table 4.5 shows that our application was significantly superior to DicomViewer.net, Image-IN, BlueLight, and VolView in terms of both loading times and reconstruction efficiency across various configurations. For example, when considering a low-size dataset series of 2.51 MB on Windows with Google Chrome, our application resulted in loading times (T1) and reconstruction times (T2) that were 63% to 85% faster than those of the competing platforms. Specifically, with Google Chrome on Windows, our application achieved a combined metric (T1+T2) of 0.374 seconds, whereas DicomViewer.net, Image-IN, BlueLight, and VolView experienced crashes or failures (shown as “x” in the table). Furthermore, when tested on a tablet, the proposed application outperformed the state-of-the-art methods by maintaining robust performance, whereas DicomViewer.net failed to build the MPR, and both Image-IN and VolView were unable to upload and build the MPR. This reinforces the scalability and versatility of the proposed software across different device types. Table 4.6 shows that our application continues to outperform DicomViewer.net, Image-IN, BlueLight, and VolView by a significant margin in the analysis of large-size data of 1.10 GB, ranging from 84% to 98%.

For example, when running on Linux with Google Chrome, our application achieved loading and reconstruction times that were notably faster than those of the competitors. However, BlueLight encountered issues and stopped at slice 1750 and at slice 520 for Linux on Google Chrome and Firefox, respectively. This suggests potential limitations in BlueLight’s ability to handle large dataset series, highlighting the robustness and scalability of our application. Similarly, VolView encounters a range error when processing a large dataset. Compared with DicomViewer.net, Image-IN, BlueLight, and VolView, our application consistently outperforms DicomViewer.net in terms of loading time and reconstruction efficiency, establishing it as a leading solution in medical image web visualization. The comparison reveals our application’s reliability and effectiveness in addressing the challenges encountered by

existing platforms, making it a compelling choice for medical image visualization tasks. On the basis of the findings presented in Table 4.5, the average number of DICOM slices used for evaluating the application is 347. This evaluation was conducted within an LAN environment on a Windows platform.

The combined performance time (T_1+T_2) ranged from 6.251 seconds when Google Chrome was used to 6.564 seconds with Microsoft Edge and 7.22 seconds with Firefox. In contrast, BlueLight, as reported in its corresponding study, uses 280 DICOM slices for evaluation. Comparative analysis revealed that our application consistently exhibited shorter combined performance times across all the browsers, with durations of 8.91 seconds (Google Chrome), 9.15 seconds (Microsoft Edge), and 16.27 seconds (Firefox). Furthermore, as shown in Figure 4.4A, our proposed MPR algorithm leverages bicubic interpolation for edge pixels and weighted bilinear interpolation for nonedge pixels. This approach yielded favorable reconstruction results, particularly for edge pixels, compared with the MPR results produced by BlueLight, as illustrated in Figure 4.4B. These results underscore the superior performance of our application in loading medical image datasets and executing MPR techniques compared with BlueLight, thereby highlighting the efficiency and effectiveness of our application in processing medical image datasets and positioning it as a more dependable option for medical image visualization.

Table 4.6 Comparison of the proposed application performances over the LAN with others, (Low-size data).

Dataset	OS/Tablet	Browser	Proposed software			DicomViewer.net [241]		Image-IN [242]	BlueLight [100]		VolView [260]
			T1	T2	T1+T2	T1	T2	T1+T2	T1	T2	T1+T2
# 2	Win	Chrome	0.285	0.088	0.374	0.629	x	1.63	0.448	0.325	1.586
		Firefox	0.103	0.101	0.204	0.393	x	1.404	0.366	0.281	1.89
	Linux	Chrome	0.125	0.095	0.22	0.45	x	1.869	0.388	0.305	1.262
		Firefox	0.16	0.107	0.267	0.605	x	2.523	0.354	0.316	1.57
	Mac	Chrome	0.228	0.115	0.343	0.421	x	2.144	0.569	0.454	3.32
		Firefox	0.179	0.124	0.303	x	x	x	0.755	0.406	1.9
	Tablet	Chrome	3.748	6.804	10.552	x	x	x	x	x	x
		Firefox	4.752	7.576	12.328	2.416	x	x	1.578	1.826	x

Table 4.7 Comparison of the proposed application performances over the LAN with others, (Large-size data).

Dataset	OS	Browser	Proposed software			DicomViewer.net [241]		Image-IN [242]	BlueLight [100]		VolView [260]
			T1	T2	T1+T2	T1	T2	T1+T2	T1	T2	x
# 17	Win	Chrome	6.021	0.170	6.192	5.85	x	x	310	9.623	x
		Firefox	7.10	0.382	7.482	5.524	x	x	319	9.669	x
	Linux	Chrome	6.326	0.151	6.478	21.939	x	x	stopped at slice 1750	x	x
		Firefox	23.366	0.037	23.403	60.02	x	x	stopped at slice 520	x	x
	Mac	Chrome	31.019	0.848	31.868	12.264	x	x	407	30.22	x
		Firefox	16.628	0.024	16.652	x	x	x	x	x	x

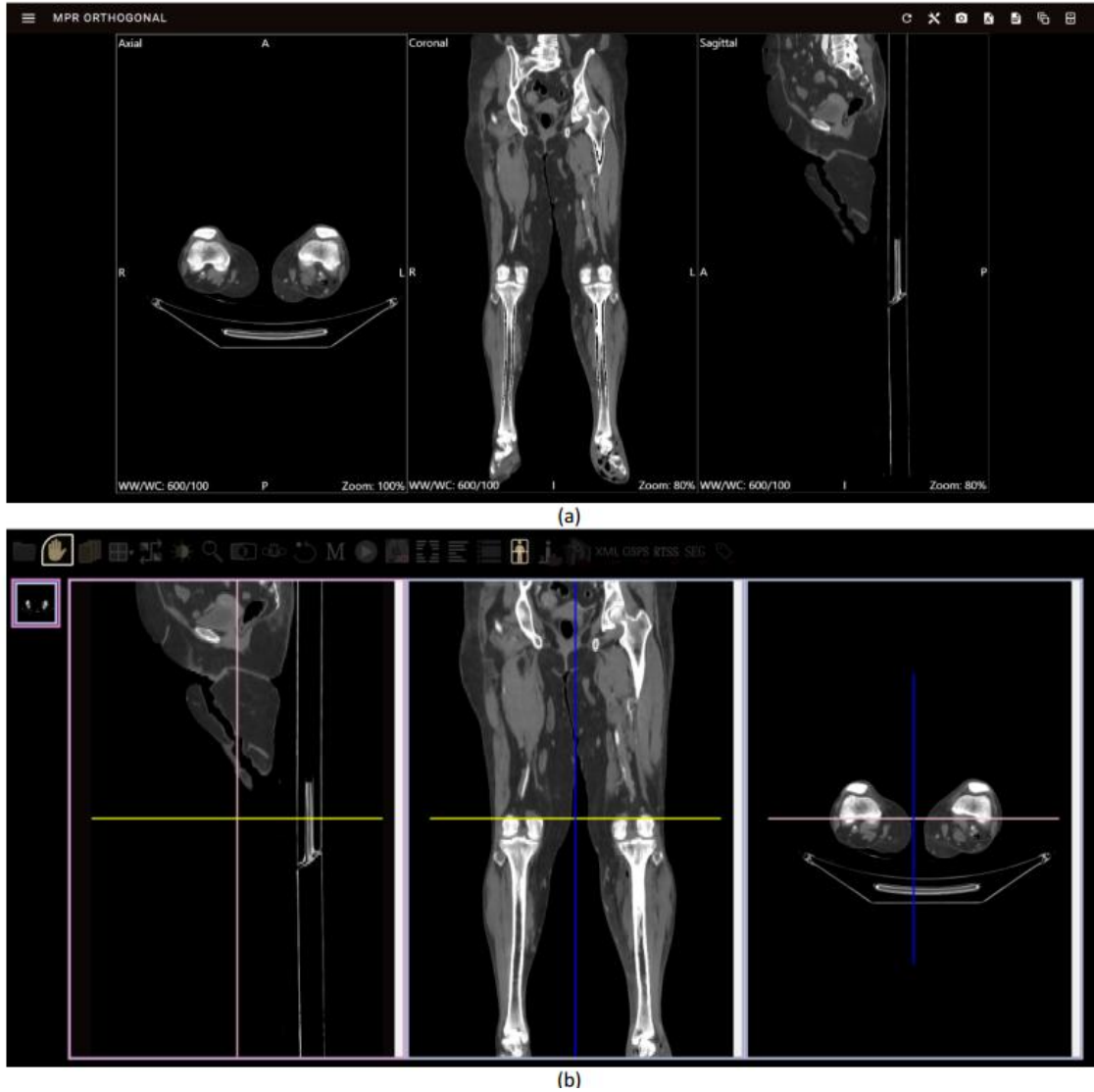


Figure 4.4 Comparison of the proposed application performances over the LAN with others, (Large-size data).

On the basis of these results, our developed application achieved compatibility with all browsers and platforms, demonstrating accurate and fast processing. In addition, users can access and upload files or folders directly from their local computers, resulting in improved user interaction. These advancements surpass the findings of a previous study [94], which used HTML5 and WebGL for web-based medical imaging but encountered limitations such as compatibility issues with internet Explorer, difficulties with user interaction for local file access, and reliance on predefined surface information for 3D visualization.

This chapter introduces PWA for DICOM and MPR visualization on the web, addressing challenges such as cross-platform compatibility, speed, and offline functionality. By leveraging PWAs, the application enhances accessibility and performance in medical imaging tasks,

including offline access, which allows it to function without internet connectivity by caching essential resources. This is particularly useful in areas with limited connectivity. In addition, improved performance is achieved through React.js and IndexedDB (via Dexie), optimizing the handling of large datasets, reducing loading times, and accelerating MPR. These features enhance usability and efficiency, improving radiologists' workflow. Furthermore, our application outperforms existing platforms such as DicomViewer.net, Image-IN, and BlueLight in terms of loading time and reconstruction efficiency, positioning itself as a robust and reliable choice for medical image visualization.

4.7 Contributions and Future Directions

This chapter effectively addresses significant gaps in web-based medical imaging applications, particularly DICOM and MPR visualization via PWAs. Leveraging the unique features of PWAs, such as uninterrupted offline access and enhanced performance, substantial progress has been made in overcoming technological barriers and advancing medical imaging functionality. Emphasizing cross-platform compatibility, integration capabilities, and speed underscores critical aspects in developing web-based medical imaging solutions. The proposed design and implementation demonstrate the feasibility and effectiveness of integrating DICOM and MPR visualization into web environments via PWAs, benefiting radiologists and health care professionals. Moreover, this chapter addresses MPR challenges, enhancing diagnostic capabilities through advanced interpolation methods and reconstruction protocols. The experimental results consistently showed superior performance compared with existing platforms, firmly establishing our application as a leading solution in medical image web visualization. The evaluation and testing were conducted using a dataset comprising CT scans from patients diagnosed with PAD, adding real-world relevance and validation to our findings. Future work will focus on visualizing 3D surfaces and performing volume rendering via MPR images.

Chapter 5: DECODE-3DViz: High-Fidelity Web-Based Visualization and Automated Risk Classification for Peripheral Artery Disease

- 5.1. Introduction
 - 5.2. Objectives
 - 5.3. System Design and Implementation
 - 5.4. Automated Risk Classification of PAD
 - 5.5. Validation and Performance Evaluation
 - 5.6. Results
 - 5.7. Discussion
 - 5.8. Conclusions
-

5.1 Introduction

The visualization of large-scale medical imaging datasets, particularly those from peripheral artery CT images, presents unique challenges owing to their high-resolution volumetric nature and the need for interactive 3D rendering. Traditional medical imaging systems are often restricted by hardware constraints and lack the scalability required for real-time visualization and diagnostic applications. To overcome these limitations, advanced web technologies such as WebGL have been leveraged, enabling efficient, high-fidelity visualization directly within web browsers without the need for additional plugins or specialized hardware [261, 262].

DECODE-3DViz introduces a significant advancement in web-based medical imaging by addressing the challenges of rendering large volumetric datasets through an innovative pipeline

that integrates LOD algorithms and progressive chunk streaming. This approach optimizes rendering performance by dynamically adjusting the resolution and streaming data in manageable chunks, effectively overcoming WebGL texture size constraints and browser memory limitations. This results in a seamless, interactive visualization experience that maintains high visual fidelity, which is essential for accurate medical diagnosis and treatment planning.

One of the core innovations of DECODE-3DViz is its dynamic LOD algorithm, which intelligently adjusts the resolution on the basis of user interactions and the importance of specific regions of interest (ROIs). By preserving high-resolution details where necessary and downsampling less critical areas, the system ensures efficient memory utilization and minimizes rendering times. This capability is particularly crucial for peripheral artery CT images, where precise visualization of complex vascular structures is required for accurate diagnostic interpretation and surgical planning. In addition to its advanced LOD implementation, DECODE-3DViz employs progressive chunk streaming to efficiently manage large datasets. This method divides the volumetric data into smaller, manageable chunks that are streamed and rendered incrementally, preventing browser crashes and maintaining application responsiveness. The integration of bicubic and trilinear interpolation techniques further enhances image quality, ensuring smooth transitions and accurate representations of anatomical structures.

The architecture of DECODE-3DViz is meticulously designed to optimize GPU memory usage and resource allocation strategies, enabling high-quality rendering even on resource-constrained devices. Comparative evaluations demonstrate that DECODE-3DViz outperforms state-of-the-art visualization tools in terms of structure definition, depth perception, texture appearance, and diagnostic capability. Its ability to deliver high-fidelity visualizations with real-time interactivity significantly enhances diagnostic accuracy and clinical decision-making. By leveraging the capabilities of WebGL and innovative data management techniques, DECODE-3DViz bridges the gap between high-fidelity visualization and web-based accessibility, enabling medical professionals to interact with complex 3D models of peripheral artery CT images in real time. This advancement not only enhances diagnostic workflows and clinical decision-making but also supports remote consultations and telemedicine applications, thereby expanding access to advanced medical imaging tools.

This chapter delves into the technical design, implementation strategies, and performance optimization techniques that make DECODE-3DViz a pioneering solution in web-based medical imaging. It explores the architectural frameworks, interpolation algorithms, and GPU optimization methods employed to achieve real-time, high-fidelity visualization. In addition, the chapter presents a comprehensive evaluation of DECODE-3DViz against state-of-the-art tools, highlighting its impact on diagnostic workflows and clinical outcomes.

5.2 Objectives

To address the challenges identified in the literature, this chapter seeks to develop innovative solutions that optimize the visualization pipeline through the application of an LOD algorithm. The specific objectives are as follows:

- a) RO1: Efficiently manage WebGL texture size limitations by developing techniques that utilize the LOD algorithm to render large peripheral artery CT datasets without performance degradation or errors, thereby overcoming texture size constraints.
- b) RO2: Implement strategies to prevent memory allocation errors, employing the LOD algorithm to ensure the complete and accurate rendering of high-resolution medical imaging data.
- c) RO3: Develop a method for chunk streaming large datasets, preventing browser crashes and maintaining application responsiveness and usability.
- d) RO4: Establish an approach to downsample only when necessary, guided by the LOD algorithm, to preserve as much detail as possible in the rendered images and maintain high visual fidelity.
- e) RO5: Provides functionality for specifying and rendering regions of interest (ROIs) in their original resolution using the LOD algorithm, ensuring that critical volumes are visualized in high detail for accurate medical diagnosis.

The overarching aim of these objectives is to increase the performance, accuracy, and usability of web-based applications for visualizing large-scale peripheral artery CT imaging datasets. This will ultimately support improved diagnostic outcomes and advance the field of medical imaging technology.

5.3 System Design and Implementation

5.3.1 System Design

The system design of DECODE-3DViz for 3D WebGL volume rendering of peripheral artery CT images involves a five-stage workflow: volume data input, resource assessment, data processing, volume rendering, and postrendering, as shown in Figure 5.1. The system begins by assessing and configuring processing resources through resource assessment, where the central processing unit (CPU) is primarily responsible for task allocation, data handling, and managing heap memory to optimize performance. The graphics processing unit (GPU) is configured for high-performance rendering, with constraints such as *MAX_3D_TEXTURE_SIZE* carefully considered to ensure efficient handling of large textures. The workflow ensures that computational demands are met while maintaining efficient memory and resource utilization.

Initially, CT slices are collected to form a detailed volumetric dataset, which undergoes resource assessment to evaluate computational requirements and configure processing resources efficiently. During data processing, the dataset is prepared using techniques such as data chunking and an LOD algorithm, which dynamically adjusts the resolution to manage large datasets efficiently. The volume rendering stage uses WebGL to cast rays through the data, creating a 3D representation with shading and lighting for enhanced visual realism. Volume clipping and interaction techniques focus on specific ROIs to improve clarity and detail. In the final postrendering stage, a transfer function maps data values to colors and opacities, allowing interactive adjustments for detailed visualization and accurate diagnosis.

5.3.2 Preprocessing Pipeline

The preprocessing pipeline of DECODE-3DViz consists of several essential steps for effective rendering. This section outlines the process starting from source data through the computation

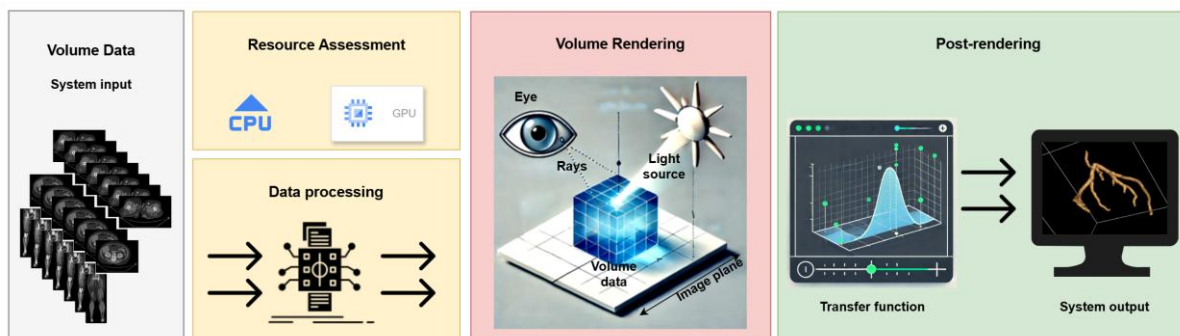


Figure 5.1 Workflow of 3D WebGL Volume Rendering for Peripheral Artery CT Imaging.

of the maximum 3D texture size, computation of total chunks required for rendering, streaming image chunks, combining chunks, and applying the LOD algorithm, which includes downsampling if necessary, as it is shown in Figure 5.2.

1) Input Data Source

The source data comprises peripheral artery CT images in DICOM or NIfTI formats [263, 264]. These images are volumetric datasets that require processing to be rendered using WebGL technology. The importance of using both DICOM and NIfTI formats lies in their widespread adoption in medical imaging and their ability to store complex image data with metadata, which is crucial for accurate visualization and analysis. The data are loaded into the browser environment where WebGL is used for rendering.

2) Maximum 3D Texture Size

Determining the maximum 3D texture size supported by WebGL 2.0 is crucial for assessing the WebGL context's ability to handle 3D textures. This process involves querying the *MAX_3D_TEXTURE_SIZE* parameter, which specifies the largest dimension in pixels for each axis of a 3D texture. Understanding that limitation is vital for partitioning volumetric data into manageable chunks, ensuring efficient rendering and optimal performance [104, 265]. In addition, optimizing the upload process involves managing the available JavaScript heap

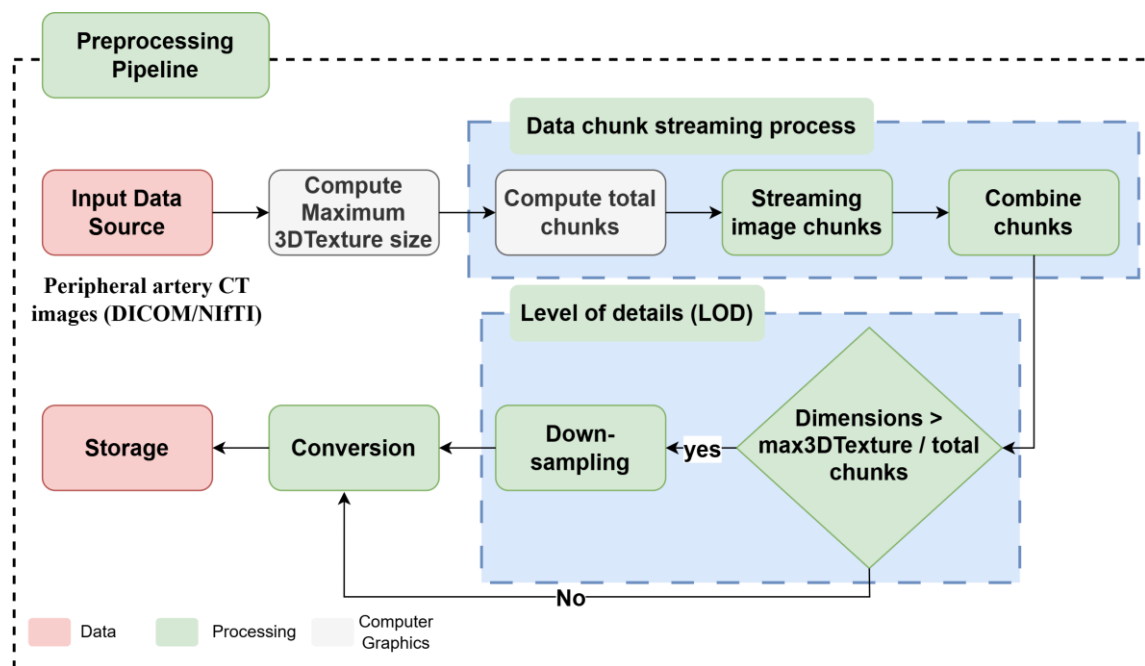


Figure 5.2 Schematic Diagram of the Preprocessing Pipeline for 3D WebGL Volume Rendering.

memory via the *performance.memory* API, with 75% of the total heap size typically allocated for texture uploads. In cases where this API is not supported, a fallback value is used to maintain a balance between maximizing memory usage for uploads and ensuring sufficient memory for other operations [266].

3) Data Chunk Streaming Process

The data chunk streaming process is critical for the efficient handling and rendering of volumetric datasets in a WebGL environment. To manage large volumes of data, the dataset is initially divided into manageable chunks. This division is guided by constraints such as the maximum 3D texture size supported by the WebGL context and the available upload memory. A chunk factor, typically set as a fraction (e.g., 0.25) of the maximum 3D texture size, determines the chunk size, ensuring that the chunks remain within feasible limits. The chunk size is computed as follows:

$$chunkSize = \min \left(\lfloor max3DTextureSize \times chunkFactor \rfloor, \left\lfloor \frac{maxUploadMemoryBytes}{2} \right\rfloor \right), \quad (5.1)$$

where *max3DTextureSize* represents the maximum allowable texture size along each dimension, *chunkFactor* is the fraction determining the size of each chunk, and *maxUploadMemoryBytes* is the available memory for uploading data. The total number of chunks required to process the dataset, denoted *totalChunks*, is determined by dividing the total depth of the dataset by the chunk size and rounding up:

$$totalChunks = \left\lceil \frac{depth}{chunkSize} \right\rceil, \quad (5.2)$$

where *depth* is the depth of the dataset along the axis being partitioned. This calculation ensures that all the data slices account for [267].

In the data chunk streaming phase, the volumetric data are dynamically partitioned into these chunks for incremental processing, which optimizes memory usage and enables smooth visualization. For each chunk, the starting and ending positions along the depth axis are calculated, and data from the original dataset are extracted accordingly. Each voxel within a

slice is mapped to the corresponding position in a new array, preserving spatial relationships. The assembled chunks, containing the extracted data with updated dimensions, are then added to a list of chunks to ensure complete coverage of the dataset [268].

The chunks are later combined into a single volumetric dataset, which is essential for reconstructing the original volume. This process assumes a consistent width and height across all chunks, as derived from the source data. The total depth of the combined dataset, denoted by *totalDepth*, is calculated by summing the individual depths of all chunks:

$$totalDepth = \sum_{i=1}^n depth_i, \quad (5.3)$$

where n is the total number of chunks and $depth_i$ is the depth of each individual chunk. This approach maintains the correct spatial relationships and ensures that the final dataset is ready for subsequent processing or rendering. If the combined dataset exceeds the maximum 3D texture size per chunk, an LOD algorithm is applied, as it is shown in Figure 5.2, to keep the dataset within these constraints and optimize it for efficient rendering.

4) Level of detail (LOD)

LOD adjustment is essential for efficient rendering within the constraints of the WebGL context, particularly for managing large volumetric datasets. This adjustment involves reducing the dataset's resolution while preserving critical features. The maximum dimension of the dataset is compared to a target maximum dimension to calculate the LOD adjustment factor. If the dataset dimensions exceed the target, an adjustment factor, *maxFactor*, is determined by the maximum ratio of the dataset dimensions to the target dimension:

$$maxFactor = \max\left(\frac{dimensions}{targetMaxDimension}\right), \quad (5.4)$$

where the dimensions represent the actual dimensions of the dataset, and *targetMaxDimension* is set to half of the maximum 3D texture size:

$$targetMaxDimension = \frac{max3DTextureSize}{2}, \quad (5.5)$$

The dataset is then resized by dividing each dimension by *maxFactor* and rounding up to the nearest integer, with the voxel spacing adjusted accordingly to maintain spatial relationships [269]. When any dimension of the combined dataset surpasses the maximum 3D texture size divided by the total number of chunks, downsampling becomes necessary. This downsampling process reduces the dataset's resolution while retaining essential features and uses trilinear interpolation to maintain data integrity [270]. Each voxel in the downsampled dataset is calculated by interpolating values from the original dataset on the basis of the indices and weights of the surrounding voxels. The outcome is a dataset with optimized dimensions and voxel spacing suitable for efficient rendering in a WebGL environment, as it is illustrated in the LOD algorithm in Figure 5.2.

5) Conversion and Storage

The process of data storage and conversion is crucial for preparing downsamples via LODs or original combined datasets for efficient rendering. This involves converting the dataset from formats such as DICOM or NIfTI to the VTK image data format [271]. This conversion is necessary for compatibility with WebGL volume rendering, specifically when *vtk.js* is utilized [272]. The converted data are stored as VTK images, which are optimized for efficient rendering in WebGL.

5.3.3 Large-Scale Volume Rendering

The WebGL volume rendering pipeline is meticulously structured into several stages, each playing a crucial role in generating high-quality, interactive 3D visualizations of peripheral

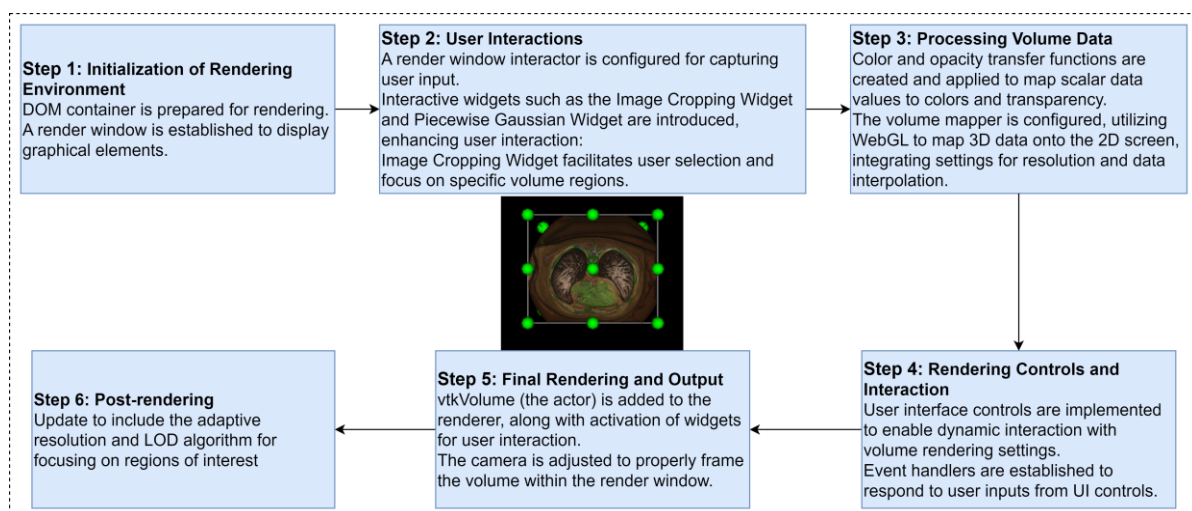


Figure 5.3 WebGL Volume Rendering Pipeline with Adaptive Resolution and LOD Algorithm.

artery CT images. This systematic approach, as it is illustrated in Figure 5.3, ensures an organized workflow, enabling efficient and effective rendering.

1) Initialization of the rendering environment

After preprocessing and conversion, the dataset is prepared for rendering. This involves acquiring input image and color data and setting up the core visualization components, including a rendering window, a renderer, and an OpenGL rendering window. The rendering container is identified within the HTML document, establishing the essential environment for visualization [273]. In addition, an interactor is initialized to facilitate responsive and interactive user experiences.

2) User Interactions

User interaction is further enhanced through a graphical overlay that provides visual feedback and a widget manager that handles interactive widgets, such as image cropping tools, allowing dynamic modification of rendering parameters with real-time updates [274]. Interactive widgets, including the image cropping width and piecewise Gaussian width, support user interaction by facilitating selection and focusing on specific volume regions.

3) Volume Render Processing

In the volume rendering processing phase, detailed volume rendering settings are configured to accurately represent the CT data. This involves setting up volume properties such as color and opacity transfer functions, shading parameters, and interpolation types. The volume mapper is linked to the input image data to ensure precise visualization [275].

A critical component of this phase is the transfer function, which controls the visualization of CT data in terms of color and opacity. The main volume rendering is [276]:

$$I(D) = I_0 e^{-\int_0^D \tau(t) dt} + \int_0^D e^{-\int_s^D \tau(t) dt} \tau(s) C(s) ds, \quad (5.6)$$

where $I(D)$ is the intensity of the light after passing through the volume at depth D , I_0 is the initial intensity of the light, $\tau(t)$ is the optical depth or attenuation coefficient at position t , and $C(s)$ is the color or emission at position s . This equation accounts for both absorption and

emission within the volume, which is critical for accurate volume rendering. The transfer function is defined [277]:

$$T(v) = (\alpha(v), c(v)),$$

$$\alpha(v) = \sum_{i=1}^n w_i G(v - v_i, \sigma_i), \quad (5.7)$$

$$c(v) = \sum_{i=1}^n c_i L(v - v_i).$$

where $\alpha(v)$ is the opacity transfer function and $c(v)$ is the color transfer function, G is a Gaussian function centered at v_i with width σ_i , w_i represents the weights, L is a linear function centered at v_i , and c_i represents the color values associated with intensity v_i .

To facilitate interactive adjustments, a *vtkPiecewiseGaussianWidget* is created and configured within a dynamically generated HTML container. This widget allows users to modify the color and opacity mappings interactively. A histogram is generated from the CT data values, providing a visual representation of the data distribution. This histogram is used to set up the data array for the widget, enabling users to see and adjust how data values are mapped to colors and opacities. The *vtkPiecewise* function is used to define the opacity transfer mapping, setting specific points to make different tissue types transparent or opaque. Simultaneously, the *vtkColorTransferFunction* assigns colors to different intensity values, enhancing the visual distinction between various tissues, such as air, lung, fat, muscle, and bone. The widget's opacity change events are closely monitored, and any user adjustments are dynamically applied to the transfer functions. This allows for real-time updates to the rendered volume representation, ensuring that users can fine-tune the visualization parameters to achieve the best possible representation of the CT data.

4) Rendering Controls and Interaction

In this stage, interactive features are meticulously refined to enhance user engagement and control. Advanced manipulators for pan, zoom, and rotation operations are seamlessly integrated, providing users with comprehensive control over the viewing experience. An orientation marker widget is added to facilitate spatial orientation within the 3D scene, ensuring that users can navigate the volume data effectively [278]. In addition, control panels are integrated to allow precise adjustments to various rendering parameters, including gradient

opacity, scalar opacity, sample distance, blending modes, visibility, and shading of the volume. These controls enable users to customize the visualization to meet specific diagnostic needs, thereby enhancing the overall utility and effectiveness of the rendered images.

5) Final Rendering and Output

The final rendering stage involves applying the configured settings and controls to produce the visual output. The rendering pipeline integrates mechanisms for updating the rendering in response to changes in cropping planes, utilizing *vtkPlane* instances for precise clipping operations. The sophisticated color and opacity transfer functions established during volume processing are crucial, ensuring that different tissue types are accurately represented and visually distinct. Initial rendering involves downsampling for performance optimization on the basis of the LOD algorithm. The final color C_{final} along a ray can be computed via the integral as:

$$C_{final} = \int_{t_0}^{t_1} c(t) \alpha(t) e^{-\int_{t_0}^{t_1} \tau(s) ds} dt, \quad (5.8)$$

where $c(t)$ is the color at point t , $\alpha(t)$ is the opacity at point t , and $\tau(s)$ is the optical depth or attenuation coefficient at position s . The compositing equation used in volume rendering can be expressed as follows [279]:

$$C = \sum_i c_i \cdot \alpha_i \cdot \prod_{j=1}^{i-1} (1 - \alpha_j), \quad (5.9)$$

where c_i is the color of the $i - th$ sample, α_i is the opacity of the $i - th$ sample, and the product term accounts for the accumulated transparency of all preceding samples.

6) Post-rendering

In the post-rendering stage, further adjustments and enhancements are made to the rendered output, benefiting significantly from the initial use of the LOD algorithm in the preprocessing phase. This stage focuses on refining the ROIs by re-rendering them at the original resolution if downsampling has occurred. Adaptive resolution changes enable selective quality improvement in specific regions [280]. The process involves several steps: storing current camera settings to

maintain the user perspective, calculating subvolume dimensions on the basis of downsampled data, cropping the relevant region from the original resolution data, creating a high-resolution subvolume, rerendering the region with its original resolution, and finally restoring camera settings to reflect the updated high-resolution view.

The methodology of the LOD algorithm, which underpins the preprocessing phase and supports these refinements, is provided in Algorithm 5.1. This pseudocode provides a structured overview of the processes involved, from initialization and volume preparation to progressive LOD rendering and final visualization.

5.4 Automated Risk Classification of PAD

5.4.1 Real-Time Dynamic Illumination

The proposed framework integrates an advanced real-time dynamic illumination model to enhance the visualization of vascular structures, especially in PAD diagnostics. This illumination approach uses Perlin noise to simulate the dynamic light direction and a damped harmonic oscillator to generate realistic variations in light intensity over time [281]. These dynamic lighting techniques improve depth perception, enhance the realism of vascular geometry, and enable a detailed visualization of intricate anatomical structures.

The dynamic behavior of the light is controlled through mathematical formulations that adapt in real time on the basis of user-defined parameters. The light direction is calculated using a frequency-controlled noise factor, ensuring smooth and natural transitions. This is vital for achieving enhanced realism in visualizing complex vascular geometries. On the other hand, the light intensity is modulated using a damped harmonic oscillator model to introduce natural decay and oscillatory effects [282]. Together, these techniques provide a highly realistic simulation of lighting, significantly improving the perception of depth and texture in medical imaging applications.

Dynamic Light Direction [283]: The light direction vector $L(t)$ is computed as:

$$L(t) = \begin{bmatrix} \sin(\omega t) + 0.2 \eta(t) \\ \cos(\omega t) - 0.2 \eta(t) \\ \sin(0.5\omega t) \end{bmatrix}, \quad (5.10)$$

Algorithm 5.1 Level of detail (LOD) optimization for efficient WebGL volume rendering.

```
1. Function InitializeSystem():
2.   Initialize WebGL 2.0:
3.     WebGL ← initializeWebGL2()
4.     if not WebGL.isCompatible():
5.       terminate("WebGL 2.0 not supported")
6.   Query hardware constraints:
7.     maxTextureSize ← queryMax3DTextureSize()
8.   Allocate memory and compute chunk size:
9.     heapMemory ← getTotalHeapMemory()
10.    maxUploadMemoryMB ← allocateMemory(heapMemory * 0.75)
11.    chunkSize ← computeChunkSize(maxUploadMemoryMB, maxTextureSize)
12. Function PrepareVolumeData():
13.   Load and validate medical data:
14.     medicalData ← loadMedicalData("DICOM/NifTI")
15.     if not validateDimensions(medicalData, WebGL.limits):
16.       terminate("Data dimensions exceed WebGL limits")
17.   Apply LOD downsampling and partition volume:
18.     downsampledData ← applyLODDownsampling(medicalData)
19.     partitionedVolume ← partitionVolume(downsampledData, chunkSize)
20. Function RenderProgressiveLOD():
21.   while not allChunksLoaded():
22.     Stream image chunks based on GPU capacity:
23.       imageChunks ← streamChunks(partitionedVolume, GPU.capacity)
24.     Detect ROI and refine resolution:
25.       ROI ← detectROI(imageChunks)
26.       replaceDownsampledRegions(ROI, medicalData)
27.     Apply LOD interpolation for seamless transitions:
28.       applyLODInterpolation(imageChunks)
29. Function OptimizeGPUAndMemory():
30.   while rendering:
31.     Monitor GPU load and adjust LOD dynamically:
32.       if monitorGPULoad() > threshold:
33.         adjustLODDynamically()
34. Function FinalizeVisualization():
35.   Convert processed data to VTK and apply color mapping:
36.     renderData ← applyLODColorMapping(convertToVTK(partitionedVolume))
37.   Render final 3D volume:
38.     render3DVolume(renderData)
```

where the noise factor $\eta(t)$ is defined as:

$$\eta(t) = \sin(\omega t) \cdot \cos(\omega t), \quad (5.11)$$

where ω is the light frequency, which is defined by the user input, and where t is the current time.

Dynamic Light Intensity: The light intensity $I(t)$ is modeled as:

$$I(t) = I_0 + A \cdot e^{-\beta t} \cdot \sin(\alpha t), \quad (5.12)$$

where I_0 is the base intensity, A is the amplitude of oscillation, β is the damping factor, and α is the angular frequency.

5.4.2 Plaque density analysis

To quantitatively assess the extent of plaque accumulation within peripheral arteries, a voxel-based plaque density analysis was conducted [284]. This method uses the intensity values derived from Hounsfield units (HUs) in CT images to segment and classify vascular tissues, enabling a precise evaluation of plaque burden [285]. The analysis hinges on defining specific HU thresholds to categorize voxels into calcified plaque, soft plaque, and vascular tissue regions.

Thresholding: The classification of voxels is guided by predefined HU ranges as follows:

$$\text{Vascular Tissue: } 45 \leq HU \leq 300, \quad (5.13)$$

$$\text{Calcified Plaque: } 130 \leq HU \leq 300, \quad (5.14)$$

$$\text{Soft Plaque: } 50 \leq HU < 130, \quad (5.15)$$

This thresholding mechanism ensures the accurate segregation of vascular elements, allowing for the extraction of biomarkers associated with arterial health and disease.

Plaque density calculation: The plaque density (ρ_p) is computed as the ratio of plaque voxels (both calcified and soft) to the total vascular voxels within the specified ROI [286]. The formula for calculating plaque density is as follows:

$$\rho_p = \frac{N_c + N_s}{N_v}, \quad (5.16)$$

where N_c is the number of calcified plaque voxels, N_s is the number of soft plaque voxels, and N_v is the total number of vascular tissue voxels.

This metric provides a quantitative measure of atherosclerotic plaque burden, offering critical insights into the severity and progression of PAD. By combining HU-based segmentation with this density calculation, the framework supports enhanced diagnostic precision and risk stratification.

5.4.3 Vascular Curvature Analysis

The analysis of vascular curvature is crucial for evaluating arterial deformation and identifying regions subjected to high morphological stress, which are significant indicators of disease severity and progression [287]. By extracting a sequence of centerline points P_{i-1} , P_i , and P_{i+1} from the arterial geometry, the local curvature at each point can be calculated. This approach provides a detailed quantification of the arterial structure, enabling the detection of irregularities and potential risk zones.

The curvature k_i at a specific centerline point P_i is determined by the angle between the vectors connecting consecutive centerline points [288]. It is expressed mathematically as:

$$k_i = \arccos\left(\frac{\vec{v}_1 \cdot \vec{v}_2}{\|\vec{v}_1\| \|\vec{v}_2\|}\right), \quad (5.17)$$

$$\vec{v}_1 = P_i - P_{i-1}, \quad (5.18)$$

$$\vec{v}_2 = P_{i+1} - P_i, \quad (5.19)$$

where \vec{v}_1 is a vector from the previous point to the current point, \vec{v}_2 is a vector from the current point to the next point, and $\|\vec{v}_1\|$, $\|\vec{v}_2\|$ are the magnitudes of vectors \vec{v}_1 and \vec{v}_2 , respectively.

Average Curvature Calculation [289]: To evaluate the overall curvature along the vascular centerline, the average curvature \bar{k} is computed as the mean of all individual curvature values:

$$\bar{k} = \frac{\sum_{i=1}^{N-1} k_i}{N - 2}, \quad (5.20)$$

where N is the total number of centerline points.

This metric provides a comprehensive assessment of arterial shape irregularities, aiding in the identification of critical morphological changes associated with vascular diseases. By integrating curvature analysis into the diagnostic process, this method enhances the precision and reliability of disease characterization.

5.4.4 PAD Risk Classification

PAD risk classification integrates both plaque density and vascular curvature metrics [290], leveraging threshold-based decision-making to stratify patients into high- or low-risk categories. This approach ensures a systematic and quantifiable framework for early identification and intervention in patients susceptible to PAD.

The framework uses predefined thresholds: the plaque density threshold ($\rho_{p,threshold} = 0.3$) and the curvature threshold ($\overline{k_{threshold}} = 0.5$). The classification rule is mathematically expressed as:

$$Risk\ Level = \begin{cases} High\ Risk, & \text{if } \rho_p > \rho_{p,threshold} \text{ or } \bar{k} > \overline{k_{threshold}}, \\ Low\ Risk, & \text{otherwise.} \end{cases} \quad (5.21)$$

where ρ_p represents the computed plaque density and \bar{k} denotes the average vascular curvature.

This methodology provides an efficient and robust tool for PAD risk assessment, enabling clinicians to prioritize patients who may benefit from advanced diagnostic and therapeutic interventions. The threshold-based approach simplifies the integration of the algorithm into real-time diagnostic systems, thereby enhancing clinical decision-making processes.

5.5 Validation and Performance Evaluation

To ensure the performance and efficiency of DECODE-3DViz, a comprehensive validation approach comprising analytical evaluation, clinical evaluation, and user feedback via a questionnaire is employed. Each method provides a distinct perspective on the system's capabilities, offering a thorough and multifaceted assessment.

5.5.1 Analytical evaluation

This evaluation focuses on quantitative performance metrics, including the rendering time (ms), frame refresh rate (FPS), and GPU memory usage (MB), which are essential for assessing computational efficiency, real-time interactivity, and resource optimization when handling large-scale medical imaging datasets [291]. The rendering time was assessed via browser developer tools (*DevTools*) available from multiple web browsers. The performance panel within the console was used to capture and profile frame execution times, providing a precise evaluation of rendering efficiency. FPS and GPU memory usage were measured through the rendering tab in *DevTools*, specifically the frame rendering stats feature.

5.5.2 Clinical evaluation

This assessment evaluated the system's effectiveness in a real-world clinical setting and involved specialists in vascular and endovascular surgery who utilized DECODE-3DViz to review and diagnose peripheral artery CT images. The clinical evaluation is conducted to determine how well the tool aids in accurate diagnosis, its usability within the clinical workflow, and its overall impact on patient care.

5.5.3 User feedback via questionnaire

User satisfaction and preferences are gathered through a questionnaire, which compares images generated by DECODE-3DViz with those from other state-of-the-art (SoTA) tools, such as IMAGE-IN [242], BlueLight [100], VolView [114], and Glance [292]. Feedback is collected on several visual characteristics via a Likert scale ranging from 1 (very unsatisfied) to 5 (very satisfied) [293]. The questionnaire covers three main areas: visual characteristics (including structure definition, depth perception, texture appearance, fidelity, and diagnostic ability), reliability ratings, and recommendations. In addition, open-ended questions invite participants to express their preferences for DECODE-3DViz and suggest improvements, providing valuable qualitative feedback to enhance the tool's capabilities. To ensure robust quantitative analysis, the collected data were subjected to statistical evaluation via analysis of variance

(ANOVA) [294] to determine the significance of differences in user ratings between the tools. ANOVA was employed to test the null hypothesis that there are no significant differences in the mean ratings across the tools. The F-statistic, calculated as the ratio of between-group variance to within-group variance, was used to assess the overall significance of the differences. The between-group variance (SSB) measures the variability of the group means from the overall mean, whereas the within-group variance (SSW) captures the variability of individual ratings within each group. The F-statistic is computed as:

$$F = \frac{SSB/(k - 1)}{SSW/(N - k)}, \quad (5.22)$$

where k is the number of tools, N is the total number of observations, SSB is the sum of squares between groups, and SSW is the sum of squares within groups. The degrees of freedom for the F -statistic are $df_1 = k - 1$ (between groups) and $df_2 = N - k$ (within groups). The resulting p -value, derived from the F -distribution, indicates the probability of observing the data if the null hypothesis is true. A p -value < 0.05 was considered statistically significant, suggesting that at least one tool's mean rating significantly differed from the others.

5.6 Results

To evaluate the performance of DECODE-3DViz, tests were conducted via two systems with distinct hardware specifications. The first system was a laptop running Windows 11 Pro 64-bit, equipped with an Intel(R) Core (TM) i7-11800H CPU at 2.30 GHz with 16 cores, 16 GB of memory, and an NVIDIA GeForce RTX 3070 GPU. The display rate for this system was 144 Hz. The second system was a desktop running Windows 10 Pro 64-bit, featuring an Intel(R) Core (TM) i7-9700F CPU at 3.00 GHz with 8 cores, 32 GB of memory, and an NVIDIA GeForce RTX 3080 GPU. These hardware configurations were selected to assess DECODE-3DViz's performance across both mobile and stationary platforms, providing insights into its ability to handle high-resolution medical imaging data.

5.6.1 Effects of Visualization Parameters on Peripheral Artery CT Images

DECODE-3DViz uses key visualization parameters, including the sample distance, gradient, and scalar opacity, to significantly enhance the quality of peripheral artery CT images:

- a) Sample Distance (0.1 to 1): Controls the interval for sampling data points along rays. Lower values provide greater detail and smoother transitions, whereas higher values prioritize performance with reduced detail.
- b) Gradient (0 to 1): Enhances shading and depth perception, with higher values increasing contrast and highlighting anatomical features such as arteries.
- c) Scalar Opacity (0 to 255): Regulates transparency, allowing for better visualization of internal structures at lower values and emphasizing specific regions at higher values.

Fine-tuning these parameters enable DECODE-3DViz to deliver high-quality, diagnostic-grade visualizations that enhance image clarity and utility for clinical evaluation.

Figure 5.4 illustrates the effects of various visualization parameters on the CT images of Patient #17, demonstrating the versatility of DECODE-3DViz across different settings:

- Figure 5.4(a): High-detail rendering with a sample distance of 0.1 and a gradient of 0.6, enhancing peripheral artery visibility with interactive adjustments for regions of interest.
- Figure 5.4(b): Focused on the feet, maintaining high detail with the same sample distance and gradient settings as in Figure 5.4(a).
- Figure 5.4(c): Comprehensive assessment of the peripheral artery system relative to the skeletal structure, using a sample distance of 0.75 and a gradient of 0.6.
- Figure 5.4(d): Detailed visualization with strong contrast to differentiate vascular structures, achieved with a sample distance of 0.1 and a gradient of 1.
- Figure 5.4(e): Balancing detail and performance, focused on the upper thighs and pelvic region, with a sample distance of 0.5 and a gradient of 1.
- Figure 5.4(f): Provides detailed, contrasting views of the peripheral arteries via the same parameters as those used in Figure 5.4(e).
- Figure 5.4(g): Impact of combined parameters (sample distance of 0.3, gradient of 1, and scalar opacity of 170) on visualization quality and detail, particularly for the pelvic arteries.

This comprehensive set of images highlights the versatility and precision of DECODE-3DViz in rendering detailed vascular anatomy.

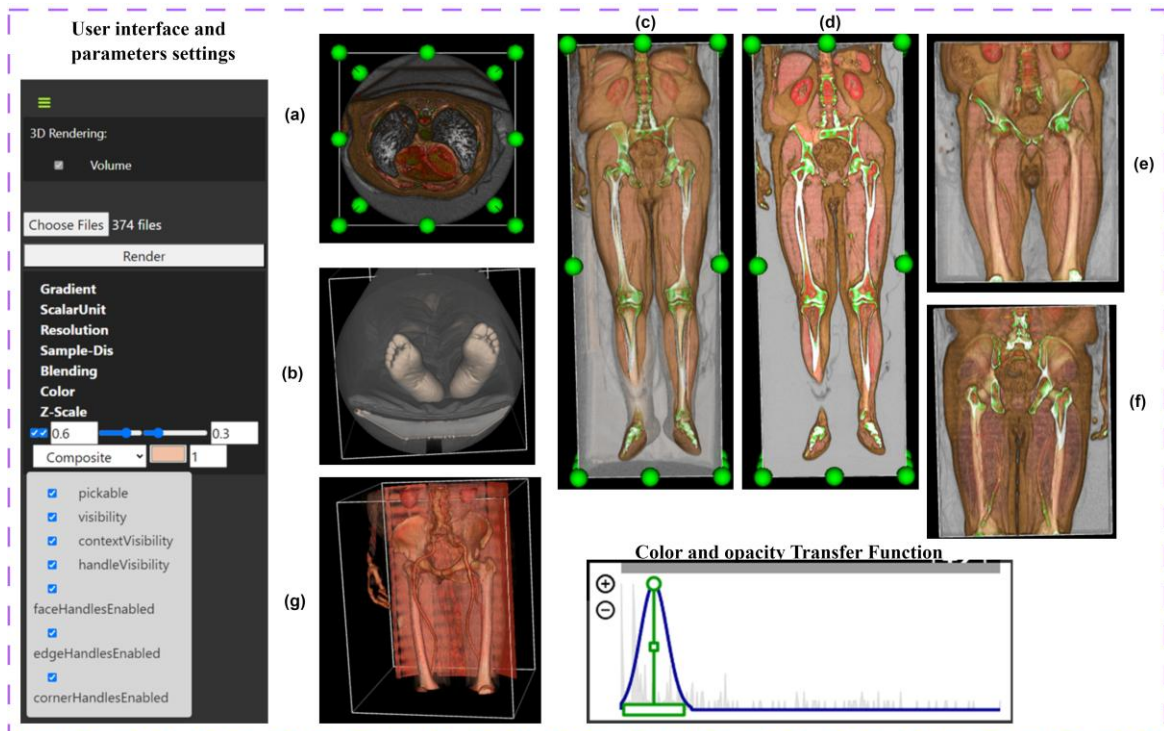


Figure 5.4 Visualization and Parameter Effects on Peripheral Artery CT Images of Patient #17: (a) Top Series Axial View, (b) Bottom Series Axial View, (c) Coronal View, (d) Cropped Coronal View, (e) Cropped Front Coronal View of Region of Interest, (f) Cropped Back Coronal View of Region of Interest, (g) Enhanced Detailed View of Pelvic Arteries with Transfer Function Adjustments.

5.6.2 Level of detail optimization in large-scale data management

To efficiently manage large volumetric datasets and prevent browser crashes, this methodology partitions the data into manageable chunks, as demonstrated by the use of the laptop and desktop systems in the evaluation and across the three case studies shown in Figure 5.5 and Table 5.1.

- Case Study 1: This case study, a series for Patient #2, focused on the aorto-iliac segment, allowing detailed visualization of the abdominal aorta and iliac arteries. For this case, the dataset was divided on the basis of WebGL's texture size limits and JavaScript heap size, optimizing memory use and maintaining responsiveness. Downsampling with the LOD algorithm was applied only when necessary to preserve crucial details, as shown in Figure 5.5(a). The pipeline allows for the rendering of ROIs at their original resolution, enhancing diagnostic capabilities. Figures 5.5(b) and (c) illustrate the progression from initial rendering to high-detail re-rendering, revealing finer vascular structures crucial for diagnosis.

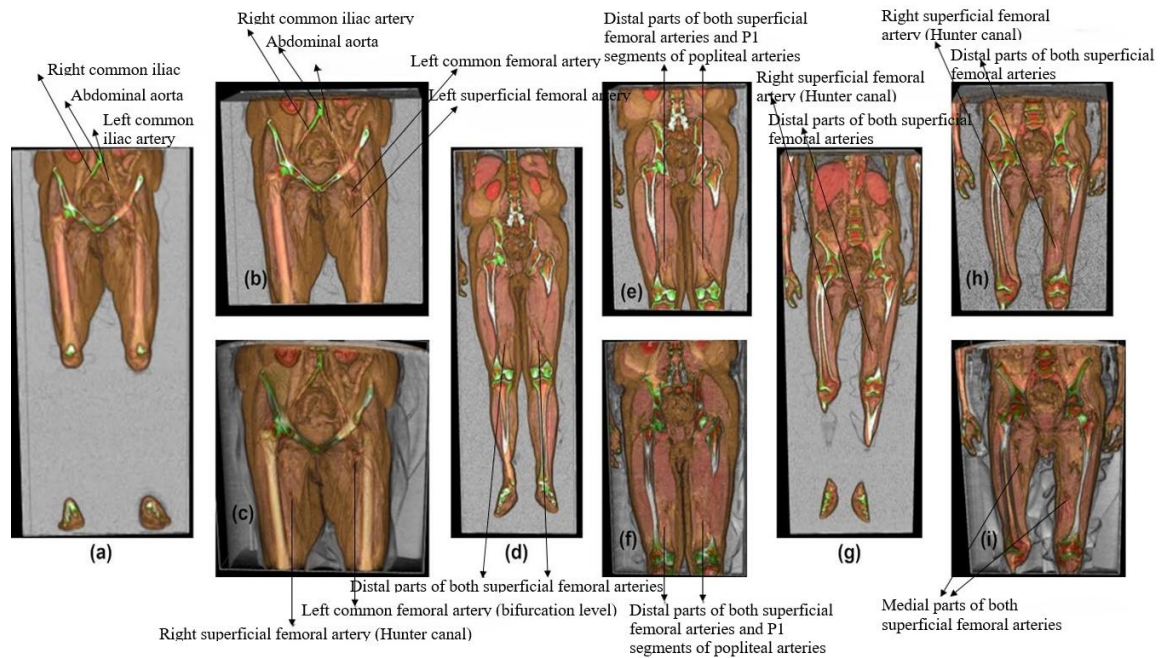


Figure 5.5 Visualization Results of Progressive Streaming and Level of Detail (LOD)

Volume Rendering for Three Case Studies (a-c: Case Study 1; d-f: Case Study 2; g-i: Case Study 3).

- Case Study 2: This case study, a series involving Patient #17, focused on the femoral arteries, specifically the distal parts of the superficial femoral arteries as they passed through the Hunter canal. As shown in Figures 5.5(d-f), this case study applies similar chunking and downsampling methods to ensure that the intricate anatomical details are clearly visualized. The LOD algorithm enables the detailed rendering of the arteries within their surrounding anatomical context, improving visualization and diagnostic interpretation of arterial segments that are critical for assessing peripheral vascular diseases.
- Case Study 3: This case study, a series for Patient #21, examines the popliteal arterial segment, particularly focusing on the knee area and the P1 segment of the popliteal artery. As illustrated in Figures 5.5(g-i), this case study uses chunked and downsampled datasets to maintain high resolution while rendering complex arterial pathways. The rerendered ROIs in this segment provided a precise view of the arterial structures, supporting accurate assessment and planning for interventions.

This progressive streaming and LOD volume rendering approach effectively manages large datasets, minimizes resolution loss, and ensures high-fidelity, interactive 3D visualizations, greatly enhancing the diagnostic accuracy of WebGL-based medical imaging tools.

Table 5.1 Parameters and results of progressive streaming and level of detail volume rendering for three case studies.

Parameters	Case study 1	Case study 2	Case study 3
Maximum 3D Texture Size	2048	2048	2048
Computed Chunk Size	512	512	512
Initial JS Heap Size Limit (MB)	4095.75	4095.75	4095.75
Total Chunks to Process	4	5	4
Processed Chunks (1/5) - Used JS Heap Size (MB)	868.8	869.46	871.43
Processed Chunks (2/5) - Used JS Heap Size (MB)	1636.81	1637.48	1639.45
Processed Chunks (3/5) - Used JS Heap Size (MB)	2404.21	2405.53	2407.49
Processed Chunks (4/5) - Used JS Heap Size (MB)	2558.64	3173.04	3164.36
Processed Chunks (5/5) - Used JS Heap Size (MB)	-	3459.37	-
Dimensions of Combined Original Data	[512, 512, 1639]	[512, 512, 2239]	[512, 512, 2041]
Dimensions of Vol_img downsampled	[320, 320, 1024]	[235, 235, 1024]	[257, 257, 1024]
Dimensions of ROI_Vol_img downsampled	[320, 190, 474]	[235, 98, 520]	[257, 124, 492]
Dimensions of ROI_Vol_img original	[512, 304, 761]	[512, 216, 1138]	[512, 248, 982]

5.6.3 Effect of Light Controls on CT DICOM Peripheral Artery Imaging

Dynamic light controls play a pivotal role in enhancing the visualization of CT DICOM images, particularly for the evaluation of PADs. Figure 5.6 illustrates the impact of three critical parameters—light rotation speed, base intensity, and intensity amplitude—on the imaging quality and clinical interpretability of vascular structures. These parameters enable tailored visualization, facilitating the identification of arterial abnormalities and enhancing diagnostic accuracy. The user interface, as shown in Figure 5.6(a), provides precise control over the lighting parameters. The light rotation speed, initially set to 0.001, governs the dynamic transitions of light over vascular surfaces, aiding in the identification of calcified plaques and soft tissue variations. The base intensity, with a default value of 0.5, modulates the ambient brightness, ensuring balanced contrast across the vascular and surrounding regions. The intensity amplitude, also set to 0.5 by default, introduces oscillatory variations in lighting, enhancing depth perception and emphasizing surface textures. Figure 5.6(b) presents the full

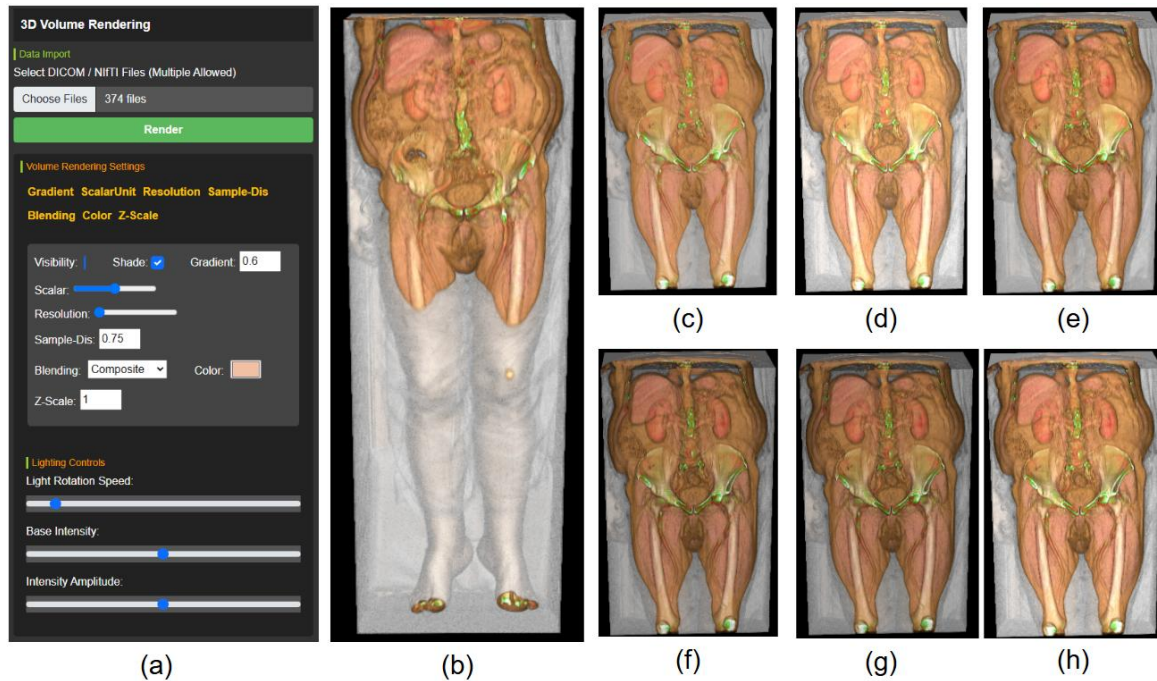


Figure 5.6 Interactive Visualization of Peripheral Artery CT Imaging for Patient 9 with Dynamic Light Controls; (a) User interface for light control parameters; (b) Full CT volume visualization; (c-e) Region of interest under dynamic light variation; (f) Increased light rotation speed and maximum intensity amplitude; (g) Maximum light rotation speed and intensity amplitude; (h) Static lighting with medium intensity.

3D CT volume of Patient 9 under the default lighting parameters. This configuration achieves balanced illumination, enabling an overall assessment of the vascular geometry.

Focused visualization of the pelvic region is shown in Figure 5.6(c), (d), and (e) under dynamic lighting with the default rotation speed (0.001), base intensity (0.5), and intensity amplitude (0.5). In Figure 5.6(c), the rotational light highlights the arterial walls and surrounding tissues, aiding in the identification of subtle vascular deformities. Figure 5.6(d) and Figure 5.6(e) further enhance depth perception and contrast, improving differentiation between calcified plaques and soft tissues, which is essential for precise plaque characterization and arterial health assessment. In Figure 5.6(f), the light rotation speed is slightly increased to 0.002, the base intensity is reduced to 0, and the intensity amplitude is set to 1. This setup generates sharper contrasts and pronounced shadowing, emphasizing the contours of the arterial walls. Figure 5.6(g) shows the maximum light rotation speed (0.01) and intensity amplitude (1), with the base intensity maintained at 0. Rapid light transitions accentuate surface textures and regions of high curvature, offering enhanced visualization of complex vascular deformations. However, rapid oscillations may introduce artifacts, potentially complicating the evaluation of smaller or less

prominent features. Figure 5.6(h) shows the effect of static lighting, which is achieved with a rotation speed of 0, a base intensity of 0.5, and an intensity amplitude of 0.5. Uniform and stable lighting facilitates a detailed evaluation of the ROI, supporting the analysis of arterial wall integrity, plaque distribution, and vascular morphology without distractions from dynamic transitions.

5.6.4 Validation of the Proposed Framework for PAD Risk Classification

The initial results of the proposed framework, as presented in Table 5.2, provide a detailed quantitative analysis of plaque density and vascular curvature metrics for five patients diagnosed with PAD. These metrics represent preliminary validation of the framework’s ability to assess vascular abnormalities and classify PAD risk effectively.

Table 5.2 Quantitative Results of Plaque Density and Vascular Curvature Metrics Across Patients.

Patient ID	Total Vascular Voxels	Calcified Plaque Voxels	Soft Plaque Voxels	Plaque Density	Total Centerline Points	Average Curvature	PAD Risk Classification
1	5534139	798390	3810908	0.8329	299684	1.132	High Risk of PAD
2	4853409	1178950	2975082	0.8559	218375	1.4366	High Risk of PAD
3	4551532	1155706	2952517	0.9026	234276	1.2712	High Risk of PAD
4	13067145	1463447	10616052	0.9244	234132	1.5417	High Risk of PAD
5	3499743	721625	2102619	0.807	255167	1.1786	High Risk of PAD

The plaque density (ρ_p) values ranged from 0.807 for Patient 5 to 0.924 for Patient 4. Elevated plaque density values indicate significant arterial plaque accumulation, reflecting advanced disease stages. For example, Patient 4, with the highest plaque density of 0.924, presented with severe arterial obstruction and pronounced disease progression. The analysis of vascular curvature revealed average curvature values (\bar{k}) ranging from 1.132 (Patient 1) to 1.541 (Patient 4). These values are calculated from the total centerline points, with the highest count of 299,684 observed in Patient 1. Higher curvature values signify tortuous arterial paths, increasing hemodynamic stress and the risk of vascular complications. Patient 4, who displays both the highest curvature ($\bar{k} = 1.541$) and plaque density ($\rho_p = 0.924$), is indicative of an advanced disease state with substantial vascular irregularities.

All five patients were classified as being at high risk of PAD, according to the framework’s thresholds for plaque density (> 0.3) and vascular curvature (> 0.5). These results

demonstrate the framework’s capacity to quantify critical vascular features and classify PAD severity effectively in its initial application.

5.6.5 Analytical Performance and Evaluation

This section compares the performance of DECODE-3DViz with that of other visualization tools (IMAGE-IN, BlueLight, VolView, and Glance) in the context of 3D WebGL volume rendering for CT peripheral artery images. Key metrics, including render time, FPS, and GPU memory usage, are evaluated across laptop and desktop environments. DECODE-3DViz demonstrates superior efficiency and effectiveness, outperforming the other tools in rendering high-quality medical images.

Table 5.3 presents a detailed comparison, showing that DECODE-3DViz consistently achieves faster render times, lower GPU memory usage, and robust FPS performance. Figure 5.7 shows the FPS performance, where DECODE-3DViz maintains a high FPS on both laptops (Figure 5.7(a)) and desktops (Figure 5.7(b)), highlighting its ability to deliver smooth and fluid visualizations. In particular, DECODE-3DViz outperforms IMAGE-IN and BlueLight, whereas Glance has the highest FPS, indicating superior optimization on desktops.

Table 5.3 Analytical performance evaluation metrics of DECODE-3DViz and state-of-the-art visualization tools for 3D WebGL volume rendering (mean \pm std).

Tool	DECODE-3DViz	IMAGE-IN	BlueLight	VolView	Glance
Laptop Render Time (ms)	26.88 \pm 2.65	41.35 \pm 3.88	604.06 \pm 108.73	42.73 \pm 4.74	73.74 \pm 5.61
Desktop Render Time (ms)	48.07 \pm 2.36	79.57 \pm 3.76	688.04 \pm 39.35	81.52 \pm 5.32	106.93 \pm 4.27
Laptop Refresh Rate (FPS)	115.2	108.5	113.4	90.4	139.5
Desktop Refresh Rate (FPS)	134.03	128.95	110.89	120.99	143.57
Laptop GPU memory usage (MB)	3.4	7	108.9	14.4	20
Desktop GPU memory usage (MB)	2.5	4.12	108.6	11.03	22.61

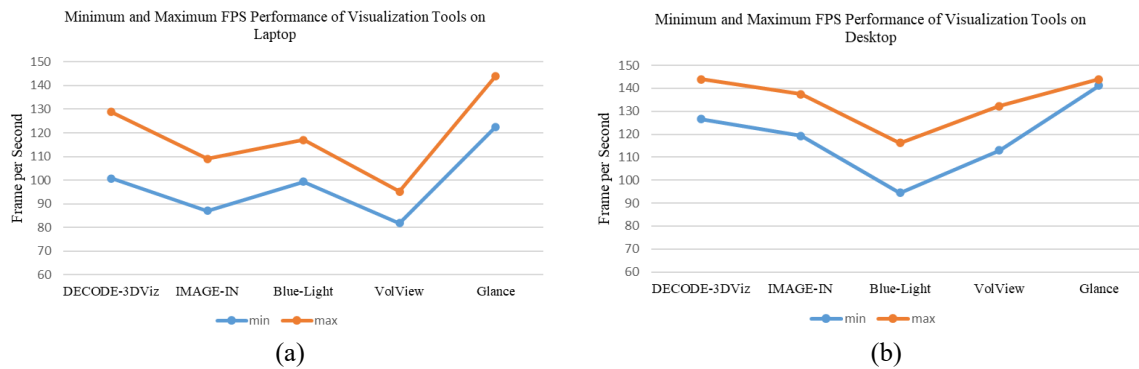


Figure 5.7 Minimum and Maximum Refresh Rate Performance of Visualization Tools on: (a) Laptop and (b) Desktop.

5.6.6 Clinical evaluation

The DECODE-3DViz tool uses an LOD algorithm, including the processes of rendering and rerendering regions of interest (ROIs), to provide detailed and clinical views of peripheral arterial segments. This capability is crucial for evaluating potential operative strategies and enhancing diagnostic accuracy. In Case Study 1 (Figure 5.5(a-c)), DECODE-3DViz facilitated clear visualization of the aortoiliac segment, effectively differentiating adjacent structures. This visualization provided critical insights into the diameters and wall morphology of the arteries and the extent of atherosclerotic, primarily calcified, lesions. In addition, the tool offered a clear view of both larger and smaller arterial branches, particularly around the femoral bifurcation. This is advantageous for planning surgical dissections and assessing the development of the collateral network.

In Studies 2 (Figures 5.5(d-f)) and 3 (Figures 5.5(g-i)), the focus was on the femoral–popliteal arterial segment, specifically the distal part of the superficial femoral artery, as it traverses the adductor (Hunter) canal and the P1 segment of the popliteal artery. DECODE-3DViz has demonstrated its ability to track the arterial pathway and its anatomical relationships with high fidelity and texture quality. This detailed level of visualization is instrumental in assessing and planning strategies for treating occlusive disease in the femoral–popliteal segment. The rerendered ROIs, processed through the LOD algorithm, provided a more precise view of the arterial structures and their relationships with surrounding tissues, enhancing the tool's clinical utility in medicine.

The ability of DECODE-3DViz to adapt to other vascular structures supports its potential use in coronary artery imaging. The system's selective rerendering ensures high-resolution

visualization of regions requiring detailed assessment, making it suitable for evaluating aneurysms, stenotic lesions, and vessel integrity in different anatomical contexts. In addition, its ability to process large volumetric datasets with adaptive resolution allows its extension to other anatomical regions, such as thoracic aortic dissection assessment. Furthermore, the system's ability to distinguish between high-density structures makes it well suited for bone visualization, including orthopedic assessments, fracture detection, and skeletal deformity analysis. This adaptability highlights its potential in neurology, cardiology, orthopedics, and oncology for precise 3D visualization of complex anatomical structures.

5.6.7 Questionnaire and Assessment Protocol

The evaluation of DECODE-3DViz was conducted with a cohort of 12 participants (four from the University of Ioannina, Greece; one from the University of Patras, Greece; one from the University of Milan, Italy; two from the University of Kragujevac, Serbia; one from the University of Montpellier, France; and three from AGH University of Krakow, Poland) from various professional backgrounds, including researchers, software engineers, PhD students, biomedical engineers, professors, and clinicians. The participants reviewed and assessed images generated by DECODE-3DViz alongside other state-of-the-art tools (IMAGE-IN, BlueLight, VolView, and Glance), providing comprehensive feedback on multiple visual attributes, as detailed in Table 5.4, using a structured questionnaire (Supplementary Questionnaire 1).

5.6.7.1 Visual characteristics

DECODE-3DViz consistently outperformed the other tools across all visual characteristics. Statistical analysis via ANOVA revealed significant differences in user ratings between the tools. For the definition of structure, the ANOVA results $F(4,15) = 164.44$, $p < 0.001$, indicated that DECODE-3DViz (mean = 4.37 ± 0.15) significantly outperformed IMAGE-IN (mean = 2.68 ± 0.16), BlueLight (mean = 2.12 ± 0.08), VolView (mean = 3.31 ± 0.11), and Glance (mean = 3.72 ± 0.16). Similarly, for depth perception, DECODE-3DViz excelled (mean = 4.26 ± 0.12) in representing spatial relationships within volumetric data, enhancing the understanding of complex anatomical features. The participants also praised DECODE-3DViz for its texture appearance (mean = 4.12 ± 0.12), noting the realistic surface textures that improved the visual realism and quality of medical images. In terms of fidelity, DECODE-3DViz demonstrated a high level of accuracy (mean = 4.30 ± 0.12) in depicting real peripheral artery tissue, which is crucial for diagnostic reliability. Finally, for diagnostic ability, DECODE-3DViz (mean = 3.87 ± 0.12) provided more diagnostically useful visualizations than the other tools did, further

enhancing its utility in medical applications. The ANOVA results confirmed these differences as statistically significant ($p < 0.001$ for all characteristics), underscoring the superior performance of DECODE-3DViz.

5.6.7.2 Additional Questions

Reliability of DECODE-3DViz: Participants rated the reliability at 4.41, which was significantly higher than the SoTA average of 2.66 ($p < 0.001$), indicating strong confidence in its performance and consistency. **Recommendation of DECODE-3DViz:** DECODE-3DViz received a high recommendation score of 4.5, whereas the SoTA average was 2.66 ($p < 0.001$), reflecting strong user preference and high satisfaction.

Table 5.4 Likert's scale evaluation of volume rendering across Peripheral arteries structures and characteristics from the DECODE-3DViz and State-of-the-Art Tools.

Characteristics	Tools	Iliac Artery	Femoral Artery	Popliteal Artery	Tibial Artery	Mean ± SD
Definition of Structure	DECODE-3DViz	4.5	4.41	4.41	4.16	4.37 ± 0.15
	IMAGE-IN	2.91	2.6	2.68	2.53	2.68 ± 0.16
	BlueLight	2.2	2.2	2.05	2.05	2.12 ± 0.08
	VolView	3.17	3.42	3.31	3.36	3.31 ± 0.11
	Glance	3.59	3.75	3.6	3.97	3.72 ± 0.16
Depth Perception	DECODE-3DViz	4.33	4.41	4.16	4.16	4.26 ± 0.12
	IMAGE-IN	2.85	2.55	2.6	2.3	2.57 ± 0.14
	BlueLight	2.15	2.2	2.11	2.04	2.12 ± 0.07
	VolView	3.2	3.45	3.35	3.35	3.31 ± 0.11
	Glance	3.6	3.8	3.7	4.0	3.77 ± 0.16
Texture Appearance	DECODE-3DViz	4.25	4.25	4	4	4.12 ± 0.12
	IMAGE-IN	2.91	2.6	2.68	2.53	2.68 ± 0.16
	BlueLight	2.15	2.1	2.07	2.1	2.10 ± 0.07
	VolView	3.2	3.45	3.35	3.35	3.31 ± 0.11
	Glance	3.6	3.8	3.7	4.0	3.77 ± 0.16
Fidelity	DECODE-3DViz	4.41	4.41	4.25	4.16	4.30 ± 0.12
	IMAGE-IN	2.91	2.6	2.68	2.53	2.68 ± 0.16
	BlueLight	2.10	2.0	2.11	2.04	2.08 ± 0.07
	VolView	3.17	3.42	3.31	3.36	3.31 ± 0.11
	Glance	3.59	3.75	3.6	3.97	3.72 ± 0.16
Diagnostic Ability	DECODE-3DViz	4.0	4.0	3.75	3.75	3.87 ± 0.12
	IMAGE-IN	2.91	2.6	2.68	2.53	2.68 ± 0.16
	BlueLight	2.0	2.2	2.14	1.94	2.02 ± 0.10
	VolView	3.5	3.4	3.3	3.3	3.45 ± 0.11
	Glance	3.6	3.8	3.6	3.9	3.67 ± 0.16

5.6.7.1 Open-End Questions

The participants highlighted several key strengths, such as the tool's reliability and superior performance on large datasets, producing clear and high-quality visualizations of the peripheral vasculature. They noted the detailed and accurate representation of anatomy and pathology, particularly in viewing the iliac and femoral arteries. Suggestions for improvement included adding rendering filters for visualizing different tissue types, which would increase the utility of DECODE-3DViz in medicine.

5.7 Discussion

The performance of DECODE-3DViz was evaluated against that of SoTA visualization tools, including IMAGE-IN, BlueLight, VolView, and Glance, which focus on render time, FPS, and GPU memory usage across laptop and desktop environments. As it is shown in Figure 5.8, DECODE-3DViz significantly outperforms the other tools in rendering time, demonstrating a 93% improvement over BlueLight on both laptops (Figure 5.8(a)) and desktops (Figure 5.8(b)), with notable advantages over IMAGE-IN, VolView, and Glance. In terms of FPS, DECODE-3DViz maintains high performance on laptops (Figure 5.8(c)), outperforms IMAGE-IN and

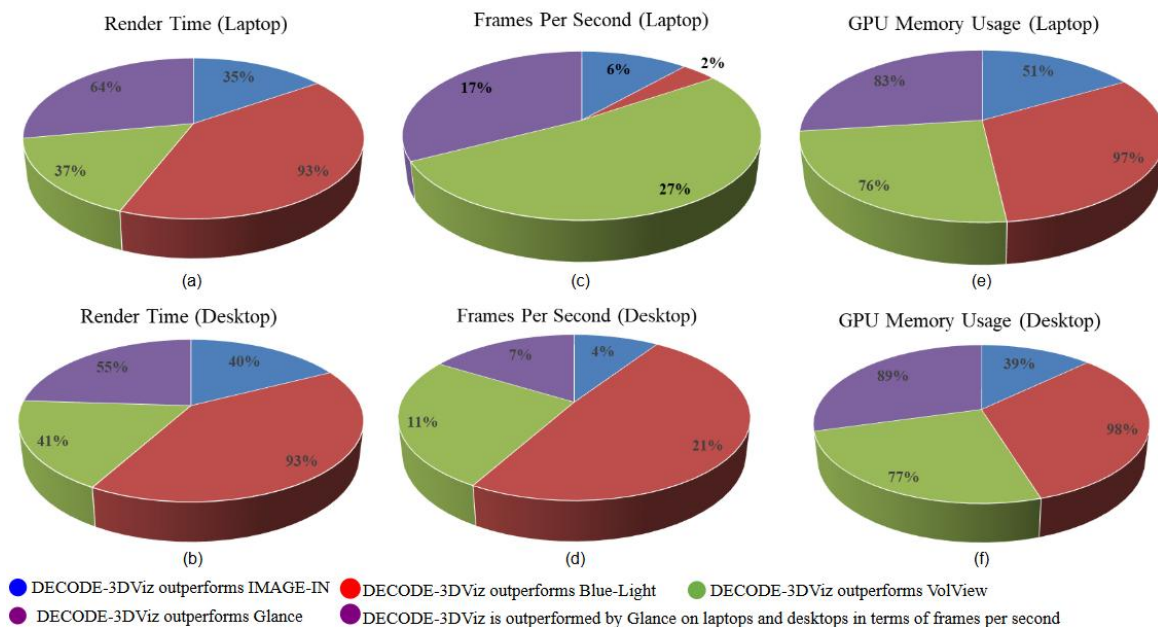


Figure 5.8 Performance Comparison of DECODE-3DViz and State-of-the-Art Visualization Tools which are IMAGE-IN, BlueLight, VolView, and Glance. (a) Render Time on Laptop, (b) Render Time on Desktop, (c) Frames Per Second (FPS) on Laptop, (d) FPS on Desktop, (e) GPU Memory Usage on Laptop, and (f) GPU Memory Usage on Desktop.

VolView, and achieves competitive results with Glance. On desktop, as shown in Figure 5.8(d), DECODE-3DViz ensures smooth and responsive visualizations, which are crucial for detailed analysis and diagnostics.

In addition, DECODE-3DViz exhibits exceptional GPU memory efficiency, using significantly less GPU memory than BlueLight 97% less on laptops (Figure 5.8(e)) and similarly reducing usage on desktops (Figure 5.8(f)). This efficiency makes DECODE-3DViz accessible with less powerful hardware, enhancing its usability and accessibility for real-time 3D visualization of large-scale peripheral artery CT images in web browsers.

5.7.1 Comparative evaluation of DECODE-3DViz and other modalities on a large-scale dataset

The evaluation of DECODE-3DViz against other SoTA visualization tools, which use large-scale CT datasets from patients #5 (series 6) and #7 (series 5), is shown in Table 5.5 and detailed in Table 5.6.

Table 5.5 Large-Size Dataset Specification for DECODE-3DViz validation and comparison with others.

Patient ID	Dimension	Size	Bits stored	Slice thickness	Spacing bet slice	Pixel spacing (mm)
5	(512, 512, 2299)	1.13	16	0.625 mm	0.625 mm	0.955078
7	(512, 512, 2305)	GB				0.912109

a) Rendering Efficiency and Performance

DECODE-3DViz significantly outperforms other tools, especially BlueLight, by reducing rendering times by approximately 98% on both laptops and desktops. It also provided smoother and more responsive visualizations, with FPS improvements of 44% on laptops and 131% on desktops.

b) GPU memory usage and resource efficiency

Compared with BlueLight, the tool demonstrated exceptional GPU memory efficiency, with 96.7% less memory on laptops and 97.4% less memory on desktops. This efficiency enhances the performance on less powerful hardware, expanding the accessibility of DECODE-3DViz.

c) Challenges in Processing Large-Scale Datasets

VolView experienced a "range error: invalid array buffer length," indicating issues with large datasets. IMAGE-IN and Glance failed to render these datasets, whereas BlueLight successfully rendered Patient #7's dataset. These difficulties, indicated by the 'x' values in Table 5.6, underscore the limitations of these tools due to high computational demands and inadequate memory management, in contrast with DECODE-3DViz's robust handling of extensive data volumes.

Table 5.6 Evaluation Metrics of DECODE-3DViz and State-of-the-Art Visualization Tools on Large-Size Dataset (mean \pm std).

	Metrics	Patient ID	DECODE-3DViz	IMAGE-IN	BlueLight	VolView	Glance
Laptop	Render Time (ms)	5	41.8 \pm 4.49	x	x	x	x
		7	38.4 \pm 1.20	x	2559 \pm 157.02	x	x
	Refresh Rate (FPS)	5	138.74 \pm 4.94	x	x	x	x
		7	142.0 \pm 1.47	x	96.38 \pm 24.62	x	x
	GPU memory usage (MB)	5	3.14	x	x	x	x
		7	3.1	x	94.7	x	x
Desktop	Render Time (ms)	5	54.6 \pm 2.65	x	x	x	x
		7	53.8 \pm 2.85	x	3185.4 \pm 394.7	x	x
	Refresh Rate (FPS)	5	135.62 \pm 3.09	x	x	x	x
		7	129.06 \pm 8.92	x	58.6 \pm 19.96	x	x
	GPU memory usage (MB)	5	2.6	x	x	x	x
		7	2.6	x	101.64	x	x

5.7.1 Innovations and Robustness in DECODE-3DViz

DECODE-3DViz introduces significant advancements in web-based medical imaging visualization, particularly for handling large-scale datasets such as peripheral artery CT images. The system overcomes WebGL texture size limitations and browser memory constraints, which have traditionally impeded real-time visualization. Key innovations include progressive chunk streaming and dynamic LOD algorithms, optimizing memory usage and enabling high-resolution rendering tailored to user interactions and the importance of specific regions. These features ensure smooth, detailed visualizations crucial for accurate diagnostics. DECODE-3DViz outperforms other SoTA methods in rendering time, refresh rate, and GPU memory usage, highlighting superior GPU resource management. Its robust performance has been validated through comprehensive evaluations, confirming its efficiency in complex medical imaging tasks. Moreover, DECODE-3DViz's web-based accessibility distinguishes it from traditional tools, broadening the availability of high-quality medical visualizations to medical professionals and patients.

5.7.2 Clinical impact of DECODE-3DViz in a real-world clinical setting

DECODE-3DViz enhances diagnostic precision and intervention planning by providing high-resolution, interactive views of peripheral artery CT images. Clinicians can assess complex pathologies such as atherosclerosis and stenosis with clarity, improving diagnostic accuracy and treatment efficacy. Surgical planning enables precise evaluation of arterial segments, facilitating accurate measurement of diameters and wall morphology, which is critical for assessing lesion severity and optimizing procedures. The tool supports noninvasive monitoring of disease progression and postoperative recovery by depicting arterial pathways with high fidelity. Its integration into digital workflows enhances real-time collaboration and multidisciplinary case discussions, streamlining decision-making in vascular diagnostics. By optimizing the diagnostic workflow, DECODE-3DViz accelerates image interpretation, reducing the time required for radiologists and vascular specialists to reach conclusions. This efficiency benefits triage and urgent interventions, ensuring quicker treatment decisions. Seamless integration with PACSs minimizes workflow disruptions, whereas enhanced visualization capabilities support telemedicine, allowing remote specialists to review cases efficiently and expand access to expert-driven diagnosis and treatment planning. Furthermore, DECODE-3DViz enables visualization of both vascular and osseous structures, enhancing orthopedic and vascular assessments by allowing simultaneous evaluation of arterial integrity and skeletal conditions. The advanced rendering pipeline ensures the precise differentiation of

vascular calcifications, fractures, and soft tissue structures, making it an effective tool for preoperative planning and post-treatment evaluation.

DECODE-3DViz significantly enhances the detection and assessment of vascular abnormalities, including arterial stenosis, occlusions, and calcifications, by providing clinicians with detailed, high-resolution images for accurate interpretation. The ability to visualize both large arterial structures and finer vascular branches ensures a comprehensive evaluation of the PAD. One of DECODE-3DViz's most impactful clinical applications is its role in telemedicine and remote diagnostics. The system's accessibility allows specialists to review cases remotely and provide expert opinions from various geographic locations. This feature is particularly beneficial for hospitals with limited vascular imaging expertise, enabling remote consultations with specialists to improve patient outcomes.

5.7.3 Limitations and Future Work

DECODE-3DViz currently processes datasets only in DICOM and NIfTI formats. In addition, advanced rendering filters for tissue differentiation, which are vital for distinguishing between similar intensity tissues such as bone, muscle, arterial, and adipose tissue, are lacking. Expanding the format support and integrating rendering filters would enhance the applicability and versatility of DECODE-3DViz, providing a more comprehensive solution for medical imaging visualization and analysis. Future work will focus on enhancing real-time volumetric rendering by integrating adaptive transfer functions to improve tissue segmentation and classification. Moreover, incorporating AI-driven automation for feature extraction and anomaly detection could further streamline clinical decision-making. A key focus will be on automated peripheral artery risk classification, leveraging ML models to assess arterial stenosis severity and predict potential occlusions. This automated risk assessment could aid clinicians in early disease detection and personalized treatment planning, reducing the likelihood of adverse cardiovascular events. Expanding cloud-based capabilities will facilitate multiuser collaboration and enable seamless access to imaging data across institutions, supporting broader clinical adoption and interoperability within modern healthcare infrastructures.

5.8 Conclusions

The development and implementation of DECODE-3DViz have enabled significant progress in medical imaging, particularly in visualizing peripheral artery CT images. This system adeptly addresses key challenges in rendering large-scale medical datasets on web platforms, overcoming WebGL texture size constraints and browser memory limitations. By using

advanced techniques such as data chunk streaming and the LOD algorithm, DECODE-3DViz dynamically adjusts resolution on the basis of user interaction and the importance of visualized regions, increasing both user engagement and visualization quality. This capability is invaluable for clinical experts, as it enhances diagnostic accuracy and supports detailed preoperative planning by delivering high-fidelity visualizations of complex vascular structures. The ability to manage extensive datasets without sacrificing performance or visual fidelity sets DECODE-3DViz apart from existing solutions, offering a more robust and user-friendly tool for medical professionals. Future developments include the integration of advanced rendering filters for visualizing different tissue types, such as bone, muscle, and adipose tissue, thereby broadening the system's applicability across various medical scenarios. In addition, further optimization is needed to improve the system's scalability and efficiency in handling even larger datasets.

Chapter 6: DECODE: An Open-Source Cloud-Based Platform for the Noninvasive Management of Peripheral Artery Disease

- 6.1. Introduction
 - 6.2. Materials and methods
 - 6.3. Modules Design and Architecture
 - 6.4. Evaluation
 - 6.5. Results
 - 6.6. Discussion
 - 6.7. Conclusions
-

6.1 Introduction

This chapter presents the development and validation of DECODE, an open-source cloud-based platform designed to transform the noninvasive management of PAD. DECODE integrates DL-powered segmentation, real-time 3D visualization, and finite element-based computational modeling within a unified cloud-native framework, addressing critical limitations of existing PAD diagnostic systems. Unlike fragmented solutions that lack comprehensive integration, DECODE seamlessly bridges AI-driven medical imaging, predictive analytics, and *in-silico* simulations to offer an automated, scalable infrastructure for vascular precision medicine [295].

The motivation behind developing DECODE lies in the increasing demand for advanced diagnostic tools that increase diagnostic accuracy, optimize treatment planning, and provide

personalized interventions for PAD. Traditional methods often rely on isolated systems with limited interoperability, manual processing, and a lack of real-time visualization, which can compromise diagnostic precision and clinical decision-making [296]. DECODE overcomes these limitations by providing a fully automated, cloud-integrated diagnostic and interventional workflow.

This chapter systematically details the architectural design, implementation, and evaluation of DECODE. It explores the platform's modular microservice architecture, which ensures secure, efficient data communication across the main, subfrontend and backend servers. The platform's core capabilities are highlighted, including DL-powered peripheral artery (PA) segmentation, intima–media thickness (IMT) segmentation, and centerline extraction, which are essential for precise vascular analysis and computational hemodynamic modeling. In addition, DECODE supports *in-silico* clinical trials through its finite element modeling (FEM) and DCB simulation modules, optimizing drug–device performance and reducing the need for physical trials [297].

A critical component of DECODE is its advanced visualization capability powered by DECODE-3DViz, a WebGL-based tool that delivers high-fidelity 3D rendering and immersive visualization experiences. This capability significantly enhances diagnostic accuracy, procedural planning, and personalized treatment strategies. The platform's cloud-native architecture ensures seamless integration, scalability, and real-time accessibility, making it adaptable for diverse clinical and research workflows.

This chapter also presents the usability and acceptance evaluations of DECODE, which are conducted via the SUS [298] and the TAM [299]. By detailing the technical design, implementation challenges, and validation outcomes, this chapter establishes DECODE as a pioneering solution in digital vascular diagnostics, paving the way for personalized PAD management and advancing the frontier of precision vascular medicine.

The platform's core capabilities include the following:

- Dataset Management Module – A secure, cloud-integrated system for uploading, managing, and sharing medical datasets among clinicians and researchers.
- Data Conversion Module – Convert the DICOM/NIFTI datasets into standardized formats for AI-based processing.
- PA segmentation module – A deep-learning-powered tool for automated arterial segmentation, ensuring high diagnostic precision.

- IMT segmentation module – AI-driven lumen-intima boundary detection, which is essential for vascular risk assessment.
- Centerline Extraction Module – Computes vascular centerlines, providing geometric profiling for computational hemodynamic modeling.
- DECODE-3DViz – A real-time 3D WebGL-based volume rendering tool that supports interactive exploration.
- Finite element modeling (FEM) module – Enables *in-silico* simulations of balloon angioplasty and vascular interventions, improving patient-specific treatment planning.
- Scalability and open-source interoperability – A RESTful API-based cloud framework ensuring seamless integration with EHRs, telemedicine platforms, and computational research workflows.

DECODE establishes a new benchmark in AI-driven PAD diagnostics and intervention planning by integrating DL-powered segmentation, real-time 3D visualization, and computational modeling within a fully automated, cloud-native ecosystem. By seamlessly bridging the domains of medical imaging, AI-enhanced decision support, and predictive modeling, DECODE delivers a comprehensive digital solution tailored for vascular precision medicine.

The primary users of the DECODE platform include clinicians, researchers, and healthcare institutions. Clinicians benefit from enhanced diagnostic accuracy and optimized intervention planning through advanced segmentation and high-fidelity visualization, improving therapeutic outcomes. Researchers utilize DECODE for *in-silico* simulations, enabling patient-specific modeling for DCB therapy and angioplasty, accelerating drug device development and optimizing therapeutic strategies. Healthcare institutions leverage their secure, scalable cloud infrastructure for multicenter data management and seamless clinical integration, enhancing interoperability and collaboration. DECODE drives innovations in vascular diagnostics, *in-silico* trials, and personalized treatment planning, revolutionizing PAD management through precision medicine.

6.2 Materials and methods

6.2.1 Conceptual Design

To align the DECODE Cloud Platform with clinical, research, and industry needs, a user-centered design approach was employed, gathering detailed requirements through a structured

questionnaire from 16 participants across leading European institutions involved in vascular research, medical imaging, and computational modeling. These included researchers from the University of Ioannina, University of Athens, University of Patras, University of Milan, University of Kragujevac, University of Montpellier, and AGH University of Krakow. The insights provided a multidisciplinary perspective, ensuring DECODE’s integration of AI-driven analytics, real-time visualization, and scalable cloud infrastructure. As illustrated in Figure 6.1, platform development followed eight phases: (1) gathering user requirements; (2) defining key architectural components such as segmentation, 3D visualization, and computational modeling; (3) establishing secure data management and sharing; (4) integrating tools for data conversion, image upscaling, and centerline extraction; (5) implementing DL for accurate artery and lumen-intima boundary detection; (6) enabling real-time DICOM rendering and WebGL-based volume visualization; (7) providing predictive simulations for PAD treatment planning; and (8) leveraging open-source cloud infrastructure with RESTful APIs for EHR and telemedicine integration. This structured approach ensures that DECODE meets the demands of modern vascular research and clinical applications.

6.2.2 Implementation

The DECODE Cloud Platform is designed as a modular, cloud-based framework that integrates AI-driven diagnostics, real-time visualization, and computational modeling to optimize the management of PAD. Figure 6.2 presents the package diagram of the platform, detailing its

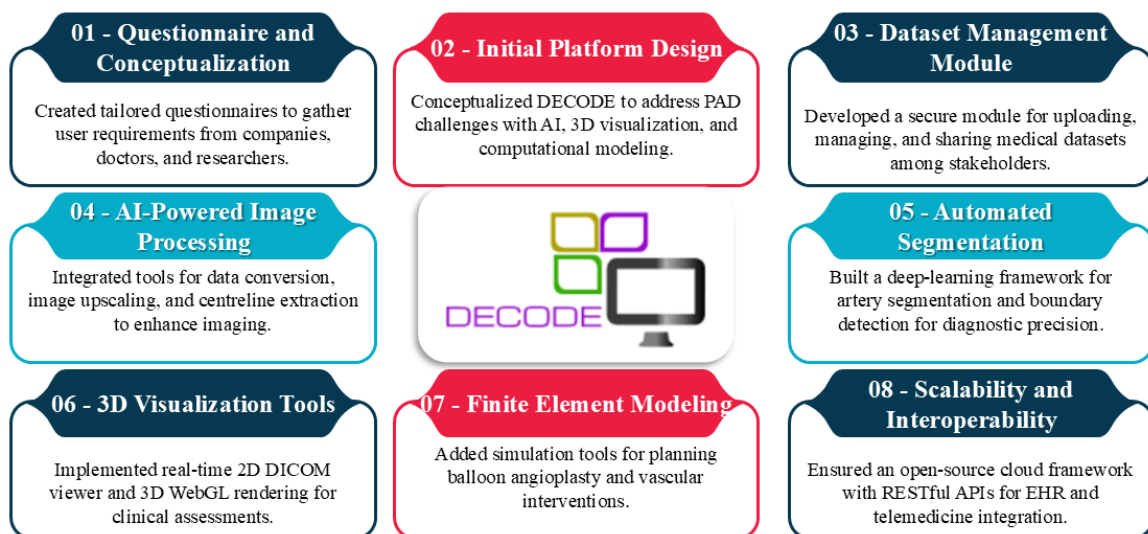


Figure 6.1 Conceptual development phases of the DECODE cloud platform.

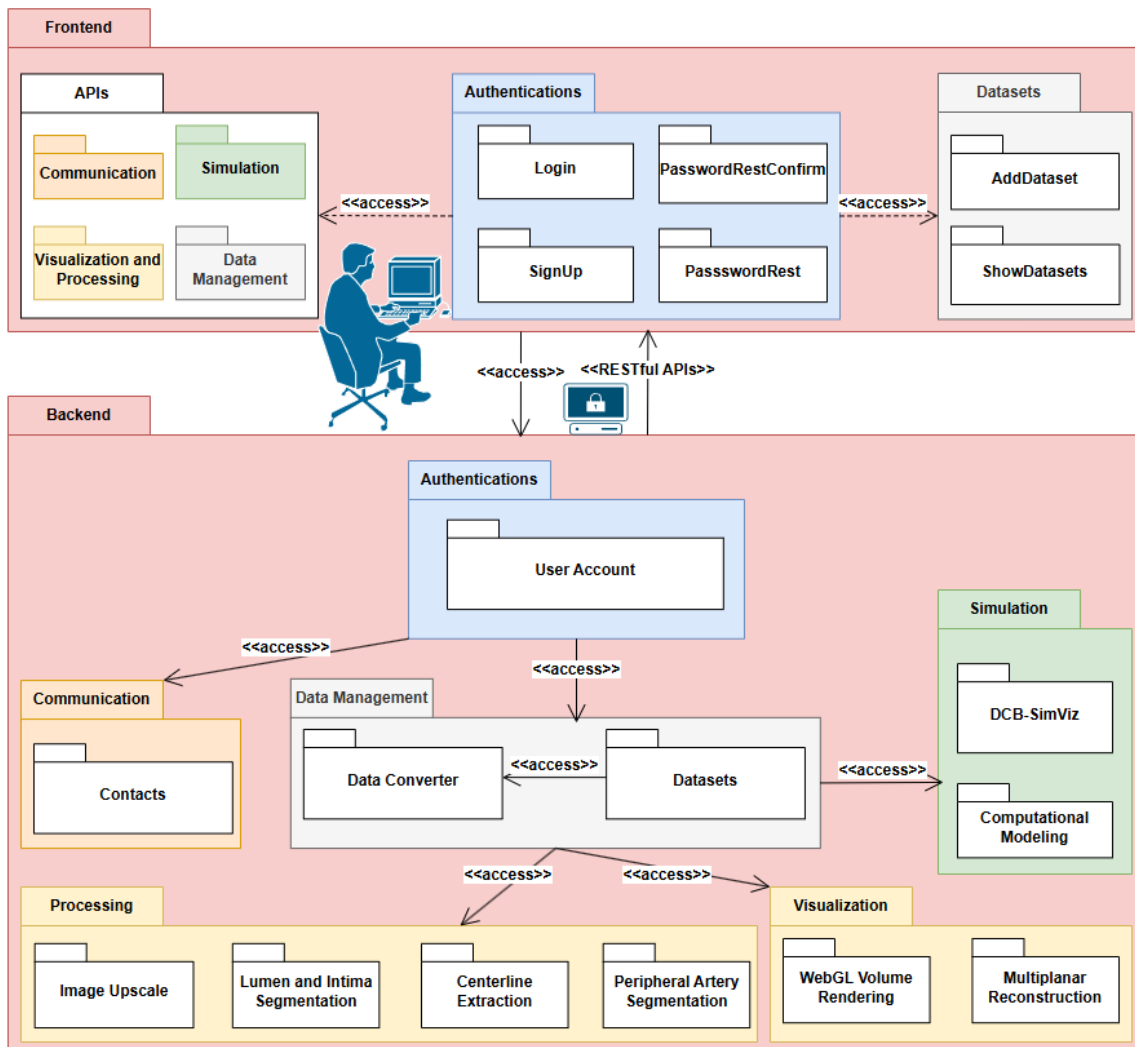


Figure 6.2 Package diagram of the DECODE Cloud Platform.

hierarchical structure, interdependence, and information flow across system modules. The architecture is structured into frontend and backend layers, each of which is responsible for specific functionalities. The frontend, implemented via React.js [238], leverages its component-based structure and virtual DOM for a highly responsive, interactive user experience. The backend, built with Django [300], provides a scalable and secure RESTful API-driven environment, facilitating efficient data processing and AI-powered analytics. This architecture ensures a seamless and dynamic workflow, allowing users to interact with medical imaging, computational modeling, and treatment planning in a cloud-based ecosystem.

6.2.3 DECODE Cloud Platform Layers

The DECODE Cloud Platform is architected as a multilayered system to deliver a scalable and secure solution for the noninvasive management of PAD, as illustrated in Figure 6.3. The architecture comprises five fundamental layers: a hardware layer, a security layer, a workflow

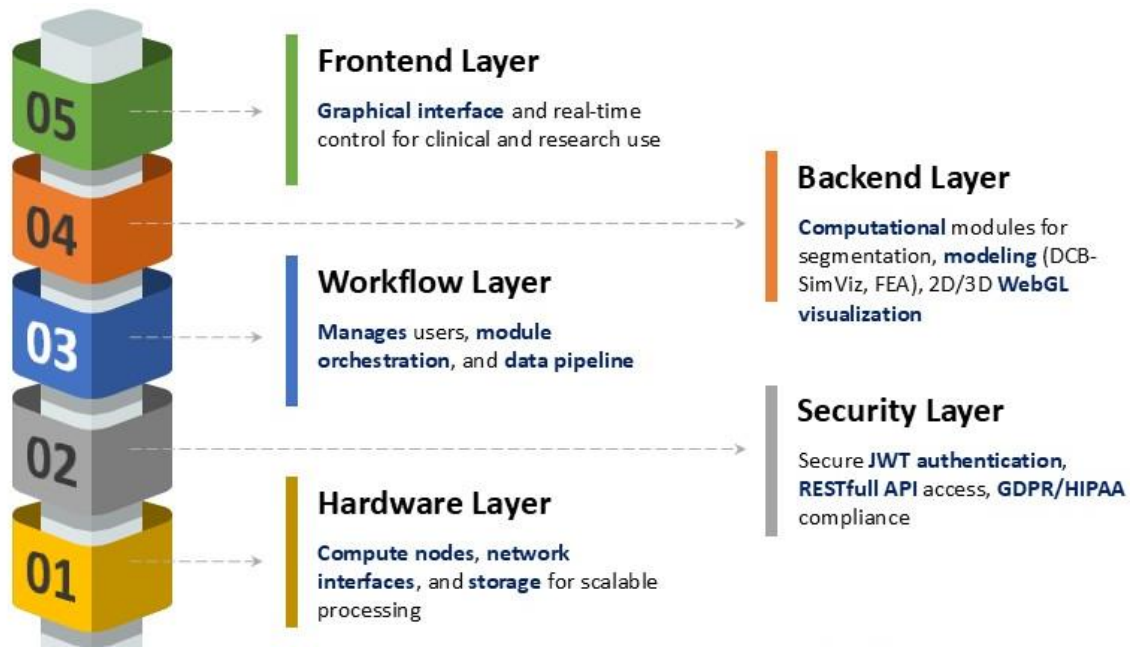


Figure 6.3 The DECODE Cloud Platform's multilayered hierarchical framework.

layer, a backend layer, and a frontend layer, each designed for seamless integration, high availability, and optimized performance. At the foundation, the hardware layer provides the core infrastructure, including networking components, storage solutions, and processing units. It is optimized for computationally intensive tasks such as medical imaging, data processing, and advanced simulations, ensuring high availability and scalability through cloud-based infrastructure.

The security layer implements robust user authentication, RESTful API security, and access control mechanisms. It ensures data integrity and privacy via advanced encryption protocols and role-based access control, maintaining strict compliance with the GDPR and HIPAA regulations [301]. The workflow layer orchestrates module interactions and manages user authentication, including login, signup, and password resets. It facilitates intermodule communication and data management, optimizing workflows for seamless data integration, transformation, and organization. The Backend Layer serves as the computational engine, hosting processing modules for image upscaling, Lumen and Intima segmentation, centerline extraction, and PA segmentation. It supports simulation and computational modeling tools such as DCB-SimViz and FEAs, enabling predictive simulations for clinical decision-making. It also includes visualization tools powered by WebGL Volume Rendering, MPR, and WebXR for high-fidelity 3D visualization.

At the top, the Frontend Layer offers a responsive user interface with APIs for visualization, image processing, data management, and simulation. It includes dataset management functionalities for adding, displaying, and organizing datasets. Built on a PWA framework, it ensures cross-platform compatibility and offline accessibility [302], enhancing productivity for surgeons, researchers, and pharmaceutical representatives. This layered architecture provides a scalable, secure, and high-performance solution for advanced medical imaging and data analytics in PAD management. By integrating hardware infrastructure, robust security, efficient workflows, powerful backend processing, and an intuitive frontend interface, the DECODE Cloud Platform sets a new benchmark for digital health solutions in vascular medicine.

6.2.4 Distribution of the DECODE Cloud Computing Services to Stakeholders

The DECODE Cloud Platform is strategically designed to distribute cloud computing services efficiently across a diverse range of stakeholders, including clinicians, researchers, developers, and patients, as illustrated in Figure 6.4. At the forefront are frontend services, which are delivered through an intuitive user interface and interactive visualization modules. These modules leverage WebGL and VR/AR technologies to provide immersive experiences, enabling clinicians to perform 3D rendering, real-time diagnostics, and precision surgical planning. These services are accessible via a PWA, ensuring cross-platform compatibility and offline accessibility.

The backend layer serves as the computational engine, hosting advanced image processing, modeling tools, and data management modules. It integrates the finite element method (FEM) and ML tools to support complex simulations, predictive analytics, and clinical data analysis. The visual analytical engine powers comprehensive data exploration, whereas the workflow manager ensures seamless communication among modules. The REST API engine facilitates secure and scalable communication between the frontend and backend components via the HTTP and JSON protocols [303].

Security is ensured through a robust security layer that employs JWT authentication for secure login sessions, transport layer security (TLS) protocols for end-to-end data encryption [304], and a private credential database for role-based access control, ensuring compliance with the GDPR and HIPAA standards. This layered security approach protects sensitive medical data while maintaining user privacy.

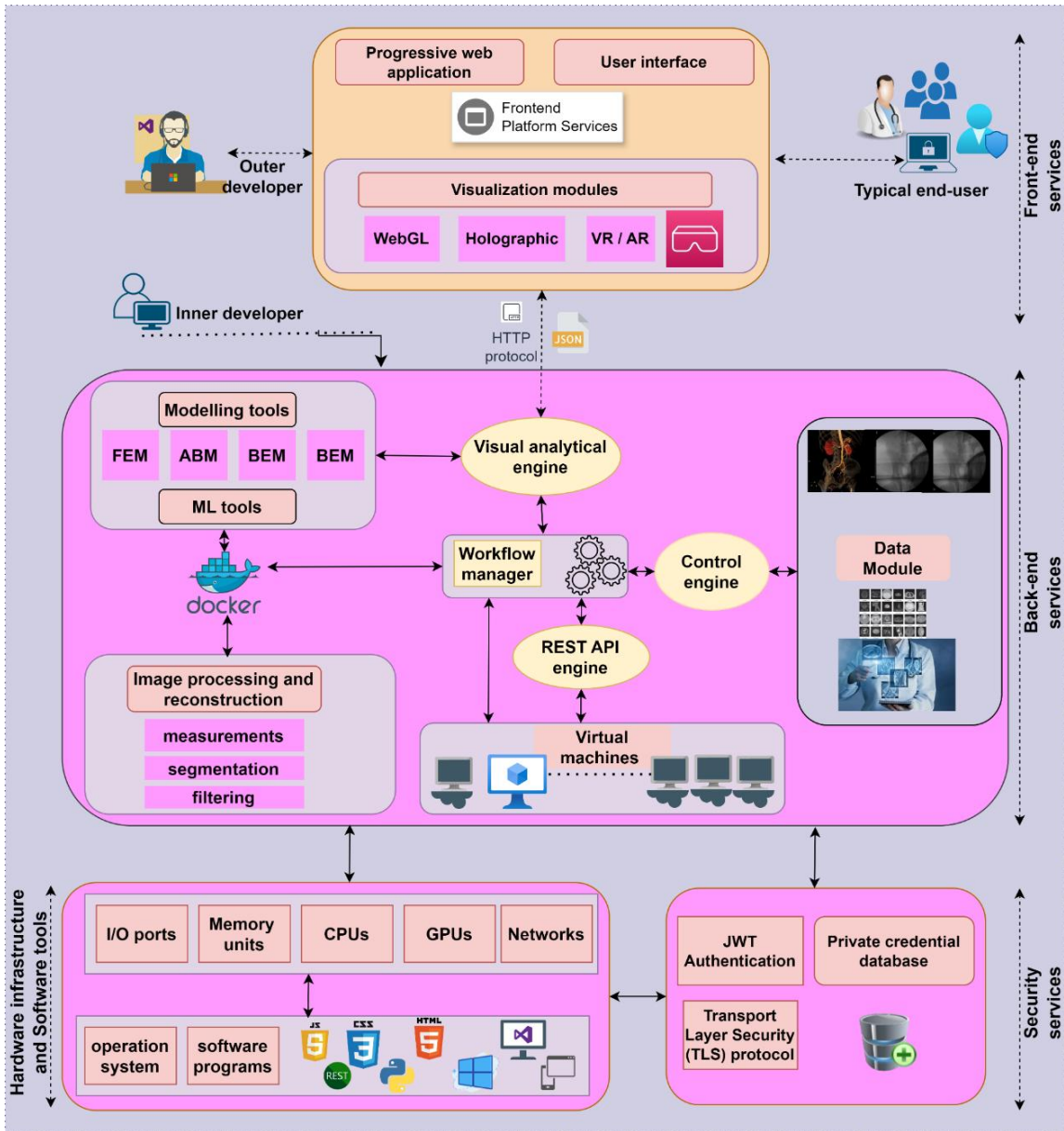


Figure 6.4 Architecture and Service Distribution of the DECODE Cloud Platform.

At the core, the hardware infrastructure provides the necessary computational resources, including I/O Ports, Memory Units, CPUs, GPUs, and Networking Components, optimized for high-performance computing in medical imaging, data processing, and simulation tasks. This infrastructure supports virtual machines and Docker containers for scalable deployment and high availability.

This architecture efficiently distributes cloud computing services to stakeholders, enabling clinicians to leverage real-time diagnostics, researchers to access advanced modeling tools and data processing modules, developers to innovate in PAD management, and patients to maintain control over their medical data. By seamlessly integrating front-end visualization, backend

computational power, security mechanisms, and scalable hardware resources, the DECODE Cloud Platform delivers a high-performance, secure, and scalable solution for vascular diagnostics, in silico trials, and personalized treatment planning.

6.3 Modules Design and Architecture

The DECODE Cloud Platform frontend is designed as a PWA that integrates AI-driven modules for real-time PAD diagnostics, computational modeling, and 3D visualization. Its modular and scalable architecture, as illustrated in Figure 6.5, ensures a seamless workflow from data acquisition to advanced treatment simulation. The system is structured into interconnected components, facilitating automated medical image processing, DL-based segmentation, FEM, and WebGL visualization. This section provides a detailed breakdown of the platform's core modules, their functionalities, and interdependencies, highlighting their impact on PAD diagnosis and intervention planning.

6.3.1 User Authentication and Access Control

The DECODE Cloud Platform employs a secure authentication system to ensure robust access control and data security, as illustrated in Figure 6.6. The authentication process is managed by an access control module that verifies user credentials, assigns roles, and enforces hierarchical security policies. This system supports various user roles, including researchers, doctors, and administrators, each with tailored access privileges to platform functionalities.

The platform uses a RESTful API-based JSON Web Token (JWT) tokenization system to securely manage user authentication and authorization. When a user attempts to log in, the User Authentication request is processed through the Frontend Authentication Module, which

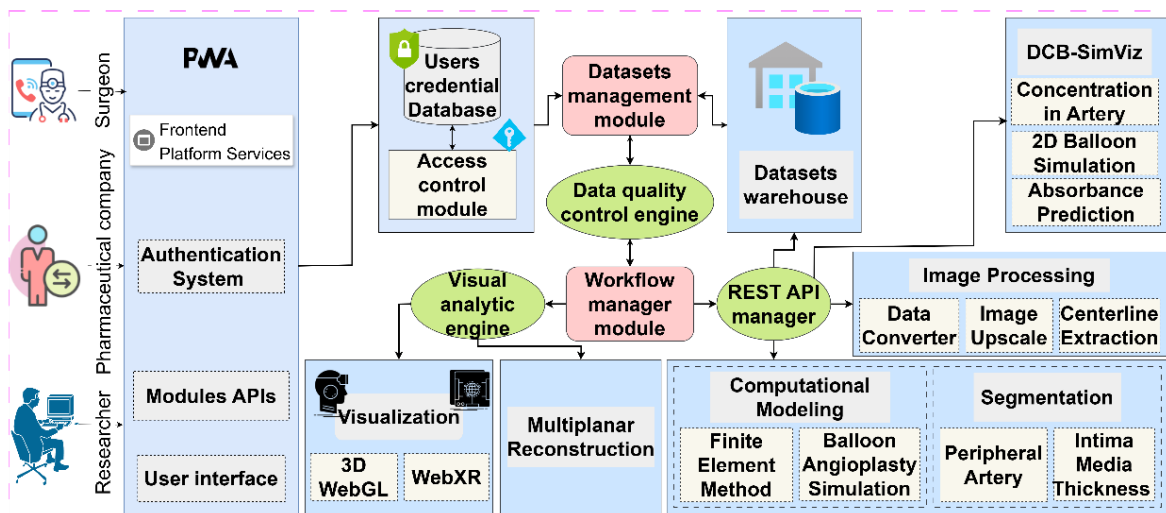


Figure 6.5 Detailed architecture of the DECODE Cloud Platform.

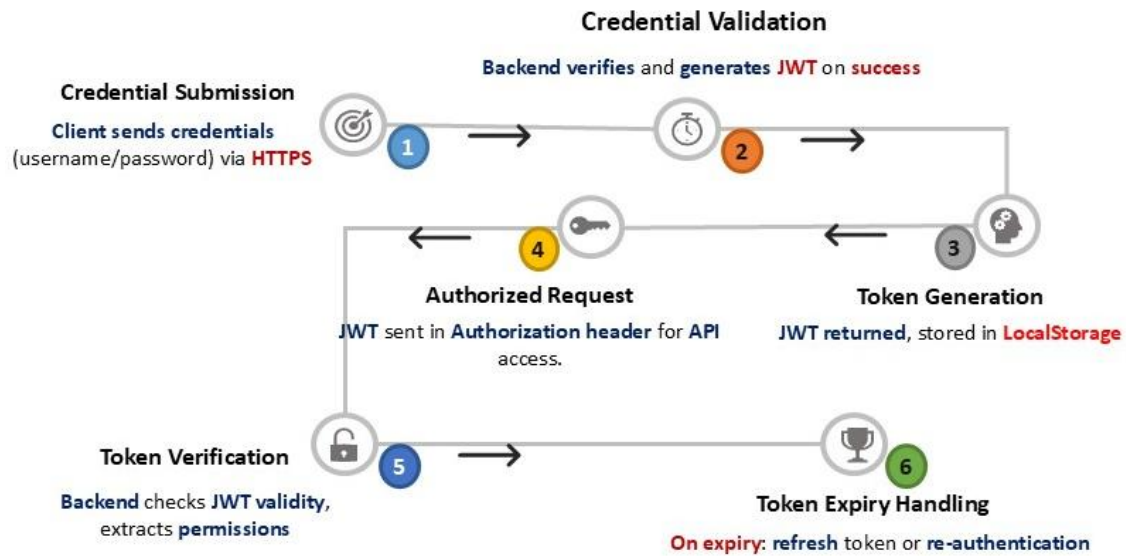


Figure 6.6 User authentication workflow in the DECODE Cloud Platform.

securely transmits the credentials to the Backend Authentication API over an encrypted HTTPS request. The server validates user credentials by cross-referencing the information with the User Credential Database. If the credentials are correct, the server generates a JWT token containing the user ID, expiration time, and a secret key signature. This token is then securely sent to the client and stored in *LocalStorage* for persistent login [305].

The system includes a token issuance and response mechanism, ensuring that each request is authenticated via the JWT token. The server verifies the JWT by checking the token's signature, expiration time, and user role. If validated, the server grants access to the requested resource, such as uploading datasets, running segmentation algorithms, or interacting with WebGL visualization tools. To maintain security and session integrity, DECODE implements a Token Expiry and Refresh mechanism. Once a token expires, users must either reauthenticate or use a refresh token to obtain a new JWT without reentering their credentials. This approach balances security and user convenience by maintaining continuous authentication sessions without frequent logins. This JWT-based authentication architecture provides persistent, role-based access management, ensuring data security and system integrity while maintaining a user-friendly experience. It supports scalable and secure communication across frontend and backend servers, enabling seamless interactions within the DECODE Cloud Platform.

6.3.2 Data Providers

The DECODE Cloud Platform relies on a data provider to ensure the availability and accessibility of medical data essential for simulations, optimizations, and treatment planning,

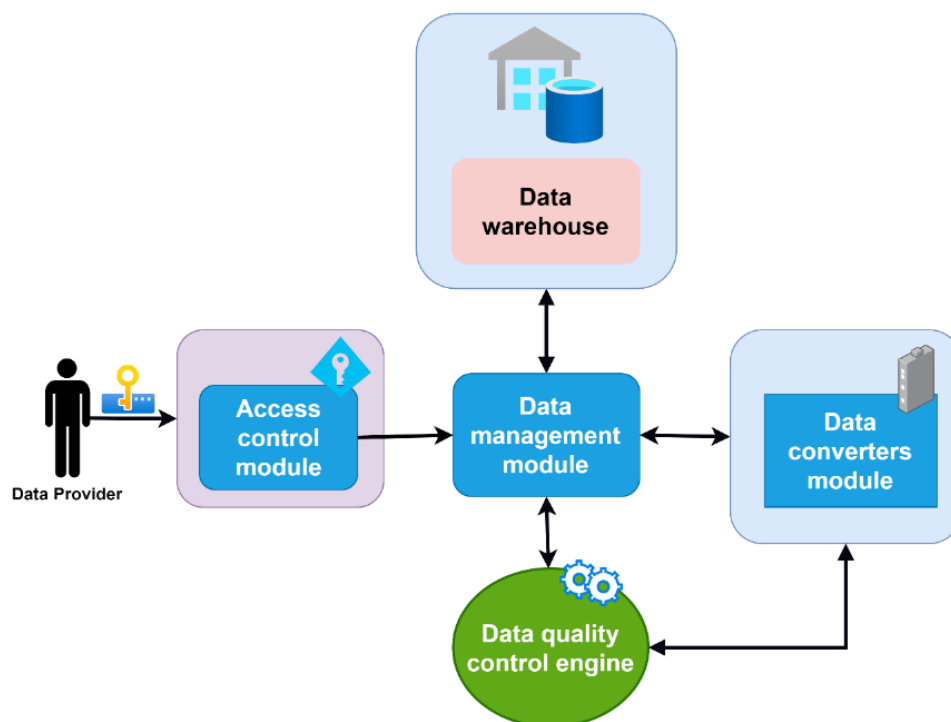


Figure 6.7 Data provider architecture within the DECODE Cloud Platform.

as illustrated in Figures 6.7 and 6.8. The data provider connects the platform's core modules with diverse analytical tools, integrating data from various sources, including medical databases, patient records, imaging systems, and research studies. It consolidates these data into a unified repository, enabling advanced analysis and high-fidelity visualization. Figure 6.7 shows the data provider architecture, highlighting the integration of key modules: access control, data management, data converters, and a data quality control engine. The access control module enforces secure authentication and authorization protocols, safeguarding data privacy and integrity. The data management module standardizes incoming data formats, ensuring compatibility across all platform modules. The Data Converters module transforms raw medical data into formats suitable for DL algorithms and computational modeling. To maintain data accuracy and reliability, the Data Quality Control Engine continuously monitors and rectifies inconsistencies, ensuring high data integrity.

Figure 6.8 illustrates the data ownership and the collaborative healthcare ecosystem within the DECODE platform. It empowers patients as Data Owners, granting them full control over their medical data, including the ability to create, read, update, and delete personal information. This feature enhances patient engagement by enabling patients to maintain data accuracy and exercise control over their participation. Researchers, developers, and doctors utilize the

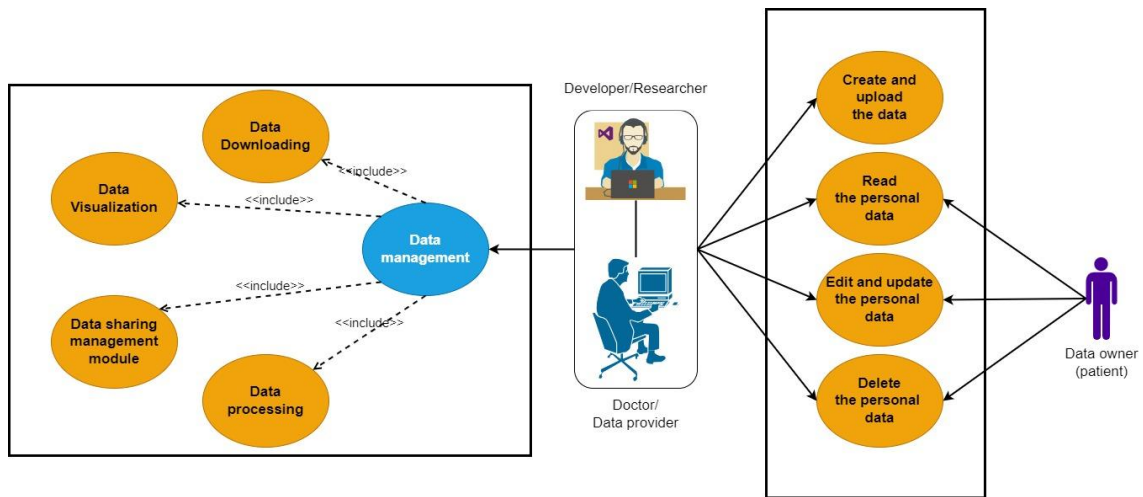


Figure 6.8 Data Ownership and Collaborative Healthcare Ecosystem.

platform’s tools to upload, read, edit, update, analyze, and visualize medical data, fostering a collaborative environment for advanced research and personalized patient care while maintaining strict compliance with ethical and regulatory standards.

The data provider supports real-time updates, ensuring that clinical decisions are informed by the latest medical insights. It employs efficient data retrieval and caching strategies to maintain platform responsiveness, even with large datasets. By enabling secure collaboration and advanced analytics, the data provider drives innovation in PAD management and DCB optimization. Its modular architecture ensures scalable performance and seamless integration with the DECODE Cloud Platform, facilitating responsible data sharing and ethical research practices.

6.3.3 Data Management and Data Quality Control

A centralized dataset warehouse functions as the primary storage and retrieval system for medical imaging data, supporting multiple formats, including DICOM [306] and NIfTI [307]. The dataset management module facilitates structured metadata indexing, ensuring that uploaded datasets remain traceable and interoperable. Before datasets are processed, they undergo a quality validation step managed by the data quality control engine, which performs format standardization. This automated pipeline ensures that only high-fidelity images proceed to AI-driven segmentation and computational analysis, minimizing errors associated with low-resolution or inconsistent datasets.

6.3.4 Workflow Manager Module

The workflow manager module is the core orchestration engine of the DECODE Cloud Platform, facilitating automated task execution, data transfer, and AI-powered image processing [308, 309]. This ensures that segmentation, computational modeling, and visualization workflows are executed in a synchronized and scalable manner. The workflow module supports asynchronous execution, allowing multiple computational tasks to run in parallel, thus optimizing processing efficiency. Through API-driven task scheduling, the module dynamically allocates computational resources, reducing latency in real-time applications such as image analysis, segmentation, and FEM simulations.

6.3.5 Visualization

6.3.5.1 WebXR (eXtended Reality)

The WebXR Viewer module enables real-time, interactive 3D model visualization and AR integration for medical imaging applications [310]. This module is designed to seamlessly render and manipulate GLB-formatted anatomical models directly within a web browser, eliminating the need for specialized software. The workflow begins with file acquisition, allowing users to upload 3D models via drag-and-drop or direct file selection, ensuring an intuitive and accessible interface for medical professionals and researchers. The module uses Google's Model Viewer API, providing high-fidelity rendering with adjustable shadow intensity, dynamic lighting, and full camera controls to facilitate detailed anatomical inspection [311]. Once loaded, interactive scene control, such as zooming, rotation, and object manipulation, enhances the ability to examine intricate structures. A key innovation is the integration of WebXR-based AR functionality, enabling users to project and visualize 3D models within real-world environments via AR-supported devices, bridging the gap between digital analysis and physical spatial assessment.

6.3.5.2 DECODE-3DViz: WebGL

The DECODE-3DViz [44, 75] module is a WebGL-powered 3D visualization framework designed for interactive volume rendering of medical imaging datasets, including DICOM and NIfTI formats. This system enables real-time rendering, dynamic parameter control, and high-fidelity volumetric analysis directly in a web environment, eliminating the need for specialized hardware. The visualization pipeline begins with data acquisition, where users can upload single or multiple medical imaging files or fetch them remotely via the URL. The preprocessing stage ensures compatibility by handling anisotropic voxel spacing, intensity normalization, and

adaptive resolution adjustments. The core volume rendering engine, built on WebGL and VTK.js, employs gradient-based opacity mapping and transfer function optimization. Users can dynamically adjust lighting conditions and perform voxel intensity scaling, refining visualization quality for diagnostic precision. In addition, the module integrates interactive clipping planes, real-time cropping, and widget-based selection tools to facilitate focused region analysis. By incorporating customizable rendering presets, multimodal blending, and high-performance GPU acceleration, DECODE-3DViz provides an advanced, browser-based solution for interactive 3D medical visualization, supporting clinical diagnostics, surgical planning, and computational modeling in vascular imaging.

6.3.6 Routing Architecture of the DECODE Cloud Platform

The routing architecture of the DECODE Cloud Platform is designed to facilitate seamless communication and efficient data flow between its functional modules. By employing RESTful API endpoints, the platform ensures standardized data exchange and secure interactions, optimizing scalability and maintainability. Table 6.1. The DECODE Cloud Platform Routes and Functional Modules illustrate the organized routing scheme categorized by modules, ensuring logical grouping and hierarchical navigation. The Authentication and General Pages module centralizes the user authentication and navigation endpoints, including /login, /signup, and /password-reset. These routes are interconnected to maintain session continuity through token-based authentication (JWT). The structured routing within this module ensures streamlined access management and secure navigation between general pages such as /home, /about, and /contact.

In the dataset management module, routes are hierarchically organized to handle medical datasets, enabling actions such as uploading (/datasets/upload-datasets), retrieving (/datasets/show-datasets/:id), and updating datasets (/datasets/show-datasets/:id/update). The modular grouping of these endpoints allows efficient data management while maintaining scalability for large dataset repositories.

The image processing module groups related routes for preprocessing tasks, including /image-processing/centerline-extraction, /image-processing/dataconverter, and /image-processing/upscale. The interrelation between these routes facilitates data transformation and consistency, ensuring compatibility across all imaging workflows. This logical grouping allows flexible extension for additional preprocessing functionalities.

Table 6.1 DECODE Cloud Platform Routes and Functional Modules.

Module/Category	Endpoints/Routes	Description
Authentication and General Pages	/login /signup /password-reset /password-reset-confirm /home /about /contact	User authentication, account management, and general navigation pages.
Datasets Management	/datasets /datasets/upload-datasets /datasets/show-datasets /datasets/show-datasets/:id /datasets/show-datasets/:id/update	Secure uploading, managing, and displaying of medical datasets.
Image Processing	/image-processing /image-processing/centerline-extraction/image-processing/dataconverter /image-processing/upscale	Image preprocessing, centerline extraction, format conversion, and upscaling.
Segmentation	/segmentation /segmentation/segmentation-imt /segmentation/segmentationPA	Deep learning-powered arterial segmentation and lumen-intima boundary detection.
Visualization	/visualization /api/DECODE-3DViz /visualization/webXR /dcb-simviz	Real-time 3D visualization, WebGL-based volume rendering, and interactive exploration.
Computational Modeling	/computational-tools /computational-tools/finite-element/computational-tools/BAsimulation	<i>In-silico</i> simulations using finite element modeling and balloon angioplasty simulation.
Multiplanar Reconstruction	/3dMPR	High-resolution multiplanar reconstruction for detailed vascular analysis.

The segmentation module organizes its routing to streamline automated segmentation workflows. The endpoints /segmentation, /segmentation/segmentation-imt, and /segmentation/segmentationPA are cohesively grouped, ensuring structured navigation through different segmentation tasks. This modular design optimizes route maintainability and scalability for evolving DL models.

The visualization module uses a cohesive routing scheme for 3D rendering and interactive exploration. Endpoints such as /visualization, /api/DECODE-3DViz, and /visualization/webXR are strategically linked to provide seamless transitions between visualization tools. The

interconnected routing structure enhances the user experience by enabling intuitive navigation across multiple visualization modes, including volume rendering and AR.

Computational modeling routes are logically grouped to support *in-silico* simulations. The hierarchical structure includes /computational-tools, /computational-tools/finite-element, and /computational-tools/BAsimulation, maintaining consistency across computational workflows. This modular routing design allows efficient model execution and integration with other computational modules.

Finally, the MPR module is managed through a single entry point (/3dMPR), maintaining simplicity and high navigational efficiency for accessing cross-sectional views. This isolated routing structure enhances maintainability and future scalability for multiplanar visualization enhancements.

The DECODE routing architecture employs a modular, hierarchical design, ensuring consistent data flow and efficient communication across all modules. By grouping related endpoints within each module, the platform maintains logical navigation and ease of extension for future functionalities. This organized routing strategy enables seamless interoperability, secure access control, and optimal user experience across the DECODE ecosystem.

6.3.7 Flowchart of the DECODE Cloud Platform

The DECODE Cloud Platform provides an integrated workflow. Users begin by signing up with their credentials, followed by authentication to access core modules. The platform enables dataset management, allowing users to add, view, update, and download datasets. Image processing supports data conversion, image upscaling, and centerline extraction for medical imaging. Segmentation facilitates PA and IMT analysis, with visualization options via DECODE-3DViz and Glance. Computational modeling provides advanced simulations, whereas MPR processes DICOM inputs for detailed imaging. The visualization module offers 3D rendering through DECODE-3DViz and WebXR, supporting interactive exploration. In addition, DCB-SimViz enables DEB analysis, including arterial drug concentration and simulation. As shown in Figure 6.9, this structured workflow streamlines medical imaging, analysis, and modeling within a cloud-based environment, enhancing precision in PAD management.

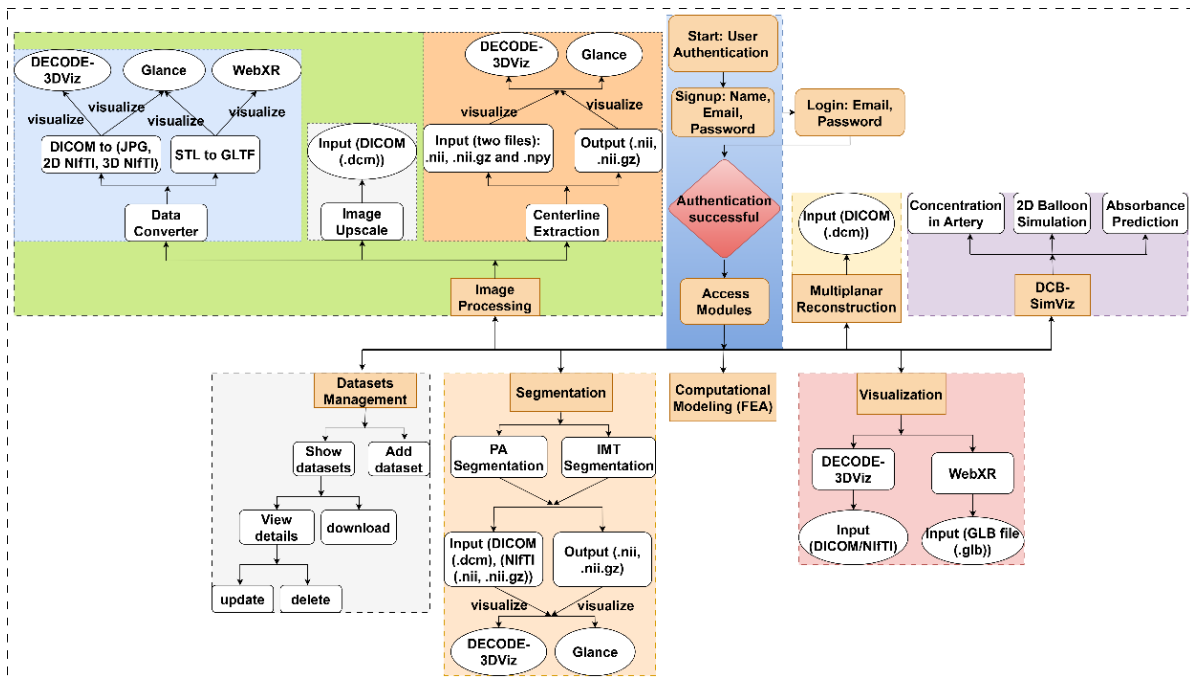


Figure 6.9 Flowchart of the DECODE Cloud Platform.

6.4 Evaluation

The usability and acceptance of the DECODE Cloud Platform were evaluated via the SUS [298] and the TAM [299]. The SUS measures perceived usability across 10 items on a 5-point Likert scale (provided in Supplementary Questionnaire 2), assessing effectiveness, efficiency, and user satisfaction. The TAM evaluated perceived usefulness (PU), perceived ease of use (PEOU), and behavioral intention (BI) through 12 items rated on a 5-point Likert scale (provided in Supplementary Questionnaire 3), with a focus on productivity, workflow integration, and user adoption intentions. Both evaluations were conducted with the 16 participants described in the Conceptual Design section. SUS scores were calculated via the standard method, yielding scores ranging from 0 to 100. TAM data were analyzed by calculating average scores for PU, PEOU, and BI, providing quantitative insights into user acceptance. In addition, correlation analysis was conducted between the SUS and TAM metrics to explore potential dependencies between usability and acceptance factors, enhancing the robustness of the evaluation.

6.5 Results

The DECODE Cloud Platform provides an intuitive web-based interface designed for seamless interaction with AI-driven medical imaging, segmentation, computational modeling, and visualization tools. The home interface, as depicted in Figure 6.10, serves as the central access point for users, including clinicians, researchers, and pharmaceutical companies, facilitating efficient navigation through the platform's core functionalities. The interface is structured around six primary modules—Datasets, Image Processing, Segmentation, Computational Modeling, MPR, Visualization, and DCB-SimViz—ensuring a streamlined workflow from medical image acquisition to advanced analysis and simulation. The navigation bar at the top provides quick access to platform information, contact support, and user authentication functionalities, whereas the social media integration panel on the right enhances collaboration and knowledge sharing. By integrating PWA principles, the platform offers real-time accessibility, cross-device compatibility, and cloud-based processing.

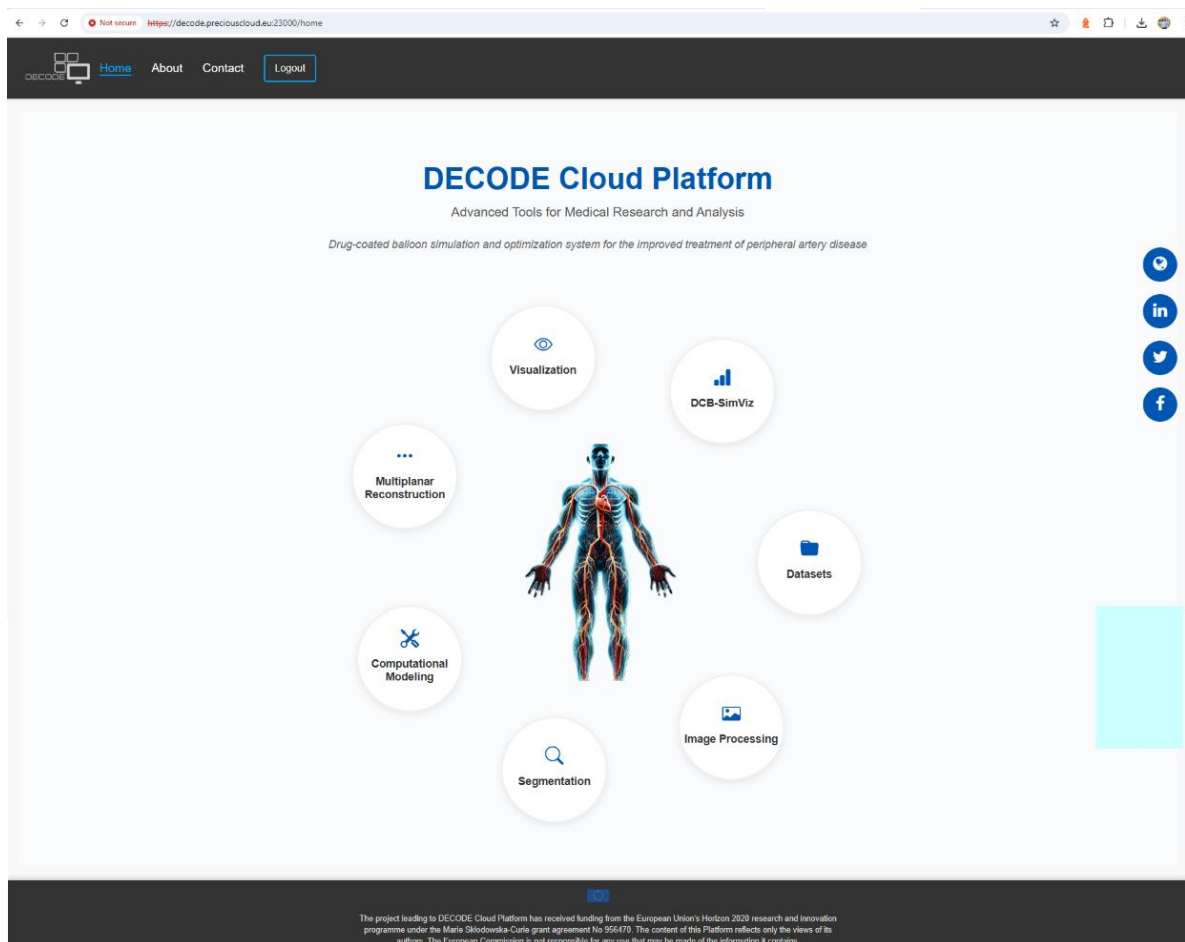


Figure 6.10 Home Interface of the DECODE Cloud Platform.

6.5.1 SUS evaluation

The SUS revealed an average score 87.5 (SD = 13.2), reflecting high perceived usability. According to industry benchmarks, scores above 85 are considered “Excellent,” validating the platform's intuitive design, ease of navigation, and effective integration of AI-driven segmentation and 3D visualization tools. These results confirm the platform’s usability and suitability for clinical and research applications in PAD management.

6.5.2 TAM evaluation

- PU: The average PU score 4.04 indicates that users perceived the platform as beneficial for enhancing efficiency in PAD imaging and computational modeling.
- PEOU: The average score 4.29 indicates high learnability and intuitive interaction with advanced features, confirming the platform's user-friendly design.
- BI: The average score 4.44 reflects strong user commitment to continue using and recommending the platform, validating its clinical relevance and utility.
- Overall TAM score: An overall average score 4.21 indicates high user acceptance and reinforces the platform's applicability in clinical and research workflows.

6.5.3 Correlation analysis between the SUS and TAM metrics

A correlation analysis was conducted to examine the interdependencies between SUS scores and TAM constructs (PU, PEOU, and BI). Pearson’s correlation coefficient (r) [312] was calculated as follows:

- SUS and PU ($r = 0.42$): A moderate positive correlation, indicating that enhanced usability contributes to greater perceived usefulness.
- PEOU and BI ($r = 0.72$): Strong correlation, emphasizing that ease of use significantly influences users' intention to continue using the platform.
- PU and BI ($r = 0.59$): Substantial correlation confirming that perceived productivity and clinical utility drive users' advocacy and adoption intentions.
- SUS and BI ($r = 0.32$): Moderate correlation, suggesting that usability indirectly influences behavioral intention through other domain-specific functionalities.

The correlation matrix, visualized in Figure 6.11, illustrates the strength and direction of these relationships, highlighting the interdependence between usability and acceptance factors. This analysis quantitatively validates the DECODE Cloud Platform’s user-centric design, demonstrating that enhanced usability and perceived value drive user acceptance and adoption.

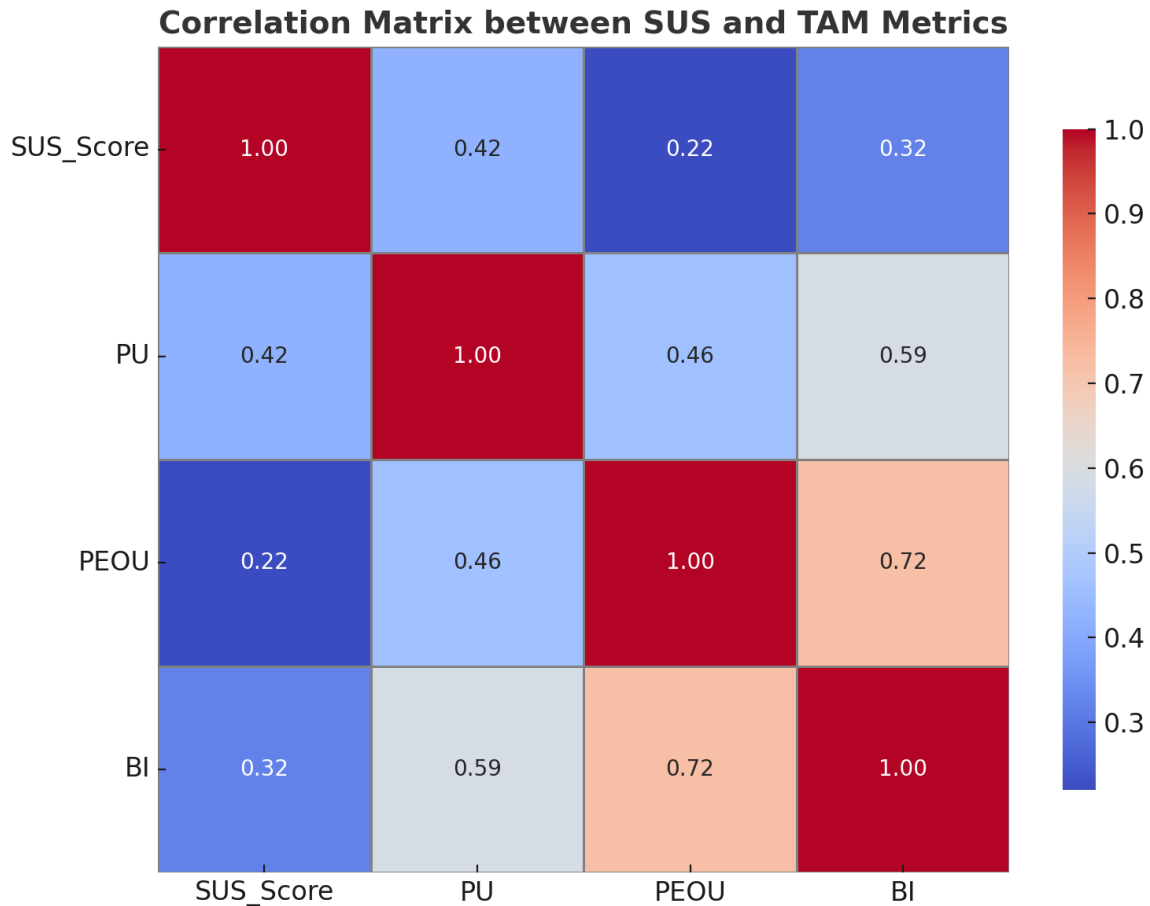


Figure 6.11 Correlation matrix between the system usability scale (SUS) and technology acceptance model (TAM) metrics.

6.6 Discussion

The DECODE Cloud Platform establishes a transformative approach to PAD management by integrating AI-driven segmentation, computational modeling, and GPU-accelerated visualization within a unified cloud-based framework. As shown in Figure 6.12, DECODE’s architecture uses a modular microservice design to enable efficient medical imaging workflows. The platform is organized into main frontend and subfrontend servers that interact with the main backend and subbackend servers via a centralized API gateway, ensuring secure and efficient data communication. Dataset retrieval is initiated from the DECODE Dataset Repository, which supports structured DICOM and NIFTI formats. The data converter module standardizes the input formats, enhancing the compatibility with DL algorithms. The PA segmentation module uses CT imaging to precisely delineate arterial structures, ensuring high accuracy in vessel extraction. The centerline extraction module computes the vascular centerline, curvature, and circularity, which are essential for computational hemodynamic modeling and predictive simulations. These parameters are processed in the main backend server, with results securely

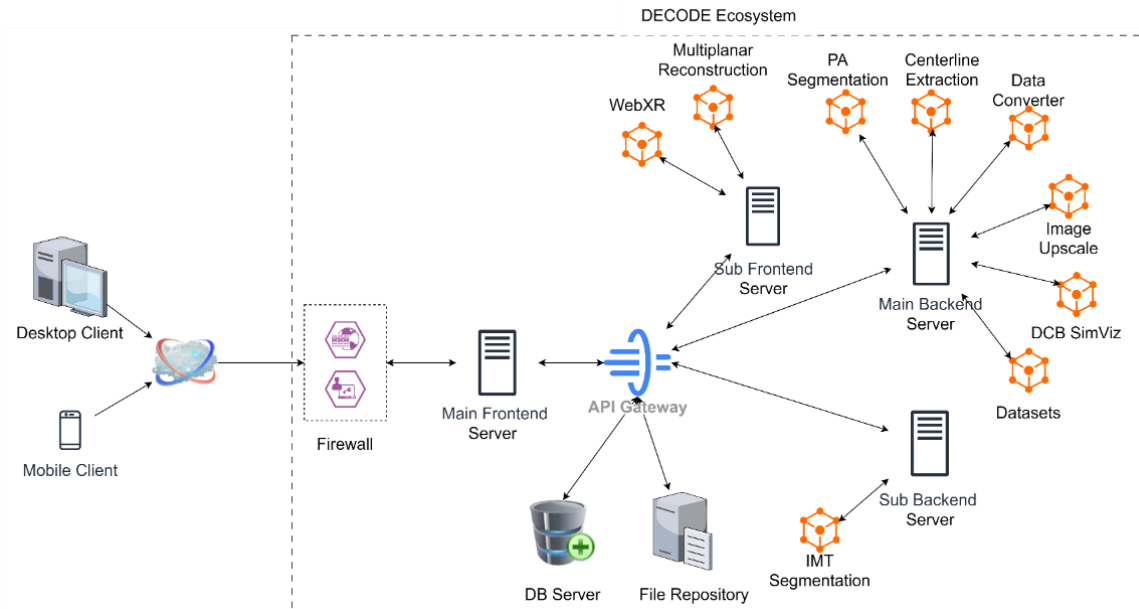


Figure 6.12 DECODE Cloud Platform ecosystem.

stored in the File Repository and DB server for scalable access. DECODE-3DViz enables real-time volumetric rendering and AR-enabled visualization through GPU-accelerated WebGL, significantly enhancing diagnostic accuracy and procedural planning. The platform supports interactive 3D visualization for comprehensive vascular analysis, enabling personalized treatment planning.

While previous mHealth interventions, such as TrackPAD [118], have improved patient adherence to SET, they lack AI-driven automation and real-time vascular analytics. Furthermore, systematic reviews have highlighted low adoption rates and the absence of AI-powered monitoring in digital SET programs [121]. In contrast, DECODE's cloud-integrated AI framework enables automated segmentation, hemodynamic analysis, and predictive modeling, addressing critical gaps in personalized PAD management. Similarly, advancements in AI-enhanced cloud computing for medical imaging have improved segmentation accuracy and predictive diagnostics. However, these approaches lack clinical validation for PAD applications and do not incorporate real-time visualization or patient-specific modeling. DECODE surpasses these limitations by integrating deep-learning-powered segmentation, real-time FEM simulations, and WebGL-based 3D visualization, providing clinically actionable insights in a scalable cloud environment.

The DECODE Cloud Platform introduces a groundbreaking cloud-based AI framework that seamlessly integrates DL segmentation, computational modeling, and real-time 3D

visualization for PAD management. Unlike previous systems that focus on isolated aspects of vascular imaging or exercise therapy, DECODE establishes a fully automated, scalable, and interoperable ecosystem that bridges the gap between AI-driven decision support, *in-silico* modeling, and interactive visualization.

- **Real-Time Cloud-Based Computation:** Unlike static image processing workflows, DECODE leverages GPU-accelerated cloud computing for automated segmentation, geometric vascular profiling, and FEM, optimizing PAD treatment planning through patient-specific simulations.
- **High-Fidelity WebGL Visualization:** DECODE-3DViz delivers real-time volumetric rendering and AR-enabled exploration, enabling interactive procedural planning in a fully cloud-integrated environment.
- **Predictive Modeling for PAD Interventions:** The DCB-SimViz module enables DCB therapy optimization, integrating computational fluid dynamics (CFD) and pharmacokinetic simulations to personalize vascular drug delivery strategies.
- **Seamless Clinical Integration:** Through RESTful APIs, DECODE ensures interoperability with PACS, EHRs, and telemedicine platforms, positioning it as a scalable and adaptable solution for precision vascular medicine.

By unifying AI-driven vascular analysis, interactive 3D visualization, and predictive modeling, DECODE establishes a new benchmark for digital PAD diagnostics, advancing data-driven and personalized vascular intervention planning.

PAD remains widely underdiagnosed owing to limited access to advanced imaging tools. DECODE automates AI-driven segmentation of PAs and the IMT, reducing interobserver variability and enhancing diagnostic confidence. Compared with CTA and MRA, its automated centerline extraction and geometric vascular profiling enable early PAD detection and disease progression monitoring with superior anatomical fidelity, which often misclassifies vascular calcifications.

Current PAD treatments lack personalization and rely on generalized protocols. DECODE integrates the FEM to simulate angioplasty and DCB interventions, optimizing vascular response prediction. The DCB-SimViz module enables real-time drug diffusion simulations, shifting treatment planning from empirical data to personalized computational modeling, reducing restenosis risk and improving long-term outcomes. In addition, DECODE supports *in-*

silico clinical trials by virtually testing DCB performance under different anatomical and hemodynamic conditions. It also enables optimized balloon design by simulating drug release kinetics and mechanical interactions with arterial walls. This allows precise adjustments in geometry, material properties, and coatings. The result is improved therapeutic efficacy and personalized treatment.

Traditional PAD diagnostic tools often rely on offline processing and can be computationally intensive, limiting real-time clinical decision-making. DECODE eliminates these bottlenecks with a cloud-integrated, RESTful API-based framework, providing instant AI-powered analysis and real-time 3D visualization. Through DECODE-3DViz, clinicians can interactively assess vascular pathologies via WebGL/WebXR-powered volumetric rendering, enabling dynamic exploration, computational flow analysis, and AR-driven visualization for precise procedural planning.

Despite its advancements, the DECODE Cloud Platform has inherent limitations that require further optimization. The centerline extraction module, while providing high-precision vascular geometry analysis, currently requires user-defined starts and endpoints, which introduces manual dependency and potential variability in arterial path selection. Future enhancements will focus on fully automated centerline detection via graph-based algorithms and topology-aware neural networks to eliminate manual input and improve reproducibility. In addition, DECODE's segmentation and computational modeling pipeline is optimized for CT-based vascular imaging, limiting its applicability to multimodal datasets such as ultrasound and MRI. Expanding compatibility to diverse imaging modalities will require modality-agnostic AI models and adaptive preprocessing pipelines to standardize input across different imaging formats. Furthermore, DECODE-3DViz's WebGL-based real-time visualization can experience latency when high-resolution datasets are rendered, particularly in low-bandwidth cloud environments. Future improvements will integrate progressive mesh streaming and WebGPU acceleration to enhance real-time interaction and scalability. Finally, while DECODE supports RESTful API integration, seamless interoperability with clinical PACS/EHR systems remains a challenge. Future iterations will incorporate FHIR-compliant APIs and encrypted cloud-based storage to ensure secure, scalable, and regulatory-compliant deployment in real-world clinical workflows.

6.7 Conclusion

This chapter presents DECODE, a cloud-based platform that transforms PAD management by integrating AI-driven segmentation, computational modeling, and real-time 3D visualization within a scalable, cloud-native framework. Unlike traditional systems, DECODE seamlessly bridges medical imaging, predictive analytics, and *in-silico* simulations, delivering a comprehensive infrastructure for vascular precision medicine. Through finite element modeling (FEM) and DCB simulations, DECODE enables patient-specific modeling of vascular interventions, optimizes therapeutic strategies, accelerates drug–device development, and reduces the need for physical trials.

The chapter demonstrates the platform’s advanced modules, including peripheral artery (PA) segmentation, intima–media thickness (IMT) segmentation, and centerline extraction, which provide high-precision vascular analysis and detailed geometric profiling for computational hemodynamics. The DECODE-3DViz tool, powered by WebGL/WebXR, delivers high-fidelity 3D visualization, enhancing clinical workflow efficiency and enabling interactive exploration of complex datasets. With RESTful API support for PACS/EHR integration, DECODE ensures seamless interoperability and cloud scalability.

The chapter also presents usability and acceptance evaluations, which were conducted via the SUS and TAM. The results revealed an average SUS score of 87.5, indicating excellent usability, and an overall TAM score of 4.21, confirming high user acceptance. Correlation analysis validated the dependencies between usability and acceptance, supporting DECODE’s user-centric design approach.

This chapter establishes DECODE as a next-generation platform for precision vascular medicine, enabling *in-silico* clinical trials and personalized PAD intervention planning. Future directions will focus on automating centerline detection, expanding imaging modality support, and optimizing real-time rendering performance. By showcasing DECODE as an open-source, AI-powered solution, this chapter sets a new benchmark in vascular diagnostics, bridging the gap between computational intelligence and real-world clinical applications. The platform code is available at <https://zenodo.org/records/14872021>, providing a foundation for continued research and development in vascular precision medicine.

Chapter 7: Conclusions and Future Work

7.1. Advancements in Cloud-Based Medical Imaging and Computational Vascular Modeling

7.2. Future Work

7.1 Advancements in Cloud-Based Medical Imaging and Computational Vascular Modeling

This dissertation addresses critical challenges in web-based medical imaging and computational modeling, contributing significantly to the advancement of cloud-based solutions for peripheral artery disease (PAD) diagnosis and treatment planning. By integrating state-of-the-art technologies in medical image analysis, WebGL-based visualization, and computational simulations, this research provides a comprehensive and scalable framework that enhances diagnostic precision, workflow efficiency, and patient-specific treatment strategies.

One of the most impactful contributions of this work is the development of a web-based DICOM and MPR visualization system within a PWA architecture. By leveraging React.js, Cornerstone.js, and Dexie.js, the system enables efficient medical image loading, real-time interaction, and optimized volume rendering, addressing key limitations in cross-platform compatibility and offline accessibility. The integration of advanced interpolation techniques (bicubic and weighted bilinear) ensures high-precision 3D image reconstructions, achieving an error margin below 0.05 mm, making it a clinically viable alternative to traditional high-performance imaging software.

A major breakthrough in this research is the DECODE-3DViz framework, which revolutionizes the web-based high-fidelity visualization of large-scale medical imaging datasets. Traditional WebGL-based rendering solutions suffer from texture constraints, high GPU memory requirements, and real-time performance bottlenecks, limiting their applicability in clinical settings. To address this, DECODE-3DViz integrates a level of detail (LOD) algorithm and progressive chunk streaming, achieving a 98% reduction in rendering latency, real-time visualization at up to 144 FPS, and a significant reduction in GPU memory usage to as low as 2.6 MB. This LOD-based adaptive resolution rendering ensures that clinically relevant vascular structures maintain high precision while optimizing computational resources, making it scalable across desktop and mobile devices.

The introduction of real-time dynamic illumination in vascular imaging represents another significant advancement. By mimicking physiological lighting variations, this approach enhances depth perception, plaque characterization, and arterial morphology visualization, addressing key challenges in atherosclerotic lesion assessment. The GPU-accelerated rendering pipeline ensures high-fidelity visualization even for large-scale DICOM datasets, enabling real-time interaction and superior diagnostic insights.

Furthermore, this dissertation presents an automated risk classification framework for PAD that uses quantitative vascular analysis. The system successfully classifies high-risk PAD cases with remarkable accuracy, achieving a plaque density averaging 0.85 and a vascular curvature averaging 1.3, providing clinicians with an objective, non-invasive tool for assessing disease severity. Compared with traditional static volume rendering techniques, this approach enhances diagnostic accuracy, reduces interobserver variability, and optimizes computational efficiency.

The DECODE Cloud Platform, another key outcome of this research, offers a fully integrated, cloud-based infrastructure for AI-powered vascular imaging and *in-silico* clinical trials. This platform combines deep learning-based vascular segmentation, real-time 3D visualization, finite element modeling (FEM), and predictive analytics for PAD intervention planning. A critical component of the DECODE Cloud Platform is its *in-silico* modeling capabilities, particularly through the balloon angioplasty FEM module and the DCB-SimViz drug-coated balloon simulation module. These computational tools provide critical insights into vascular mechanics, arterial stress distribution, and drug diffusion kinetics, ensuring optimized intervention strategies tailored to individual patient profiles. The integration of patient-specific

arterial reconstructions further enhances treatment personalization, reducing restenosis risk and improving drug delivery outcomes.

From a usability and clinical adoption standpoint, this research has demonstrated strong acceptance among radiologists, vascular specialists, and medical imaging researchers. The system usability scale (SUS) and technology acceptance model (TAM) evaluations yielded an SUS score of 87.5 (excellent usability) and a TAM score of 4.21 (high acceptance), confirming the effectiveness and practicality of the DECODE ecosystem. This positive correlation between usability, AI-driven automation, and real-time visualization capabilities underscores the clinical viability of this platform for real-world PAD diagnostics and intervention planning.

In addition to technical innovations, this dissertation underscores the transformative impact of AI, cloud computing, and computational modeling in digital healthcare. By pushing the boundaries of automated vascular analysis, scalable 3D visualization, and personalized treatment simulations, this research establishes a new benchmark for AI-driven PAD management. The combination of deep learning, *in-silico* modeling, and cloud-based diagnostic platforms lays the groundwork for next-generation digital health solutions, facilitating more efficient, accessible, and precise cardiovascular disease diagnostics.

This thesis presents a paradigm shift in vascular imaging and PAD diagnostics, demonstrating that real-time WebGL visualization, computational modeling, and cloud-integrated analytics can significantly enhance clinical decision-making. The DECODE Cloud Platform, with its multi-faceted approach to vascular diagnostics, risk classification, and *in-silico* simulations, represents a scalable, clinically validated framework that bridges research advancements with real-world medical applications. By combining state-of-the-art web technologies, GPU-accelerated processing, and AI-driven medical imaging, this work establishes a solid foundation for future advancements in digital health, AI-assisted diagnosis, and cloud-based medical imaging ecosystems.

7.2 Future Work

Building upon the advancements presented in this thesis, several research directions can further enhance the capabilities of web-based medical imaging, AI-driven vascular diagnostics, and computational modeling for PAD treatment. Future developments will focus on scalability, real-time AI integration, cloud-enabled imaging, and personalized *in-silico* clinical trials, ensuring

clinical viability, regulatory compliance, and expanded applicability across multiple imaging modalities.

A key area of future work is enhancing 3D volume rendering with real-time GPU acceleration. While WebGL-based visualization has demonstrated high performance, future iterations will integrate WebGPUs for even greater efficiency in handling large-scale volumetric datasets. The introduction of adaptive transfer functions and real-time shading models will further improve tissue differentiation, vascular structure clarity, and contrast-enhanced visualization of arterial lesions. In addition, AI-driven segmentation models are incorporated into the rendering pipeline, allowing automated feature extraction and pathology segmentation in real time.

Cloud-based storage and distributed processing play crucial roles in scaling DICOM and 3D medical visualization for multi-institutional collaboration. By leveraging cloud computing frameworks such as AWS, Microsoft Azure, and Google Cloud, future implementations will enable remote GPU acceleration, federated AI model training, and real-time collaborative imaging analysis. The integration of edge computing architectures allows AI models to run directly on low-power clinical devices, reducing latency and dependency on centralized cloud infrastructure while ensuring on-demand access to diagnostic imaging.

The expansion of real-time multi-user collaboration tools is another essential direction for future work. Implementing synchronous communication protocols such as Web real-time communication (WebRTC) will enable live diagnostic discussions, shared image annotation, and collaborative decision-making between radiologists, vascular specialists, and computational researchers. This feature will be particularly beneficial in telemedicine applications, allowing clinicians in remote regions to consult complex PAD cases via real-time AI-enhanced visualization.

Another avenue for expansion is extending imaging modalities beyond CT-based visualization. While this thesis has focused primarily on peripheral artery CT imaging, future research will incorporate MRI, ultrasound, and PET scans into the DECODE Cloud Platform. By developing multimodal fusion networks, the system enables cross-modality imaging analysis, improved tissue characterization, and better integration of physiological data into computational models. This will provide a comprehensive, AI-enhanced imaging pipeline for vascular diagnostics and cardiothoracic assessments.

For clinical deployment, regulatory and security compliance must be further strengthened to meet the Digital Imaging and Communications in Medicine Web Services (DICOMweb), Health Level Seven Fast Healthcare Interoperability Resources (HL7 FHIR), General Data Protection Regulation (GDPR), and Health Insurance Portability and Accountability Act (HIPAA) standards. The implementation of privacy-preserving AI models, federated learning for secure model training across institutions, and end-to-end encryption protocols ensures compliance with data protection regulations. Moreover, integrating blockchain-based audit trails will enhance data integrity, traceability, and interoperability across clinical imaging networks.

In terms of computational modeling, the expansion of personalized drug delivery simulations via finite element modeling (FEM) and fluid–structure interaction (FSI) will be a major focus. The development of real-time pharmacokinetic models for DCBs will allow individualized simulation of drug diffusion, arterial wall interactions, and restenosis risk prediction. By integrating AI-powered predictive analytics, patient-specific vascular geometries can be used to optimize DCB deployment, drug absorption rates, and long-term treatment efficacy.

Another critical advancement will be AI-powered automated report generation and decision support. By incorporating natural language processing (NLP) models, the platform will be able to generate AI-augmented radiology reports, highlight abnormal findings, and provide clinical decision recommendations. This will streamline workflow efficiency, reduce reporting errors, and enhance the interpretability of AI-driven vascular imaging results. Furthermore, large-scale clinical validation is essential for transitioning DECODE-3DViz and the DECODE Cloud Platform into real-world medical applications. Future research will focus on conducting multicenter trials to validate AI-based PAD risk classification models.

By advancing these research directions, the DECODE Cloud Platform will continue to evolve as a gold standard in AI-driven PAD diagnostics, high-fidelity web-based visualization, and computational modeling for vascular interventions. These future innovations will further push the boundaries of digital health, AI-assisted diagnosis, and cloud-based *in-silico* clinical trials, ensuring scalability, efficiency, and widespread clinical adoption.

Bibliography

- [1] K. E. Haile, Y. S. Asgedom, G. A. Azeze, A. A. Amsalu, G. A. Kassie, and A. Y. Gebrekidan, "Burden of peripheral artery disease and risk factors among patients with diabetes mellitus in sub-Saharan Africa: a systematic review and meta-analysis," *BMC Endocrine Disorders*, vol. 25, no. 1, p. 42, 2025.
- [2] "Peripheral Artery Disease." <https://my.clevelandclinic.org/health/diseases/17357-peripheral-artery-disease-pad> (accessed 2024).
- [3] M. Piechocki, T. Przewłocki, P. Pieniążek, M. Trystuła, J. Podolec, and A. Kabłak-Ziembicka, "A non-coronary, peripheral arterial atherosclerotic disease (carotid, renal, lower limb) in elderly patients—A review: Part I—Epidemiology, risk factors, and atherosclerosis-related diversities in elderly patients," *Journal of Clinical Medicine*, vol. 13, no. 5, p. 1471, 2024.
- [4] M. M. Radwan, S. Sunny, and S. Thomas, "Environmental Factors and Peripheral Artery Disease," in *Environmental Factors in the Pathogenesis of Cardiovascular Diseases*, Eds.: Springer, pp. 193-208, 2024.
- [5] C. P. Porras, M. L. Bots, M. Teraa, S. van Doorn, and R. W. Vernooij, "Differences in symptom presentation in women and men with confirmed lower limb peripheral artery disease: a systematic review and meta-analysis," *European Journal of Vascular and Endovascular Surgery*, vol. 63, no. 4, pp. 602-612, 2022.
- [6] M. Takahara, "Diabetes mellitus and peripheral artery disease," *Diabetology International*, pp. 1-6, 2025.
- [7] M. G. Levin, V. Zuber, V. M. Walker, D. Klarin, J. Lynch, R. Malik, A. W. Aday, L. Bottolo, A. D. Pradhan, and M. Dichgans, "Prioritizing the role of major lipoproteins and subfractions as risk factors for peripheral artery disease," *Circulation*, vol. 144, no. 5, pp. 353-364, 2021.
- [8] F. Riveros-Mckay, C. Oliver-Williams, S. Karthikeyan, K. Walter, K. Kundu, W. H. Ouwehand, D. Roberts, E. Di Angelantonio, N. Soranzo, and J. Danesh, "The influence of rare variants in circulating metabolic biomarkers," *PLoS Genetics*, vol. 16, no. 3, p. e1008605, 2020.
- [9] M. Pabon, S. Cheng, S. E. Altin, S. S. Sethi, M. D. Nelson, K. L. Moreau, N. Hamburg, and C. N. Hess, "Sex differences in peripheral artery disease," *Circulation research*, vol. 130, no. 4, pp. 496-511, 2022.
- [10] J. Golledge, "Update on the pathophysiology and medical treatment of peripheral artery disease," *Nature reviews cardiology*, vol. 19, no. 7, pp. 456-474, 2022.

- [11] F. G. R. Fowkes, V. Aboyans, F. J. Fowkes, M. M. McDermott, U. K. Sampson, and M. H. Criqui, "Peripheral artery disease: epidemiology and global perspectives," *Nature Reviews Cardiology*, vol. 14, no. 3, pp. 156-170, 2017.
- [12] J. A. Barnes, M. A. Eid, M. A. Creager, and P. P. Goodney, "Epidemiology and risk of amputation in patients with diabetes mellitus and peripheral artery disease," *Arteriosclerosis, thrombosis, and vascular biology*, vol. 40, no. 8, pp. 1808-1817, 2020.
- [13] V. Chuter, N. Schaper, J. Mills, R. Hinchliffe, D. Russell, N. Azuma, C. A. Behrendt, E. J. Boyko, M. S. Conte, and M. Humphries, "Effectiveness of bedside investigations to diagnose peripheral artery disease among people with diabetes mellitus: a systematic review," *Diabetes/metabolism research and reviews*, vol. 40, no. 3, p. e3683, 2024.
- [14] D. O. Soyoye, O. O. Abiodun, R. T. Ikem, B. A. Kolawole, and A. O. Akintomide, "Diabetes and peripheral artery disease: A review," *World journal of diabetes*, vol. 12, no. 6, p. 827, 2021.
- [15] K. Matsushita, M. J. Salameh, and M. Allison, "Peripheral Artery Disease in Regions with Limited Socioeconomic Resources," in *Global Challenges in Cardiovascular Prevention in Populations with Low Socioeconomic Status*, Eds.: Springer, pp. 63-88, 2025.
- [16] M. T. B. Abola, J. Golledge, T. Miyata, S.-W. Rha, B. P. Yan, T. C. Dy, M. S. V. Ganzon, P. K. Handa, S. Harris, and J. Zhisheng, "Asia-Pacific consensus statement on the management of peripheral artery disease: a report from the Asian Pacific society of atherosclerosis and vascular disease Asia-Pacific peripheral artery disease consensus statement project committee," *Journal of Atherosclerosis and Thrombosis*, vol. 27, no. 8, pp. 809-907, 2020.
- [17] K. G. Smolderen, Z. Samaan, C. Decker, T. Collins, R. M. Lazar, N. K. Itoga, C. Mena-Hurtado, A. H. A. C. o. P. V. Disease, C. o. Cardiovascular, S. Nursing, C. o. C. Cardiology, C. o. Lifestyle, C. Health, C. o. Q. o. Care, and O. Research, "Association between mental health burden, clinical presentation, and outcomes in individuals with symptomatic peripheral artery disease: a scientific statement from the American Heart Association," *Circulation*, vol. 148, no. 19, pp. 1511-1528, 2023.
- [18] A. W. Aday and K. Matsushita, "Epidemiology of peripheral artery disease and polyvascular disease," *Circulation research*, vol. 128, no. 12, pp. 1818-1832, 2021.
- [19] E. E. Buschmann, L. Li, M. Brix, A. Zietzer, P. Hillmeister, A. Busjahn, P. Bramlage, and I. Buschmann, "A novel computer-aided diagnostic approach for detecting peripheral arterial disease in patients with diabetes," *PloS one*, vol. 13, no. 6, p. e0199374, 2018.

- [20] D. Kovacs, B. Csiszar, K. Biro, K. Koltai, D. Endrei, I. Juricskay, B. Sandor, D. Praksch, K. Toth, and G. Kesmarky, "Toe-brachial index and exercise test can improve the exploration of peripheral artery disease," *Atherosclerosis*, vol. 269, pp. 151-158, 2018.
- [21] A. G. Blum, R. Gillet, L. Athlani, A. Prestat, S. Zuily, D. Wahl, G. Dautel, and P. Gondim Teixeira, "CT angiography and MRI of hand vascular lesions: technical considerations and spectrum of imaging findings," *Insights Into Imaging*, vol. 12, pp. 1-22, 2021.
- [22] H. Wolf and N. Singh, "Using Multidisciplinary Teams to Improve Outcomes for Treating Chronic-Limb Threatening Ischemia," *Annals of Vascular Surgery*, vol. 107, pp. 37-42, 2024.
- [23] L. Tang, S. C. Paravastu, S. D. Thomas, E. Tan, E. Farmer, and R. L. Varcoe, "Cost analysis of initial treatment with endovascular revascularization, open surgery, or primary major amputation in patients with peripheral artery disease," *Journal of Endovascular Therapy*, vol. 25, no. 4, pp. 504-511, 2018.
- [24] E. L. Hackler III, N. M. Hamburg, and K. T. White Solaru, "Racial and ethnic disparities in peripheral artery disease," *Circulation research*, vol. 128, no. 12, pp. 1913-1926, 2021.
- [25] M. M. McDermott, K. J. Ho, O. Alabi, M. H. Criqui, P. Goodney, N. Hamburg, D. M. McNeal, A. Pollak, K. G. Smolderen, and M. Bonaca, "Disparities in diagnosis, treatment, and outcomes of peripheral artery disease: JACC scientific statement," *Journal of the American College of Cardiology*, vol. 82, no. 24, pp. 2312-2328, 2023.
- [26] H. Guan, Y. Wang, P. Niu, Y. Zhang, Y. Zhang, R. Miao, X. Fang, R. Yin, S. Zhao, and J. Liu, "The role of machine learning in advancing diabetic foot: a review," *Frontiers in Endocrinology*, vol. 15, p. 1325434, 2024.
- [27] Y. Lu, X. Cui, L. Zhang, X. Wang, Y. Xu, Z. Qin, G. Liu, Q. Wang, K. Tian, and K. S. Lim, "The functional role of lipoproteins in atherosclerosis: novel directions for diagnosis and targeting therapy," *Aging and disease*, vol. 13, no. 2, p. 491, 2022.
- [28] M. Zakir, N. Ahuja, M. A. Surksha, R. Sachdev, Y. Kalariya, M. Nasir, M. Kashif, F. Shahzeen, A. Tayyab, and M. S. moazzam Khan, "Cardiovascular complications of diabetes: from microvascular to macrovascular pathways," *Cureus*, vol. 15, no. 9, 2023.
- [29] A. Achim, A. Stanek, C. Homorodean, M. Spinu, H. L. Onea, L. Lazăr, M. Marc, Z. Ruzsa, and D. M. Olinic, "Approaches to peripheral artery disease in diabetes: are there any differences?," *International Journal of Environmental Research and Public Health*, vol. 19, no. 16, p. 9801, 2022.

- [30] M. P. Bonaca, N. M. Hamburg, and M. A. Creager, "Contemporary medical management of peripheral artery disease," *Circulation research*, vol. 128, no. 12, pp. 1868-1884, 2021.
- [31] M. Piechocki, T. Przewłocki, P. Pieniążek, M. Trystuła, J. Podolec, and A. Kabłak-Ziembicka, "A non-coronary, peripheral arterial atherosclerotic disease (carotid, renal, lower limb) in elderly patients—A review PART II—Pharmacological approach for management of elderly patients with peripheral atherosclerotic lesions outside coronary territory," *Journal of Clinical Medicine*, vol. 13, no. 5, p. 1508, 2024.
- [32] R. Y. Kherallah, M. Khawaja, M. Olson, D. Angiolillo, and Y. Birnbaum, "Cilostazol: a review of basic mechanisms and clinical uses," *Cardiovascular drugs and therapy*, pp. 1-16, 2022.
- [33] V. A. Myasoedova, M. Bozzi, V. Valerio, D. Moschetta, I. Massaiu, V. Rusconi, D. Di Napoli, M. Ciccarelli, V. Parisi, and P. Agostoni, "Anti-inflammation and anti-oxidation: the key to unlocking the cardiovascular potential of SGLT2 inhibitors and GLP1 receptor agonists," *Antioxidants*, vol. 13, no. 1, p. 16, 2023.
- [34] J. K. Ehrman, A. W. Gardner, D. Salisbury, K. Lui, and D. Treat-Jacobson, "Supervised exercise therapy for symptomatic peripheral artery disease: a review of current experience and practice-based recommendations," *Journal of Cardiopulmonary Rehabilitation and Prevention*, vol. 43, no. 1, pp. 15-21, 2023.
- [35] J. A. Beckman, P. A. Schneider, and M. S. Conte, "Advances in revascularization for peripheral artery disease: revascularization in PAD," *Circulation research*, vol. 128, no. 12, pp. 1885-1912, 2021.
- [36] J. Nicolas, C. A. Pivato, M. Chiarito, F. Beerkens, D. Cao, and R. Mehran, "Evolution of drug-eluting coronary stents: a back-and-forth journey from the bench to bedside," *Cardiovascular research*, vol. 119, no. 3, pp. 631-646, 2023.
- [37] O. Martinelli, A. Alunno, F. M. Drudi, A. Malaj, and L. Irace, "Duplex ultrasound versus CT angiography for the treatment planning of lower-limb arterial disease," *Journal of Ultrasound*, vol. 24, pp. 471-479, 2021.
- [38] M. Miceli, D. Baldi, C. Cavaliere, A. Soricelli, M. Salvatore, and C. Napoli, "Peripheral artery disease: the new frontiers of imaging techniques to evaluate the evolution of regenerative medicine," *Expert Review of Cardiovascular Therapy*, vol. 17, no. 7, pp. 511-532, 2019.

- [39] A. I. Gardezi and A. S. Yevzlin, "Overview of PAD Treatment in the CKD Population: Indications, Medical Strategies, and Endovascular Techniques," in *Interventional Nephrology: Principles and Practice*, Eds.: Springer, pp. 45-51, 2021.
- [40] S. Misra, M. H. Shishehbor, E. A. Takahashi, H. D. Aronow, L. P. Brewster, M. C. Bunte, E. S. Kim, J. R. Lindner, K. Rich, A. H. A. C. o. P. V. Disease, C. o. C. Cardiology, C. o. Cardiovascular, and S. Nursing, "Perfusion assessment in critical limb ischemia: principles for understanding and the development of evidence and evaluation of devices: a scientific statement from the American Heart Association," *Circulation*, vol. 140, no. 12, pp. e657-e672, 2019.
- [41] F. Vancheri, G. Longo, S. Vancheri, and M. Henein, "Coronary microvascular dysfunction," *Journal of Clinical Medicine*, vol. 9, no. 9, p. 2880, 2020.
- [42] T. X. Hoang, L. M. T. Phan, T. A. T. Vo, and S. Cho, "Advanced signal-amplification strategies for paper-based analytical devices: A comprehensive review," *Biomedicines*, vol. 9, no. 5, p. 540, 2021.
- [43] M. A. AboArab, V. T. Potsika, A. Theodorou, S. Vagena, M. Gravanis, F. Sigala, and D. I. Fotiadis, "Advancing Progressive Web Applications to Leverage Medical Imaging for Visualization of Digital Imaging and Communications in Medicine and Multiplanar Reconstruction: Software Development and Validation Study," *JMIR Medical Informatics*, vol. 12, p. e63834, 2024.
- [44] M. A. AboArab, V. T. Potsika, F. Sigala, A. Theodorou, S. Vagena, and D. I. Fotiadis, "GPU-Driven Optimization of Web-Based Volume Rendering in Peripheral Artery Disease CT Imaging," in *IEEE 24th International Conference on Bioinformatics and Bioengineering (BIBE): IEEE*, pp. 1-8, 2024.
- [45] L. Salvolini, E. B. Secchi, L. Costarelli, and M. De Nicola, "Clinical applications of 2D and 3D CT imaging of the airways—a review," *European journal of radiology*, vol. 34, no. 1, pp. 9-25, 2000.
- [46] G. Aceto, V. Persico, and A. Pescapé, "Industry 4.0 and health: Internet of things, big data, and cloud computing for healthcare 4.0," *Journal of Industrial Information Integration*, vol. 18, p. 100129, 2020.
- [47] A. Patra, N. B. Pushpa, and K. S. Ravi, "Visualization in anatomy education," in *Biomedical Visualisation: Volume 15—Visualisation in Teaching of Biomedical and Clinical Subjects: Anatomy, Advanced Microscopy and Radiology*, Eds.: Springer, pp. 171-186, 2023.

- [48] H. Pereira, L. Romero, and P. Miguel Faria, "Web-Based DICOM Viewers: A Survey and a Performance Classification," *Journal of Imaging Informatics in Medicine*, pp. 1-19, 2024.
- [49] M. Y. Shakor and M. I. Khaleel, "Recent Advances in Big Medical Image Data Analysis Through Deep Learning and Cloud Computing," *Electronics*, vol. 13, no. 24, p. 4860, 2024.
- [50] M. Deb and A. Choudhury, "Hybrid cloud: A new paradigm in cloud computing," *Machine learning techniques and analytics for cloud security*, pp. 1-23, 2021.
- [51] S. M. Williamson and V. Prybutok, "Balancing privacy and progress: a review of privacy challenges, systemic oversight, and patient perceptions in AI-driven healthcare," *Applied Sciences*, vol. 14, no. 2, p. 675, 2024.
- [52] N. Gupta, R. Agrawal, and K. Arora, "Cloud Computing in Healthcare: Risks and Security Measures," *Artificial Intelligence and Cybersecurity in Healthcare*, pp. 221-242, 2025.
- [53] M. Ullah, S. Hamayun, A. Wahab, S. U. Khan, M. U. Rehman, Z. U. Haq, K. U. Rehman, A. Ullah, A. Mehreen, and U. A. Awan, "Smart technologies used as smart tools in the management of cardiovascular disease and their future perspective," *Current Problems in Cardiology*, vol. 48, no. 11, p. 101922, 2023.
- [54] Z. Chen, Y. Lou, B. Wang, H. Lei, and P. Yang, "Application of Cloud-Driven Intelligent Medical Imaging Analysis in Disease Detection," *Journal of Theory and Practice of Engineering Science*, vol. 4, no. 05, pp. 64-71, 2024.
- [55] B. R. Cherukuri, "Progressive Web Apps (PWAs): Enhancing User Experience through Modern Web Development."
- [56] B. Li, R. Nassereldine, F. Shaikh, H. Younes, B. AbuHalimeh, A. Zamzam, R. Abdin, and M. Qadura, "Inflammatory Protein Panel: Exploring Diagnostic Insights for Peripheral Artery Disease Diagnosis in a Cross-Sectional Study," *Diagnostics*, vol. 14, no. 17, p. 1847, 2024.
- [57] P. Jiang, Q. Li, Y. Luo, F. Luo, Q. Che, Z. Lu, S. Yang, Y. Yang, X. Chen, and Y. Cai, "Current status and progress in research on dressing management for diabetic foot ulcer," *Frontiers in Endocrinology*, vol. 14, p. 1221705, 2023.
- [58] S. Greengard, "The internet of things," MIT press, pp., 2021.
- [59] A. Liao and E. Seeram, "Enterprise Imaging: The Next Frontier in Healthcare Technology—A Literature Review," *Radiology*, vol. 3, no. 1, pp. 4-11, 2019.
- [60] E. Martelli, L. Capoccia, M. Di Francesco, E. Cavallo, M. G. Pezzulla, G. Giudice, A. Bauleo, G. Coppola, and M. Panagrosso, "Current applications and future perspectives of

artificial and biomimetic intelligence in vascular surgery and peripheral artery disease," *Biomimetics*, vol. 9, no. 8, p. 465, 2024.

[61] A. Singh, A. Payal, and S. Bharti, "A walkthrough of the emerging IoT paradigm: Visualizing inside functionalities, key features, and open issues," *Journal of Network and Computer Applications*, vol. 143, pp. 111-151, 2019.

[62] A. Fedorov, R. Beichel, J. Kalpathy-Cramer, J. Finet, J.-C. Fillion-Robin, S. Pujol, C. Bauer, D. Jennings, F. Fennessy, and M. Sonka, "3D Slicer as an image computing platform for the Quantitative Imaging Network," *Magnetic resonance imaging*, vol. 30, no. 9, pp. 1323-1341, 2012.

[63] I. Wolf, M. Vetter, I. Wegner, M. Nolden, T. Bottger, M. Hastenteufel, M. Schobinger, T. Kunert, and H.-P. Meinzer, "The medical imaging interaction toolkit (MITK): a toolkit facilitating the creation of interactive software by extending VTK and ITK," in *Medical imaging: Visualization, image-guided procedures, and display: SPIE*, pp. 16-27, 2004.

[64] Z. Wang, R. Yi, X. Wen, C. Zhu, and K. Xu, "Cardiovascular Medical Image and Analysis based on 3D Vision: A Comprehensive Survey," *Meta-Radiology*, p. 100102, 2024.

[65] C. A. Carrasco, I. Lombillo, J. M. Sánchez-Espeso, and F. J. Balbás, "Quantitative and qualitative analysis on the integration of geographic information systems and building information modeling for the generation and management of 3D models," *Buildings*, vol. 12, no. 10, p. 1672, 2022.

[66] J. Xiang, L. Antiga, N. Varble, K. V. Snyder, E. I. Levy, A. H. Siddiqui, and H. Meng, "AView: an image-based clinical computational tool for intracranial aneurysm flow visualization and clinical management," *Annals of biomedical engineering*, vol. 44, pp. 1085-1096, 2016.

[67] D. Fadilazim, "The Effectiveness of a Personalized Digital Health Intervention Plan (Naluri App) on Clinical and Psychological Outcomes Among Cardiac Patients at The National Heart Institute (IJN): A Randomized Controlled Trial," Royal College of Surgeons in Ireland, 2023.

[68] A.-M. Ştefan, N.-R. Rusu, E. Ovreiu, and M. Ciuc, "Empowering Healthcare: A Comprehensive Guide to Implementing a Robust Medical Information System—Components, Benefits, Objectives, Evaluation Criteria, and Seamless Deployment Strategies," *Applied System Innovation*, vol. 7, no. 3, p. 51, 2024.

[69] L. Franke and D. Haehn, "Modern scientific visualizations on the web," in *Informatics: MDPI*, pp. 37, 2020.

- [70] S. Dykstra, "Integrating Multi-Domain Electronic Health Data, Machine Learning, and Automated Cardiac Phenomics for Personalized Cardiovascular Care," 2024.
- [71] A. M. Arruda-Olson, N. Afzal, V. Priya Mallipeddi, A. Said, H. Moussa Pacha, S. Moon, A. P. Chaudhry, C. G. Scott, K. R. Bailey, and T. W. Rooke, "Leveraging the electronic health record to create an automated real-time prognostic tool for peripheral arterial disease," *Journal of the American Heart Association*, vol. 7, no. 23, p. e009680, 2018.
- [72] C. Brandon, S. Boßelmann, A. Singh, S. Ryan, A. Schieweck, E. Fennell, B. Steffen, and T. Margaria, "Cinco de Bio: A Low-Code Platform for Domain-Specific Workflows for Biomedical Imaging Research," *BioMedInformatics*, vol. 4, no. 3, pp. 1865-1883, 2024.
- [73] A. M. Anwer, H. Karacan, L. Enver, and G. Cabuk, "Machine learning applications for vascular stenosis detection in computed tomography angiography: a systematic review and meta-analysis," *Neural Computing and Applications*, vol. 36, no. 29, pp. 17767-17786, 2024.
- [74] A. I. Iqbal, A. Aamir, A. Hammad, H. Hafsa, A. Basit, M. O. Oduoye, M. W. Anis, S. Ahmed, M. I. Younus, and S. Jabeen, "Immersive technologies in healthcare: An in-depth exploration of virtual reality and augmented reality in enhancing patient care, medical education, and training paradigms," *Journal of Primary Care & Community Health*, vol. 15, p. 21501319241293311, 2024.
- [75] M. A. AboArab, V. T. Potsika, A. Skalski, M. Stanuch, G. Gkois, I. Koncar, D. Matejevic, A. Theodorou, S. Vagena, and F. Sigala, "DECODE-3DViz: Efficient WebGL-Based High-Fidelity Visualization of Large-Scale Images using Level of Detail and Data Chunk Streaming," *Journal of Imaging Informatics in Medicine*, pp. 1-19, 2025.
- [76] A. Panta, X. Huang, N. McCurdy, D. Ellsworth, A. A. Gooch, G. Scorzelli, H. Torres, P. Klein, G. A. Ovando-Montejo, and V. Pascucci, "Web-based visualization and analytics of petascale data: Equity as a tide that lifts all boats," in *IEEE 14th Symposium on Large Data Analysis and Visualization (LDAV)*: IEEE, pp. 1-11, 2024.
- [77] N. Cornelis, R. Buys, T. Dewit, D. Benoit, J. Claes, I. Fourneau, and V. Cornelissen, "Satisfaction and acceptability of telemonitored home-based exercise in patients with intermittent claudication: pragmatic observational pilot study," *JMIR rehabilitation and assistive technologies*, vol. 8, no. 1, p. e18739, 2021.
- [78] A. Castiglione, R. Pizzolante, A. De Santis, B. Carpentieri, A. Castiglione, and F. Palmieri, "Cloud-based adaptive compression and secure management services for 3D healthcare data," *Future Generation Computer Systems*, vol. 43, pp. 120-134, 2015.

- [79] S. R. Khoury, E. V. Ratchford, and K. J. Stewart, "Supervised exercise therapy for patients with peripheral artery disease: clinical update and pathways forward," *Progress in Cardiovascular Diseases*, vol. 70, pp. 183-189, 2022.
- [80] A. M. Alyami, M. T. Kirimi, S. L. Neale, and J. R. Mercer, "Implantable Biosensors for Vascular Diseases: Directions for the Next Generation of Active Diagnostic and Therapeutic Medical Device Technologies," *Biosensors*, vol. 15, no. 3, p. 147, 2025.
- [81] J. F. LaDisa Jr, A. Ghorbannia, D. S. Marks, P. Mason, and H. Otake, "Advancements and opportunities in characterizing patient-specific wall shear stress imposed by coronary artery stenting," *Fluids*, vol. 7, no. 10, p. 325, 2022.
- [82] A. Molloy, K. Beaumont, A. Alyami, M. Kirimi, D. Hoare, N. Mirzai, H. Heidari, S. Mitra, S. L. Neale, and J. R. Mercer, "Challenges to the development of the next generation of self-reporting cardiovascular implantable medical devices," *IEEE Reviews in Biomedical Engineering*, vol. 15, pp. 260-272, 2021.
- [83] K. A. Gallagher, J. L. Mills, D. G. Armstrong, M. S. Conte, R. S. Kirsner, S. D. Minc, J. Plutzky, K. W. Southerland, M. Tomic-Canic, A. H. A. C. o. P. V. Disease, C. o. Cardiovascular, S. Nursing, C. o. C. Cardiology, C. o. Lifestyle, and C. Health, "Current status and principles for the treatment and prevention of diabetic foot ulcers in the cardiovascular patient population: a scientific statement from the American Heart Association," *Circulation*, vol. 149, no. 4, pp. e232-e253, 2024.
- [84] Y.-W. Wu, C.-Y. Wang, N.-C. Cheng, H.-J. Lin, H.-L. Huang, J.-H. Huang, C.-C. Chen, J.-K. Lee, P.-L. Chen, and P.-C. Hsu, "2024 TSOC/TSPS joint consensus: Strategies for advanced vascular wound management in arterial and venous diseases," *Acta Cardiologica Sinica*, vol. 40, no. 1, p. 1, 2024.
- [85] W. A. Campbell IV, J. F. Chick, D. S. Shin, and M. S. Makary, "Value of interventional radiology and their contributions to modern medical systems," *Frontiers in Radiology*, vol. 4, p. 1403761, 2024.
- [86] Z. Lin, C. Lei, and L. Yang, "Modern image-guided surgery: A narrative review of medical image processing and visualization," *Sensors*, vol. 23, no. 24, p. 9872, 2023.
- [87] S. Suganthi and T. Poongodi, "Interactive Visualization for Understanding and Analyzing Medical Data," in *Exploratory Data Analytics for Healthcare*, Eds.: CRC Press, pp. 101-123, 2021.
- [88] R. Khan, I. Kumar, and P. Praveen, "Applications of parallel data processing for biomedical imaging," IGI global, pp., 2024.

- [89] S. Sachdeva, S. Bhatia, A. Al Harrasi, Y. A. Shah, K. Anwer, A. K. Philip, S. F. A. Shah, A. Khan, and S. A. Halim, "Unraveling the role of cloud computing in health care system and biomedical sciences," *Heliyon*, 2024.
- [90] D. Haak, C.-E. Page, and T. M. Deserno, "A survey of DICOM viewer software to integrate clinical research and medical imaging," *Journal of digital imaging*, vol. 29, pp. 206-215, 2016.
- [91] M. Miller, "Cloud computing: Web-based applications that change the way you work and collaborate online," Que publishing, pp., 2008.
- [92] D. Kweche Ebechue, "Progressive Web Applications and Users' Engagement," 2024.
- [93] J. C. Hellinger, L. S. Medina, and M. Epelman, "Pediatric advanced imaging and informatics: state of the art," in *Seminars in Ultrasound, CT and MRI*: Elsevier, pp. 171-193, 2010.
- [94] Q. Min, Z. Wang, and N. Liu, "An evaluation of HTML5 and WebGL for medical imaging applications," *Journal of healthcare engineering*, vol. 2018, no. 1, p. 1592821, 2018.
- [95] H. J. Hazarika and A. Handique, "DICOM-based medical image repository using DSpace," *Collection and Curation*, vol. 39, no. 4, pp. 105-115, 2020.
- [96] H. J. Hazarika, S. Ravikumar, and A. Handique, "Developed DICOM standard schema with DSpace," *Collection and Curation*, vol. 41, no. 2, pp. 50-61, 2022.
- [97] J. S. Wadali, S. P. Sood, R. Kaushish, S. Syed-Abdul, P. K. Khosla, and M. Bhatia, "Evaluation of free, open-source, web-based DICOM viewers for the Indian national telemedicine service (eSanjeevani)," *Journal of Digital Imaging*, vol. 33, pp. 1499-1513, 2020.
- [98] C. Gorman, D. Punzo, I. Octaviano, S. Pieper, W. J. Longabaugh, D. A. Clunie, R. Kikinis, A. Y. Fedorov, and M. D. Herrmann, "Interoperable slide microscopy viewer and annotation tool for imaging data science and computational pathology," *Nature communications*, vol. 14, no. 1, p. 1572, 2023.
- [99] E. Ziegler, T. Urban, D. Brown, J. Petts, S. D. Pieper, R. Lewis, C. Hafey, and G. J. Harris, "Open health imaging foundation viewer: an extensible open-source framework for building web-based imaging applications to support cancer research," *JCO clinical cancer informatics*, vol. 4, pp. 336-345, 2020.
- [100] T.-T. Chen, Y.-C. Sun, W.-C. Chu, and C.-Y. Lien, "BlueLight: an open source DICOM viewer using low-cost computation algorithm implemented with javascript using advanced medical imaging visualization," *Journal of Digital Imaging*, vol. 36, no. 2, pp. 753-763, 2023.

- [101] S. Ghoshal, S. Banu, A. Chakrabarti, S. Sur-Kolay, and A. Pandit, "3D reconstruction of spine image from 2D MRI slices along one axis," *IET Image Processing*, vol. 14, no. 12, pp. 2746-2755, 2020.
- [102] A. Fajar, R. Sarno, C. Fatichah, and A. Fahmi, "Reconstructing and resizing 3D images from DICOM files," *Journal of King Saud University-Computer and Information Sciences*, vol. 34, no. 6, pp. 3517-3526, 2022.
- [103] K. Matsuda and R. Lea, "WebGL programming guide: interactive 3D graphics programming with WebGL," Addison-Wesley, pp., 2013.
- [104] W. Li, S. Wang, W. Xie, K. Yu, and C. Feng, "Large scale medical image online three-dimensional reconstruction based on WebGL using four tier client server architecture," *Information Visualization*, vol. 22, no. 2, pp. 100-114, 2023.
- [105] M. J. Leming, E. E. Bron, R. Bruffaerts, Y. Ou, J. E. Iglesias, R. L. Gollub, and H. Im, "Challenges of implementing computer-aided diagnostic models for neuroimages in a clinical setting," *NPJ Digital Medicine*, vol. 6, no. 1, p. 129, 2023.
- [106] Z. Cui, "Towards Efficient Presentation and Interaction in Visual Data Analysis," University of Maryland, College Park, 2019.
- [107] J. Díaz García, P. Brunet Crosa, I. Navazo Álvaro, and P. P. Vázquez Alcocer, "Downsampling methods for medical datasets," in Proceedings of the International conferences Computer Graphics, Visualization, Computer Vision and Image Processing and Big Data Analytics, Data Mining and Computational Intelligence 2017: Lisbon, Portugal, July 21-23, 2017: IADIS Press, pp. 12-20, 2017.
- [108] R. JohnsonChris, "A review of three-dimensional medical image visualization," *Health Data Science*, 2022.
- [109] H. Zhang, Q. Liu, D. Qu, Y. Hou, and B. Chen, "SAMP-Viz: An interactive multivariable volume visualization framework based on subspace analysis and multidimensional projection," *IEEE Access*, vol. 5, pp. 7636-7647, 2017.
- [110] Q. Zhang, "Web-based medical data visualization and information sharing towards application in distributed diagnosis," *Informatics in medicine unlocked*, vol. 14, pp. 69-81, 2019.
- [111] Q. Zhang, "Medical data visual synchronization and information interaction using internet-based graphics rendering and message-oriented streaming," *Informatics in Medicine Unlocked*, vol. 17, p. 100253, 2019.

- [112] N. Lajara, J. L. Espinosa-Aranda, O. Deniz, and G. Bueno, "Optimum web viewer application for DICOM whole slide image visualization in anatomical pathology," *Computer Methods and Programs in Biomedicine*, vol. 179, p. 104983, 2019.
- [113] P. Visutsak, "Marching cubes and histogram pyramids for 3d medical visualization," *Journal of imaging*, vol. 6, no. 9, p. 88, 2020.
- [114] J. Xu, G. Thevenon, T. Chabat, M. McCormick, F. Li, T. Birdsong, K. Martin, Y. Lee, and S. Aylward, "Interactive, in-browser cinematic volume rendering of medical images," *Computer Methods in Biomechanics and Biomedical Engineering: Imaging & Visualization*, vol. 11, no. 4, pp. 1019-1026, 2023.
- [115] A.-M. Boutsis, C. Ioannidis, and S. Verykokou, "Multi-resolution 3D rendering for high-performance web AR," *Sensors*, vol. 23, no. 15, p. 6885, 2023.
- [116] Z. Zhu, X. He, C. Li, S. Liu, K. Jiang, K. Li, and J. Wang, "Adaptive resolution enhancement for visual attention regions based on spatial interpolation," *Sensors*, vol. 23, no. 14, p. 6354, 2023.
- [117] A. Kumar, X. Zhang, H. L. Xin, H. Yan, X. Huang, W. Xu, and K. Mueller, "Radvolviz: an information display-inspired transfer function editor for multivariate volume visualization," *IEEE Transactions on Visualization and Computer Graphics*, 2023.
- [118] K. Paldán, M. Steinmetz, J. Simanovski, C. Rammos, G. Ullrich, R. A. Jánosi, S. Moebus, T. Rassaf, and J. Lortz, "Supervised exercise therapy using mobile health technology in patients with peripheral arterial disease: pilot randomized controlled trial," *JMIR mHealth and uHealth*, vol. 9, no. 8, p. e24214, 2021.
- [119] H. Paredes, D. Paulino, J. Barroso, C. Abrantes, I. Machado, and I. Silva, "Supervised physical exercise therapy of peripheral artery disease patients: M-health challenges and opportunities," 2021.
- [120] M. Kim, Y. Kim, and M. Choi, "Mobile health platform based on user-centered design to promote exercise for patients with peripheral artery disease," *BMC Medical Informatics and Decision Making*, vol. 22, no. 1, p. 206, 2022.
- [121] F.-Q. Wu, Q.-W. Deng, J.-G. Wang, and W.-Z. Li, "The Role of Supervised Exercise Therapy in the Management of Symptomatic Peripheral Artery Disease with Intermittent Claudication," *Current Treatment Options in Cardiovascular Medicine*, vol. 25, no. 10, pp. 501-513, 2023.
- [122] A. Shalan, A. Abdulrahman, I. Habli, G. Tew, and A. Thompson, "YORwalk: designing a smartphone exercise application for people with intermittent claudication," in Building

Continents of Knowledge in Oceans of Data: The Future of Co-Created eHealth, Eds.: IOS Press, pp. 311-315, 2018.

[123] A. Harzand, A. A. Vakili, A. Alrohaibani, S. M. Abdelhamid, N. F. Gordon, J. Thiel, J. Benarroch-Gampel, V. J. Teodorescu, K. Minton, and N. K. Wenger, "Rationale and design of a smartphone-enabled, home-based exercise program in patients with symptomatic peripheral arterial disease: The smart step randomized trial," *Clinical Cardiology*, vol. 43, no. 6, pp. 537-545, 2020.

[124] J. Lortz, J. Simanovski, T. Kuether, I. Kreitschmann-Andermahr, G. Ullrich, M. Steinmetz, C. Rammos, R. A. Jánosi, S. Moebus, and T. Rassaf, "Needs and requirements in the designing of mobile interventions for patients with peripheral arterial disease: questionnaire study," *JMIR formative research*, vol. 4, no. 8, p. e15669, 2020.

[125] A. M. Flores, F. Demsas, N. J. Leeper, and E. G. Ross, "Leveraging machine learning and artificial intelligence to improve peripheral artery disease detection, treatment, and outcomes," *Circulation research*, vol. 128, no. 12, pp. 1833-1850, 2021.

[126] N. Forghani, K. Maghooli, N. J. Dabanloo, A. V. Farahani, and M. Forouzanfar, "Intelligent oscillometric system for automatic detection of peripheral arterial disease," *IEEE Journal of Biomedical and Health Informatics*, vol. 25, no. 8, pp. 3209-3218, 2021.

[127] T. Collins, M. Geana, K. Overton, M. Benton, L. Lu, F. Khan, M. Rohleder, J. Ahluwalia, K. Resnicow, and Y. Zhu, "Use of a smartphone app versus motivational interviewing to increase walking distance and weight loss in overweight/obese adults with peripheral artery disease: pilot randomized trial," *JMIR Formative Research*, vol. 6, no. 2, p. e30295, 2022.

[128] A. Sakellarios, J. Correia, S. Kyriakidis, E. Georga, N. Tachos, P. Siogkas, F. Sans, P. Stofella, V. Massimiliano, and A. Clemente, "A cloud-based platform for the non-invasive management of coronary artery disease," *Enterprise Information Systems*, vol. 14, no. 8, pp. 1102-1123, 2020.

[129] J. Wu, H. Wang, C. Ni, C. Zhang, and W. Lu, "Case Study of Next-Generation Artificial Intelligence in Medical Image Diagnosis Based on Cloud Computing," *Journal of Theory and Practice of Engineering Science*, vol. 4, no. 02, pp. 66-73, 2024.

[130] M. Putzier, T. Khakzad, M. Dreischarf, S. Thun, F. Trautwein, and N. Taheri, "Implementation of cloud computing in the German healthcare system," *npj digital medicine*, vol. 7, no. 1, p. 12, 2024.

- [131] M. Schweitzer, P. Ostheimer, A. Lins, V. Romano, B. Steger, D. Baumgarten, and M. Augustin, "Transforming Tele-Ophthalmology: Utilizing Cloud Computing for Remote Eye Care," in *dHealth 2024*, Eds.: IOS Press, pp. 215-220, 2024.
- [132] Y. Zhang, J. Li, M. Liao, Y. Yang, G. He, Z. Zhou, G. Feng, F. Gao, L. Liu, and X. Xue, "Cloud platform to improve efficiency and coverage of asynchronous multidisciplinary team meetings for patients with digestive tract cancer," *Frontiers in Oncology*, vol. 13, p. 1301781, 2024.
- [133] W. Peng, Y. Hong, Y. Chen, and Z. Yi, "AIScholar: An OpenFaaS-enhanced cloud platform for intelligent medical data analytics," *Computers in Biology and Medicine*, vol. 186, p. 109648, 2025.
- [134] M. Lindstrom, N. DeCleene, H. Dorsey, V. Fuster, C. O. Johnson, K. E. LeGrand, G. A. Mensah, C. Razo, B. Stark, and J. Varieur Turco, "Global burden of cardiovascular diseases and risks collaboration, 1990-2021," *Journal of the American College of Cardiology*, vol. 80, no. 25, pp. 2372-2425, 2022.
- [135] L. Horváth, N. Németh, G. Fehér, Z. Kívés, D. Endrei, and I. Boncz, "Epidemiology of peripheral artery disease: narrative review," *Life*, vol. 12, no. 7, p. 1041, 2022.
- [136] J. Nordanstig, C. Behrendt, A. Bradbury, G. De Borst, F. Fowkes, J. Golledge, A. Gottsater, R. Hinchliffe, S. Nikol, and L. Norgren, "Peripheral arterial disease (PAD)—A challenging manifestation of atherosclerosis," *Preventive Medicine*, vol. 171, p. 107489, 2023.
- [137] M. S. Rohman, Y. Waranugraha, A. N. Masbuchin, S. S. Baskoro, L. W. Sishartami, and B. B. Pratiwi, "Coronary in-stent restenosis predictors following drug-eluting stent implantation: A meta-analysis study," *Journal of Vascular Diseases*, vol. 2, no. 3, pp. 266-281, 2023.
- [138] T. Muramatsu, K. Kozuma, K. Tanabe, Y. Morino, J. Ako, S. Nakamura, K. Yamaji, S. Kohsaka, T. Amano, and Y. Kobayashi, "Clinical expert consensus document on drug-coated balloon for coronary artery disease from the Japanese Association of Cardiovascular Intervention and Therapeutics," *Cardiovascular Intervention and Therapeutics*, vol. 38, no. 2, pp. 166-176, 2023.
- [139] X. Yu, X. Zhang, Z. Lai, J. Shao, R. Zeng, W. Ye, Y. Chen, B. Zhang, B. Ma, and W. Cao, "One-year outcomes of drug-coated balloon treatment for long femoropopliteal lesions: a multicentre cohort and real-world study," *BMC Cardiovascular Disorders*, vol. 21, no. 1, p. 326, 2021.

- [140] J. Escuer, A. F. Schmidt, E. Pena, M. A. Martínez, and S. McGinty, "Mathematical modelling of endovascular drug delivery: Balloons versus stents," *International Journal of Pharmaceutics*, vol. 620, p. 121742, 2022.
- [141] C. Zhao, J. L. Heuslein, Y. Zhang, B. H. Annex, and A. S. Popel, "Dynamic multiscale regulation of perfusion recovery in experimental peripheral arterial disease: a mechanistic computational model," *Basic to Translational Science*, vol. 7, no. 1, pp. 28-50, 2022.
- [142] R. Batra, Y. N. Talluri, S. Sankaranarayanan, and H. C. Fry, "Discovery of Unconventional and Non-intuitive Self-assembling Peptide Materials using Experiment Driven Machine Learning," 2024.
- [143] J. Ipema, E. Huizing, M. A. Schreve, J.-P. P. de Vries, and Ç. Ünlü, "Editor's choice—drug coated balloon angioplasty vs. standard percutaneous transluminal angioplasty in below the knee peripheral arterial disease: a systematic review and meta-analysis," *European journal of vascular and endovascular surgery*, vol. 59, no. 2, pp. 265-275, 2020.
- [144] P. Palmisciano, S. S. Hoz, H. A. Algburi, G. Ventre, S. Street, N. Agyeman, M. W. Robinson, M. S. Smith, P. Shirani, and A. W. Grossman, "Percutaneous transluminal angioplasty and/or stenting for the treatment of basilar artery stenosis: a systematic review and meta-analysis," *Neuroradiology*, vol. 65, no. 6, pp. 985-1000, 2023.
- [145] T. Li, Z. Zhang, W. Wang, A. Mao, Y. Chen, Y. Xiong, and F. Gao, "Simulation and experimental investigation of balloon folding and inserting performance for angioplasty: a comparison of two materials, polyamide-12 and Pebax," *Journal of Functional Biomaterials*, vol. 14, no. 6, p. 312, 2023.
- [146] S. Shaikh, M. Hamza, P. Upreti, M. Akkawi, K. Rajak, M. Z. Haider, N. Kumar, M. Turkmani, F. Kathawa, and S. A. Basit, "Meta-Analysis Comparing Drug-Coated Balloon Versus Plain Old Balloon Angioplasty for In-stent Restenosis of Coronaries," *The American Journal of Cardiology*, 2024.
- [147] P. Sharma, D. Ortiz, M. F. Jan, J. Khitha, S. Q. Allaqaband, T. Bajwa, M. W. Mewissen, and T. Nfor, "Effectiveness and safety of atherectomy versus plain balloon angioplasty for limb salvage in tibioperoneal arterial disease," *Journal of Vascular and Interventional Radiology*, vol. 34, no. 3, pp. 428-435, 2023.
- [148] N. Verde, G. Ciliberti, L. Pittorino, M. Ferrone, M. Franzese, M. Russo, A. Cioppa, G. Popusoi, L. Salemme, and T. Tesorio, "Contemporary Use of Drug-Coated Balloons for Coronary Angioplasty: A Comprehensive Review," *Journal of Clinical Medicine*, vol. 13, no. 20, p. 6243, 2024.

- [149] M. Anantha-Narayanan, S. M. Shah, Q. U. A. Jelani, S. Garcia, C. Ionescu, C. Regan, and C. Mena-Hurtado, "Drug-coated balloon versus plain old balloon angioplasty in femoropopliteal disease: an updated meta-analysis of randomized controlled trials," *Catheterization and Cardiovascular Interventions*, vol. 94, no. 1, pp. 139-148, 2019.
- [150] U. Teichgräber, T. Lehmann, R. Aschenbach, D. Scheinert, T. Zeller, K. Brechtel, E. Blessing, M. Lichtenberg, P. von Flotow, and B. Heilmeyer, "Drug-coated balloon angioplasty of femoropopliteal lesions maintained superior efficacy over conventional balloon: 2-year results of the randomized EffPac trial," *Radiology*, vol. 295, no. 2, pp. 478-487, 2020.
- [151] D.-A. Tataru, F.-L. Lazar, H.-L. Onea, C. Homorodean, M.-C. Ober, M. Olinic, M. Spinu, and D.-M. Olinic, "Benefits and Challenges of Drug-Coated Balloons in Peripheral Artery Disease: From Molecular Mechanisms to Clinical Practice," *International Journal of Molecular Sciences*, vol. 25, no. 16, p. 8749, 2024.
- [152] M. Verdoia, F. Negro, E. Kedhi, H. Suryapranata, M. Marcolongo, and G. De Luca, "Benefits with drug-coated balloon as compared to a conventional revascularization strategy for the treatment of coronary and non-coronary arterial disease: A comprehensive meta-analysis of 45 randomized trials," *Vascular Pharmacology*, vol. 138, p. 106859, 2021.
- [153] M. H. Shishehbor, D. Scheinert, A. Jain, M. Brodmann, G. Tepe, K. Ando, P. Krishnan, O. Iida, J. R. Laird, and P. A. Schneider, "Comparison of drug-coated balloons vs bare-metal stents in patients with femoropopliteal arterial disease," *Journal of the American College of Cardiology*, vol. 81, no. 3, pp. 237-249, 2023.
- [154] C. Yerasi, B. C. Case, B. J. Forrestal, R. Torguson, W. S. Weintraub, H. M. Garcia-Garcia, and R. Waksman, "Drug-coated balloon for de novo coronary artery disease: JACC state-of-the-art review," *Journal of the American College of Cardiology*, vol. 75, no. 9, pp. 1061-1073, 2020.
- [155] J. Wang, X. Chen, J. Zhao, and W. W. Zhang, "Systematic review and meta-analysis of the outcomes of drug-eluting stent versus drug-coated balloon angioplasty for lower extremity peripheral artery diseases," *Annals of Vascular Surgery*, vol. 85, pp. 1-8. e5, 2022.
- [156] A. Kayssi, T. Al-Atassi, G. Oreopoulos, G. Roche-Nagle, K. T. Tan, and D. K. Rajan, "Drug-eluting balloon angioplasty versus uncoated balloon angioplasty for peripheral arterial disease of the lower limbs," *Cochrane Database of Systematic Reviews*, no. 8, 2016.
- [157] C. M. Kinstner, J. Lammer, A. Willfort-Ehringer, W. Matzek, M. Gschwandtner, D. Javor, M. Funovics, M. Schoder, R. Koppensteiner, and C. Loewe, "Paclitaxel-eluting balloon versus standard balloon angioplasty in in-stent restenosis of the superficial femoral and

proximal popliteal artery: 1-year results of the PACUBA trial," *JACC: Cardiovascular Interventions*, vol. 9, no. 13, pp. 1386-1392, 2016.

[158] M. P. Kohi, M. Brodmann, T. Zeller, A. Micari, I. Baumgartner, H. Wang, B. Wall, and M. K. Razavi, "Sex-related differences in the long-term outcomes of patients with femoropopliteal arterial disease treated with the IN. PACT drug-coated balloon in the IN. PACT SFA randomized controlled trial: a post hoc analysis," *Journal of Vascular and Interventional Radiology*, vol. 31, no. 9, pp. 1410-1418. e10, 2020.

[159] U. Frank, S. Nikol, J. Belch, V. Boc, M. Brodmann, P. H. Carpentier, A. Chraim, C. Canning, E. Dimakakos, and A. Gottsäter, "ESVM Guideline on peripheral arterial disease," *Vasa*, 2019.

[160] T. Zeller, R. Langhoff, K. J. Rocha-Singh, M. R. Jaff, E. Blessing, B. Amann-Vesti, M. Krzanowski, P. Peeters, D. Scheinert, and G. Torsello, "Directional atherectomy followed by a paclitaxel-coated balloon to inhibit restenosis and maintain vessel patency: twelve-month results of the DEFINITIVE AR study," *Circulation: Cardiovascular Interventions*, vol. 10, no. 9, p. e004848, 2017.

[161] H. Briody, C. A. Kearns, and M. J. Lee, "Mortality, safety, and effectiveness of paclitaxel-containing balloons and stents in the femoropopliteal artery: systematic review and meta-analysis of randomized controlled trials since 2018," *Journal of Vascular and Interventional Radiology*, vol. 35, no. 10, pp. 1423-1434, 2024.

[162] T. Shazly, W. M. Torres, E. A. Secemsky, V. C. Chitalia, F. A. Jaffer, and V. B. Kolachalama, "Understudied factors in drug-coated balloon design and evaluation: A biophysical perspective," *Bioengineering & Translational Medicine*, vol. 8, no. 1, p. e10370, 2023.

[163] E. Huizing, S. Kum, G. Adams, R. Ferraresi, J. P. P. de Vries, and Ç. Ünlü, "High-pressure, non compliant balloon angioplasty for long and calcified infrapopliteal and inframalleolar lesions is feasible," *International angiology*, vol. 39, no. 5, pp. 390-397, 2020.

[164] Y. Li, W. Cui, J. Wang, C. Zhang, and T. Luo, "Efficacy of high-pressure balloon for the treatment of arteriovenous fistula stenosis: a meta-analysis," *Journal of Endovascular Therapy*, vol. 29, no. 4, pp. 627-636, 2022.

[165] S. Xia, J. Li, L. Ma, Y. Cui, T. Liu, Z. Wang, F. Li, X. Liu, S. Li, and L. Sun, "Ultra-high pressure balloon angioplasty for pulmonary artery stenosis in children with congenital heart defects: Short-to mid-term follow-up results from a retrospective cohort in a single tertiary center," *Frontiers in Cardiovascular Medicine*, vol. 9, p. 1078172, 2023.

- [166] D. Pan, J. Guo, Z. Su, W. Meng, J. Wang, J. Guo, and Y. Gu, "Efficacy and safety of atherectomy combined with balloon angioplasty vs balloon angioplasty alone in patients with femoro-popliteal lesions: a systematic review and meta-analysis of randomized controlled trials," *Journal of Endovascular Therapy*, p. 15266028231215354, 2023.
- [167] S. Giannopoulos, R. L. Varcoe, M. Lichtenberg, J. Rundback, M. Brodmann, T. Zeller, P. A. Schneider, and E. J. Armstrong, "Balloon angioplasty of infrapopliteal arteries: a systematic review and proposed algorithm for optimal endovascular therapy," *Journal of Endovascular Therapy*, vol. 27, no. 4, pp. 547-564, 2020.
- [168] X. Song, T. Adachi, Y. Kawase, T. Kimura, and N. Saito, "Efficacy of the Wolverine cutting balloon on a circumferential calcified coronary lesion: bench test using a three-dimensional printer and computer simulation with the finite element method," *Cardiovascular Intervention and Therapeutics*, pp. 1-11, 2022.
- [169] X. Zhu, M. Umezu, and K. Iwasaki, "Finite element analysis of cutting balloon expansion in a calcified artery model of circular angle 180: Effects of balloon-to-diameter ratio and number of blades facing calcification on potential calcification fracturing and perforation reduction," *PloS one*, vol. 16, no. 5, p. e0251404, 2021.
- [170] M. Kronlage, C. Werner, M. Dufner, E. Blessing, O. J. Müller, B. Heilmeyer, H. A. Katus, and C. Erbel, "Long-term outcome upon treatment of calcified lesions of the lower limb using scoring angioplasty balloon (AngioSculpt™)," *Clinical Research in Cardiology*, vol. 109, pp. 1177-1185, 2020.
- [171] J.-B. Dexpert, D. Hayoz, R. P. Engelberger, C. Krieger, M.-A. R. Meyer, and D. Périard, "Arterial preparation by longitudinal micro-incisions before balloon angioplasty of the superficial femoral and popliteal artery: acute and 12-month results," *Journal of Endovascular Therapy*, vol. 29, no. 3, pp. 420-426, 2022.
- [172] K. Kang and J. Wilson, "Intravascular lithotripsy of underexpanded and recoiled freshly implanted internal carotid stents," *Cardiovascular Revascularization Medicine*, vol. 40, pp. 200-204, 2022.
- [173] K. Lu, X. Ye, Y. Chen, P. Wang, M. Gong, B. Xuan, Z. Tang, M. Li, J. Hou, and K. Peng, "Research progress of drug eluting balloon in arterial circulatory system," *Frontiers in Cardiovascular Medicine*, vol. 11, p. 1287852, 2024.
- [174] J. Lindquist and K. Schramm, "Drug-eluting balloons and drug-eluting stents in the treatment of peripheral vascular disease," in *Seminars in interventional radiology*: Thieme Medical Publishers, pp. 443-452, 2018.

- [175] K. Yalta, E. Yetkin, and T. Yalta, "Harnessing drug-coated balloons for the management of left main coronary disease: A promising strategy?," *Polish Heart Journal (Kardiologia Polska)*, vol. 80, no. 6, pp. 717-718, 2022.
- [176] I. Salahshoori, M. Golriz, M. A. Nobre, S. Mahdavi, R. E. Malekshah, A. Javdani-Mallak, M. N. Jorabchi, H. A. Khonakdar, Q. Wang, and A. H. Mohammadi, "Simulation-based approaches for drug delivery systems: Navigating advancements, opportunities, and challenges," *Journal of Molecular Liquids*, vol. 395, p. 123888, 2024.
- [177] A. Athani, N. N. N. Ghazali, I. A. Badruddin, A. Y. Usmani, M. Amir, D. Singh, and S. H. Khan, "Image-Based Hemodynamic and Rheological Study of Patient's Diseased Arterial Vasculatures Using Computational Fluid Dynamics (CFD) and Fluid-Structure Interactions (FSI) Analysis: A review," *Archives of Computational Methods in Engineering*, pp. 1-31, 2024.
- [178] L. K. Vora, A. D. Gholap, K. Jetha, R. R. S. Thakur, H. K. Solanki, and V. P. Chavda, "Artificial intelligence in pharmaceutical technology and drug delivery design," *Pharmaceutics*, vol. 15, no. 7, p. 1916, 2023.
- [179] P. G. Dake, J. Mukherjee, K. C. Sahu, and A. B. Pandit, "Computational fluid dynamics in cardiovascular engineering: a comprehensive review," *Transactions of the Indian National Academy of Engineering*, vol. 9, no. 2, pp. 335-362, 2024.
- [180] U. Shahrulakmar, M. Omar, and N. Johari, "Brief review on recent advancement of computational analysis on hemodynamics in peripheral artery disease," in *International Conference on Mechanical Engineering Research: Springer*, pp. 555-572, 2021.
- [181] M. Mohammad and A. Trounev, "An advanced algorithm for solving incompressible fluid dynamics: from Navier-Stokes to Poisson equations," *The European Physical Journal Special Topics*, pp. 1-18, 2024.
- [182] C. Hirsch, "Numerical computation of internal and external flows: The fundamentals of computational fluid dynamics," Elsevier, pp., 2007.
- [183] V. Carvalho, D. Pinho, R. A. Lima, J. C. Teixeira, and S. Teixeira, "Blood flow modeling in coronary arteries: A review," *Fluids*, vol. 6, no. 2, p. 53, 2021.
- [184] F. Rikhtegar, E. R. Edelman, U. Olgac, D. Poulidakos, and V. Kurtcuoglu, "Drug deposition in coronary arteries with overlapping drug-eluting stents," *Journal of Controlled Release*, vol. 238, pp. 1-9, 2016.
- [185] A. R. Tzafiriri, F. Garcia-Polite, X. Li, J. Keating, J.-M. Balaguer, B. Zani, L. Bailey, P. Markham, T. C. Kiorpes, and W. Carlyle, "Defining drug and target protein distributions after

stent-based drug release: Durable versus deployable coatings," *Journal of Controlled Release*, vol. 274, pp. 102-108, 2018.

[186] A. Jain, S. McGinty, G. Pontrelli, and L. Zhou, "Theoretical modeling of endovascular drug delivery into a multilayer arterial wall from a drug-coated balloon," *International Journal of Heat and Mass Transfer*, vol. 187, p. 122572, 2022.

[187] A.-F. Totorean, S. I. Bernad, T. Ciocan, I.-C. Totorean, and E. S. Bernad, "Computational fluid dynamics applications in cardiovascular medicine—from medical image-based modeling to simulation: numerical analysis of blood flow in abdominal aorta," in *Advances in Fluid Mechanics: Modelling and Simulations*, Eds.: Springer, pp. 1-42, 2022.

[188] S. M. Black, C. Maclean, P. Hall Barrientos, K. Ritos, A. McQueen, and A. Kazakidi, "Calibration of patient-specific boundary conditions for coupled CFD models of the aorta derived from 4D Flow-MRI," *Frontiers in Bioengineering and Biotechnology*, vol. 11, p. 1178483, 2023.

[189] L. Xu, Z. Tang, H. Zou, Y. Jiang, Y. Shen, X. Zhang, A. Elkoumy, X. Guan, L. Wu, and X. Wu, "Angiography-based computational modeling for in vivo assessment of endothelial dynamic strain in coronary arteries with de novo lesions: comparison of treatment effects of drug-coated balloons between small and large arteries," *Cardiovascular Innovations and Applications*, vol. 9, no. 1, p. 945, 2024.

[190] V. S. Loukas, D. S. Pleouras, G. S. Karanasiou, S. Kyriakidis, A. I. Sakellarios, A. Semertzioglou, L. K. Michalis, and D. I. Fotiadis, "Investigation of Drug Eluting Stents Performance Through in silico Modeling," in *8th European Medical and Biological Engineering Conference: Proceedings of the EMBEC*, November 29–December 3, Portorož, Slovenia: Springer, pp. 712-721, 2020.

[191] M. Myneni and K. Rajagopal, "Constitutive modeling of the mechanical response of arterial tissues," *Applications in Engineering Science*, vol. 11, p. 100111, 2022.

[192] H. B. Khaniki, M. H. Ghayesh, R. Chin, and M. Amabili, "Hyperelastic structures: A review on the mechanics and biomechanics," *International Journal of Non-Linear Mechanics*, vol. 148, p. 104275, 2023.

[193] V. Gupta, A. Jameel, S. K. Verma, S. Anand, and Y. Anand, "An insight on NURBS based isogeometric analysis, its current status and involvement in mechanical applications," *Archives of Computational Methods in Engineering*, vol. 30, no. 2, pp. 1187-1230, 2023.

[194] M. Z. Gładysz, M. Stevanoska, M. K. Włodarczyk-Biegun, and A. Nagelkerke, "Breaking through the barrier: Modelling and exploiting the physical microenvironment to

enhance drug transport and efficacy," *Advanced Drug Delivery Reviews*, vol. 184, p. 114183, 2022.

[195] Vanshita, A. Garg, and H. K. Dewangan, "Recent advances in drug design and delivery across biological barriers using computational models," *Letters in drug design & discovery*, vol. 19, no. 10, pp. 865-876, 2022.

[196] C. Noble, K. D. Carlson, E. Neumann, B. Lewis, D. Dragomir-Daescu, A. Lerman, A. Erdemir, and M. D. Young, "Finite element analysis in clinical patients with atherosclerosis," *Journal of the mechanical behavior of biomedical materials*, vol. 125, p. 104927, 2022.

[197] P. K. Mandal, Sarifuddin, and V. B. Kolachalama, "Computational model of drug-coated balloon delivery in a patient-specific arterial vessel with heterogeneous tissue composition," *Cardiovascular engineering and technology*, vol. 7, pp. 406-419, 2016.

[198] Sarifuddin and P. K. Mandal, "Effect of interstitial fluid flow on drug-coated balloon delivery in a patient-specific arterial vessel with heterogeneous tissue composition: A simulation study," *Cardiovascular Engineering and Technology*, vol. 9, pp. 251-267, 2018.

[199] J. Escuer, M. Cebollero, E. Pena, S. McGinty, and M. A. Martínez, "How does stent expansion alter drug transport properties of the arterial wall?," *Journal of the Mechanical Behavior of Biomedical Materials*, vol. 104, p. 103610, 2020.

[200] A. McQueen, J. Escuer, A. Aggarwal, S. Kennedy, C. McCormick, K. Oldroyd, and S. McGinty, "Do we really understand how drug eluted from stents modulates arterial healing?," *International Journal of Pharmaceutics*, vol. 601, p. 120575, 2021.

[201] S. N. Angili, M. R. Morovvati, M. Kardan-Halvaei, S. Saber-Samandari, K. Razmjooee, A. M. Abed, D. Toghraie, and A. Khandan, "Fabrication and finite element simulation of antibacterial 3D printed Poly L-lactic acid scaffolds coated with alginate/magnesium oxide for bone tissue regeneration," *International Journal of Biological Macromolecules*, vol. 224, pp. 1152-1165, 2023.

[202] S. Psarras, A.-N. Skafidas, and V. Kostopoulos, "In Silico Investigation of the Interlaminar and Mechanical Fracture of Arteries with Atheromatic Plaque during Angioplasty Treatment," *Biomedicines*, vol. 12, no. 9, p. 2105, 2024.

[203] J. Kim, J. H. Lee, E. A. Choi, H. J. Lee, J. Oh, D. H. Byeon, and C. H. Park, "A comparative in vitro study of distinct and novel stent geometries on mechanical performances of poly-L-lactic acid cardiovascular stents," *Artificial Organs*, 2025.

[204] T. Shazly, J. F. Eberth, C. J. Kostelnik, M. J. Uline, V. C. Chitalia, F. G. Spinale, A. Alshareef, and V. B. Kolachalama, "Hydrophilic coating microstructure mediates acute drug

transfer in drug-coated balloon therapy," *ACS applied bio materials*, vol. 7, no. 5, pp. 3041-3049, 2024.

[205] A. Abdelaziz, A. Hafez, K. Atta, H. Elsayed, M. Abdelaziz, A. Elaraby, H. Kadhim, A. Mechi, M. Ezzat, and A. Fadel, "Drug-coated balloons versus drug-eluting stents in patients with acute myocardial infarction undergoing percutaneous coronary intervention: an updated meta-analysis with trial sequential analysis," *BMC Cardiovascular Disorders*, vol. 23, no. 1, p. 605, 2023.

[206] A. Shamanskiy and B. Simeon, "Mesh moving techniques in fluid-structure interaction: robustness, accumulated distortion and computational efficiency," *Computational Mechanics*, vol. 67, no. 2, pp. 583-600, 2021.

[207] D. S. Pleouras, A. I. Sakellarios, P. Tsompou, V. Kigka, S. Kyriakidis, S. Rocchiccioli, D. Neglia, J. Knuuti, G. Pelosi, and L. K. Michalis, "Simulation of atherosclerotic plaque growth using computational biomechanics and patient-specific data," *Scientific Reports*, vol. 10, no. 1, p. 17409, 2020.

[208] D.-H. Lee and J. M. de la Torre Hernandez, "The newest generation of drug-eluting stents and beyond," *European Cardiology Review*, vol. 13, no. 1, p. 54, 2018.

[209] C. M. McKittrick, S. McKee, S. Kennedy, K. Oldroyd, M. Wheel, G. Pontrelli, S. Dixon, S. McGinty, and C. McCormick, "Combining mathematical modelling with in vitro experiments to predict in vivo drug-eluting stent performance," *Journal of Controlled Release*, vol. 303, pp. 151-161, 2019.

[210] K. Anbalakan, H. W. Toh, H. Y. Ang, M. L. Buist, and H. L. Leo, "Assessing the influence of atherosclerosis on drug coated balloon therapy using computational modelling," *European Journal of Pharmaceutics and Biopharmaceutics*, vol. 158, pp. 72-82, 2021.

[211] N. A. Fadhil, K. A. Hammoodi, L. Jassim, H. A. Al-Asadi, and L. J. Habeeb, "Multiphysics analysis for fluid-structure interaction of blood biological flow inside three-dimensional artery," *Curved and Layered Structures*, vol. 10, no. 1, p. 20220187, 2023.

[212] U. Z. Shahrulakmar, N. H. Johari, M. F. M. Fauzi, J. Haron, C. Nadarajan, and M. N. Omar, "Numerical approach for the evaluation of hemodynamic behaviour in peripheral arterial disease: a systematic review," *J Adv Res Fluid Mech Therm Sci*, vol. 103, no. 2, pp. 95-117, 2023.

[213] A. Khairulin, A. G. Kuchumov, and V. V. Silberschmidt, "In silico model of stent performance in multi-layered artery using 2-way fluid-structure interaction: Influence of

boundary conditions and vessel length," *Computer Methods and Programs in Biomedicine*, vol. 255, p. 108327, 2024.

[214] S. A. Adcock and J. A. McCammon, "Molecular dynamics: survey of methods for simulating the activity of proteins," *Chemical reviews*, vol. 106, no. 5, pp. 1589-1615, 2006.

[215] M. E. Tuckerman, "Statistical mechanics: theory and molecular simulation," Oxford university press, pp., 2023.

[216] N. Chopin and O. Papaspiliopoulos, "An introduction to sequential Monte Carlo," Springer, pp., 2020.

[217] W. Zhang, E. W. Bell, M. Yin, and Y. Zhang, "EDock: blind protein–ligand docking by replica-exchange monte carlo simulation," *Journal of cheminformatics*, vol. 12, pp. 1-17, 2020.

[218] P. Geerlings, E. Chamorro, P. K. Chattaraj, F. De Proft, J. L. Gázquez, S. Liu, C. Morell, A. Toro-Labbé, A. Vela, and P. Ayers, "Conceptual density functional theory: status, prospects, issues," *Theoretical Chemistry Accounts*, vol. 139, no. 2, p. 36, 2020.

[219] Y. Shi and A. Wasserman, "Inverse Kohn–Sham density functional theory: Progress and challenges," *The journal of physical chemistry letters*, vol. 12, no. 22, pp. 5308-5318, 2021.

[220] S. He, L. G. Leanse, and Y. Feng, "Artificial intelligence and machine learning assisted drug delivery for effective treatment of infectious diseases," *Advanced Drug Delivery Reviews*, vol. 178, p. 113922, 2021.

[221] N. Serov and V. Vinogradov, "Artificial intelligence to bring nanomedicine to life," *Advanced Drug Delivery Reviews*, vol. 184, p. 114194, 2022.

[222] A. J. Gormley, "Machine learning in drug delivery," *Journal of Controlled Release*, vol. 373, pp. 23-30, 2024.

[223] R. Gupta, D. Srivastava, M. Sahu, S. Tiwari, R. K. Ambasta, and P. Kumar, "Artificial intelligence to deep learning: machine intelligence approach for drug discovery," *Molecular diversity*, vol. 25, pp. 1315-1360, 2021.

[224] W. Wang, Z. Ye, H. Gao, and D. Ouyang, "Computational pharmaceuticals-A new paradigm of drug delivery," *Journal of Controlled Release*, vol. 338, pp. 119-136, 2021.

[225] B. M. Castro, M. Elbadawi, J. J. Ong, T. Pollard, Z. Song, S. Gaisford, G. Pérez, A. W. Basit, P. Cabalar, and A. Goyanes, "Machine learning predicts 3D printing performance of over 900 drug delivery systems," *Journal of Controlled Release*, vol. 337, pp. 530-545, 2021.

[226] M. Staszak, K. Staszak, K. Wieszczycka, A. Bajek, K. Roszkowski, and B. Tylkowski, "Machine learning in drug design: Use of artificial intelligence to explore the chemical

structure–biological activity relationship," *Wiley Interdisciplinary Reviews: Computational Molecular Science*, vol. 12, no. 2, p. e1568, 2022.

[227] V. Patel and M. Shah, "Artificial intelligence and machine learning in drug discovery and development," *Intelligent Medicine*, vol. 2, no. 3, pp. 134-140, 2022.

[228] E. D. F. D. Lupuliasa, D. F. de Farmacie, and S. d. Ș. F. din România, "Farmacia azi: de la tradiție la interdisciplinaritate și inteligență artificială," 2023.

[229] Z. F. Greenberg, K. S. Graim, and M. He, "Towards artificial intelligence-enabled extracellular vesicle precision drug delivery," *Advanced Drug Delivery Reviews*, vol. 199, p. 114974, 2023.

[230] A. Dedeloudi, E. Weaver, and D. A. Lamprou, "Machine learning in additive manufacturing & Microfluidics for smarter and safer drug delivery systems," *International Journal of Pharmaceutics*, vol. 636, p. 122818, 2023.

[231] S. Hamilton and B. R. Kingston, "Applying artificial intelligence and computational modeling to nanomedicine," *Current Opinion in Biotechnology*, vol. 85, p. 103043, 2024.

[232] H. Xin, A. S. Virk, S. S. Virk, F. Akin-Ige, and S. Amin, "Applications of artificial intelligence and machine learning on critical materials used in cosmetics and personal care formulation design," *Current opinion in colloid & interface science*, p. 101847, 2024.

[233] M. Colombo, A. Corti, S. Berceci, F. Migliavacca, S. McGinty, and C. Chiastra, "3D modelling of drug-coated balloons for the treatment of calcified superficial femoral arteries," *PLoS one*, vol. 16, no. 10, p. e0256783, 2021.

[234] R. V. Pai, J. D. Monpara, and P. R. Vavia, "Exploring molecular dynamics simulation to predict binding with ocular mucin: An in silico approach for screening mucoadhesive materials for ocular retentive delivery systems," *Journal of Controlled Release*, vol. 309, pp. 190-202, 2019.

[235] A. Bunker and T. Róg, "Mechanistic understanding from molecular dynamics simulation in pharmaceutical research 1: drug delivery," *Frontiers in Molecular Biosciences*, vol. 7, p. 604770, 2020.

[236] M. Parsaei and K. Akhbari, "MOF-801 as a nanoporous water-based carrier system for in situ encapsulation and sustained release of 5-FU for effective cancer therapy," *Inorganic Chemistry*, vol. 61, no. 15, pp. 5912-5925, 2022.

[237] M. Öeren, P. J. Walton, P. A. Hunt, D. J. Ponting, and M. D. Segall, "Predicting reactivity to drug metabolism: beyond P450s—modelling FMOs and UGTs," *Journal of Computer-Aided Molecular Design*, vol. 35, no. 4, pp. 541-555, 2021.

- [238] S. Aggarwal, "Modern web-development using reactjs," *International Journal of Recent Research Aspects*, vol. 5, no. 1, pp. 133-137, 2018.
- [239] "cornerstone3D." <https://github.com/cornerstonejs/cornerstone3D> (accessed July, 2024).
- [240] V. K. Kotaru, "Dexie. js for IndexedDB," in *Building Offline Applications with Angular: Develop Reliable, Performant Web Applications for Desktop and Mobile Platforms*, Eds.: Springer, pp. 213-233, 2022.
- [241] "Dicom Viewer." <https://dicomviewer.net/viewer> (accessed 14 February, 2024).
- [242] Y. Gupta, C. Costa, E. Pinho, L. A. Bastião Silva, and R. Heintzmann, "IMAGE-IN: Interactive web-based multidimensional 3D visualizer for multi-modal microscopy images," *Plos one*, vol. 17, no. 12, p. e0279825, 2022.
- [243] R. E. Cooke Jr, M. G. Gaeta, D. M. Kaufman, and J. G. Henrici, "Picture archiving and communication system," ed: Google Patents, 2003.
- [244] S. Bai, C. Ma, X. Wang, S. Zhou, H. Jiang, L. Ma, and H. Jiang, "Application of medical image 3D visualization web platform in auxiliary diagnosis and preoperative planning," *Journal of Image and Graphics*, vol. 11, no. 1, pp. 32-39, 2023.
- [245] M. Mariani, M. Bonanni, A. D'Agostino, G. Iuliano, A. Gimelli, M. A. Coceani, S. Celi, G. M. Sangiorgi, and S. Berti, "Multimodality imaging approach for planning and guiding direct transcatheter tricuspid valve annuloplasty," *Journal of the American Society of Echocardiography*, 2024.
- [246] R. Pemmaraju, R. Minahan, E. Wang, K. Schadl, H. Daldrup-Link, and F. Habte, "Web-based application for biomedical image registry, analysis, and translation (BiRAT)," *Tomography*, vol. 8, no. 3, 2022.
- [247] B. Pervan, S. Tomic, H. Ivandic, and J. Knezovic, "MIDOM—a DICOM-based medical image communication system," *Applied Sciences*, vol. 13, no. 10, p. 6075, 2023.
- [248] Z. Huang and L. Cao, "Bicubic interpolation and extrapolation iteration method for high resolution digital holographic reconstruction," *Optics and Lasers in Engineering*, vol. 130, p. 106090, 2020.
- [249] B. Boroomand and S. Parand, "Towards a general interpolation scheme," *Computer Methods in Applied Mechanics and Engineering*, vol. 381, p. 113830, 2021.
- [250] J. Jin, "An adaptive image scaling algorithm based on continuous fraction interpolation and multi-resolution hierarchy processing," *Fractals*, vol. 28, no. 08, p. 2040016, 2020.

- [251] J. Leng, G. Xu, and Y. Zhang, "Medical image interpolation based on multi-resolution registration," *Computers & Mathematics with Applications*, vol. 66, no. 1, pp. 1-18, 2013.
- [252] M.-s. Pan, X.-l. Yang, and J.-t. Tang, "Research on interpolation methods in medical image processing," *Journal of Medical Systems*, vol. 36, pp. 777-807, 2012.
- [253] A. Atangana and S. Í. Araz, "New numerical scheme with Newton polynomial: theory, methods, and applications," Academic Press, pp., 2021.
- [254] "webnamics / u-dicom-viewer." <https://github.com/webnamics/u-dicom-viewer> (accessed 29 April, 2024).
- [255] S. Tandel and A. Jamadar, "Impact of progressive web apps on web app development," *International Journal of Innovative Research in Science, Engineering and Technology*, vol. 7, no. 9, pp. 9439-9444, 2018.
- [256] E. Elrom, "React and Libraries: Your Complete Guide to the React Ecosystem," Springer, pp., 2021.
- [257] R. A. Rodrigues Zalipynis and N. Terlych, "WebArrayDB: a geospatial array DBMS in your web browser," *Proceedings of the VLDB Endowment*, vol. 15, no. 12, pp. 3622-3625, 2022.
- [258] L. N. Sabaren, M. A. Mascheroni, C. L. Greiner, and E. Irrazábal, "A systematic literature review in cross-browser testing," *Journal of Computer Science & Technology*, vol. 18, 2018.
- [259] R. Kikinis, S. D. Pieper, and K. G. Vosburgh, "3D Slicer: a platform for subject-specific image analysis, visualization, and clinical support," in *Intraoperative imaging and image-guided therapy*, Eds.: Springer, pp. 277-289, 2013.
- [260] S. Jodogne, "Simple, effective deployment of Web viewers for medical imaging in an open platform," in *EuSoMII Annual Meeting 2023. AI: Connecting the dots*, pp., Year.
- [261] I. Marinho, "3D Visualizations in Web Based Environment," Universidade do Porto (Portugal), 2020.
- [262] S. Scanzio, E. Lombardi, K. May, and S. G. Zambrano, "Efficient Hybrid Rendering of Large-scale Data for Simulations on Cloud-based Platform for a Fluid User Experience," 2023.
- [263] W. T. Clarke, T. K. Bell, U. E. Emir, M. Mikkelsen, G. Oeltzschner, A. Shamaei, B. J. Soher, and M. Wilson, "NIfTI-MRS: a standard data format for magnetic resonance spectroscopy," *Magnetic resonance in medicine*, vol. 88, no. 6, pp. 2358-2370, 2022.
- [264] J. Polzehl and K. Tabelow, "Medical Imaging Data Formats," in *Magnetic Resonance Brain Imaging: Modelling and Data Analysis Using R*, Eds.: Springer, pp. 17-27, 2023.

- [265] J. Huixian, "The construction of virtual simulation platform for pingtan experimental area based on HTML5 and WebGL," *Enterprise Information Systems*, vol. 14, no. 9-10, pp. 1457-1474, 2020.
- [266] K. Sareen, S. M. Blackburn, S. S. Hamouda, and L. Gidra, "Memory Management on Mobile Devices," in Proceedings of the ACM SIGPLAN International Symposium on Memory Management, pp. 15-29, 2024.
- [267] M. Ibrahim, P. Rautek, G. Reina, M. Agus, and M. Hadwiger, "Probabilistic occlusion culling using confidence maps for high-quality rendering of large particle data," *IEEE Transactions on Visualization and Computer Graphics*, vol. 28, no. 1, pp. 573-582, 2021.
- [268] P. Ksieniewicz, "Processing data stream with chunk-similarity model selection," *Applied Intelligence*, vol. 53, no. 7, pp. 7931-7956, 2023.
- [269] R. Sicat, M. Ibrahim, A. Ageeli, F. Mannuss, P. Rautek, and M. Hadwiger, "Real-Time Visualization of Large-Scale Geological Models with Nonlinear Feature-Preserving Levels of Detail," *IEEE Transactions on Visualization and Computer Graphics*, vol. 29, no. 2, pp. 1491-1505, 2021.
- [270] O. Zachariadis, A. Teatini, N. Satpute, J. Gómez-Luna, O. Mutlu, O. J. Elle, and J. Olivares, "Accelerating B-spline interpolation on GPUs: Application to medical image registration," *Computer methods and programs in biomedicine*, vol. 193, p. 105431, 2020.
- [271] J. Chaki and N. Dey, "Data tagging in medical images: A survey of the state-of-art," *Current Medical Imaging Reviews*, vol. 16, no. 10, pp. 1214-1228, 2020.
- [272] "Visualize Your Data With vtk.js." <https://kitware.github.io/vtk-js/> (accessed Jul. 26, 2024).
- [273] M. Schwab, D. Saffo, N. Bond, S. Sinha, C. Dunne, J. Huang, J. Tompkin, and M. A. Borkin, "Scalable scalable vector graphics: Automatic translation of interactive svgs to a multithread vdom for fast rendering," *IEEE Transactions on Visualization and Computer Graphics*, vol. 28, no. 9, pp. 3219-3234, 2021.
- [274] W. Yang, Y. Tao, and H. Lin, "Voxer—a platform for creating, customizing, and sharing scientific visualizations," *Journal of Visualization*, vol. 22, pp. 1161-1176, 2019.
- [275] A. Chaudhary, S. J. Jhaveri, A. Sanchez, L. S. Avila, K. M. Martin, A. Vacanti, M. D. Hanwell, and W. Schroeder, "Cross-platform ubiquitous volume rendering using programmable shaders in VTK for scientific and medical visualization," *IEEE Computer Graphics and Applications*, vol. 39, no. 1, pp. 26-43, 2019.

- [276] L. Yariv, J. Gu, Y. Kasten, and Y. Lipman, "Volume rendering of neural implicit surfaces," *Advances in Neural Information Processing Systems*, vol. 34, pp. 4805-4815, 2021.
- [277] M. A. Selver, "Exploring brushlet based 3D textures in transfer function specification for direct volume rendering of abdominal organs," *IEEE transactions on visualization and computer graphics*, vol. 21, no. 2, pp. 174-187, 2014.
- [278] M. Sereno, X. Wang, L. Besançon, M. J. Mcguffin, and T. Isenberg, "Collaborative work in augmented reality: A survey," *IEEE transactions on visualization and computer graphics*, vol. 28, no. 6, pp. 2530-2549, 2020.
- [279] M. Kolos, A. Sevastopolsky, and V. Lempitsky, "TRANSPR: Transparency ray-accumulating neural 3D scene point renderer," in *International Conference on 3D Vision (3DV): IEEE*, pp. 1167-1175, 2020.
- [280] L. Yang, Y. Han, X. Chen, S. Song, J. Dai, and G. Huang, "Resolution adaptive networks for efficient inference," in *Proceedings of the IEEE/CVF conference on computer vision and pattern recognition*, pp. 2369-2378, 2020.
- [281] P. Gómez, M. Semmler, A. Schützenberger, C. Bohr, and M. Döllinger, "Low-light image enhancement of high-speed endoscopic videos using a convolutional neural network," *Medical & biological engineering & computing*, vol. 57, pp. 1451-1463, 2019.
- [282] Z. Li, N. V. Myung, and Y. Yin, "Light-powered soft steam engines for self-adaptive oscillation and biomimetic swimming," *Science Robotics*, vol. 6, no. 61, p. eabi4523, 2021.
- [283] P.-P. Sloan, J. Kautz, and J. Snyder, "Precomputed radiance transfer for real-time rendering in dynamic, low-frequency lighting environments," in *Seminal Graphics Papers: Pushing the Boundaries, Volume 2, Eds.*, pp. 339-348, 2023.
- [284] L. Saba, P. L. Antignani, A. Gupta, R. Cau, K. I. Paraskevas, P. Poredos, B. A. Wasserman, H. Kamel, E. D. Avgerinos, and R. Salgado, "International Union of Angiology (IUA) consensus paper on imaging strategies in atherosclerotic carotid artery imaging: From basic strategies to advanced approaches," *Atherosclerosis*, vol. 354, pp. 23-40, 2022.
- [285] A. J. Buckler, A. M. Gotto Jr, A. Rajeev, A. Nicolaou, A. Sakamoto, S. St Pierre, M. Phillips, R. Virmani, and T. C. Villines, "Atherosclerosis risk classification with computed tomography angiography: a radiologic-pathologic validation study," *Atherosclerosis*, vol. 366, pp. 42-48, 2023.
- [286] G. Sangiorgi, J. A. Rumberger, A. Severson, W. D. Edwards, J. Gregoire, L. A. Fitzpatrick, and R. S. Schwartz, "Arterial calcification and not lumen stenosis is highly correlated with atherosclerotic plaque burden in humans: a histologic study of 723 coronary

artery segments using nondecalcifying methodology," *Journal of the American College of Cardiology*, vol. 31, no. 1, pp. 126-133, 1998.

[287] M. Ghasemi, D. R. Nolan, and C. Lally, "Assessment of mechanical indicators of carotid plaque vulnerability: Geometrical curvature metric, plaque stresses and damage in tissue fibres," *Journal of the mechanical behavior of biomedical materials*, vol. 103, p. 103573, 2020.

[288] M. Kobayashi, K. Hoshina, Y. Nemoto, S. Takagi, M. Shojima, M. Hayakawa, S. Yamada, and M. Oshima, "A penalized spline fitting method to optimize geometric parameters of arterial centerlines extracted from medical images," *Computerized Medical Imaging and Graphics*, vol. 84, p. 101746, 2020.

[289] M.-Y. Eun, H. N. Song, J. U. Choi, H. H. Cho, H. J. Kim, J.-W. Chung, T.-J. Song, J.-M. Jung, O. Y. Bang, and G. M. Kim, "Global intracranial arterial tortuosity is associated with intracranial atherosclerotic burden," *Scientific Reports*, vol. 14, no. 1, p. 11318, 2024.

[290] A. B. Consortium, Y.-J. Jia, J. Wang, J.-R. Ren, P. Chan, S. Chen, X.-C. Chen, J. K. Chhetri, J. Guo, and Q. Guo, "A framework of biomarkers for brain aging: a consensus statement by the Aging Biomarker Consortium," *Life Medicine*, vol. 2, no. 3, p. lnad017, 2023.

[291] H. Zhang, J. Ma, Z. Qiu, J. Yao, M. A. A. Sibahee, Z. A. Abduljabbar, and V. O. Nyangaresi, "Multi-gpu parallel pipeline rendering with splitting frame," in *Computer Graphics International Conference*: Springer, pp. 223-235, 2023.

[292] "Glance – Medical Imaging Data Visualization." <https://github.com/Kitware/glance> (accessed July 2024).

[293] M. R. Islam, S. Akter, L. Islam, I. Razzak, X. Wang, and G. Xu, "Strategies for evaluating visual analytics systems: A systematic review and new perspectives," *Information Visualization*, vol. 23, no. 1, pp. 84-101, 2024.

[294] P. Stoker, G. Tian, and J. Y. Kim, "Analysis of variance (ANOVA)," in *Basic quantitative research methods for urban planners*, Eds.: Routledge, pp. 197-219, 2020.

[295] T. Alsaigh, B. A. Di Bartolo, J. Mulangala, G. A. Figtree, and N. J. Leeper, "Bench-to-bedside in vascular medicine: optimizing the translational pipeline for patients with peripheral artery disease," *Circulation research*, vol. 128, no. 12, pp. 1927-1943, 2021.

[296] B. Almadani, H. Kaiser, I. R. Thoker, and F. Aliyu, "A Systematic Survey of Distributed Decision Support Systems in Healthcare," *Systems*, vol. 13, no. 3, p. 157, 2025.

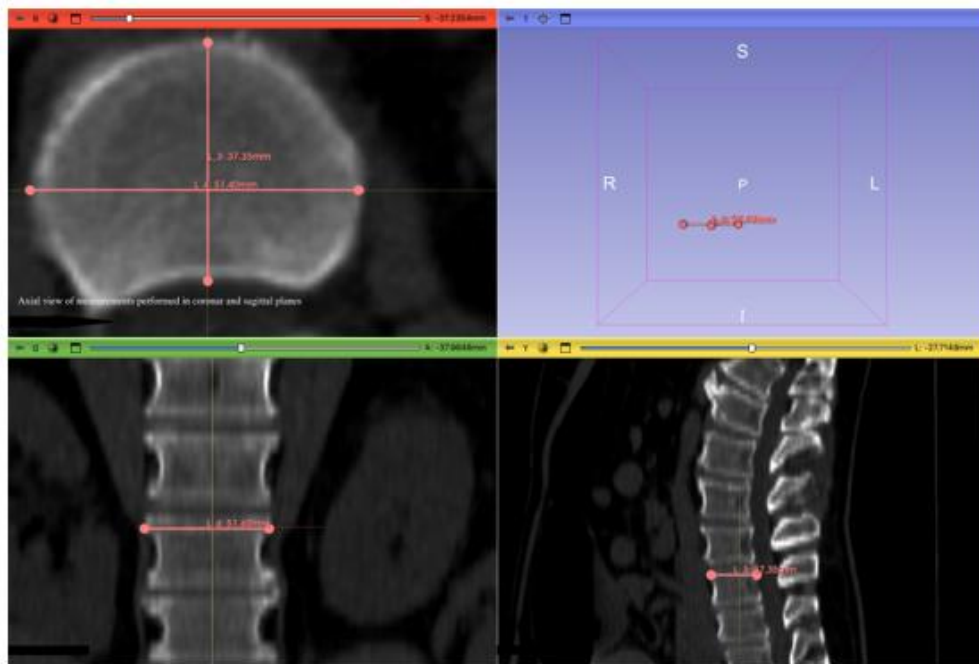
[297] N. Filipović, "In Silico Clinical Trials for Cardiovascular Disease: A Finite Element and Machine Learning Approach," Springer Nature, pp., 2024.

- [298] A. Kaya, R. Ozturk, and C. Altin Gumussoy, "Usability measurement of mobile applications with system usability scale (SUS)," in *Industrial Engineering in the Big Data Era: Selected Papers from the Global Joint Conference on Industrial Engineering and Its Application Areas*, GJCIE, June 21–22, Nevsehir, Turkey: Springer, pp. 389-400, 2018.
- [299] P. Silva, "Davis' technology acceptance model (TAM)(1989)," *Information seeking behavior and technology adoption: Theories and trends*, pp. 205-219, 2015.
- [300] D. Rubio, "Beginning django," Springer, pp., 2017.
- [301] D. Sargiotis, "Data security and privacy: Protecting sensitive information," in *Data governance: a guide*, Eds.: Springer, pp. 217-245, 2024.
- [302] V. Andersson and J. Seller Fredlund, "A Comparison of User Experience in Progressive Web Apps and Cross-platform Framework Apps: Performance, Appearance and Functionality of a React Progressive Web App and a React Native App," ed: KTH Royal Institute of Technology, 2024.
- [303] H. Subramanian and P. Raj, "Hands-On RESTful API Design Patterns and Best Practices: Design, develop, and deploy highly adaptable, scalable, and secure RESTful web APIs," Packt Publishing Ltd, pp., 2019.
- [304] S. K. Sahu, "Protocol Security," in *Building Secure PHP Applications: A Comprehensive Guide to Protecting Your Web Applications from Threats*, Eds.: Springer, pp. 315-346, 2024.
- [305] Q. T. Cao, "Authentication mechanisms for a web developer," 2023.
- [306] D. A. Clunie, "DICOM format and protocol standardization—a core requirement for digital pathology success," *Toxicologic Pathology*, vol. 49, no. 4, pp. 738-749, 2021.
- [307] M. Larobina and L. Murino, "Medical image file formats," *Journal of digital imaging*, vol. 27, pp. 200-206, 2014.
- [308] M. A. AboArab, V. T. Potsika, D. I. Fotiadis, and G. Gkois, "DECODE: A New Cloud-Based Framework for Advanced Visualization, Simulation, and Optimization Treatment of Peripheral Artery Disease," in *IEEE 23rd International Conference on Bioinformatics and Bioengineering (BIBE)*: IEEE, pp. 303-307, 2023.
- [309] M. A. AboArab, V. T. Potsika, N. Petrović, and D. I. Fotiadis, "DECODE cloud platform: A new cloud platform to combat the burden of peripheral artery disease," in *Panhellenic Conference on Electronics & Telecommunications (PACET)*: IEEE, pp. 1-6, 2022.

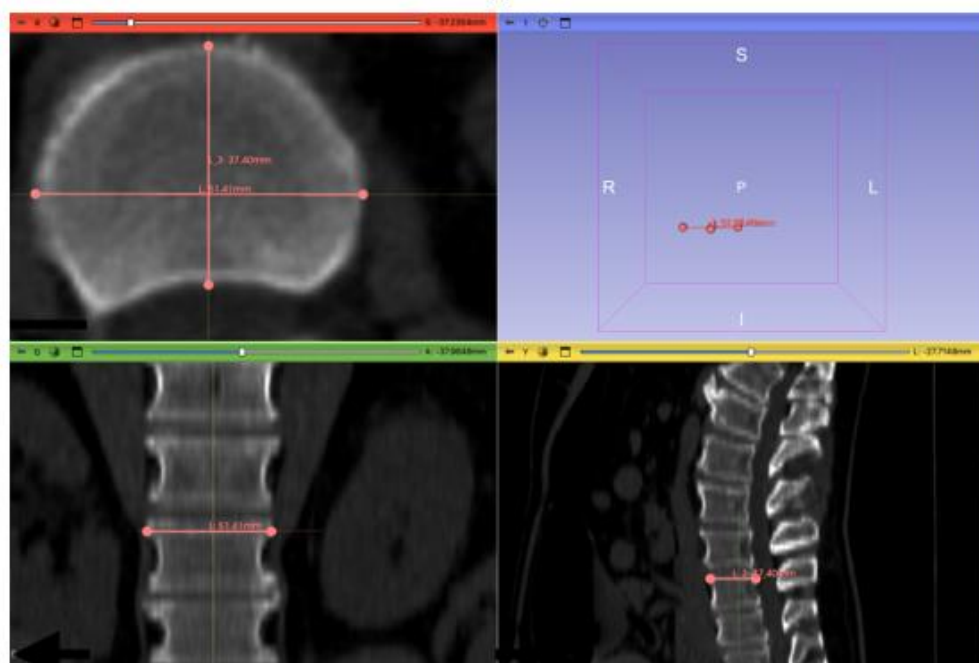
- [310] G. Yu, C. Liu, T. Fang, J. Jia, E. Lin, Y. He, S. Fu, L. Wang, L. Wei, and Q. Huang, "A survey of real-time rendering on Web3D application," *Virtual Reality & Intelligent Hardware*, vol. 5, no. 5, pp. 379-394, 2023.
- [311] C. Green, "Optimising for holistic VR interaction," 2024.
- [312] P. Schober, C. Boer, and L. A. Schwarte, "Correlation coefficients: appropriate use and interpretation," *Anesthesia & analgesia*, vol. 126, no. 5, pp. 1763-1768, 2018.

Appendix.

Supplementary Figure 1. Multiplanar Validation Views in 3D Slicer Software



(a)



(b)

Supplementary Figure 1. Control measurements of the distal edge of the L1 vertebra for patient #1 using 3D Slicer (Version 5.6.2). (a) Measurements performed in the axial view, automatically reflected in the coronal and sagittal planes. (b) Manual measurements repeated in the coronal and sagittal planes. Minor differences ($<0.5\text{mm}$) observed between the views are attributed to the manual measurement process using the mouse cursor.

Supplementary Questionnaire 1. DECODE-3DViz Tool

A. Visual Characteristics Questions

For each set of images, rate the following characteristics:

1. Definition of Structure, please rate the sharpness of the edges of the anatomical structures in the images: 1 - Very Unsatisfied | 2 - Unsatisfied | 3 - Neutral | 4 - Satisfied | 5 - Very Satisfied

Iliac Arteries: _____

Femoral Arteries: _____

Popliteal Arteries: _____

Tibial Arteries: _____

2. Depth Perception, please rate the ability to perceive spatial relationships in the images: 1 - Very Unsatisfied | 2 - Unsatisfied | 3 - Neutral | 4 - Satisfied | 5 - Very Satisfied

Iliac Arteries: _____

Femoral Arteries: _____

Popliteal Arteries: _____

Tibial Arteries: _____

3. Texture Appearance, please rate the realism of the surface textures in the images: 1 - Very Unsatisfied | 2 - Unsatisfied | 3 - Neutral | 4 - Satisfied | 5 - Very Satisfied

Iliac Arteries: _____

Femoral Arteries: _____

Popliteal Arteries: _____

Tibial Arteries: _____

4. Fidelity, please rate how closely the images resemble real peripheral artery tissue: 1 - Very Unsatisfied | 2 - Unsatisfied | 3 - Neutral | 4 - Satisfied | 5 - Very Satisfied

Iliac Arteries: _____

Femoral Arteries: _____

Popliteal Arteries: _____

Tibial Arteries: _____

5. Diagnostic Ability, please rate the effectiveness of the images in supporting clinical diagnosis/your work: 1 - Very Unsatisfied | 2 - Unsatisfied | 3 - Neutral | 4 - Satisfied | 5 - Very Satisfied

Iliac Arteries: _____

Femoral Arteries: _____

Popliteal Arteries: _____

Tibial Arteries: _____

B. Additional Questions

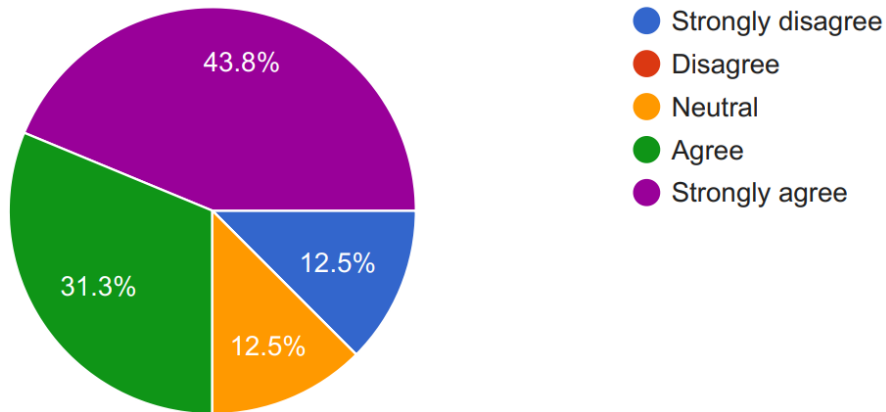
6. Reliability of this Tool, please rate the reliability of our tool for 3D volume rendering: 1 - Very Unsatisfied | 2 - Unsatisfied | 3 - Neutral | 4 - Satisfied | 5 - Very Satisfied
7. Recommendation of this Tool, would you recommend our tool to others for advanced rendering? 1 - Very Unsatisfied | 2 - Unsatisfied | 3 - Neutral | 4 - Satisfied | 5 - Very Satisfied

C. Open-Ended Questions

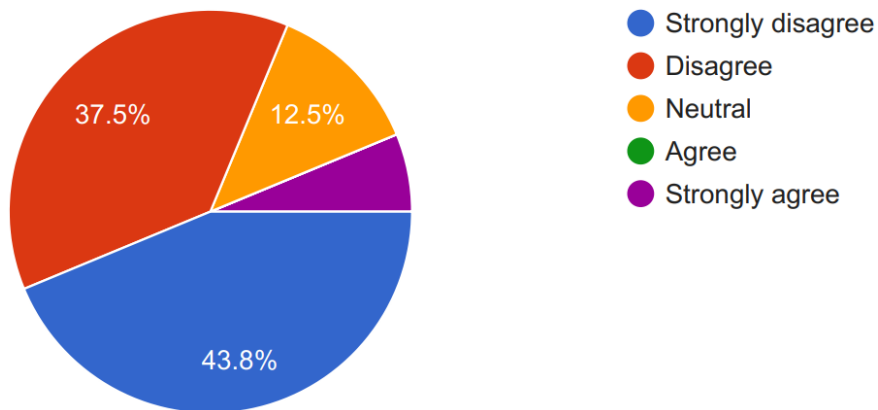
8. Please provide your preference for using our tool or the other state-of-the-art tools for advanced rendering and explain your reasoning.
9. Please provide any additional comments or suggestions to help improve the rendering techniques.

Supplementary Questionnaire 2. SUS for DECODE Cloud Platform

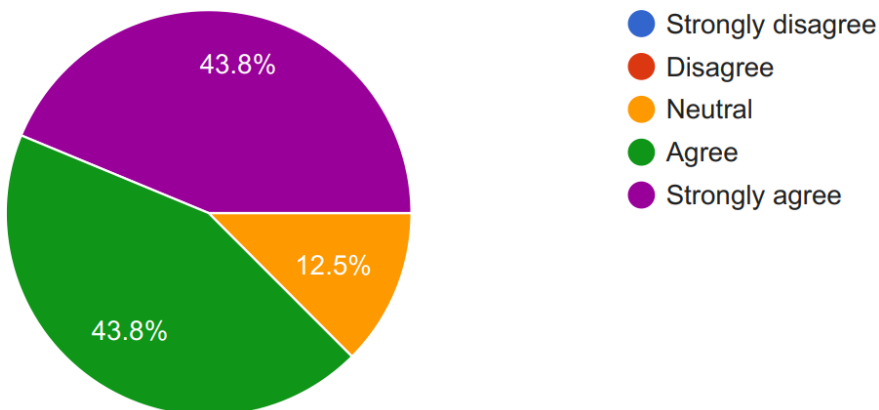
1. I think that I would like to use the DECODE Cloud Platform frequently.



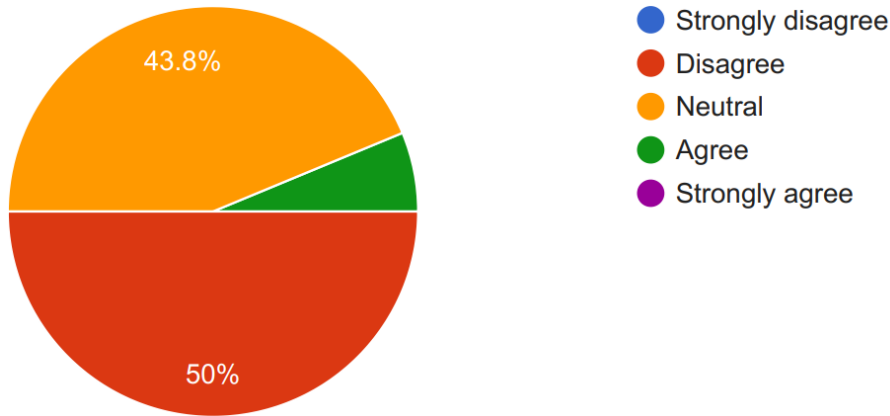
2. I found the DECODE Cloud Platform unnecessarily complex.



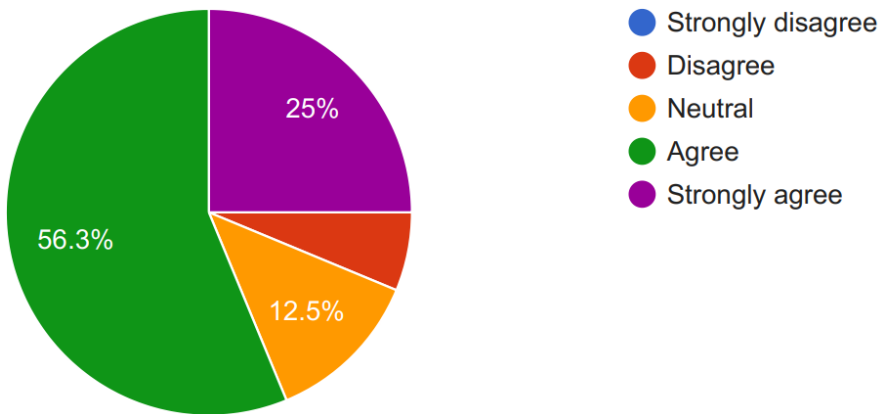
3. I thought the DECODE Cloud Platform was easy to use.



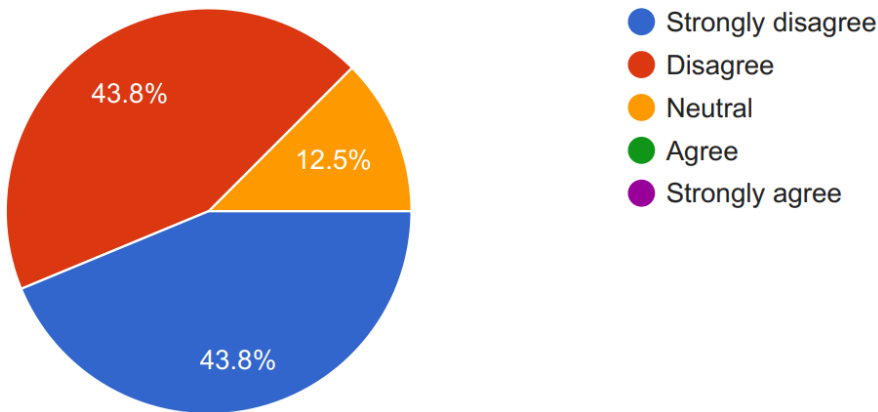
4. I think that I would need the support of a technical person to use this platform.



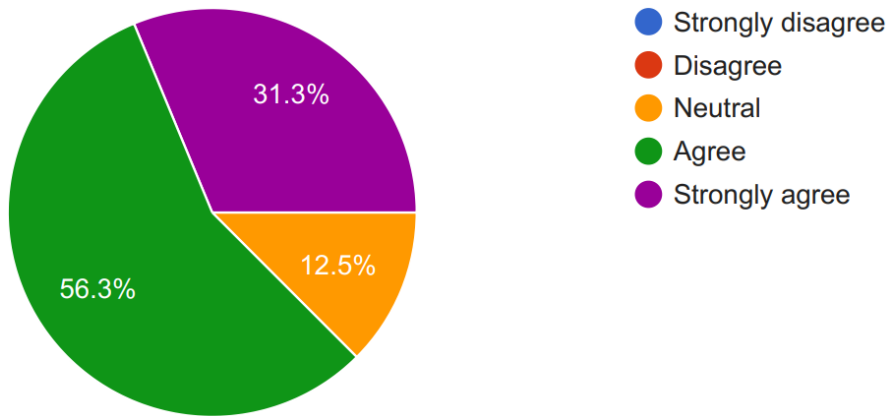
5. I found the various functions of the DECODE Cloud Platform were well integrated.



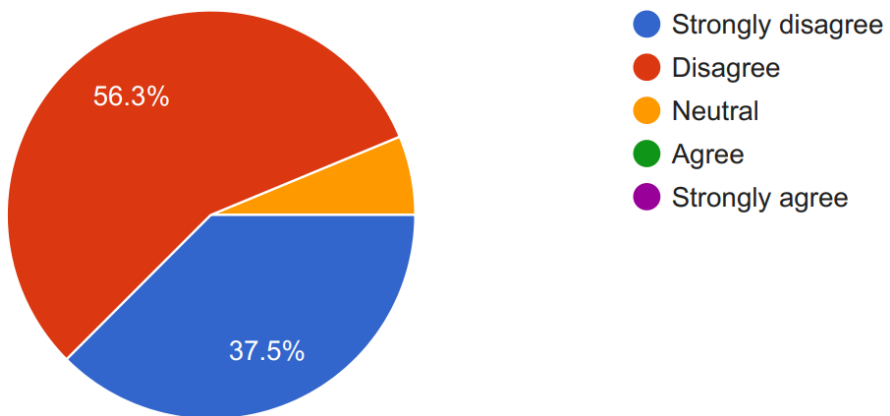
6. I thought there was too much inconsistency in this platform.



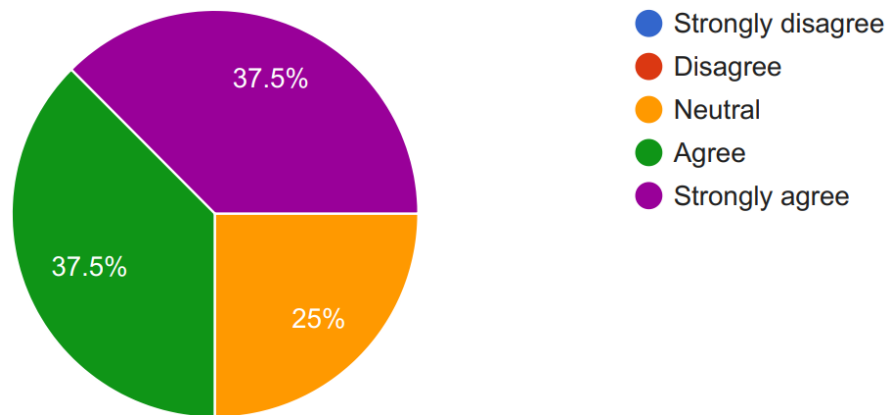
7. I would imagine that most people would learn to use this platform very quickly.



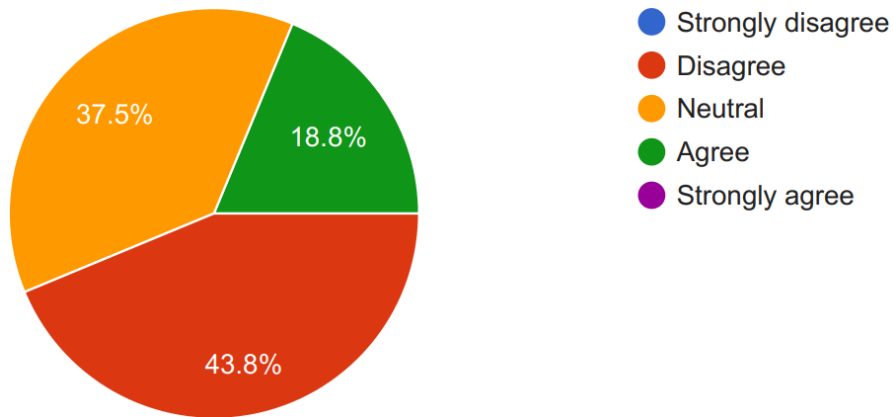
8. I found the DECODE Cloud Platform very cumbersome to use.



9. I felt very confident using the DECODE Cloud Platform.



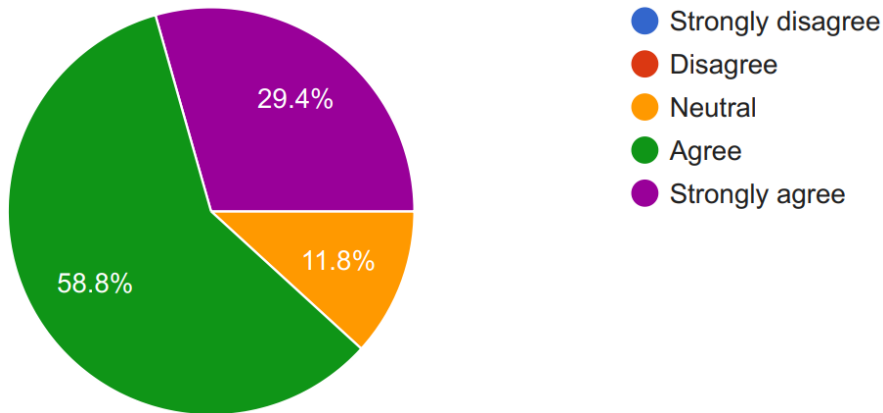
10. I needed to learn a lot of things before I could get going with this platform.



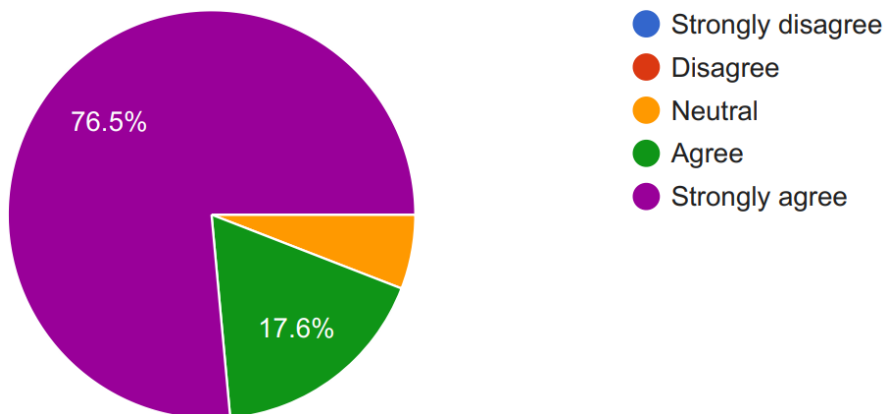
Supplementary Questionnaire 3. TAM for DECODE Cloud Platform

A. Perceived Usefulness (PU)

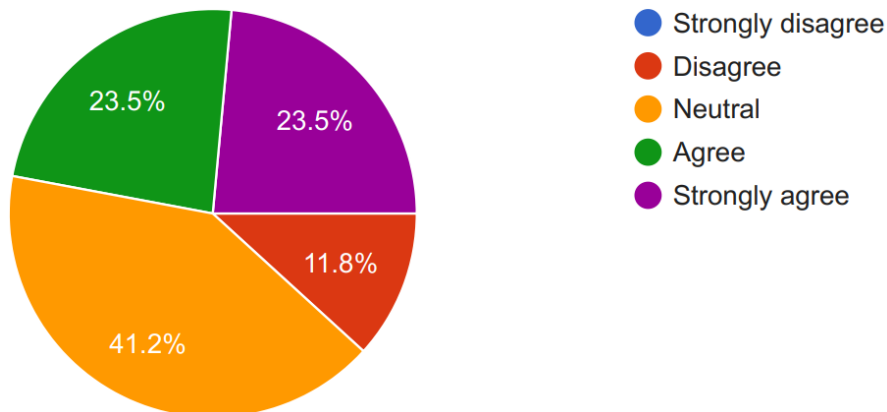
1. Using the DECODE Cloud Platform improves my efficiency in analyzing PAD imaging.



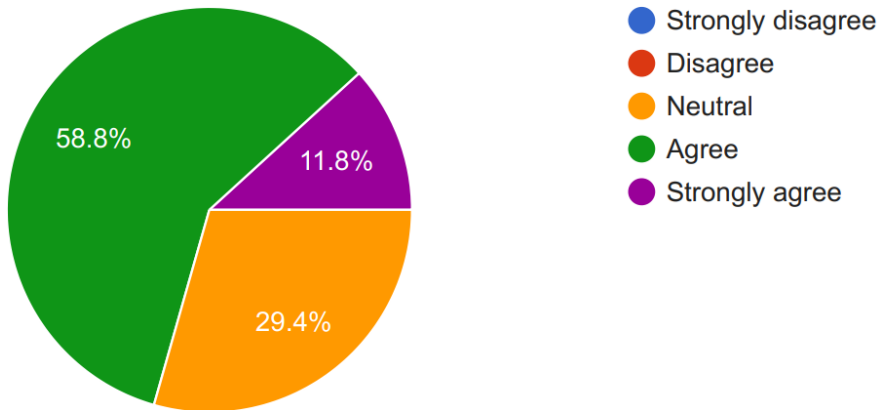
2. The DECODE Cloud Platform enhances my ability to process and visualize vascular imaging data.



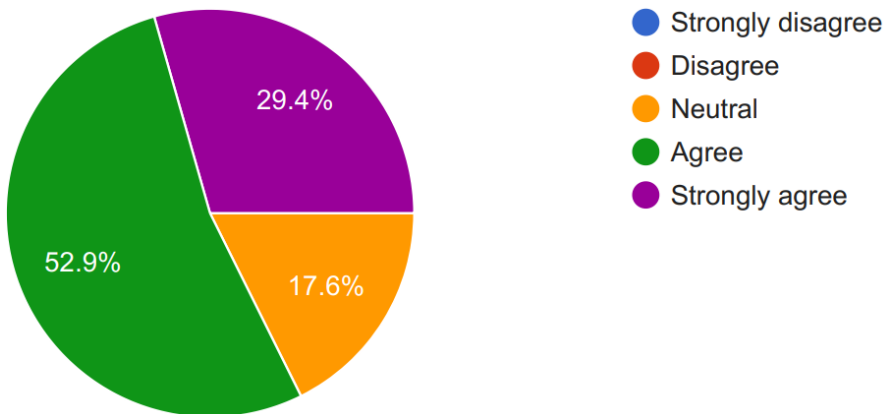
3. Using this platform increases my productivity in computational modeling and PAD diagnosis.



4. The DECODE Cloud Platform makes it easier to manage patient-specific PAD diagnosis and intervention planning.

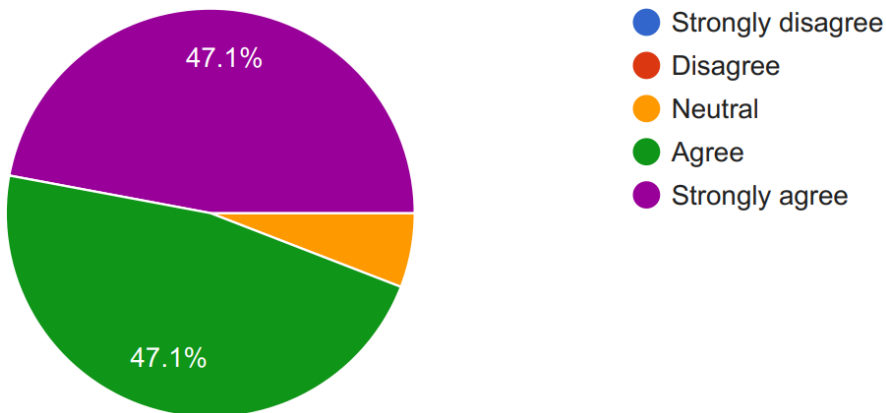


5. I find the DECODE Cloud Platform useful for my research or clinical work.

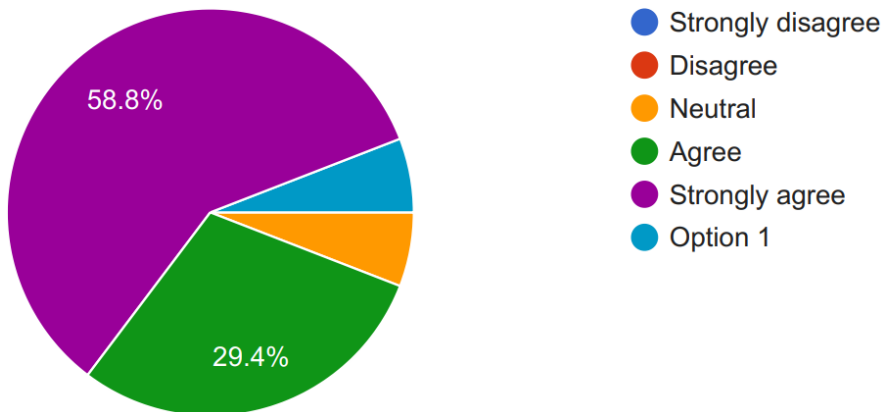


B. Perceived Ease of Use (PEOU)

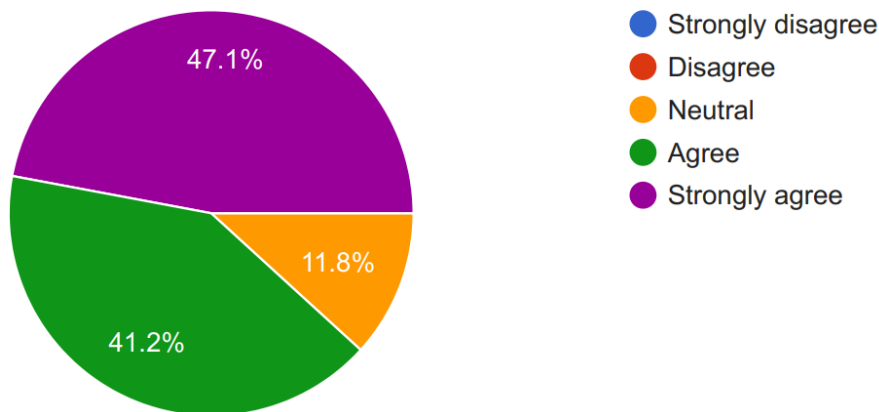
6. Learning to use the DECODE Cloud Platform is easy for me.



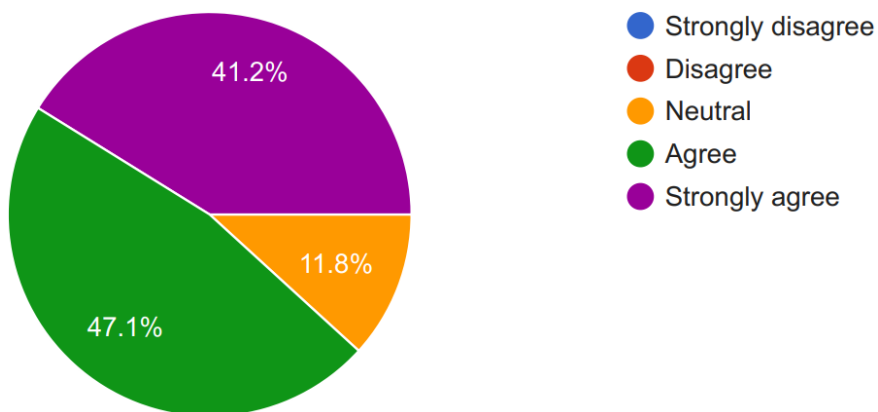
7. I find it easy to interact with the platform's AI-driven segmentation and visualization features.



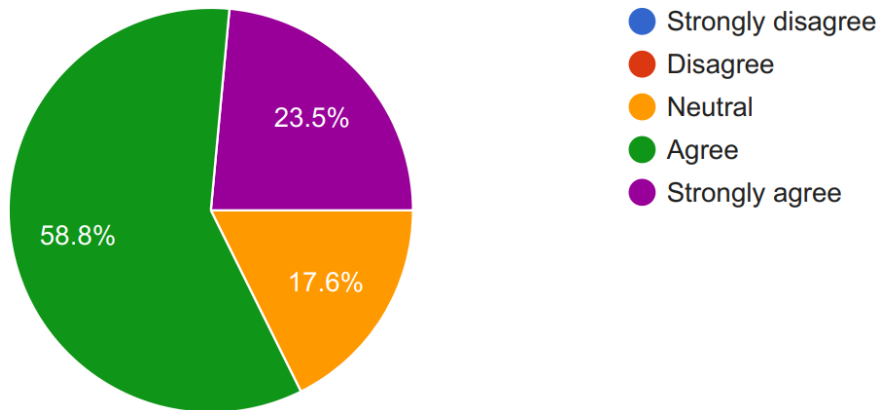
8. My experience with the DECODE Cloud Platform has been smooth and without complications.



9. The platform is user-friendly and well-structured for medical imaging workflows.

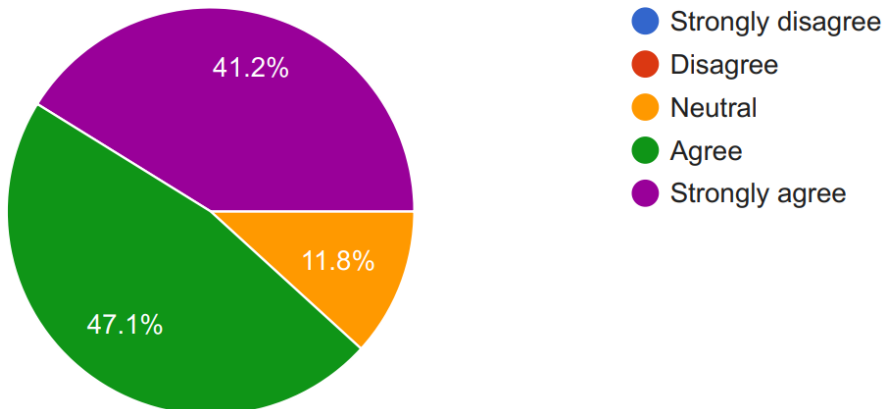


10. It is easy for me to become skilled at using the DECODE Cloud Platform.

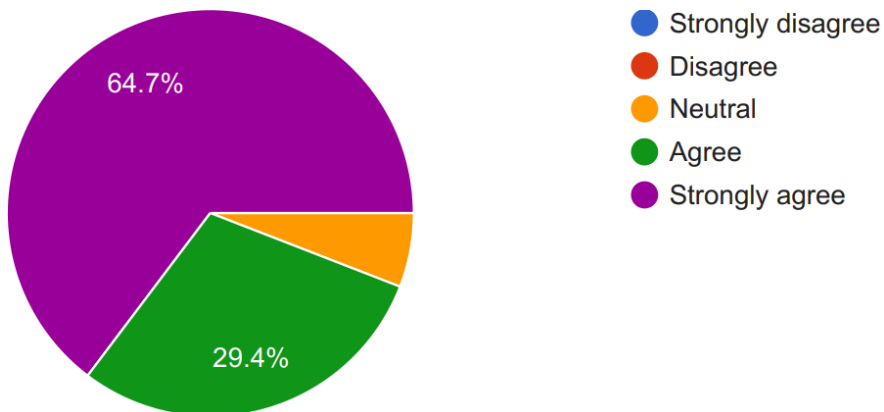


C. Behavioral Intention to Use (BI)

11. I intend to continue using the DECODE Cloud Platform for medical imaging and analysis.



12. I would recommend the DECODE Cloud Platform to other researchers and clinicians working with PAD imaging.



Author's Publications

Journal Publications

1. **AboArab, M. A.**, Potsika, V. T., Theodorou, A., Vagena, S., Gravanis, M., Sigala, F., & Fotiadis, D. I. (2024). Advancing Progressive Web Applications to Leverage Medical Imaging for Visualization of Digital Imaging and Communications in Medicine and Multiplanar Reconstruction: Software Development and Validation Study. *JMIR Medical Informatics*, 12, e63834.
2. **AboArab, M. A.**, Potsika, V. T., & Fotiadis, D. I. (2024). Advanced cloud-based solutions for peripheral artery disease: Diagnosis, analysis, and visualization. *Journal of Engineering Research and Sciences*, 3(12), 24–35.
3. **AboArab, M.A.**, Potsika, V.T., Skalski, A., Stanuch, M., Gkois, G., Koncar, I., Matejevic, D., Theodorou, A., Vagena, S., Sigala, F. and Fotiadis, D.I., 2025. DECODE-3DViz: Efficient WebGL-Based High-Fidelity Visualization of Large-Scale Images using Level of Detail and Data Chunk Streaming. *Journal of Imaging Informatics in Medicine*, pp.1-19.
4. **AboArab, M. A.**, Potsika, V. T., Pleouras, D. S., & Fotiadis, D. I. (2025). (2025). Computational Modeling of Drug-Eluting Balloons in Peripheral Artery Disease: Mechanisms, Optimization, and Translational Insights. *Computational and Structural Biotechnology Journal* (**under review**).
5. **AboArab, M. A.**, Anić, M., Potsika, V. T., Saeed, H., Zulfiqar, M., Skalski, A., Strettie, E., Kostopoulos, V., Psarras, S., Pennati, G., Berti, F., Spahić, L., Benolić, L., Filipović, N., & Fotiadis, D. I. (2025). DECODE: An Open-Source Cloud-Based Platform for the Noninvasive Management of Peripheral Artery Disease. *Computer Methods and Programs in Biomedicine journal* (**under review**).

Conference Publications

1. **AboArab, M. A.**, Potsika, V. T., Petrović, N., & Fotiadis, D. I. (2022, December). DECODE cloud platform: A new cloud platform to combat the burden of peripheral artery disease. In 2022 Panhellenic Conference on Electronics & Telecommunications (PACET) (pp. 1-6). IEEE.
2. **AboArab, M. A.**, Potsika, V. T., Fotiadis, D. I., & Gkois, G. (2023, December). DECODE: A New Cloud-Based Framework for Advanced Visualization, Simulation, and Optimization Treatment of Peripheral Artery Disease. In 2023 IEEE 23rd International Conference on Bioinformatics and Bioengineering (BIBE) (pp. 303-307). IEEE.
3. **AboArab, M. A.**, Potsika, V. T., Sigala, F., Theodorou, A., Vagena, S., & Fotiadis, D. I. (2024, November). GPU-Driven Optimization of Web-Based Volume Rendering in Peripheral Artery Disease CT Imaging. In 2024 IEEE 24th International Conference on Bioinformatics and Bioengineering (BIBE) (pp. 1-8). IEEE.
4. **AboArab, M. A.**, Potsika, V. T., & Fotiadis, D. I., DECODE: AI-Driven Segmentation, Visualization, and In-Silico Modeling for Peripheral Artery Disease Management, Poster presented at the Biomaterials Conference, University of Ioannina, Greece, 28–29 March 2025.
5. **AboArab, M. A.**, Potsika, V. T., Theodorou, A., Vagena, S., Sigala, F., and Fotiadis, D. I., "Automated Risk Stratification of Peripheral Artery Disease via Optimized Volume Rendering and Vascular Biomarkers," 12th International Conference on Biomedical Engineering and Systems (ICBES 2025) August 17 - 19, 2025, Paris, France.

Short CV

Mohammed A. AboArab was born in Gharbia Governorate, Egypt, in 1994. He is a Ph.D. candidate in Biomedical Engineering at the School of Engineering, University of Ioannina, Greece, under the DECODE project, funded by Marie Skłodowska-Curie (February 2022 – June 2025). Prior to his doctoral studies, he was an Assistant Lecturer in the Electronics and Electrical Communications Engineering (EECE) Department, Faculty of Engineering, Tanta University, Egypt (March 2019 – February 2022). He earned his M.Sc. in Biomedical Engineering from Tanta University in October 2021, where his thesis, "A Novel Image Registration Technique in Medical Applications," focused on advanced methodologies for medical image alignment. He received his B.Sc. (Hons.) in EECE in 2017, graduating first in his class of 85 students. From February 2018 to March 2019, he served in the Egyptian Armed Forces, where he was promoted to the rank of Corporal. His research interests include medical imaging, biomedical image analysis, artificial intelligence (AI), cloud-based solutions, and 3D visualization.